METEO FRANCE

CENTRE NATIONAL DE LA RECHERCHE SCIENTIFIQUE

The Meso-NH Atmospheric Simulation System:

Scientific Documentation

Part III: Physics

Acknowledgments

This volume contains contributions from P. Bechtold, S. Belair, Ph. Bougeault, J.M. Carrière, J. Cuxart, V. Ducrocq, C. Fischer, M. Georgelin, P. Héreil, J.P. Lafore, C. Liousse, C. Mari, I. Mallet, P. J. Mascart, V. Masson, J.P. Pinty, E. Richard, K. Suhre, J. Stein, P. Tulet, and J. Vilà-Guerau de Arellano. As editors, we would like to express our deep appreciation for the dedicated work of all contributors. The Méso-NH project is the achievement of a much larger team. Our thanks extend to all those who are not cited here, but have given their best to create this unique tool.

Philippe Bougeault and Patrick Mascart

Since the 2002 edition, in addition to the contributors cited above, thanks have to be extended to D. Barbary, Y. Bouteloup, O. Caumont, J.-P. Chaboureau, O. Geoffroy, O. Nuissier, C. Lac, T. Marić, P. Le Moigne, M. Leriche, J. Pergaud, F. Solmon, and M. Tomasini.

Jean-Pierre Chaboureau

Chapter 1

The radiation parameterization

Contents

1.1 Introduction to the radiation code

1.1.1 Purpose

This chapter summarizes the salient features concerning the radiation scheme in Meso-NH. In collaboration with J.-J. Morcrette (ECMWF), a new set of routines corresponding to the version of the radiation codes running at ECMWF on March 2002 have been interfaced with Meso-NH. The detailed original ECMWF scientific documentation is available online at http://www.ecmwf.int/research/ifsdocs/CY23r4/

The package calculates the radiative fluxes taking into account absorption-emission of longwave radiation and reflection, scattering and absorption of solar radiation by the earth's atmosphere and surfaces. Notice that although the radiation parameterization can deliver a great deal of fluxes (up/down LW/SW in several bands), the package and its interface with Meso-NH only provides the surface shortwave and longwave fluxes with slope angle corrections and the 3D net radiative tendency of the thermodynamical variable θ to the regular user. In addition, some specific configurations of the scheme are available to save computation ressources when a great accuracy of the radiative effects is superfluous. This includes the possibility of calling the package at a different rate of the model timestep, with the "clear sky" approximation, for the "cloud only" air columns or for a larger step of the horizontal sweep out of the air columns. All the details of the parameterization and calling interface will be exposed in this section.

The aim of the routine RADIATIONS is to produce the net total radiative heat flux F used to evaluate the potential temperature tendency term:

$$\frac{\partial \theta}{\partial t} = \frac{g}{C_{ph}} \Pi \frac{\partial F}{\partial p},$$

where F is a net flux: i.e. $F = F^{\uparrow} + F^{\downarrow}$ sum of the upward $F^{\uparrow}$ and downward $F^{\downarrow}$ fluxes, and a total flux: i.e. $F = F_{LW} + F_{SW}$ sum of the solar or shortwave F_{SW} and atmospheric or longwave F_{LW} fluxes. Also in order to drive the surface process scheme, the routine RADIATIONS provides the total downward surface flux in the shortwave and longwave part of the spectrum. All these fluxes are expressed in W m^{-2} unit. The downward SW surface flux is partitioned into direct and diffuse contributions. Note that the radiation output fluxes are defined on a flat surface. A topographic correction is then applied (routine SURF_RAD_MODIF) to get the effective surface fluxes entering in the ISBA scheme (see the specific documentation). A number of other fields are available running the DIAG program as for example the LW and SW flux profiles, the specific LW and SW radiative tendencies, the cloud optical properties, etc (see the DIAG documentation).

1.1.2 The ECMWF radiation code and its Meso-NH interface

The code treats successively the longwave and shortwave radiative transfers for independent air columns. The routine named ECMWF_RADIATION_VERS2 is the interface between the physical variables available in Meso-NH through routine RADIATIONS and the ECMWF LW and SW codes. This routine is used also to initialise cloud radiative properties that do not directly belong to the radiation scheme. It calls the subroutine LW (SW) which handles the infrared (solar) part, respectively.

1.2 Longwave radiation

Two different LW schemes can be activated in Meso-NH (namelist CLW).

- The first one (CLW='MORC') corresponds to the LW scheme operationnal at ECMWF from may 1989 to June 2000 (Morcrette 1991; Gregory et al. 2000). The main characteristics of the scheme are given below (Table 1.1). Physical basis of this model are described in the ECMWF radiation documentation (Chapter 2.2.1 to 2.2.4) and are reproduced below.
- The second one (CLW='RRTM') corresponds to the Rapid Radiation Transfer Model which is currently operational at ECMWF. The main characteristics of RRTM are recalled below (Table 1.1). More details as well as bibliographic references are given in the ECMWF radiation documentation (Chapter 2.2.5) and are reproduced below.

Table 1.1: Main characteristics of LW schemes

	RRTM	MORC
Solution of radiative transfer equation	Two-stream method	Spectral emissivity method
Number of spectral intervals	16	6
Absorbers	H_2O, CO_2, $O3$, CH_4, N_2O, $CFC11$, $CFC12$, aerosols	H_2O, CO_2, $O3$, CH_4, N_2O, $CFC11$, $CFC12$, aerosols
Spectroscopic data base	HITRAN 1996	HITRAN 1992
Absorption coefficient	From LBLRTM line-by-line model	Fits on statistical model of transmission
Cloud handling	True cloud fraction	Effective cloud fraction (CF * emissivity)
Cloud optical properties: method	16-band spectral emissivity	Whole spectrum emissivity
Cloud overlap assumption	Maximum random	Maximum random (maximum and random also possible)
References	Mlawer et al. (1997)	Morcrette et al. (1986, 1991); Gregory et al. (2000)

1.2.1 The Morcrette longwave radiation

1.2.2 First glance

The rate of net atmospheric cooling by emission-absorption of longwave radiation (PDTLOG is given in Kelvin/hour in the code) is:

$$\frac{\partial T}{\partial t} = \frac{g}{C_{ph}} \frac{\partial F}{\partial p}, \tag{1.1}$$

where $F = F_{LW}$ is the net total longwave flux.

Assuming a non-scattering atmosphere in local thermodynamic equilibrium, $F \equiv F^{\uparrow\downarrow}$ is given by:

$$F^{\uparrow\downarrow} = \int_{-1}^{+1} \mu \, d\mu \int_{0}^{\infty} \left[L_\nu(p_s, \mu) \, t_\nu(p_s, p, \mu) + \int_{p_s}^{0} L_\nu(p', \mu) \, dt_\nu \right] d\nu \tag{1.2}$$

where $L_\nu(p_s, \mu)$ is the monochromatic radiance of wavenumber ν at level p propagating in a direction such as $\mu \cos\vartheta$ is the cosine of the angle ϑ that this direction makes with the vertical and $t_\nu(p, p', \mu)$ is the monochromatic transmission through a layer whose limits are at p and p', seen under the same angle.
After separating the upward and downward components and integrating by parts, we obtain the radiation transfer equation as it is actually estimated in the radiation code

$$\begin{aligned} F_\nu^{\uparrow}(p) &= \left[B_\nu(T_s) - B_\nu(T_{0^+}) \right] t_\nu(p_s, p; r) + B_\nu(T_p) + \int_{p_s}^{p} t_\nu(p, p'; r) \, dB_\nu, \\ F_\nu^{\downarrow}(p) &= \left[B_\nu(T_t) - B_\nu(T_\infty) \right] t_\nu(p, 0; r) - B_\nu(T_p) - \int_{p}^{0} t_\nu(p', p; r) \, dB_\nu. \end{aligned} \tag{1.3}$$

Taking benefit of the isotropic nature of the longwave radiations, the radiance L_ν of (1.2) is replaced by the Planck function $B_\nu(T)$ in unit of flux W m^{-2} (subroutine LWB) (hereafter B_ν always includes the π factor). Notice that T_s is the surface temperature (in fact a radiative surface temperature PTSRAD issuing from a surface process scheme such as ISBA) and that T_{0^+} is the temperature of the air just above the surface. T_p is the air temperature (PT) at the Meso-NH mandatoy levels where the atmospherique pressure p needs also to be calculated. T_t is the temperature at the top of the atmosphere (standard atmosphere extension above the last atmospheric level) and $B_\nu(T_\infty$ is set to zero. The transmission t_ν is evaluated as the radiance transmission in a direction ϑ to the vertical such that $r = \sec\vartheta$ is the diffusivity factor (Elsasser 1942). Such an approximation for the integration over the angle is usual in radiative transfer calculations and tests on the validity of this approximation have been presented by Rodgers and Walshaw (1966) among others. The use of the diffusivity factor gives cooling rates within 2% of those obtained with a 4-point Gaussian quadrature.

1.2.3 Vertical integration

Integrals in (1.3) are evaluated numerically, after discretization over the vertical grid, considering the atmosphere as a pile of homogeneous layers (subroutine LWV). As the cooling rate is strongly

dependent on local conditions of temperature and pressure and energy is mainly exchanged with the layers adjacent to the level where fluxes are calculated, the contribution of the distant layers is simply computed using a trapezoidal rule integration (subroutine LWVD), but the contribution of the adjacent layers is evaluated with a 2-point Gaussian quadrature (subroutine LWVN; see common YOMLW), thus

$$\int_{p_s}^{p_i} t_\nu(p,p';r) = \sum_{l=1}^{2} w_l\, t_\nu(p_i,p_l;r)\, dB_\nu(l) + \frac{1}{2}\sum_{j=1}^{i-2} \left[t_\nu(p_i,p_j;r) + t_\nu(p_i,p_{j-1};r)\right] dB_\nu(j) \quad (1.4)$$

where p_l and w_l are the pressure corresponding to the Gaussian root and the Gaussian weight, respectively. $dB_\nu(j)$ (PDBDT) and $dB_\nu(l)$ (PDBSL) are the Planck function gradients calculated between two interfaces and between mid-layer and interface, respectively.

1.2.4 Spectral integration

The integration over wavenumber ν is performed using a band emissivity method, as first discussed by Rodgers (1967). The longwave spectrum is divided into six spectral regions:

1	0 - 350 cm^{-1}	+	1450 - 1880 cm^{-1}
2	500 - 800 cm^{-1}		
3	800 - 970 cm^{-1}	+	1110 - 1250 cm^{-1}
4	970 - 1110 cm^{-1}		
5	350 - 500 cm^{-1}		
6	1250 - 1450 cm^{-1}	+	1880 - 2820 cm^{-1}

corresponding to the centers of the rotation and vibration-rotation bands of H_2O, the 15-μm band of CO_2, the atmospheric window, the 9.6-μm band of O_3, the 25-μm "window" region and the wings of the vibration-rotation band of H_2O, respectively. Over these spectral regions, band fluxes are evaluated with the help of band transmissivities precalculated from the narrow-band model of Morcrette and Fouquart (1985) – See Appendix of Morcrette et al. (1986) for details.

Integration of (1.3) over wavenumber ν within the wide k^{th} spectral region gives the upward and downward fluxes as

$$\begin{aligned} F_k^{\uparrow}(p) &= \left[B_k(T_s) - B_k(T_{0^+})\right] t_{B_k}(ru(p_s,p), T_u(p_s,p)) \\ &\quad + B_k(T_p) + \int_{p_s}^{p} t_{dB_k}(ru(p,p'), T_u(p,p'))\, dB_k, \\ F_k^{\downarrow}(p) &= \left[B_k(T_0) - B_k(T_\infty)\right] t_{B_k}(ru(p,0), T_u(p,0)) \\ &\quad - B_k(T_p) - \int_{p}^{0} t_{dB_k}(ru(p',p), T_u(p',p))\, dB_k. \end{aligned} \quad (1.5)$$

The formulation accounts for the different temperature dependences involved in atmospheric flux calculations, namely that on T_p, the temperature at the level where fluxes are calculated and that

on T_u, the temperature that governs the transmission through the temperature dependence of the intensities and half-widths of the lines absorbing in the concerned spectral region. The band transmissivities are non-isothermal accounting for the temperature dependence that arises from the wavenumber integration of the product of the monochromatic absorption and the Planck function. Two normalized band transmissivities are used for each absorber in a given spectral region (subroutine SWTT1): the first one $t_B(\overline{up}, T_p, T_u)$ for calculating the first r.h.s. term in (1.3) involving the boundaries; it corresponds to the weighted average of the transmission function by the Planck function

$$t_B(\overline{up}, T_p, T_u) = \frac{\int_{\nu_1}^{\nu_2} B_\nu(T_p)\, t_\nu(\overline{up}, T_u)\, d\nu}{\int_{\nu_1}^{\nu_2} B_\nu(T_p)\, d\nu} \tag{1.6}$$

and the second one $t_{dB}(\overline{up}, T_p, T_u)$ for calculating the integral terms in (1.3) is the weighted average of the transmission function by the derivative of the Planck function

$$t_{dB}(\overline{up}, T_p, T_u) = \frac{\int_{\nu_1}^{\nu_2} dB_\nu(T_p)/dT\ t_\nu(\overline{up}, T_u)\, d\nu}{\int_{\nu_1}^{\nu_2} dB_\nu(T_p)/dT\ d\nu} \tag{1.7}$$

where $\overline{up}$ is the pressure weighted amount of absorber (computed in SWU).
In the scheme, the actual dependence on T_p is carried out explicity in the Planck functions integrated over the spectral regions. Although normalized relative to $B(T_p)$ (or $dB(T_p)/dT$), the transmissivities still depend on T_u both through Wien's displacement of the maximum of the Planck function with temperature and through the temperature dependence of the absorption coefficients. O_3 transmissivity is obtained using the Malkmus band model and CH_4, N_2O, $CFC-11$ and $CFC-12$ transmissivities with a statistical model. For computational efficiency, H_2O and CO_2 transmissivities have been developed into Padé approximants

$$t(\overline{up}, T_u) = \frac{\sum_{i=0}^{2} C_i\, u_{eff}^{i/2}}{\sum_{j=0}^{2} D_j\, u_{eff}^{j/2}}, \tag{1.8}$$

where $u_{eff} = r\,\overline{up}\, f(T_u, \overline{up})$ is an effective amount of absorber which incorporates the diffusivity factor r, the weighting of the absorber amount by pressure, $\overline{up}$ and the temperature dependence of the absorption coefficients f, with

$$f(T_u, \overline{up}) = \exp[a(\overline{up})\,(T_u - 250) + b(\overline{up})\,(T_u - 250)^2]. \tag{1.9}$$

The temperature dependence due to Wien's law is incorporated although there is no explicit variation of the coefficients C_i and D_j with temperature. These coefficients have been computed for temperatures between 187.5 and 312.5 K with a 12.5 K step and transmissivities corresponding to the reference temperature the closest to the pressure weighted temperature T_u are actually used in the scheme.

1.2.5 Incorporation of the effects of clouds

The incorporation of the effects of clouds on the longwave fluxes follows the treatment discussed by Washington and Williamson (1977). Whatever the state of cloudiness of the atmosphere, the scheme starts by calculating the clear-sky fluxes and stores the terms representing exchanges of energy between the levels (integrals in (1.3).
Let $F_0^{\uparrow}(i)$ and $F_0^{\downarrow}(i)$ be the upward and downward clear-sky fluxes (PFUP and PFDN in LWC). For any cloud layer actually present in the atmosphere, the scheme then evaluates the fluxes assuming a unique overcast cloud of unity emissivity. Let $F_n^{\uparrow}(i)$ and $F_n^{\downarrow}(i)$ the upward and downward fluxes when such a cloud is present in the n^{th} layer of the atmosphere. Downward fluxes above the cloud and upward fluxes below it have kept their clear-sky values that is:

$$\begin{array}{rcll} F_n^{\uparrow}(i) & = & F_0^{\uparrow}(i) & for \quad i \leq n, \\ F_n^{\downarrow}(i) & = & F_0^{\downarrow}(i) & for \quad i > n. \end{array} \tag{1.10}$$

Upward fluxes above the cloud ($F_n^{\uparrow}(k)$ for $k \geq n+1$) and downward fluxes below it ($F_n^{\downarrow}(k)$ for $k < n$) can be expressed with expressions similar to (1.3) provided the boundary terms are now replaced by terms corresponding to possible temperature discontinuities between the cloud and the surrounding air

$$\begin{aligned} F_n^{\uparrow}(k) &= \left[F_{cld}^{\uparrow} - B(n+1)\right] t(p_k, p_{n+1}; r) + B(k) + \int_{p_{n+1}}^{p_k} t(p_k, p'; r)\, dB, \\ F_n^{\downarrow}(k) &= \left[F_{cld}^{\downarrow} - B(n)\right] t(p_k, p_n; r) + B(k) + \int_{p_k}^{p_n} t(p', p_k; r)\, dB. \end{aligned} \tag{1.11}$$

where $B(i)$ is now the total Planck function (integrated over the whole longwave spectrum) at level i and $F_{cld}^{\uparrow}$ and $F_{cld}^{\downarrow}$ are the fluxes at the upper and lower boundaries of the cloud. Terms under the integrals correspond to exchange of energy between layers in the clear-sky atmosphere and have already been computed in the first step of the calculations. This step is repeated for all cloudy layers. The fluxes for the actual atmosphere (with semi-transparent, fractional and/or multi-layered clouds) are derived from a linear combination of the fluxes calculated in previous steps with some cloud overlap assumption in the case of clouds present in several layers. Let N be the index of the layer containing the highest cloud. C_i the fractional cloud cover in layer i, with $C_0 = 1$ for the upward flux at the surface and with $C_{N+1} = 1$ and $F_{N+1}^{\downarrow} = F_0^{\downarrow}$ to have the right boundary condition for downward fluxes above the highest cloud. The cloudy upward ($F^{\uparrow}$) and downward ($F^{\downarrow}$) fluxes are obtained, with the hypothesis of a random covering of clouds, as:

$$\begin{aligned} F^{\uparrow}(i) &= F_0^{\uparrow}(i) \qquad for\, i = 1 \\ F^{\uparrow}(i) &= C_{i-1} F_{i-1}^{\uparrow}(i) + \sum_{n=0}^{i-2} C_n F_n^{\uparrow}(i) \prod_{l=n+1}^{i-1} (1 - C_l) \qquad for\, 2 \leq i \leq N+1 \\ F^{\uparrow}(i) &= C_N F_N^{\uparrow}(i) + \sum_{n=0}^{N-1} C_n F_n^{\uparrow}(i) \prod_{l=n+1}^{N} (1 - C_l) \qquad for\, i \geq N+2 \end{aligned} \tag{1.12}$$

In case of semi-transparent clouds, the fractional cloudiness entering the calculations is an effective cloud cover equal to the product of the emissivity by the horizontal coverage of the cloud layer, with the emissivity related to the condensed water amount by:

$$\epsilon_i = 1 - \exp(-K^L_{abs}\, u_{LWP} - K^I_{abs}\, u_{IWP}) \tag{1.13}$$

where K^L_{abs} is the condensed water mass absorption coefficient (in m^2 kg^{-1}) and K^I_{abs}, the corresponding one for ice phase. Different parameterisations are avalaible (see subsection 1.4.5).

1.2.6 The Rapid Radiation Transfer Model (RRTM)

As stated in Mlawer et al. (1997), the objective in the development of RRTM has been to obtain an accuracy in the calculation of fluxes and heating rates consistent with the best line-by-line models. It utilizes the correlated-k methode and shows its filiation to the Atmospheric and Environmental Research, Inc. (AER) line-by-line model (LBLRTM; Clough et al. 1989, 1992; Clough and Iacono 1995) through its use of absorption coefficients for the relevant k-distributions derived from LBLRTM. Therefore the k-coefficients in RRTM include the effect of the CKD2.2 water vapour continuum (Clough et al. 1989).
The main point in the correlated-k method (Lacis and Oinas 1991; Fu and Liou 1992) is the mapping of the absorption coefficient $k(\nu)$ from the spectral space (where it varies irregularly with wavenumber ν) to the g-space (where $g(k)$ is the probability distribution function, i.e. the fraction of the absorption coefficients in the set smaller than k). The effect of this reordering is a rearrangement of the sequence of terms in the integral over wavenumber in the radiative transfer equation (RTE), which makes it equivalent to what would be done for monochromatic radiation.
In the ECMWF (hence, Meso-NH) model, no provision is presently taken for scattering in the longwave. Therefore, in order to get the downward radiance, the integration over the vertical dimension is simply done starting from the top of the atmosphere, going downward layer by layer. At the surface, the boundary condition (in terms of spectral emissivity, and potential reflection of downward radiance) is computed, then, in order to get the upward radiance, the integration over the vertical dimension is repeated, this from the surface upward.
The spectrally averaged radiance (between ν_1 and ν_2) emerging from an atmospheric layer is

$$\overline{R} = \frac{1}{(\nu_1 - \nu_2)} \int_{\nu_2}^{\nu_1} d\nu \left\{ R_0(\nu) + \int_{t_\nu}^{1} \left[B(\nu, T(t'_\nu))\, R_0(\nu) \right] dt' \right\} \tag{1.14}$$

where R_0 is the incoming radiance to the layer, $B(\nu, T)$ is the Planck function at wavenumber ν and temperature T, t_ν is the transmittance for the layer optical path, and t'_ν is the transmittance at a point along the optical path in the layer. Under the mapping $\nu \rightarrow g$, this becomes

$$\overline{R} - \int_0^1 dg \left\{ B_{\text{eff}}(g, T_g) + \left[R_0(g) - B_{\text{eff}}(g, T_g) \right] \exp\left[-k(g, P, T) \frac{\rho \delta z}{\cos\phi} \right] \right\} \tag{1.15}$$

where $B_{\text{eff}}(g, T)$ is an effective Planck function for the layer that varies with the layer's transmittance such as to ensure continuity of flux across layer boundaries for opaque conditions. The dependence of the transmittance is now written in terms of the absorption coefficient $k(g, P, T)$ at

layer pressure P and temperature T, the absorber density ρ, the vertical thickness of the layer δz, and the angle ϕ of the optical path.

For a given spectral interval, the domain of the variable g is partitioned into subintervals (see Table 1.2, number of g-points), each corresponding to a limited range of $k(g)$ values and for which a characteristic value κ_j of the absorption coefficient is chosen. These κ_j are then used to compute the outgoing radiance

$$\overline{R} = \Sigma_j W_f \left[B_{\text{eff}_j} + (R_0(g) - B_{\text{eff}_j}) \exp\left(\kappa_j \frac{\rho \delta z}{\cos \phi} \right) \right] \tag{1.16}$$

where W_j is the size of the sub-intervals ($\Sigma W_f = 1$).

The accuracy of these absorption coefficients has been established by numerous and continuing high-resolution validations of LBLRTM with spectroscopic measurements, in particular those from the Atmospheric Radiation Measurement program (ARM). Compared to the original RRTM (Mlawer et al. 1997), the version used at ECMWF (hence, Meso-NH) has been slightly modified to account for cloud optical properties and surface emissivity defined for each of the 16 bands over which spectral fluxes are computed. For efficiency reason, the original number of g-points ($256 = 16 \times 16$) has been reduced to 140 (see Table 1.2). Other changes are the use of a diffusivity approximation (instead of the three-angle integration over the zenith angle used in the original scheme) to derive upward and downward fluxes from the radiances, and the modification of the original cloud random overlapping assumption to include (to the same degree of approximation as used in the operational SW scheme) a maximum-random overlapping of cloud layers. Given the monochromatic form of the RTE, the vertical integration is simply carried out one layer at a time from the top-of-the-atmosphere to the surface to get the downward fluxes. The downward fluxes at the surface are then used with the spectral surface emissivities and the surface temperature to get the upward longwave fluxes in each of the 140 subintervals. Then the upward fluxes are obtained in a similar fashion from the surface to the ToA.

Table 1.2: Spectral distribution of the absorption by atmospheric gases in RRTM

Spectral intervals cm^{-1}	Number of g-points	Gases included	
		Troposphere	Stratosphere
10-250	8	H2O	H2O
250-500	14	H2O	H2O
500-630	16	H2O, CO2	H2O, CO2
630-700	14	H2O, CO2	O3, CO2
700-820	16	H2O, CO2, CCl4	O3, CO2, CCl4
820-980	8	H2O, CFC11, CFC12	CFC11, CFC12
980-1080	12	H2O, O3	O3
1080-1180	8	H2O, CFC12, CFC22	O3, CFC12, CFC22
1180-1390	12	H2O, CH4	CH4

1.3 Shortwave radiation

The ECMWF operational SW scheme results from successive developments from the initial Morcrette et al. version. In Meso-NH, the SW scheme corresponds to the version which was operational at ECMWF until March 2002. Main characteristics are sumarised below. The physical content of this scheme is described in the ECMWF radiation documentation (Chapter 2.3 to 2.4).

- The scheme is based upon a two-stream formulation employed together with photon path distribution method (Fouquart and Bonnel 1980) in 6 spectral intervals (0.185-0.25-0.44-0.69-1.19-2.38-4.00 μm).[1]
- Rayleigh scattering (parametric expression of the Rayleigh optical thickness)
- Aerosol scattering and absorption (Mie parameters for 6 types of aerosols based on climatological models, see further for details on aerosol distributions)
- H_2O (two intervals)
- Uniformly mixed gases (one interval)
- O_3 (two intervals)
- Droplet absorption and scattering (employs a Delta-Eddington method with τ, ω and g determined from the liquid water path u_{LWP} and a parameterization of the effective radius r_e). See the further part for details on cloud optical properties.
- Gas absorption (included separately through the photon path distribution method)

1.3.1 First glance

The rate of atmospheric warming by absorption and scattering of shortwave radiation is:

$$\frac{\partial T}{\partial t} = \frac{g}{C_{ph}} \frac{\partial F}{\partial p} \tag{1.17}$$

where $F = F_{SW}$ is the net total shortwave flux, expressed in W m^{-2} and positive when downward:

$$F = \int_0^\infty d\nu \int_0^\pi d\phi \int_{-1}^{+1} \mu \, L_\nu(\delta, \mu, \phi) \, d\mu \, d\phi \tag{1.18}$$

L_ν is the diffuse radiance at wavenumber ν, in a direction given by ϕ, the azimuth angle and ϑ the zenith angle such as $\mu = \cos\vartheta$. Notice that ϕ (`PAZIMSOL`) and μ (`PMU0`) are computed in routine SUNPOS described in the last subsection. In (1.18), we assume a plane parallel atmosphere with the optical depth δ, as a convenient vertical coordinate when the energy source is outside the medium

[1]The first three intervals are further referenced as the VISible domain while the others are the Near Infra-Red domain for the surface albedo nomenclature.

$$\delta(p) = \int_p^0 \beta_\nu(p)\, dp \tag{1.19}$$

where $\beta_\nu^{ext}(p)$ is the extinction coefficient equal to the sum of the scattering coefficient β_ν^{sca} of the aerosol and cloud particle absorption coefficient β_ν^{abs} and of the purely molecular absorption coefficient k_ν. The diffuse radiance L_ν is governed by the radiation transfer equation

$$\begin{aligned} \mu \frac{dL_\nu(\delta,\mu,\phi)}{d\delta} &= L_\nu(\delta,\mu,\phi) - \frac{\overline{\omega}_\nu(\delta)}{4} P_\nu(\delta,\mu,\phi,\mu_0,\phi_0)\, E_\nu^0 e^{-\frac{\delta}{\mu_0}} \\ &\quad - \frac{\overline{\omega}_\nu(\delta)}{4} \int_0^{2\pi}\int_{-1}^{+1} P_\nu(\delta,\mu,\phi,\mu',\phi')\, L_\nu(\delta,\mu',\phi')\, d\mu'\, d\phi'. \end{aligned} \tag{1.20}$$

E_ν^0 is the incident solar irradiance in the direction $\mu_0 = cos\vartheta_0$, $\overline{\omega}_\nu$ is the single scattering albedo ($= \beta_\nu^{sca}/k_\nu$) and $P_\nu(\delta,\mu,\phi,\mu',\phi')$ is the scattering phase function which defines the probability that radiation coming from direction (μ',ϕ') is scattered in direction (μ,ϕ). The shortwave part of the scheme, originally developed by Fouquart and Bonnel (1980) solves the radiation transfer equation and integrates the fluxes over the whole shortwave spectrum between 0.2 and 4 μm. Upward and downward fluxes are obtained from the reflectances and transmittances of the layers, and the photon path distribution method allows to separate the parametrization of the scattering processes from that of the molecular absorption.

1.3.2 Spectral integration

Solar radiation is attenuated by absorbing gases, mainly water vapor, uniformly mixed gases (oxygen, carbon dioxide, methane, nitrous oxide) and ozone, and scattered by molecules (Rayleigh scattering), aerosols and cloud particles. Since scattering and molecular absorption occur simultaneously, the exact amount of absorber along the photon path length is unknown, and band models of the transmission function cannot be used directly as in the shortwave radiation transfer (see subsection 1.2.3). The approach of the photon path distribution method is to calculate the probability $p(U)\, dU$ that a photon contributing to the flux F_c in the conservative case (i.e. no absorption, $\overline{\omega}_\nu = 1, k_\nu = 0$) has encountered an absorber amount between U and $U + dU$. With this distribution, the radiative flux at wavenumber ν is related to F_c by

$$F_\nu = F_c \int_0^\infty p(U)\, \exp(-k_\nu U)\, dU \tag{1.21}$$

and the flux averaged over the spectral interval $\Delta\nu$ can then be calculated with the help of any band model of the transmission function $t_{\Delta\nu}$

$$F = \frac{1}{\Delta\nu} \int_{\Delta\nu} F_\nu\, d\nu = F_c \int_0^\infty p(U)\, t_{\Delta\nu}(U)\, d\nu. \tag{1.22}$$

To find the distribution function $p(U)$, the scattering problem is solved first, by any method, for a set of arbitrarily fixed absorption coefficients k_l, thus giving a set of simulated fluxes F_{k_l}. An inverse Laplace transform is then performed on (1.21) to get $p(U)$ (Fouquart 1974). The main

advantage of the method is that the actual distribution $p(U)$ is smooth enough that (1.21) gives accurate results even if $p(U)$ itself is not known accurately. In fact, $p(U)(U)$ needs not be calculated explicitly as the spectrally integrated fluxes are, in the two limiting cases of weak and strong absorption:

$$\begin{aligned} F &= F_c\, t_{\Delta\nu}(< U >) \qquad \text{where} \qquad < U >= \int_0^\infty p(U)\, U\, dU \\ F &= F_c\, t_{\Delta\nu}(< U^{\frac{1}{2}} >) \qquad \text{where} \qquad < U^{\frac{1}{2}} >= \int_0^\infty p(U)\, U^{\frac{1}{2}}\, dU \end{aligned} \tag{1.23}$$

respectively. The atmospheric absorption in the water vapor bands is generally strong and the scheme determines an effective absorber amount U_e between $< U >$ and $< U^{\frac{1}{2}} >$ derived from

$$U_e = \frac{1}{k_e}\, \ln(\frac{F_{k_e}}{F_c}) \tag{1.24}$$

where k_e is an absorption coefficient chosen to approximate the spectrally averaged transmission of the clear-sky atmosphere:

$$k_e = (\frac{U_{tot}}{\mu_0})^{-1}\, \ln(t_{\Delta\nu}\frac{U_{tot}}{\mu_0}) \tag{1.25}$$

with U_{tot} the total amount of absorber in a vertical column and $\mu_0 = \cos\vartheta_0$ (PMU0 computed in routine SUNPOS). Once the effective absorber amounts of H_2O and uniformly mixed gases are found, the transmission functions are computed using Padé approximants:

$$t_{\Delta\nu}(U) = \frac{\sum_{i=0}^{N} a_i U^{i-1}}{\sum_{j=0}^{N} b_j U^{j-1}}. \tag{1.26}$$

Absorption by ozone is also taken into account, but since ozone is located at low pressure levels for which molecular scattering is small and Mie scattering is negligible, interactions between scattering processes and ozone absorption are neglected. Transmission through ozone is computed using (1.26) where the amount of ozone U_{O_3} is (POZON is the concentration in ozone (Pa/Pa) taken from a standard atmosphere):

$$U^d_{O_3} = M \int_p^0 dU_{O_3}$$

for the downward transmission of the direct solar beam, and:

$$U^u_{O_3} = r \int_{p_s}^p dU_{O_3} + U^d_{O_3}(p_s)$$

for the upward transmission of the diffuse radiation with $r = 1.66$ the diffusivity factor and M (PSEC in SWU), the magnification factor (Rodgers 1967) used instead of μ_0 to account for the sphericity of the atmosphere at very small solar elevations:

$$M = \frac{35}{\sqrt{1224\,\mu_0^2 + 1}}. \tag{1.27}$$

To perform the spectral integration, it is convenient to discretize the solar spectral interval into subintervals in which the surface reflectance can be considered as constant. Since the main cause of the important spectral variation of the surface albedo is the sharp increase in the reflectivity of the vegetation in the near infrared and since water vapor does not absorb below 0.68 μm, the shortwave scheme considers two spectral intervals, one for the visible (0.2 - 0.68 μm, subroutine SW1S) containing a fraction of 0.441676 the incoming solar energy and second one for the near infrared (0.68 - 4.0 μm, subroutine SW2S) for the 0.558324 remaining part of the solar spectrum. This cut-off at 0.68 μm also makes the scheme more computationally efficient, in as much as the interactions between gaseous absorption (by water vapor and uniformly mixed gases) and scattering processes are accounted for only in the near-infrared interval.

1.3.3 Vertical integration

Considering an atmosphere where a fraction C_{tot} (as seen from the surface or the top of the atmosphere) is covered by clouds (the fraction C_{tot} depends on which cloud overlap assumption is assumed for the calculations), the final fluxes are given as

$$F^{\downarrow} = C_{tot}\, F^{\downarrow}_{cloudy} \;+\; (1 - C_{tot})\, F^{\downarrow}_{clear} \tag{1.28}$$

with a similar expression holding for the upward flux. Contrarily to the scheme of Geleyn and Hollingsworth (1979), the fluxes are not obtained through the solution of a system of linear equations in a matrix form. Rather, assuming an atmosphere divided into N homogeneous layers, the upward and downward fluxes at a given interface j are given by:

$$\begin{aligned} F^{\downarrow}(j) &= F_0 \prod_{k=j}^{N} T_b(k), \\ F^{\uparrow}(j) &= F^{\downarrow}(j)\, R_t(j-1), \end{aligned} \tag{1.29}$$

where $R_t(j)$ and $T_b(j)$ are the reflectance at the top and the transmittance at the bottom of the j^{th} layer. Computations of R_t's start at the surface and work upward, whereas those of T_b's start at the top of the atmosphere and work downward. R_t and T_b account for the presence of cloud in the layer:

$$R_t \;=\; C_j\, R_{cdy} + (1 - C_j)\, R_{clr},$$

$$T_b \;=\; C_j\, T_{cdy} + (1 - C_j)\, T_{clr}. \tag{1.30}$$

The subscripts $_{clr}$ and $_{cdy}$ respectively refer to the clear-sky and cloudy fractions of the layer with C_j the cloud fraction of the layer j.

Cloudy fraction of the layers

$R_{t_{cdy}}$ and $T_{b_{cdy}}$ are the reflectance at the top and transmittance at the bottom of the cloudy fraction of the layer calculated with the Delta-Eddington approximation. Given δ_c (PTAU) and δ_a (PAER), the optical thicknesses for the cloud and the aerosol, g_c (PCG) and g_a (CGA) the cloud and aerosol asymmetry factors, $R_{t_{cdy}}$ and $T_{b_{cdy}}$ are calculated as functions of:

- the total optical thickness of the layer δ^*:

$$\delta^* = \delta_c + \delta_a$$

- the total single scattering albedo:

$$\omega^* = \frac{\omega_c\, \delta_c + \omega_a\, \delta_a}{\delta_c + \delta_a} \tag{1.31}$$

- the total asymmetry factor:

$$g^* = \frac{\omega_c\, \delta_c\, g_c + \omega_a\, \delta_a\, g_a}{\omega_c\, \delta_c + \omega_a\, \delta_a}$$

of the reflectance $R_{\_}$ of the underlying medium (surface or layers below the j^{th} interface) and of the effective solar zenith angle $\mu_e(j)$ which accounts for the decrease of the direct solar beam and the corresponding increase of the diffuse part of the downward radiation by the upper scattering layers (see further).
The scheme follows the Eddington approximation, first proposed by Shettle and Weiman (1970), then modified by Joseph et al. (1976) to account more accurately for the large fraction of radiation directly transmitted in the forward scattering peak in case of highly asymmetric phase functions. Eddington's approximation assumes that, in a scattering medium of optical thickness δ^*, of single scattering albedo ω, and of asymmetry factor g, the radiance L entering (1.20) can be written as:

$$L(\delta, \mu) = L_0(\delta) + \mu\, L_1(\delta). \tag{1.32}$$

In that case, when the phase function is expanded as a series of associated Legendre functions, all terms of order greater than one vanish when (1.20) is integrated over μ and ϕ. The phase function is therefore given by

$$P(\theta) = 1 + \beta_1(\theta)\, \cos\theta,$$

where θ is the angle between incident and scattered radiances. The integral in (1.20) thus becomes

$$\int_0^{2\pi}\int_{-1}^{+1} P(\mu,\phi,\mu',\phi')\,L(\mu',\phi')\,d\mu'\,d\phi' = 4\pi\,(L_0+\pi L_1) \tag{1.33}$$

where g, the asymmetry factor identifies as

$$g = \frac{\beta}{3} = \frac{1}{2}\int_{-1}^{+1} P(\theta)\,\cos\theta\,d(\cos\theta).$$

Using (1.33) in (1.20) after integrating over μ and dividing by 2π, we get

$$\mu\,\frac{d(L_0+\mu L_1)}{d\delta} = -(L_0+\mu L_1) + \omega\,(L_0+g\mu L_1) + \frac{1}{4}\omega\,F_0\,\exp(\frac{-\delta}{\mu_0})\,(1+3g\mu_0\,\mu). \tag{1.34}$$

We obtain a pair of equations for L_0 and L_1 by integrating (1.34) over μ:

$$\frac{d(L_0)}{d\delta} = -3(1-\omega)\,L_0 + \frac{3}{4}\omega\,F_0\,\exp(\frac{-\delta}{\mu_0}), \tag{1.35}$$

$$\frac{d(L_1)}{d\delta} = -(1-\omega g)\,L_1 + \frac{3}{4}\omega\,g\,\mu_0\,F_0\,\exp(\frac{-\delta}{\mu_0}). \tag{1.36}$$

For the cloudy layer assumed non-conservative ($\omega < 1$), the solutions to (1.35) and (1.36) are, in the range $0 \le \delta \le \delta^*$:

$$\begin{aligned} L_0(\delta) &= C_1\,\exp(-k\delta) + C_2\,\exp(+k\delta) - \alpha\,\exp(\frac{-\delta}{\mu_0}),\\ L_1(\delta) &= p(C_1\,\exp(-k\delta) - C_2\,\exp(+k\delta)) - \beta\,\exp(\frac{-\delta}{\mu_0}), \end{aligned} \tag{1.37}$$

where

$$\begin{aligned} k &= \left[3\,(1-\omega)\,(1-\omega g)\right]^{\frac{1}{2}}\\ p &= \left[3\,(1-\omega)/(1-\omega g)\right]^{\frac{1}{2}}\\ \alpha &= 3\,\omega\,F_0\,\mu_0^2\,\frac{\left[1+g\,(1-\omega)\right]}{4\,(1-k^2\mu_0^2)}\\ \beta &= 3\,\omega\,F_0\,\mu_0\,\frac{\left[1+3\,g\,(1-\omega)\,\mu_0^2\right]}{4\,(1-k^2\mu_0^2)}. \end{aligned}$$

The two boundary conditions allow to solve the system for C_1 and C_2. First, the downward directed diffuse flux at the top of the layer is zero

$$F^{\downarrow}(0) = \left[L_0(0) + \frac{2}{3}L_1(0)\right] = 0,$$

which translates into

$$(1 + \frac{2p}{3})\, C_1 + (1 - \frac{2p}{3})\, C_2 = \alpha + \frac{2\beta}{3}. \tag{1.38}$$

For the second condition, one assumes that the upward directed flux at the bottom of the layer is equal to the product of the downward directed diffuse and direct fluxes by the corresponding diffuse and direct reflectances (R_d and $R_{\_}$, respectively) of the underlying medium

$$F^{\uparrow}(\delta^*) = \left[L_0(\delta^*) - \frac{2}{3}\, L_1(\delta^*)\right] = R_{\_}\left[L_0(\delta^*) + \frac{2}{3}\, L_1(\delta^*)\right] + R_d\, \mu_0\, F_0\, \exp(\frac{-\delta^*}{\mu_0}),$$

which translates into

$$\begin{aligned}(1 - R_{\_} - \frac{2p}{3}\,(1 + R_{\_}))\, C_1\, \exp(-k\,\delta^*) + (1 - R_{\_} + \frac{2p}{3}\,(1 + R_{\_}))\, C_2 \quad \exp(+k\,\delta^*) \\ = ((1 - R_{\_})\alpha - \frac{2}{3}\,(1 + R_{\_})\beta + R_d\,\mu_0\,F_0) \quad \exp(\tfrac{-\delta^*}{\mu_0})\end{aligned} \tag{1.39}$$

In the Delta-Eddington approximation, the phase function is approximated by a Dirac delta function (forward scatter peak) and a two-term expansion of the phase function

$$P(\theta) = 2f\,(1 - \cos\theta) + (1 - f)\,(1 + 3g'\,\cos\theta),$$

where f is the fractional scattering into the forward peak and g' the asymmetry factor of the truncated phase function. As shown by Joseph et al. (1976), these parameters are:

$$\begin{aligned} f &= \frac{\omega_c\,\delta_c\,g_c^2 + \omega_a\,\delta_a\,g_a^2}{\omega_c\,\delta_c + \omega_a\,\delta_a} \\ g' &= \frac{g}{1+g}. \end{aligned} \tag{1.40}$$

The solution of the Eddington's equations remains the same provided that the total optical thickness, single scattering albedo and asymmetry factor entering (1.34)-(1.39) take their transformed values:

$$\begin{aligned} \delta' &= (1 - \omega f)\,\delta^*, \\ \omega' &= \frac{(1-f)\,\omega}{1 - \omega f}. \end{aligned} \tag{1.41}$$

Practically, the optical thickness, single scattering albedo, asymmetry factor, and solar zenith angle entering (1.38)-(1.41) are δ^*, ω^*, g^* and u_e defined in (1.31) and (1.47).

The effective solar zenith angle $\mu_e(j)$ is equal to:

$$\mu_e(j) = \left[\frac{(1 - C^{al}(j))}{\mu} + r\, C^{al}(j) \right]^{-1}, \tag{1.42}$$

with r is the diffusivity factor and is prescribed at 1.66, that corresponds to a zenith angle of 52.95°. The accuracy of this approximation in fact depends on the actual solar zenith angle, which implies that the fluxes cannot be determined at all the incoming solar zenith angles with the same accuracy. $C^{al}(j)$ is the cumulated scattering efficiency from the top of the atmosphere to the layer j:

$$C^{al}(j) = 1 - \prod_{i=j+1}^{N} (1 - CC(j))$$

with $CC(j)$ is the direct solar light scattering efficiency defined in each layer of the cloud column as:

$$CC(j) = C'_j \left(1 - \exp\left[-\frac{\delta_c^{*'}(j)}{\mu}\right]\right) + (1 - C'_j) \left(1 - \exp\left[-\frac{\delta_a^{*'}(j)}{\mu}\right]\right) \tag{1.43}$$

with C'_j the cloud sub-fraction of the layer j defined with respect to the column fraction C_{tot} as:

$$C'_j = C_j / C_{tot} \tag{1.44}$$

Clear-sky fraction of the layers

In the clear-sky fraction of the layers, the shortwave scheme accounts for scattering and absorption by molecules and aerosols. As optical thickness for both Rayleigh and aerosol scattering is small, $R_{clr}(j-1)$ and $T_{clr}(j)$ the reflectance at the top and transmittance at the bottom of the j^{th} layer can be calculated using respectively a first and a second-order expansion of the analytical solutions of the two-stream equations similar to that of Coakley and Chylek (1975). For Rayleigh scattering (subroutine SW1S), the optical thickness, single scattering albedo and asymmetry factor are respectively δ_R, $\omega_R = 1$ and $g_R = 0$, so that

$$\begin{aligned} R_R &= \frac{\delta_R}{2\,\mu + \delta_R}, \\ T_R &= \frac{2\mu}{2\,\mu + \delta_R}. \end{aligned} \tag{1.45}$$

The optical thickness δ_R of an atmospheric layer is simply:

$$\delta_R = \delta_R^* \frac{(p(j) - p(j-1))}{p_{surf}},$$

where δ_R^* is the Rayleigh optical thickness of the whole atmosphere parameterized as a function of solar zenith angle (Deschamps et al. 1983):

$$\delta_R^* = \sum_{i=0}^{5} a_i \, \mu_0^{i-1}.$$

For aerosol scattering and absorption, the optical thickness, single scattering albedo and asymmetry factor are respectively δ_a, ω_a (with $1 - \omega_a \ll 1$) and g_a so that:

$$\begin{aligned} den &= 1 + (1 - \omega_a + back(\mu_e)\,\omega_a)\,\frac{\delta_a}{\mu_e} + (1 - \omega_a)\,(1 - \omega_a + 2\,back(\mu_e)\,\omega_a)\,\frac{{\delta_a}^2}{{\mu_e}^2} \\ R(\mu_e) &= \frac{back(\mu_e)\,\omega_a\,\delta_a/\mu_e}{den} \\ T(\mu_e) &= \frac{1}{den} \end{aligned} \tag{1.46}$$

where $back(\mu_e) = (2 - 3\mu_e g_a)/4$ is the backscattering factor and $\mu_e(j)$ is the effective solar zenith angle:

$$\mu_e(j) = \left[\frac{(1 - C^{al}(j))}{\mu} + r\,C^{al}(j)\right]^{-1}, \tag{1.47}$$

with r is the diffusivity factor and is prescribed at 1.66, that corresponds to a zenith angle of 52.95°. The accuracy of this approximation in fact depends on the actual solar zenith angle, which implies that the fluxes cannot be determined at all the incoming solar zenith angles with the same accuracy. $C^{al}(j)$ is the cumulated scattering efficiency from the top of the atmosphere to the layer j:

$$C^{al}(j) = 1 - \prod_{i=j+1}^{N} (1 - CC(j))$$

with $CC(j)$ is the direct solar light scattering efficiency defined in each layer of the cloud column as:

$$CC(j) = 1 - \exp\left[-\frac{\delta_a^{*'}(j)}{\mu}\right] \tag{1.48}$$

Practically, R_{clr} and T_{clr} are computed using (1.46) and the combined effect of aerosol and Rayleigh scattering comes from using modified parameters corresponding to the addition of the two scatters with provision for the highly asymmetric aerosol phase function through a Delta-Eddington approximation of the forward scattering peak (as in (1.40)-(1.41)):

$$\begin{aligned} f &= \frac{\delta_R + \omega_a\,\delta_a\,g_a^2}{\delta_R + \omega_a\,\delta_a} \\ g^{'} &= \frac{g}{1+g}. \\ \delta^{'} &= (1 - \omega f)\,\delta, \\ \omega^{'} &= \frac{(1-f)\,\omega}{1 - \omega f}. \end{aligned} \tag{1.49}$$

with:

$$\begin{aligned} \delta &= \delta_R + \delta_a \\ g &= \frac{\delta_R + \omega_a \, \delta_a \, g_a}{\delta_R + \omega_a \, \delta_a} \\ \omega &= \frac{\delta_R + \omega_a \, \delta_a}{\delta_R + \delta_a} \end{aligned} \tag{1.50}$$

As for their cloudy counterparts, R_{clr} and T_{clr} must account for the multiple reflections due to the layers underneath:

$$\begin{aligned} R_{clr} &= R(\mu_e) + \frac{T(\mu_e)}{1 - R^* \, R_-} \, R_-, \\ T_{clr} &= \frac{T(\mu_e)}{1 - R^* \, R_-}, \end{aligned} \tag{1.51}$$

with $R^* = R(1/r)$, $T^* = T(1/r)$, $R_- = R_t(j-1)$ is the reflectance of the underlying medium and r is the diffusivity factor.
Since interactions between molecular absorption and Rayleigh and aerosol scattering are negligible, the radiative fluxes in a clear-sky atmosphere are simply those calculated from (1.29) and (1.51) attenuated by the gaseous transmissions (1.26) (subroutine SW2S).

These calculations are practically done twice, the first time for the clear-sky fraction $(1 - C_{tot})$ of the atmospheric column with μ_e computed using (1.48), simply modified for the effect of Rayleigh and aerosol scattering (subroutine SWCLR), the second time for the clear-sky fraction $(1 - C'_j)$ of each individual layer within the fraction C_{tot} of the atmospheric column with μ_e computed using (1.43) (subroutine SWR).

1.3.4 Multiple reflections between layers

To deal properly with the multiple reflections between the surface and the cloud layers, it should be necessary to separate the contribution of each individual reflecting surface to the layer reflectances and transmittances inasmuch as each such surface gives rise to a particular distribution of absorber amount. In case of an atmosphere including N cloud layers, the reflected light above the highest cloud consists of photons directly reflected by the highest cloud without interaction with the underlying atmosphere and of photons that have passed through this cloud layer and undergone at least one reflection on the underlying atmosphere. In fact, (1.22) should be written

$$F = \sum_{l=0}^{N} F_{cl} \int_0^\infty p_l(U) \, t_{\Delta\nu}(U) \, d\nu, \tag{1.52}$$

where F_{cl} and $p_l(U)$ are the conservative fluxes and the distributions of absorber amount corresponding to the different reflecting surfaces.
Fouquart and Bonnel (1980) have shown that a very good approximation to this problem is obtained by evaluating the reflectance and transmittance of each layer (using (1.39) and (1.51)),

assuming successively a non-reflecting underlying medium ($R_{\_} = 0$), then a reflecting underlying medium ($R_{\_} \neq 0$). First calculations provide the contribution to reflectance and transmittance of those photons interacting only with the layer into consideration, whereas the second ones give the contribution of the photons with interactions also outside the layer itself.
From these two sets of layer reflectances and transmittances (R_{t_0}, T_{t_0}) and ($R_{t_\neq}, T_{t_\neq}$) respectively, effective absorber amounts to be applied to computing the transmission functions for upward and downward fluxes are then derived using (1.24) and starting from the surface and working the formulas upward:

$$\begin{aligned} U^{\downarrow}_{e_0} &= \frac{1}{k_e} \ln(\frac{T_{b_0}}{T_{b_c}}), \\ U^{\downarrow}_{e_\neq} &= \frac{1}{k_e} \ln(\frac{T_{b_\neq}}{T_{b_c}}), \\ U^{\uparrow}_{e_0} &= \frac{1}{k_e} \ln(\frac{R_{t_0}}{R_{t_c}}), \\ U^{\uparrow}_{e_\neq} &= \frac{1}{k_e} \ln(\frac{R_{t_\neq}}{R_{t_c}}), \end{aligned} \tag{1.53}$$

where R_{t_c} and T_{b_c} are the layer reflectance and transmittance corresponding to a conservative scattering medium. Finally the upward and downward fluxes are obtained as:

$$F^{\uparrow}(j) = F_0 \left[R_{t_0}\, t_{\Delta\nu}(U^{\uparrow}_{e_0}) + (R_{t_\neq} - R_{t_0})\, t_{\Delta\nu} U^{\uparrow}_{e_\neq}) \right] \tag{1.54}$$

$$F^{\downarrow}(j) = F_0 \left[T_{b_0}\, t_{\Delta\nu}(U^{\downarrow}_{e_0}) + (T_{b_\neq} - T_{b_0})\, t_{\Delta\nu} U^{\downarrow}_{e_\neq}) \right] \tag{1.55}$$

1.3.5 Cloud shortwave optical properties

As seen in section (1.3.3), the cloud radiative properties depend on three different parameters: the optical thickness δ_c, the asymmetry factor g_c and the single scattering albedo ω_c. Presently the cloud optical properties are derived from Fouquart (1987) for the cloud water droplets and from Ebert and Curry (1992) for the cloud ice crystals. Alternate sets of cloud optical properties are also available, see subsection 1.4.5. In case of mixed phase cloud, one has to consider the combination formula:

$$\begin{aligned} \delta_c &= \delta_L + \delta_I \\ \omega_c &= (\omega_L\, \delta_L + \omega_I\, \delta_I)/\delta_c \\ g_c &= (\omega_L\, \delta_L\, g_L + \omega_I\, \delta_I\, g_I)/(\omega_L\, \delta_L + \omega_I\, \delta_I) \end{aligned} \tag{1.56}$$

Warm cloud case

By default, the option **Fouquart** is used for the computation of the warm cloud optical properties. In that case, the optical thickness δ_L depends on the cloud liquid water path u_{LWP} and on the mean effective radius of the cloud droplets size distribution r_e (Fouquart 1987):

$$\delta_L = (a + b/r_e)u_{LWP}$$

The liquid water path u_{LWP} is defined by $\int_{\Delta z} \rho r_c dz = \int_{\Delta p} r_c/g dp$. r_e can be computed either through Martin 1994 parameterization (for the one-moment cloud schemes) or directly as the ratio of the 3$^{\text{rd}}$ and the 2$^{\text{nd}}$ moments of the cloud droplets distribution (for the two-moment cloud schemes).
The cloud single scattering albedo is computed in each of the six shortwave bands as a function of the cloud droplet chemical composition and diameter. In a first approximation, the cloud droplet composition can be retrived assuming that the cloud droplets form from the aerosols given by the global climatologies (Tegen 1997 or Tanre 1984).
The global climatologies supply the extinction coefficient for 6 aerosol classes (Continental, Maritime, Desert, Urban, Volcanic and Stratospherical background). Each of these classes can be decomposed in five elementary aerosol types: dust, water soluble compounds, soot, sea-salt, sulphates (d'Almeida et al. 1991). Using the percentage of elementary aerosol types entering in one class and their normalized extinction coefficients (for 1 particle/cm^3) (Table 4.3 of d'Almeida et al. 1991), one can deduce the normalized extinction coefficients of the 6 aforementioned classes. The number concentration in each class and the total number concentration (cm^{-3}) of the elementary types can be retrieved from the total number of aerosols entering in one class (derived as the ratio between the total extinction and the normalised extinction for 1 particle for that class).
The volume fraction of one aerosol type into the cloud droplet is then computed as the ratio of the volume of all the particles of that type corresponding to one droplet and the droplet's volume: $v_f^i = (N_i/N_c) \cdot (R_i/R_e)^3$. N_i and R_i are the number concentration and a typical value of the mean radius of the aerosol of type i, N_c and R_e are the number concentration and the effective radius of the cloud droplets.

Table 1.3: Percentage of the aerosol types in the ECMWF classes (d'Almeida et al 1991)

ECMWF classes	dust	water soluble	soot	sea salts	sulfates
marine	-	-	-	65 %	35 %
continental	$2.27 \cdot 10^{-4}$ %	93.877 %	6.123 %	-	-
urban	$1.67 \cdot 10^{-5}$ %	59.45 %	40.55 %	-	-
desert	100 %	-	-	-	-
volcanic	40 %	-	40 %	-	20 %
stratospherical background	100 %	-	-	-	-

Ice cloud case

For the optical properties of ice clouds, we have

$$\begin{aligned} \delta_I &= \mathrm{IWP}\,(a_I + b_I/r_e) \\ \omega_I &= c_I + d_I\, r_e \\ g_I &= c_I + f_I\, r_e \end{aligned} \tag{1.57}$$

By default, the coefficients have been derived from Ebert and Curry (1992), and r_e is parameterized (see subsection 1.4.5). Alternate sets of cloud optical properties are also available.

1.4 Input to the radiation scheme

1.4.1 Pressure, temperature, humidity, cloud water and ice fields

They are directly provided by the corresponding prognostic variables of Meso-NH. In order to allow for better fluxes in the stratosphere and above, the vertical profiles of temperature and humidity are completed aloft by using reference atmospheres (Mc Clatchey et al. 1972). One among the five different standard atmospheres:

- tropical
- mid-latitude in summer and winter
- polar in summer and winter

is selected to extend the relevant fields up to 50 km high.

The TSRAD radiative surface temperature calculated from surface scheme is used for lower boundary conditions. Presently, no radiative effects of rain water, graupel and snow are considered.

1.4.2 Ground albedo and emissivity

The SW radiation scheme requires albedo for each spectral band (6 bands in the most recent version, 0.185-0.25-0.44-0.69-1.19-2.38-4.00 μm). In Meso-NH, only visible and near infra-red bands are differentiated: the albedo components entering effectively in the SW scheme are then defined according to these two main bands. The SW radiation code requires also a distinction between "direct" albedo (i.e. for direct radiation) and diffuse albedo. Such a distinction does not exist in Meso-NH so a single albedo value is used for diffuse and direct fluxes. The LW surface emissivity directly corresponds to the value calculated in Meso-NH.

1.4.3 Aerosols

Aerosol effects on SW and LW radiations are now taken into account provided that CAER is set to a value different of 'NONE'. Presently, six classes of aerosols are considered in the radiation scheme: The continental class including organic and sulfate-type aerosols, the sea class (i.e. sea-salt aerosols), the urban class (mainly black-carbon type aerosols), the desert class (soil dust type aerosols), the volcanic class and a stratospheric background class. Each one of these class are characterized by specific optical properties (optical depth, single scattering albedo, asymmetry factor,

...). The optical depth is directly linked to the effective concentration of aerosol and therefore must be spatially and temporally specified. Presently the spatial and temporal distributions of optical thickness are defined in the model initialisation step (subroutine INI_RADIATIONS).

- The 'TANR' option directly refers to Tanré et al. (1984) climatological distributions. Total optical thickness (ground to top of the atmosphere TOA) associated to the land, sea, desert, and continental class are horizontally distributed on a T5 grid. This spectral distribution has been redefined on a regular "lat-lon" grid by the Arpege-climat team and imported in Meso-NH. The horizontal fields are interpolated on the Meso-NH domain (INI_HOR_AERCLIM routine). Then the total optical thickness are associated to typical vertical distribution (based on pressure levels) depending on the aerosol class, this leading to the 3D aerosol fields. Note that the resulting fields are very smooth, and no temporal evolution is considered here.

- The 'TEGE' option refers to the Tegen et al. (1997) climatological distribution. The total optical thickness fields are monthly provided at a $(4^\circ \times 5^\circ)$ resolution. Time and spatial interpolation on the Meso-NH domain are made in the INI_HOR_AERCLIM routine. The same vertical profiles as in TANR case are considered.

- The 'SURF' option provides an alternative method compared to climatical distributions. In this case the total optical thickness is directly linked to the nature and the percent of ground covers in the grid cell (sea, desert, urban, continental). This option allows to better represent localized sources like urban area at fine resolution. The considered vertical distribution are the same than in TANR and TEGE cases. Note that the user can easily modify the maximum total optical thickness associated to the aerosol classes in the INI_RADIATIONS routine.

Remark: The stratospheric background represents a horizontally homogenous field defined by default in all cases.
The optical depth associated to the volcanic class are forced to an "epsilon" value in INI_RADIATIONS step but, this can be modified easily if necessary. A historical climatology for volcanic aerosol is also available in the routines called by the TEGE option. This option is not activated.
It is always possible to define the aerosol fields from user's own data base at the INI_RADIATIONS step.

1.4.4 Radiatively active compounds

The concentrations of trace gases other than ozone are supposed to be constant spatially and temporally with the following characteristic values:

- CO_2: 360 ppm
- CH_4: 1.72 ppm
- N_2O: 0.31 ppm
- $CFC11$: 280 ppt
- $CFC12$: 484 ppt

- $O3$: The ozone field is defined from the Fortuin and Langematz (1994) climatology. The concentration depends on height, latitude and month. The 3-D climatology is loaded and interpolated on the Meso-NH domain in the INI_RADIATIONS step. The ozone field can be visualised running DIAG (see DIAG documentation).

1.4.5 Cloud optical properties

For the SW radiation, the cloud radiative properties depend on three different parameters: the optical thickness, the asymmetry factor and the single scattering albedo of particles. For LW the cloud properties (linked to emissivity and spectral optical thickness) depends of the scheme used (MORC or RRTM). All these properties are defined for water and ice particles in the ecmwf_radiation_vers2 routine. They depend on liquid (or ice) water path or on the effective radius of the particles. This characteristic parameter can be calculated by different ways according to CEFRADL and CEFRADI (ice particles) keywords:

Cloud liquid particles

- CEFRADL='PRES': the cloud water effective radius is calculated as a function of pressure (old parameterisation).
- CEFRADL='OCLN': the cloud effective radius is equal to 10 μm over land and equal to 13 μm over the ocean.
- CEFRADL='MART': parameterisation based on Martin et al. (1994).
- CEFRADL='C2R2': the effective radius of cloud particle is calculated from the 2-moment microphysical scheme C2R2 when explicitly called (see the microphyical scheme section for the nomenclature).

$$r_e = 0.5\frac{\int_0^{+\infty} D^3 n(D) dD}{\int_0^{+\infty} D^2 n(D) dD} 0.5 \frac{\Gamma(\nu+3/\alpha)^{2/3}}{\Gamma(\nu+2/\alpha)} \left(\frac{\Gamma(\nu)}{\pi/6\rho_w}\frac{\rho\, r_c}{N_c}\right)^{1/3}$$

Cloud ice particles

- CEFRADI='FX40': the ice particle effective radius is fixed at 40 μm. The user can eventually change this value by modifying the ecmwf_radiation_vers2 routine.
- CEFRADI='LIOU': ice particle effective radius calculated as f(T) from Liou and Ou (1994).
- CEFRADI='SURI': Ice effective radius calculated as a function of temperature and ice content from Sun and Rikus (1999).
- CEFRADI='C3R5': the effective radius of ice particle is calculated from C3R5 prognostic particle concentrations. Of course it works only when C3R5 microphysical scheme is activated (not yet available).

Several options are also possible to define the optical properties from the primary parameters:

SW radiation

Cloud water optical properties depend on COPWSW:

- COPWSW ='SLIN', refers to Slingo (1989).
- COPWSW ='FOUQ', refers to Fouquart (1987).
- COPWSW ='MALA', refers to Malavelle (2007): Optical thickness of Savijarvi (1997), asymetry factor of Fouquart (1991) and single scaterring albedo of Slingo (1989). Good compromise for the C2R2 and KHKO scheme in regard on the size distribution hypothesis

Ice water optical properties depend on COPISW:

- COPISW =' FULI', refers to Fu and Liou (1993).
- COPISW =' EBCU', refers to Ebert and Cury (1992).
- COPISW =' FU96', refers to Fu (1996).

MORC LW radiation

Cloud water optical properties depend on COPWLW:

- COPWLW='SMSH', refers to Smith and Shi (1992).
- COPWLW='SAVI', refers to Savijarvi and Raisanen (1997).
- COPWLW='MALA', refers to Malavelle (2008): parameterization of the optical thickness of the cloud droplets and rain drops adapted to the size distribution hypothesis used in the C2R2 and KHKO scheme.

Ice water optical properties depend on COPILW:

- COPILW='EBCU', refers to Ebert and Cury (1992).
- COPILW='SMSH', refers to Smith and Shi (1992).
- COPILW='FULI', refers to Fu and Liou (1993).
- COPILW='FU98', refers to Fu et al. (1998).

RRTM LW radiation

Cloud water optical properties depend on COPWLW:

- COPWLW='SMSH', refers to Smith and Shi (1992).
- COPWLW='SAVI', refers to Savijarvi and Raisanen (1997).
- COPWLW='LILI', refers to Lindner and Li (2000).

Ice water optical properties depend on COPILW

- COPILW='EBCU', refers to Ebert and Cury (1992).
- COPILW='FULI', refers to Fu and Liou (1993).
- COPILW='FU98', refers to Fu et al. (1998).

Note: The resulting cloud optical properties as well as effective radius, liquid and ice water path can be visualized, running DIAG program (see DIAG documentation).

1.4.6 Cloud inhomogenity factor and cloud overlap assumption

In the initial ECMWF radiation code, an empirical cloud factor XFUDG is introduced to account for cloud subgrid inhomogenity in large cells following Tiedke (1996). This factor weights the above defined optical properties and is initially set to 0.7. But it has been resized to 1 by default for Meso-NH applications, assuming that grid cell are smaller than in ECMWF model. However, as Meso-NH can be used on a wide range of resolution the value of XFUDG can be fixed by namelist.

The cloud overlap assumption is used for the determination of C_{tot} (see the SW documentation) and is important for the determination of radiation in cloudy columns when the subgrid condensation scheme is actived. It is determined by the NOVLP variable: NOVLP=5 means "random overlap", NOVLP=6 means "maximum-random overlap " and NOVLP=7 means "maximum overlap". By default NOVLP is set to 6 in the INI_RADCONF routine except if the Morcrette longwave radiation scheme is used. In this case, NOVLP is set to 5.

1.4.7 Solar astronomy

To run the shortwave radiative computations it is necessary to feed the code with the time varying solar zenithal and azimuthal angles and the daily solar constant, all derived by analytical formulae of astronomy (Paltridge and Platt 1976). For instance, the daily solar constant S_{sun}, the solar declination angle δ_{sun}, the cosine of the solar zenithal angle μ and the azimuthal solar angle β are given by:

$$\begin{aligned} S_{sun} &= S_0(1.000110 + 0.034221\cos(d_r) + 0.001280\sin(d_r) \\ &\quad + 0.000719\cos(2d_r) + 0.000077\sin(2d_r)), \qquad (1.58) \\ \delta_{sun} &= 0.006918 - 0.399912\cos(d_r) + 0.070257\sin(d_r) \\ &\quad - 0.006758\cos(2d_r) + 0.000907\sin(2d_r) \\ &\quad - 0.002697\cos(3d_r) + 0.001480\sin(3d_r), \qquad (1.59) \\ \mu &= \cos(\phi)\cos(\delta_{sun})\cos(h_r) + \sin(\phi)\sin(\delta_{sun}), \qquad (1.60) \\ \beta &= \sin^{-1}\left(\frac{\cos(\delta_{sun})\sin(h_r)}{\sin(arcos(\mu))}\right), \qquad (1.61) \end{aligned}$$

respectively where $S_0 = 1370$ W/m^2, ϕ is the latitude, $d_r = 2\pi n_{day}/365$ (n_{day} is the day number) and $h_r = 2\pi hour/24$ with $hour$, the true hour of the day at the time t and at the longitude λ, defined by:

$$hour = \mod(24 + \mod(t/3600, 24), 24) + \lambda(12/\pi) - t^{cor}_{sideral}, \qquad (1.62)$$

with mod, the modulo arithmetic function and the sideral time correction $t^{cor}_{sideral}$ given by:

$$\begin{aligned} t^{cor}_{sideral} &= (7.67825\sin(1.00554 * n_{day} - 6.28306) + \\ &\quad 10.09176\sin(1.93946 * n_{day} + 23.35089))/60. \end{aligned} \tag{1.63}$$

All these calculations are performed in routine SUNPOS prior calling the radiation code.

1.5 Intermittent radiation call

Due to its relatively high cost, the radiation code can be unreasonably expensive if called at each model time step. Furthermore as the radiative time scales are significantly larger than the time step involved in the integration of a mesoscale model, it is recommended to refresh the radiative thermal tendency and downward surface fluxes at an adapted rate. To run even faster, some approximations of the radiative computations have been made available. The basic time step to call the radiation computation is `XDTRAD`. Il must be a multiple of the model time step `XTSTEP` and a default value is set to 900 s. Note that the radiative code operates on instantaneous fields but the angular position of the sun is calculated at the current time plus `XDTRAD`/2. Actually, three parameters can be set to enable partial radiative computations:

- LCLEAR_SKY when .TRUE. means that radiative computations over clear sky columns are made for the ensemble mean column only. This option is meaningful if the terrain is flat.
- XDTRAD_CLONLY is the time step of refreshment of the radiative fluxes and tendency for the cloudy columns and the "new" clear columns i.e. where the cloud have just disappeared. Choosing XDTRAD_CLONLY as a divider of XDTRAD allows a faster update of the radiative transfer through cloudy columns as they are known to be the most perturbating ones for the radiations.

1.6 References

Bohren, C. F., and D.R.Hauffman, 1993: Absorption and Scattering of Light by Small Particles, Wiley, New York.

Bonnel, B., Y. Fouquart, J.-C. Vanhoutte, C. Fravalo, and R. Rosset, 1983: Radiative properties of some African and mid-latitude stratocumulus clouds. *Beitr. Phys. Atmosph.*, **56**, 409-428.

Chuang, C. C., J. E. Penner, J. M. Prospero, K. E. Grant, G. H. Rau, and K. Kawamoto, 2002: Cloud susceptibility and the first aerosol indirect forcing: Sensitivity to black carbon and aerosol concentrations, *J. Geophys. Res.*, **107**, 4564.

Chylek, P., G. Lesins, G. Videen, J. G. D. Wong, R. G. Pinnick, D. Ngo, and J. D. Klett, 1996: Black carbon and absorption of solar radiation by clouds, *J. Geophys. Res.*, **101**, 23365-23372.

Coakley, J. A., Jr., and P. Chylek, 1975: The two-stream approximation in radiation transfer: Including the angle of the incident radiation. *J. Atmos. Sci.*, **32**, 409-418.

Clough, S. A. and M. I. Iacono, 1995: Line-by-line calculation of atmospheric fluxes and cooling rates, 2. Application to carbon dioxide, ozone, methane, nitrous oxide and the halocarbons. *J. Geophys. Res.*, **100D**, 16519-16536

Clough, S. A., F.X. Kneizys, and R. W. Davies, 1989: Line shape and the water vapor continuum. *Atmos. Res.*, **23**, 229-241.

Clough, S. A., M. J. Iacono, and J.-L. Moncet, 1992: Line-by-line calculations of atmospheric fluxes and cooling rates: Application to water vapor. *J. Geophys. Res.*, **97D**, 15761-15786.

d'Almeida, G. A., P. Koepke, and E. P. Shettle, 1991: Atmospheric aerosols: Global climatology and Radiative characteristics, A. Deepak, Hampton, Va.

Dandin, Ph., 1995: The radiation code in ARPEGE-Climat AGCM. *Technical documentation*, in preparation.

Deschamps, P.-Y., M. Herman, and D. Tanré, 1983: Modélisation du rayonnement solaire réfléchi par l'atmosphère et la Terre, entre 0,35 et 4 microns. *Rapport ESA 4393/80/F/DD(SC)*, 156 pp.

Ebert, E. E., and J. A. Curry, 1992: A parameterization of ice cloud optical properties for climate models. *J. Geophys. Res.*, **97D**, 3831-3836.

Ebert, E. E. and Curry, J. A., 1993: An intermediate one-dimensional thermodynamic sea ice model for investigating ice-atmosphere interactions. *J. Geophys. Res.*, **98C**, 10 085-10 109.

ECMWF, 1989: Physical Parametrization, ECMWF Forecast Model. *Research Manual RM-3*, 3rd ed.

Elsasser, W. M., 1942: Heat Transfer by infrared Radiation in the Atmosphere. *Harvard University Press*, 43 pp.

Fels, S. B., 1979: Simple strategies for inclusion of Voigt effects in infrared cooling rate calculations. *Appl. Optics*, **18**, 2634-2637.

Fortuin, J. P. F., and Langematz, U., 1994: An update on the global ozone climatology and on concurrent ozone and temperature trends. *Proceedings SPIE, Atmos. Sensing and Modeling*, **2311**, 207-216.

Fouquart, Y., 1974: Utilisation des approximants de Padé pour l'étude des largeurs équivalentes des raies formées en atmosphère diffusante. *J. Quant. Spectrosc. Radiat. Transfer*, **14**, 497-506.

Fouquart, Y., 1987: Radiative transfer in climate modeling. *NATO Advanced Study Institute on Physically-Based Modeling and Simulation of Climate and Climatic Changes*. Erice, Sicily, 11-23 May 1986. M.E. Schlesinger, Ed., 223-283.

Fouquart, Y., and B. Bonnel, 1980: Computations of solar heating of the earth's atmosphere: A new parametrization. *Beitr. Phys. Atmosph.*, **53**, 35-62.

Fu, Q. and K.-N. Liou, 1992: On the correlated k-distribution method for radiative transfer in non-homogeneous atmosphere. *J. Atmos. Sci.*, **49**, 2139-2156.

Fu, Q. A., 1996: An accurate parameterization of the solar radiative properties of cirrus clouds for climate models. *J. Climate*, **9**, 2058-2082.

Fu, Q., P. Yang, and W. B. Sun, 1998: An accurate parametrization of the infrared radiative properties of cyrrus clouds of climate models. *J. Climate*, **11**, 2223-2237.

Geleyn, J.-F., and A. Hollingsworth, 1979: An economical analytical method for the computation of the interaction between scattering and line absorption of radiation. *Beitr. Phys. Atmosph.*, **52**, 1-16.

Gregory, D., J.-J. Morcrette, C. Jakob, and A. C. M. Beljaars, and T. Stockdale, 2000: Revision of convection, radiation, and cloud schemes in the ECMWF integrated forecasting system. *Quart. J. Roy. Meteor. Soc.*, **126A**, 1685-1710.

Giorgetta, M. A. and Morcrette, J.-J., 1995: Voigt line approximation in the ECMWF radiation scheme. *Mon. Weather Rev.*, **123**, 3381-3383.

Joseph, J. H., W. J. Wiscombe, and J. A. Weinman, 1976: The Delta-Eddington approximation for radiative flux transfer. *J. Atmos. Sci.*, **33**, 2452-2459.

Kondratyev, J., 1969: *Radiations in the Atmosphere*. Academic Press.

Lacis, A. A., and V. Oinas, 1991: A description of the correlated k distribution method for modeling nongray gaseous absorption, thermal emission, and multiple scattering in vertically inhomogeneous atmospheres. *J. Geophys. Res.*, **96D**, 9027-9063.

Lindner, T.H., and J. Li, 2000: Parameterization of the optical properties for water clouds in the infrared. *J. Climate*, **13**, 1797-1805.

Liu, Q. and Schmetz, J., 1988: On the problem of an analytical solution to the diffusivity factor. *Beitr. Phys. Atmos.* **61** 23-29.

Martin, G. M., D. W. Johnson, and A. Spice, 1994: The measurement and parameterization of effective radius of droplets in warm stratocumulus. *J. Atmos. Sci.*, **51**, 1823-1842

Mlawer, E. J., S. J. Taubman, P. D. Brown, M. J. Iacono, and S. A. Clough, 1997: Radiative transfer for inhomogeneous atmospheres: RRTM, a validated correlated-k model for the longwave. *J. Geophys. Res.*, **102D**, 16 663-16 682.

Morcrette, J.-J., and Y. Fouquart, 1985: On systematic errors in parametrized calculations of longwave radiation transfer. *Quart. J. Roy. Meteor. Soc.*, **111**, 691-708.

Morcrette, J.-J., L. Smith, and Y. Fouquart, 1986: Pressure and temperature dependence of the absorption in longwave radiation parametrizations. *Beitr. Phys. Atmosph.*, **59**, 455-469.

Morcrette, J.-J., 1991: Radiation and cloud radiative properties in the ECMWF operational weather forecast model. *J. Geophys. Res.*, **96D**, 9121-9132.

Morcrette, J.-J., S.A. Clough, E.J. Mlawer, and M.J. Iacono, 1998: Impact of a validated radiative transfer scheme, RRTM, on the ECMWF model climate and 10-day forecasts. *ECMWF Technical Memo.*, **No. 252**.

Morcrette, J.-J., E. J. Mlawer, M. J. Iacono, and S. A. Clough, 2001: Impact of the radiation transfer scheme RRTM in the ECMWF forecasting system. *ECMWF Newsletter*, **91**, 2-9.

Paltridge, G. W. and C. M. R. Platt, 1976: *Radiative Processes in Meteorology and Climatology*. Elsevier.

Rodgers, C. D., and C. D. Walshaw, 1966: The computation of infrared cooling rate in planetary atmospheres. *Quart. J. Roy. Meteor. Soc.*, **92**, 67-92.

Rodgers, C. D., 1967: The radiative Heat Budget of the troposphere and lower stratosphere. *Report $N^0 12$*, A2, Planetary Circulation Project, Dept. of Meteorology, Mass. Instit. Technology, Cambridge, Mass., 99 pp.

Rothman, L. S., 1981: AFGL atmospheric absorption line parameters compilation: 1980 version. *Appl. Opt.*, **21**, 791-795.

Sandu, I., P. Tulet, and J.-L. Brenguier, 2005: Parameterization of the cloud droplet single scattering albedo based on aerosol chemical composition for LES modelling of boundary layer clouds. *Geophys. Res. Lett.*, **32**, L19814, doi:10.1029/2005GL023994.

Savijarvi, H. and P. Raisanen, 1997: Long-wave optical properties of water clouds and rain. *Tellus*, **50A**, 1-11

Shettle, E. P., and J. A. Weinman, 1970: The transfer of solar irradiance through inhomogeneous turbid atmospheres evaluated by Eddington's approximation. *J. Atmos. Sci.*, **27**, 1048-1055.

Slingo, A., 1989: A GCM parameterization for the shortwave radiative properties of water clouds. *J. Atmos. Sci.*, **46**, 1419-1427

Smith, E. A., and L. Shi, 1992: Surface forcing of the infrared cooling profile over the Tibetan plateau. Part I: Influence of relative longwave radiative heating at high altitude. *J. Atmos. Sci.*, **49**, 805-822.

Stephens, G. L., 1984: The parametrization of radiation for numerical weather prediction and climate models. *Mon. Wea. Rev.*, **112**, 826-867.

Stephens, G. L., 1979: Optical properties of eight water cloud types. *CSIRO, Div. Atmos. Phys.*, Technical Paper n°12.36, Australia.

Stephens, G. L., 1978: Radiative properties of extended water clouds. Part II. *J. Atmos. Sci.*, **35**, 2111-2132.

Sun, Z., and K. P. Shine, 1995: Parameterization of ice cloud radiative properties and its application to the potential climatic importance of mixed-phase clouds. *J. Climate*, **8**, 1874-1888.

Tanré, D., J.-F. Geleyn, and J. Slingo, 1984: First results of the introduction of an advanced aerosol-radiation interaction in the ECMWF low resolution global model. *Aerosols and their Climatic Effects*, H.E. Gerber and A. Deepak, Eds., A. Deepak Publishing, Hampton, Va., 133-177.

Tegen, I, P. Hoorigl, M. Chin, I. Fung, D. Jacob, and J. Penner, 1997: Contribution of different aerosol species to the global aerosol extinction optical thickness: Estimates from model results. *J. Geophys. Res.*, **102**, 23,895-23,915.

Tiedtke, M., 1996: An Extension of Cloud-Radiation Parameterization in the ECMWF Model: The Representation of Subgrid-Scale Variations of Optical Depth. *Mon. Wea. Rev.*, **124**, 745-750.

Washington, W.M., and D.L. Williamson, 1977: A description of the NCAR GCMs. *General Circulation Models of the Atmosphere*, J. Chang, Ed., Methods in Computational Physics, vol. 17, Academic Press, 111-172.

WMO-ICSU, 1984: Optical properties for the standard aerosols of the Radiation Commission, *WCP-55*, World Climate Program, Geneva, Switzerland.

Xu, K.-M., and D. A. Randall, 1995: Impact of interactive radiative transfer on the macroscopic behavior of cumulus ensembles. Part I: Radiation parameterization ans sensitivity tests. *J. Atmos. Sci.*, **52**, 785-799.

Chapter 2

Turbulence Scheme

Contents

2.1 Introduction

The Meso-NH model intends to emulate the capacities of various models, such as mesoscale meteorological models, cloud resolving models (CRM), and even Large Eddy Simulation (LES) models. One of the main differences between these models is the treatment of turbulence. In mesoscale

hydrostatic models, the turbulence scheme is usually quasi-1D (on the vertical), since the horizontal resolution cannot resolve large gradients. In CRM and LES, this is not the case anymore, and 3D schemes, able to see turbulence sources by shear in all three spatial dimensions, are to be used. The current turbulence scheme of Meso-NH is therefore a first step towards a unified approach. It takes its roots in the two schemes which were used in the Meso-NH group, namely the quasi 1D turbulence scheme of Bougeault and Lacarrère (1989) (BL89 in the following), which was used in Peridot and Salsa models, and the 3D scheme of Redelsperger et Sommeria (1981), (RS81 in the following), which was used in the CNRM cloud model.
The approach followed is very close to the RS81 derivation of the parameterization of the three-dimensional turbulent fluxes. The second-order moments equations are separated into isotropic and anisotropic parts, and the equations for the anisotropic parts are stationnarized. This leads to diagnostic expressions for the fluxes. On the other hand, the isotropic part reverts to a prognostic equation for the turbulence kinetic energy (TKE). In this derivation, the Coriolis effects, and the Earth curvature are neglected, as well as the third order moments in the anisotropic equations. A detailed derivation of the scheme and a discussion of present limitations is given by Cuxart (1997). Note that a parameterization of third order moments of heat fluxes for the dry convective boundary layer was recently implemented into Meso-NH. The reader is referred to Tomas and Masson (2006).
The scheme offers a choice of three closure methods (currently only two are implemented). These may be selected by the parameter HTURBLEN (see sections 4 and 5). It may be run in either of two "modes": 1DIM and 3DIM. In "1DIM" mode, the horizontal gradients are not considered. This is appropriate where the horizontal resolution is coarse, and saves computer resources. In "3DIM" mode, the full computations are performed.

2.2 Turbulent fluxes in a Cartesian frame

We will first present the formulation of the scheme in a Cartesian frame of reference (x, y, z). The above mentioned treatment of the anisotropic part of the second-order moment equations leads to the following diagnostic equations:

$$\overline{u_i'\theta'} = -\frac{2}{3}\frac{L}{C_s}e^{\frac{1}{2}}\frac{\partial\overline{\theta}}{\partial x_i}\phi_i, \tag{2.1}$$

$$\overline{u_i'r_v'} = -\frac{2}{3}\frac{L}{C_h}e^{\frac{1}{2}}\frac{\partial\overline{r_v}}{\partial x_i}\psi_i, \tag{2.2}$$

$$\overline{u_i'\,u_j'} = \frac{2}{3}\delta_{ij}\,e - \frac{4}{15}\frac{L}{C_m}e^{\frac{1}{2}}(\frac{\partial u_i}{\partial x_j}+\frac{\partial u_j}{\partial x_i}-\frac{2}{3}\delta_{ij}\frac{\partial u_m}{\partial x_m}), \tag{2.3}$$

$$\overline{\theta'r_v'} = C_2L^2(\frac{\partial\overline{\theta}}{\partial x_m}\frac{\partial\overline{r_v}}{\partial x_m})(\phi_m+\psi_m), \tag{2.4}$$

$$\overline{\theta'^2} = C_1L^2(\frac{\partial\overline{\theta}}{\partial x_m}\frac{\partial\overline{\theta}}{\partial x_m})\phi_m, \tag{2.5}$$

$$\overline{r_v'^2} = C_1L^2(\frac{\partial\overline{r_v}}{\partial x_m}\frac{\partial\overline{r_v}}{\partial x_m})\psi_m. \tag{2.6}$$

Note that the Einstein summation convention applies above to all m subscripts, even in the last three equations.

The quantity L is the eddy length scale. Its specification is discussed below. The quantity e is the kinetic energy of the turbulence.
Whenever necessary, the flux of potential virtual temperature may be retrieved from the fluxes of temperature and moisture using the two coefficients $E_\theta = \frac{\overline{\theta_v}}{\overline{\theta}}$, and $E_{moist} = 0.61\overline{\theta}$:

$$\overline{u_i'\theta_v'} = E_\theta \overline{u_i'\theta'} + E_{moist}\overline{u_i'r_v'} \tag{2.7}$$

These factors have different expressions in presence of clouds (see Chapter on the subgrid condensation schemes).
The numerical coefficients appearing in the above equations arise from the closures, and take the following values (after RS81):

$$\begin{aligned}
C_s &= 4. && (2.8)\\
C_h &= 4. && (2.9)\\
C_m &= 4. && (2.10)\\
C_1 &= \frac{2}{3}\frac{1}{C_s C_\theta} && (2.11)\\
C_2 &= \frac{2}{3}\frac{1}{C_s C_{q\theta}} && (2.12)\\
C_\theta &= 1.2 && (2.13)\\
C_{q\theta} &= 2.4 && (2.14)
\end{aligned}$$

Finally, the above equations use stability functions ϕ_i and ψ_i, to describe the enhancement or inhibition of turbulent transfers by stability effects. These functions have been defined by RS81 as:

$$\phi_i = \begin{cases} 1 & \text{for i=1,2} \\ 1 - \frac{(1+C_1R_{r1})(2C_2R_{\theta r3}^2+C_1R_{\theta 3}^2)\frac{1}{R_{\theta 1}}+C_1C_2(R_{\theta 3}^2-R_{r3}^2)}{1+(C_1+C_2)(R_{\theta 1}+R_{r1})+C_1(C_2(R_{\theta 1}^2+R_{r1}^2)+C_1R_{\theta 1}R_{r1})} & \text{for i=3} \end{cases} \tag{2.15}$$

$$\psi_i = \begin{cases} 1 & \text{for i=1,2} \\ 1 - \frac{(1+C_1R_{\theta 1})(2C_2R_{\theta r3}^2+C_1R_{r3}^2)\frac{1}{R_{r1}}+C_1C_2(R_{r3}^2-R_{\theta 3}^2)}{1+(C_1+C_2)(R_{\theta 1}+R_{r1})+C_1(C_2(R_{\theta 1}^2+R_{r1}^2)+C_1R_{\theta 1}R_{r1})} & \text{for i=3} \end{cases} \tag{2.16}$$

This uses the so-called Redelsperger (or Richardson) numbers

$$\begin{aligned}
R_{\theta 1} &= \frac{g}{\theta_{v\,ref}}\frac{L^2}{e}E_\theta\frac{\partial\overline{\theta}}{\partial x_3}, && (2.17)\\
R_{\theta 3} &= \frac{g}{\theta_{v\,ref}}\frac{L^2}{e}E_\theta(\frac{\partial\overline{\theta}}{\partial x_m}\frac{\partial\overline{\theta}}{\partial x_m})^{\frac{1}{2}}, && (2.18)\\
R_{r1} &= \frac{g}{\theta_{v\,ref}}\frac{L^2}{e}E_{moist}\frac{\partial\overline{r_v}}{\partial x_3}, && (2.19)\\
R_{r3} &= \frac{g}{\theta_{v\,ref}}\frac{L^2}{e}E_{moist}(\frac{\partial\overline{r_v}}{\partial x_m}\frac{\partial\overline{r_v}}{\partial x_m})^{\frac{1}{2}}, && (2.20)\\
R_{\theta r3}^2 &= (\frac{g}{\theta_{v\,ref}}\frac{L^2}{e})^2E_\theta\frac{\partial\overline{\theta}}{\partial x_m}E_{moist}\frac{\partial\overline{r_v}}{\partial x_m}. && (2.21)
\end{aligned}$$

2.3 Turbulence kinetic energy equation

We use the well known prognostic equation for the turbulence kinetic energy (TKE), expressed as

$$\begin{aligned}\frac{\partial e}{\partial t} &= -\frac{1}{\rho_{dref}}\frac{\partial}{\partial x_j}(\rho_{dref}e\overline{u_j}) - \overline{u_i'u_j'}\frac{\partial \overline{u_i}}{\partial x_j} + \frac{g}{\theta_{vref}}\overline{u_3'\theta_v'} \\ &\quad + \frac{1}{\rho_{dref}}\frac{\partial}{\partial x_j}(C_{2m}\rho_{dref}Le^{\frac{1}{2}}\frac{\partial e}{\partial x_j}) - C_\epsilon\frac{e^{\frac{3}{2}}}{L} \qquad (2.22)\end{aligned}$$

The source terms appearing in (2.22) are respectively the advection of TKE, the shear production, the buoyancy production, the diffusion, and the dissipation.
The additional numerical constants take the values (RS81)

$$C_{2m} = 0.2, \qquad (2.23)$$
$$C_\epsilon = 0.7. \qquad (2.24)$$

2.4 Closure by mixing length

There are currently two choices of mixing length formulations.

2.4.1 The grid-size

The grid size of the model is commonly used as the characteristic length scale of the sub-grid eddies. This is justified when the grid size falls into the inertial subrange of the turbulent flow. In Meso-NH, the formulation must take into account the possible anisotropy of the grid. For the standard 3D version of the model,

$$L = (d_{xx}.d_{yy}.d_{zz})^{1/3}. \qquad (2.25)$$

For the 2D version,

$$L = (d_{xx}.d_{zz})^{1/2}, \qquad (2.26)$$

and for the 1D, column version,

$$L = d_{zz}. \qquad (2.27)$$

L is further limited in all cases to be smaller than kz, k being the Karman constant 0.4.
To activate this option, the parameter HTURBLEN has to be given the value 'DELT'. This is recommended when the model has high resolution and when the grid is nearly isotropic. Even in this case however, the assumption that the grid size falls within the inertial subrange may be in error, due for instance to the effects of stable stratification. This is to some extent mitigated by the use of the stability functions ϕ_i and ψ_i.

2.4.2 Bougeault-Lacarrère mixing length

BL89 postulate that the mixing length at any level in the atmosphere can be related to the distance a parcel of air having the initial kinetic energy of the level, can travel upwards (l_{up}) and downwards

(l_{down}) before being stopped by buoyancy effects. These distances are defined by

$$\begin{aligned}
\int_z^{z+l_{up}} \frac{g}{\theta_{v\,ref}}(\theta(z)-\theta(z'))dz' &= -e(z), \\
\int_{z-l_{down}}^{z} \frac{g}{\theta_{v\,ref}}(\theta(z')-\theta(z))dz' &= -e(z), \qquad (2.28)\\
l_{down} &\leq z, \\
L &= \left[\frac{(l_{up})^{-2/3}+(l_{down})^{-2/3}}{2}\right]^{-3/2} \qquad (2.29)
\end{aligned}$$

where $e(z)$ is the turbulent kinetic energy at level z. This method allows the length scale at any level to be influenced not only by the stability at this level, but by the effect of remote stable zones, or the presence of the ground.
This formulation is recommended when the model is used in "meso-scale mode", with highly anisotropic grids. It assumes that all of turbulence is parameterized, and will for instance lead to underestimation of dissipation if used in the LES mode. To activate this option, set HTURBLEN='BL89'.
The code is based on a second order accuracy algorithm that provides better resolution in the stable layers. We will shortly describe the difference between the first and the second order approaches. In the computation of the BL length, when the residual TKE is not large enough to reach the next level of the model, an estimation of how far this particle can travel between the two levels must be given. This is very important for stably stratified layers. First of all, we will see how this length should behave analytically, and then compare to the first and second order approximations.

Value for stably stratified layers In that case, assuming the gradient of θ constant between two adjacent layers ($\alpha \equiv \frac{\partial\theta}{\partial z} = ct$),

$$\begin{aligned}
\theta(z)-\theta(z') &= \alpha(z-z') \qquad (2.30)\\
\int_{z_n}^{z_n+L} \beta\alpha(z-z')dz' &= -e(z) \qquad (2.31)
\end{aligned}$$

where $\beta = \frac{g}{\theta_0}$, z is the departing layer and z' the heights that the particle travels throughout. The integration gives

$$\begin{aligned}
\left[zz' - \frac{z'^2}{2}\right]_z^{z+L} &= \frac{-e(z)}{\alpha\beta} \qquad (2.32)\\
L &= \sqrt{\frac{2e(z)}{\alpha\beta}} \qquad (2.33)
\end{aligned}$$

First order development In a first order approach, the length (the proportion of the layer that the particle can travel) is estimated as

$$\begin{aligned}
e &= \int_{z_n}^{z_n+L} \beta\Delta\theta\delta z \qquad (2.34)\\
\Delta\theta &= \theta(z_{n+1})-\theta(z_n) \qquad (2.35)
\end{aligned}$$

and from here the following expression can be derived

$$L = \frac{e}{\beta \Delta\theta} \tag{2.36}$$

which do not fit the analytical expression.

Second order development For a second order approach, the following relation is taken

$$\theta(z') = \theta(z_n) + \frac{\partial\theta}{\partial z}(z' - z_n) \tag{2.37}$$

Then, for the jump from the last reached level (with $E_p(z, z_n)$ energy wasted, and $e(z) - E_p(z, z_n)$ as energy available to rise the particle against negative buoyancy)

$$\begin{aligned} e(z) - E_p(z, z_n) &= \int_{z_n}^{z_n+L} \beta(\theta(z') - \theta(z))dz' \\ &\approx \int_{z_n}^{z_n+L} \beta\left[\theta(z_n) + \frac{\theta(z_{n+1}) - \theta(z_n)}{z_{n+1} - z_n}(z' - z_n) - \theta(z)\right] dz' \\ &= [\beta\theta(z_n)z']_{z_n}^{z_n+L} + \left[\beta\frac{\theta(z_{n+1}) - \theta(z_n)}{z_{n+1} - z_n}(\frac{z'^2}{2} - z_n z')\right]_{z_n}^{z_n+L} \\ &\quad - [\beta\theta(z)z']_{z_n}^{z_n+L} \end{aligned} \tag{2.38}$$

and a quadratic equation for L is obtained:

$$\frac{\beta}{2}\left[\frac{\theta(z_{n+1}) - \theta(z_n)}{z_{n+1} - z_n}\right] L^2 + \beta\left[\theta(z_n) - \theta(z)\right] L - (e(z) - E_p(z, z_n)) = 0. \tag{2.39}$$

In stably stratified layers, for $L = \frac{-b \pm \sqrt{b^2 - 4ac}}{2a}$, for a single layer elevation,

$$a = \frac{\beta}{2}\left[\frac{\theta(z_{n+1}) - \theta(z_n)}{z_{n+1} - z_n}\right] \tag{2.40}$$

$$b = \beta\left[\theta(z_n) - \theta(z)\right] = 0. \tag{2.41}$$

$$c = -(e(z) - E_p(z, z_n)) = -e(z) \tag{2.42}$$

so, $L = +\frac{\sqrt{-4ac}}{2a}$, with a $+$ sign since $a > 0$ and $c < 0$, and the expression for L is

$$L = \sqrt{\frac{2e}{\beta\left[\frac{\theta(z_{n+1}) - \theta(z_n)}{z_{n+1} - z_n}\right]}} \tag{2.43}$$

which fits the analytical expression.

2.4.3 Qualitative behavior of the 1D dry system with BL length

Critical Richardson number Let us write the 1D TKE evolution equation introducing into it the expressions for the fluxes, and neglecting the turbulent transport for this particular case:

$$\frac{\partial e}{\partial t} = \frac{4L}{15C_m} e^{\frac{1}{2}} (\frac{\partial U}{\partial z})^2 - \frac{g}{\theta_{v0}} \frac{2L}{3C_s} e^{\frac{1}{2}} \frac{\partial\theta}{\partial z}\left(1 + C_1 \frac{L^2}{e}\frac{g}{\theta_{v0}}\frac{\partial\theta}{\partial z}\right)^{-1} - C_\epsilon \frac{e^{\frac{3}{2}}}{L} \tag{2.44}$$

where the term $(\ )^{-1}$ is the developed expression for ϕ_3 in 1D dry mode. Introducing the value for BL in stable layers ($L = \sqrt{\frac{2e(z)}{\alpha\beta}}$) and defining the buoyancy as $B = \beta\alpha$,

$$\frac{\partial e}{\partial t} = e\left[\frac{4\sqrt{2}}{15C_m}(\frac{\partial U}{\partial z})^2\frac{1}{\sqrt{B}} - \sqrt{B}\sqrt{2}\frac{2}{3C_s}(\frac{1}{1+2C_1}) - \frac{C_\epsilon}{\sqrt{2}}\sqrt{B}\right] \tag{2.45}$$

The critical Richardson number is the one that nullifies the previous equation,

$$Ri_c = \frac{B}{(\frac{\partial U}{\partial z})^2} = \frac{\frac{4\sqrt{2}}{15C_m}}{\frac{2\sqrt{2}}{3C_s}(\frac{1}{1+2C_1}) + \frac{C_\epsilon}{\sqrt{2}}} \tag{2.46}$$

and entering the values of the constants (RS81), $C_m = C_s = 4, C_1 = 0.139, C_\epsilon = 0.7$, the critical Richardson of the 1D proposed scheme is $Ri_c = 0.139$.

2.4.4 Mixing length in clouds

From the masdev46 version a namelist `NAM_TURB_CLOUD` allows us to differentiate the mixing length inside and outside a cloud, for the chosen model `NMODEL_CLOUD`. Indeed, in a convective atmosphere, the cloud interface (but also inside the cloud) undergoes a small scale instabilities of a few meters which enhances the mixing (Squire 1958; Klaassen and Clark 1985; Emanuel 1994). The clear sky mixing length cannot be sufficient to take into account this turbulence enhancement when the physical gradients are not resolved. The proposed simple solution consists in chosen a specific cloud mixing length (`CTURBLEN_CLOUD`) which can be increased in the 3D turbulence scheme following an instability criterion. At each time step and in each horizontal direction, if a grid point satisfies all the following conditions:

- itself or its adjacent points are cloudy ($r_c + r_i > 0.001$ g/kg);
- G, the horizontal gradient of the non precipitating total water ($r_v + r_c + r_i$) is strong enough ($|G| \leq 0.1$ g/kg/km);
- G amplifies itself with time by advection, that is to say the frontogenetic type term $Q = dG/dt$ is of the same sign as G.

The mixing length at this point which appears in the diffusion coefficient $K = L\sqrt{e}$ of the horizontal fluxes is multiplied by the coefficient α, a linear function of Q (averaged in both horizontal directions) between two limits to be prescribed in the namelist ($Q_{\min}$ and $Q_{\max}$), with a maximum $\alpha_{\max}$ also to choose (Fig. 2.1). This local enhancement of the mixing length in clouds has been tested at resolutions of 2-3 km in a thunderstorm with extreme vertical velocities. With the following values, taken by default in the namelist, the vertical velocities and fluxes are reasonable compared to the high resolution simulation (400 m): $\alpha_{\max} = 5$, $Q_{\min} = 0.001$ g/kg/km/s, $Q_{\max} = 0.01$ g/kg/km/s.

2.5 Closure by dissipation equation

This is an alternative way to close the system (Hanjalic and Launder 1972), obtaining a value for L from an additional prognostic equation. The most popular method is the so-called $k - \epsilon$ approach, in the engineering vocabulary, where k stands for the TKE and ϵ for its dissipation.

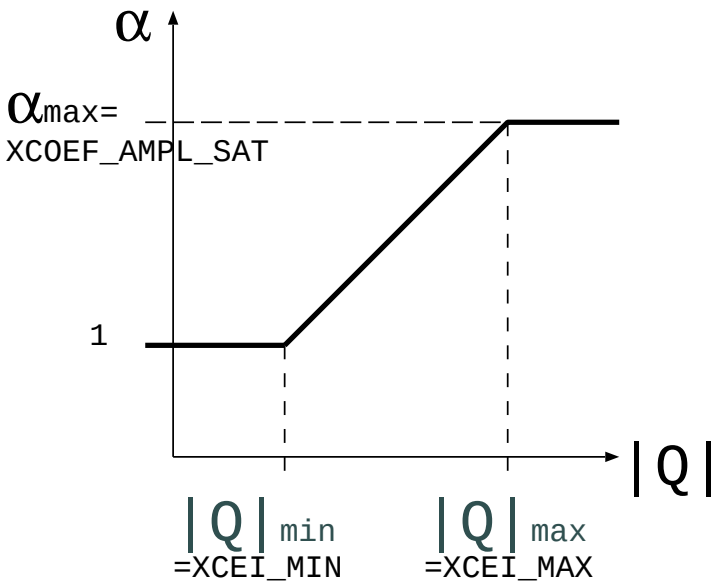

Figure 2.1: Coefficient α of in-cloud mixing length enhancement as function of the instability criterion Q.

The prognostic equation for ϵ reads

$$\frac{D\epsilon}{Dt} = P(\epsilon) - D(\epsilon) + T(\epsilon), \tag{2.47}$$

where the source terms are defined as

$$P(\epsilon) = -C_{\epsilon 1}\frac{\epsilon}{e}\overline{u_i' u_k'}\frac{\partial U_i}{\partial x_k} = C_{\epsilon 1}\frac{\epsilon}{e}P(e), \tag{2.48}$$

$$D(\epsilon) = C_{\epsilon 2}\frac{\epsilon^2}{e}, \tag{2.49}$$

$$T(\epsilon) = -\frac{\partial}{\partial x_j}(-c_\epsilon\frac{e}{\epsilon}\overline{u_j' u_k'}\frac{\partial \epsilon}{\partial x_k}) = -\frac{\partial \overline{w'\epsilon'}}{\partial z} \tag{2.50}$$

However, in the presence of stratification Duynkerke (1988) showed that it is necessary to use

$$P(\epsilon) = S + \max(0, B) + \max(0, T(e)) \tag{2.51}$$

where S, B and T stand for the shear production, buoyancy production and turbulent transport in the TKE evolution equation.

Knowing ϵ, the mixing length is recovered by inverting the Kolmogorov relation

$$\epsilon = C_\epsilon \frac{e^{\frac{3}{2}}}{L}. \tag{2.52}$$

Although it has been coded, this formulation is not yet giving satisfactory results, and is not currently available.

2.6 Conservation of the energy in Meso-NH

The examination of the energy conservation in a model of atmosphere is a very difficult task. In numerical models, this question is even untractable. However, a recent study of Blister and Emanuel (1998) pointed out that a thermodynamic energy arising from dissipative heating is always neglected in mesoscale models. Indeed this should not be the case when simulating hurricanes or very turbulent flows as omitting this term may lead to an appreciable underestimation of the intensity of tropical cyclones.
It is well known that the frictional dissipation of kinetic energy occurs at molecular scales where it is ultimately converted into thermal energy or heat. As numerical models perform a time integration of the "mean" (grid-averaged) momentum equations, an additional equation is used to parameterize the sub-grid scale motions and their up-scaling fluxes.
The momentum conservation equation is rewritten here for convenience:

$$\frac{\partial}{\partial t}(\rho_{deff}U_i) + \frac{\partial}{\partial x_j}(\rho_{deff}U_i \cdot U_j) + \rho_{deff}\mathcal{F}_\Pi + \rho_{deff}\delta_{i3}g\frac{\theta_v - \theta_{vref}}{\theta_{vref}} + \rho_{deff}f\epsilon_{ij3}U_j = \\ +\nu\frac{\partial^2}{\partial x_j^2}(\rho_{deff}U_i) + \rho_{deff}\mathcal{F}, \tag{2.53}$$

where $\rho_{deff}\boldsymbol{\mathcal{F}_\Pi}$ is the pressure gradient force, which takes different forms in the three anelastic systems:

$$\rho_{deff}\boldsymbol{\mathcal{F}_\Pi} = \begin{cases} \rho_{deff}\boldsymbol{\nabla}(C_{pd}\theta_{vref}\Pi'), & \text{(Lipps-Hemler)} \quad (2.54) \\ \rho_{deff}C_{pd}\theta_{vref}\boldsymbol{\nabla}\Pi', & \text{(Mod. Anelastic Eq.)} \quad (2.55) \\ \rho_{deff}C_{pd}\theta_v\boldsymbol{\nabla}\Pi'. & \text{(Durran)} \quad (2.56) \end{cases}$$

Expansion of the mean and turbulent parts ($U_i = \overline{U_i} + u_i'$) and applying Reynolds averaging rules on the momentum equation leads to

$$\frac{\partial}{\partial t}(\rho_{deff}\overline{U_i}) + \frac{\partial}{\partial x_j}(\rho_{deff}\overline{U_i} \cdot \overline{U_j}) + \rho_{deff}\overline{\mathcal{F}}_\Pi + \rho_{deff}\delta_{i3}g\frac{\overline{\theta_v} - \theta_{vref}}{\theta_{vref}} + \rho_{deff}f\epsilon_{ij3}\overline{U_j} = \\ +\nu\frac{\partial^2}{\partial x_j^2}(\rho_{deff}\overline{U_i}) - \frac{\partial}{\partial x_j}(\rho_{deff}\overline{u_i'u_j'}) + \rho_{deff}\overline{\mathcal{F}}, \tag{2.57}$$

where $\rho_{deff}\overline{u_i'u_j'}$ is the turbulent mean flux. The conservation equation of the turbulent part is obtained by subtracting equation (2.57) to (2.53)

$$\frac{\partial}{\partial t}(\rho_{deff}u_i') + \frac{\partial}{\partial x_j}(\rho_{deff}u_i' \cdot \overline{U_j}) + \rho_{deff}(\mathcal{F}_\Pi)' + \rho_{deff}\delta_{i3}g\frac{\theta_v'}{\theta_{vref}} + \rho_{deff}f\epsilon_{ij3}u_j' = \\ -\frac{\partial}{\partial x_j}(\rho_{deff}u_i'u_j') - \frac{\partial}{\partial x_j}(\rho_{deff}\overline{U_i} \cdot u_j') \\ +\nu\frac{\partial^2}{\partial x_j^2}(\rho_{deff}u_i') + \frac{\partial}{\partial x_j}(\rho_{deff}\overline{u_i'u_j'}) + \rho_{deff}(\mathcal{F})', \tag{2.58}$$

Multiplying equation (2.57) by $\overline{U_i}$ leads to the mean kinetic energy equation with $K = \rho_{deff}(\overline{U_i} \cdot$

$\overline{U_i}/2)$ and using the anelastic continuity equation $\partial/\partial x_i(\rho_{deff}\overline{U_i}) = 0$ of the mean flow

$$\frac{\partial}{\partial t}K + \frac{\partial}{\partial x_j}(K\cdot\overline{U_j}) + \left[\rho_{deff}\overline{\mathcal{F}}_\Pi + \rho_{deff}\delta_{i3}g\frac{\overline{\theta_v}-\theta_{vref}}{\theta_{vref}} + \rho_{deff}f\epsilon_{ij3}\overline{U_j}\right]\cdot\overline{U_i} = \\ +\left[\nu\frac{\partial^2}{\partial x_j^2}(\rho_{deff}\overline{U_i}) - \frac{\partial}{\partial x_j}(\rho_{deff}\overline{u_i'u_j'}) + \rho_{deff}\overline{\mathcal{F}}\right]\cdot\overline{U_i}, \tag{2.59}$$

while multiplying equation (2.58) by u_i' and averaging after rearrangement leads to the turbulent kinetic energy equation with $TKE = \rho_{deff}(\overline{u_i'u_i'}/2)$ (the anelastic continuity equation $\partial/\partial x_i(\rho_{deff}u_i') = 0$ of the turbulent flow is used)

$$\frac{\partial}{\partial t}TKE + \frac{\partial}{\partial x_j}(TKE\cdot\overline{U_j}) + \rho_{deff}\overline{(\mathcal{F}_\Pi)'u_i'} + \rho_{deff}\delta_{i3}g\frac{\overline{\theta_v'u_i'}}{\theta_{vref}} + \rho_{deff}f\epsilon_{ij3}\overline{u_i'u_j'} = \\ -\overline{u_i'\frac{\partial}{\partial x_j}(\rho_{deff}u_i'u_j')} - \overline{u_i'\frac{\partial}{\partial x_j}(\rho_{deff}\overline{U_i}\cdot u_j')} + \overline{\nu u_i'\frac{\partial^2}{\partial x_j^2}(\rho_{deff}u_i')} + \rho_{deff}\overline{(\mathcal{F})'u_i'}, \tag{2.60}$$

which is equivalent to:

$$\frac{\partial}{\partial t}TKE + \frac{\partial}{\partial x_j}(TKE\cdot\overline{U_j}) + \rho_{deff}\overline{(\mathcal{F}_\Pi)'u_i'} + \rho_{deff}\delta_{i3}g\frac{\overline{\theta_v'u_i'}}{\theta_{vref}} + \rho_{deff}f\epsilon_{ij3}\overline{u_i'u_j'} = \\ -\frac{\partial}{\partial x_j}\overline{TKE'u_j'} - (\rho_{deff}\overline{u_i'u_j'})\frac{\partial}{\partial x_j}\overline{U_i} \\ +\frac{\nu}{\rho_{deff}}\left[\frac{\partial}{\partial x_j}\rho_{deff}\left[\frac{\partial}{\partial x_j}TKE\right]\right] - \frac{\nu}{\rho_{deff}}\overline{\left[\frac{\partial}{\partial x_j}\left(\rho_{deff}u_i'\right)\right]^2} + \rho_{deff}\overline{(\mathcal{F})'u_i'}, \tag{2.61}$$

where the flux-like notation $\overline{TKE'u_j'}$ stands for $\rho_{deff}\overline{(u_i'u_i'/2)u_j'}$. In the rhs of equation (2.61), the TKE-diffusion term, proportional to the molecular viscosity ν, is split in two terms. The "Laplacian" term is a redistribution term which is often neglected. The second term is much larger and is always negative (minus a squared quantity). This term corresponds to the viscous dissipation rate ε

$$\varepsilon_{TKE} = \frac{\nu}{\rho_{deff}}\overline{\left[\frac{\partial}{\partial x_j}\left(\rho_{deff}u_i'\right)\right]^2}, \tag{2.62}$$

Adding equations (2.59) and (2.61) gives the evolution of the total kinetic energy equation ($K + TKE$) which explicitly contains the momentum dissipation term ε. By virtue of the total energy conservation, a counterpart dissipative energy must be added to the thermodynamic equation. This can be simply done by the introduction of a dissipative heating term of the form

$$\frac{\partial}{\partial t}(\rho_{deff}\theta) + \boldsymbol{\nabla}\cdot(\rho_{deff}\theta\,\boldsymbol{U}) = \cdots + \frac{\rho_{deff}\varepsilon_e}{\Pi_{ref}C_{ph}}. \tag{2.63}$$

The turbulence scheme in Meso-NH is based on a turbulent kinetic equation of e defined as $e = TKE/\rho_{deff}$. Most of the second order terms in equation (2.61) including $\varepsilon_{TKE} = \varepsilon_e \times \rho_{deff}$ are parameterized according to Cuxart et al. (2000).

2.7 Terrain-following coordinate system

In Meso-NH, the coordinate system is not Cartesian, in order to account for steep terrain, and the sphericity of the earth. As explained in Part I, Chapters 3 and 4 on coordinate systems and discretization, respectively, we use a $(\overline{x}, \overline{y}, \overline{z})$ coordinate system, and the contravariant components

of the velocity. By inserting these various elements in the basic equations, the form of the turbulent terms is readily obtained. For instance, the turbulent terms in the equation for the mean x momentum component read

$$\begin{aligned}\frac{\partial\tilde{\rho}\overline{u}}{\partial t} = \cdots \quad - \quad & \left[\frac{\partial}{\partial\overline{x}}(\tilde{\rho}\frac{\overline{u'u'}}{d_{xx}}) + \frac{\partial}{\partial\overline{y}}(\tilde{\rho}\frac{\overline{u'v'}}{d_{yy}}) + \frac{\partial}{\partial\overline{z}}(\tilde{\rho}\frac{\overline{w'u'}}{d_{zz}} - \tilde{\rho}\overline{u'u'}\frac{d_{zx}}{d_{xx}d_{zz}} - \tilde{\rho}\overline{v'u'}\frac{d_{zy}}{d_{yy}d_{zz}})\right] \\ + \quad & \overline{u'v'}\frac{\tilde{\rho}cos\gamma}{rcos\varphi}(sin\varphi - K) + \overline{v'v'}\frac{\tilde{\rho}sin\gamma}{rcos\varphi}(sin\varphi - K) - \tilde{\rho}\frac{\overline{u'w'}}{r}. \qquad (2.64)\end{aligned}$$

The last line of this expression arises from the curvature terms generated by the sphericity of the Earth. In the following, we will assume that these sphericity terms have negligible contributions on the turbulence, and therefore ignore them.

On the other hand, we should stress that the (u, v, w) used in the equations are still the Cartesian components of the velocity. So, the terms that the turbulence scheme will supply to Meso-NH are

$$\begin{aligned}\frac{\partial}{\partial t}(\tilde{\rho}u) &= \cdots - \left[\frac{\partial}{\partial\overline{x}}(\tilde{\rho}\frac{\overline{u'u'}}{d_{xx}}) + \frac{\partial}{\partial\overline{y}}(\tilde{\rho}\frac{\overline{u'v'}}{d_{yy}}) + \frac{\partial}{\partial\overline{z}}(\tilde{\rho}\frac{\overline{w'u'}}{d_{zz}} - \tilde{\rho}\overline{u'u'}\frac{d_{zx}}{d_{xx}d_{zz}} - \tilde{\rho}\overline{v'u'}\frac{d_{zy}}{d_{yy}d_{zz}})\right], \\ \frac{\partial}{\partial t}(\tilde{\rho}v) &= \cdots - \left[\frac{\partial}{\partial\overline{x}}(\tilde{\rho}\frac{\overline{u'v'}}{d_{xx}}) + \frac{\partial}{\partial\overline{y}}(\tilde{\rho}\frac{\overline{v'v'}}{d_{yy}}) + \frac{\partial}{\partial\overline{z}}(\tilde{\rho}\frac{\overline{v'w'}}{d_{zz}} - \tilde{\rho}\overline{u'v'}\frac{d_{zx}}{d_{xx}d_{zz}} - \tilde{\rho}\overline{v'v'}\frac{d_{zy}}{d_{yy}d_{zz}})\right], \\ \frac{\partial}{\partial t}(\tilde{\rho}w) &= \cdots - \left[\frac{\partial}{\partial\overline{x}}(\tilde{\rho}\frac{\overline{w'u'}}{d_{xx}}) + \frac{\partial}{\partial\overline{y}}(\tilde{\rho}\frac{\overline{w'v'}}{d_{yy}}) + \frac{\partial}{\partial\overline{z}}(\tilde{\rho}\frac{\overline{w'w'}}{d_{zz}} - \tilde{\rho}\overline{u'w'}\frac{d_{zx}}{d_{xx}d_{zz}} - \tilde{\rho}\overline{v'w'}\frac{d_{zy}}{d_{yy}d_{zz}})\right], \\ \frac{\partial}{\partial t}(\tilde{\rho}s) &= \cdots - \left[\frac{\partial}{\partial\overline{x}}(\tilde{\rho}\frac{\overline{s'u'}}{d_{xx}}) + \frac{\partial}{\partial\overline{y}}(\tilde{\rho}\frac{\overline{s'v'}}{d_{yy}}) + \frac{\partial}{\partial\overline{z}}(\tilde{\rho}\frac{\overline{w's'}}{d_{zz}} - \tilde{\rho}\overline{u's'}\frac{d_{zx}}{d_{xx}d_{zz}} - \tilde{\rho}\overline{v's'}\frac{d_{zy}}{d_{yy}d_{zz}})\right],\end{aligned}$$

where s is any scalar.

In addition, all the gradients appearing in the flux formulation and in the TKE prognostic equation must be evaluated in the model coordinate system by the chain rule (see below).

2.8 Spatial discretization

The location of the different variables on the computation grid is shown in Fig. 2.2. All the variables shown share the same index values i,j,k. In the following, we will use the Schuman discretization operators, as defined in Part I, Chapter 4 on discretization (section 4.3).

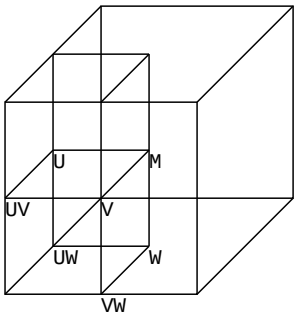

	Meso-NH	Turbulence
M	θ,ρ,λ,φ,π r,J,m,f	u'2,v'2,w'2 e,L
V	V,dyy	H2,Q2,v'S'
U	U,dxx	H1,Q1,u'S'
W	W,dzz	H3,Q3,w'S', ϕ3
UW	dzx	u'w'
VW	dzy	v'w'
UV	---	u'v'

Figure 2.2: Location of variables on the grid for turbulence computation.

The discretized form of the turbulence terms in the main equations reads

$$
\begin{aligned}
\delta_t\left[\overline{(\overline{\tilde{\rho}}^{x}u)}^{t}\right] = \cdots \quad &- \quad \delta_x(\tilde{\rho}\frac{\overline{u'u'}}{\overline{\overline{d_{xx}}^{x}}}) - \delta_y(\overline{\tilde{\rho}}^{x,y}\frac{\overline{u'v'}}{\overline{\overline{d_{yy}}^{x}}}) \\
&- \quad \delta_z(\overline{\tilde{\rho}}^{z,x}\frac{\overline{w'u'}}{\overline{\overline{d_{zz}}^{x}}} - \overline{\tilde{\rho}}^{z,x}\overline{\overline{u'u'}}^{z,x}\frac{d_{zx}}{\overline{\overline{d_{xx}}^{z}\overline{d_{zz}}^{x}}} - \overline{\tilde{\rho}}^{z,x}\overline{\overline{v'u'}}^{z,y}\frac{\overline{d_{zy}}^{x,y}}{\overline{\overline{d_{yy}}^{x,y,z}\overline{d_{zz}}^{x}}}) \\
\delta_t\left[\overline{(\overline{\tilde{\rho}}^{y}v)}^{t}\right] = \cdots \quad &- \quad \delta_x(\overline{\tilde{\rho}}^{x,y}\frac{\overline{u'v'}}{\overline{\overline{d_{xx}}^{y}}}) - \delta_y(\tilde{\rho}\frac{\overline{v'v'}}{\overline{\overline{d_{yy}}^{y}}}) \\
&- \quad \delta_z(\overline{\tilde{\rho}}^{z,y}\frac{\overline{w'v'}}{\overline{\overline{d_{zz}}^{y}}} - \overline{\tilde{\rho}}^{z,y}\overline{\overline{u'v'}}^{z,x}\frac{\overline{d_{zx}}^{y,x}}{\overline{\overline{d_{xx}}^{xyz}\overline{d_{zz}}^{y}}} - \overline{\tilde{\rho}}^{z,y}\overline{\overline{v'v'}}^{z,y}\frac{d_{zy}}{\overline{\overline{d_{yy}}^{z}\overline{d_{zz}}^{y}}}) \\
\delta_t\left[\overline{(\overline{\tilde{\rho}}^{z}w)}^{t}\right] = \cdots \quad &- \quad \delta_x(\overline{\tilde{\rho}}^{z,x}\frac{\overline{u'w'}}{\overline{\overline{d_{xx}}^{z}}}) - \delta_y(\overline{\tilde{\rho}}^{z,y}\frac{\overline{v'w'}}{\overline{\overline{d_{yy}}^{z}}}) \\
&- \quad \delta_z(\tilde{\rho}\frac{\overline{w'w'}}{\overline{\overline{d_{zz}}^{z}}} - \tilde{\rho}\overline{\overline{u'w'}}^{z,x}\frac{\overline{d_{zx}}^{x,z}}{\overline{\overline{d_{xx}}^{x}\overline{d_{zz}}^{z}}} - \tilde{\rho}\overline{\overline{v'w'}}^{y,z}\frac{\overline{d_{zy}}^{y,z}}{\overline{\overline{d_{yy}}^{x}\overline{d_{zz}}^{z}}}) \\
\delta_t\left[\overline{(\tilde{\rho}s)}^{t}\right] = \cdots \quad &- \quad \delta_x(\overline{\tilde{\rho}}^{x}\frac{\overline{u's'}}{d_{xx}}) - \delta_y(\overline{\tilde{\rho}}^{y}\frac{\overline{v's'}}{d_{yy}}) \\
&- \quad \delta_z(\overline{\tilde{\rho}}^{z}\frac{\overline{w's'}}{d_{zz}} - \overline{\tilde{\rho}}^{z}\overline{\overline{u's'}}^{z,x}\frac{\overline{d_{zx}^{x}}}{\overline{\overline{d_{xx}}^{z,x}}d_{zz}} - \overline{\tilde{\rho}}^{z}\overline{\overline{v's'}}^{z,y}\frac{\overline{d_{zy}}^{y}}{\overline{\overline{d_{yy}}^{z,y}}d_{zz}})
\end{aligned}
\tag{2.65}
$$

Here, we have assumed that the time discretization is fully explicit, and all the terms on the right hand side are taken at time $t - \Delta t$. As explained in the final section however, we allow for some degree of implicitness in the time discretization of the purely vertical diffusion terms, in order to allow for longer time steps when the model is used in meso-scale mode.

In (2.65), we still use the expression of the turbulent fluxes in the Cartesian frame. Those must be expressed as a function of the gradients of the mean variables in the Cartesian frame. To ease this formulation, we have developed 15 different "Cartesian gradient operators", depending of the direction in which the gradient is taken, and the precise locations on the grid where the information is available. The generic notation for these operators is $GX_i\_A\_B$: X_i refers to the

(Cartesian) direction where the gradient is taken, A to the variable location, and B to the location where the gradients must be known. The detailed expression of these operators is the following.

1) Gradients at mass points for variables located at mass points:

$$\begin{aligned}
\frac{\partial \bullet}{\partial x} &= \frac{1}{\overline{d_{xx}}^{x}} \left[\delta_x \overline{\bullet}^{x} - \overline{\left(\frac{\overline{d_{zx}}^{x} \delta_z \bullet}{d_{zz}} \right)}^{z} \right] && \equiv GX_M_M \\
\frac{\partial \bullet}{\partial y} &= \frac{1}{\overline{d_{yy}}^{y}} \left[\delta_y \overline{\bullet}^{y} - \overline{\left(\frac{\overline{d_{zy}}^{y} \delta_z \bullet}{d_{zz}} \right)}^{z} \right] && \equiv GY_M_M \\
\frac{\partial \bullet}{\partial z} &= \overline{\left(\frac{\delta_z \bullet}{d_{zz}} \right)}^{z} && \equiv GZ_M_M
\end{aligned} \tag{2.66}$$

2) Gradients at wind points for variables located at mass points: ($\overline{u_i' \theta'} \Longleftrightarrow \frac{\partial \theta}{\partial x_i}$)

$$\begin{aligned}
\frac{\partial \bullet}{\partial x} &= \frac{1}{d_{xx}} \left[\delta_x \bullet - \overline{\left(\frac{d_{zx} \overline{\delta_z \bullet}^{x}}{d_{zz}} \right)}^{z} \right] && \equiv GX_M_U \\
\frac{\partial \bullet}{\partial y} &= \frac{1}{d_{yy}} \left[\delta_y \bullet - \overline{\left(\frac{d_{zy} \overline{\delta_z \bullet}^{y}}{d_{zz}} \right)}^{z} \right] && \equiv GY_M_V \\
\frac{\partial \bullet}{\partial z} &= \frac{1}{d_{zz}} \delta_z \bullet && \equiv GZ_M_W
\end{aligned} \tag{2.67}$$

3) Gradients at mass points of variables located at wind points: ($\overline{u_i'^2} \Longleftrightarrow \frac{\partial u_i}{\partial x_i}$ unsummed)

$$\begin{aligned}
\frac{\partial \bullet}{\partial x} &= \frac{1}{\overline{d_{xx}}^{x}} \left[\delta_x \bullet - \overline{\left(\frac{\overline{d_{zx} \delta_z \bullet}^{x}}{d_{zz}} \right)}^{z} \right] && \equiv GX_U_M \\
\frac{\partial \bullet}{\partial y} &= \frac{1}{\overline{d_{yy}}^{y}} \left[\delta_y \bullet - \overline{\left(\frac{\overline{d_{zy} \delta_z \bullet}^{y}}{d_{zz}} \right)}^{z} \right] && \equiv GY_V_M \\
\frac{\partial \bullet}{\partial z} &= \frac{1}{\overline{d_{zz}}^{z}} \delta_z \bullet && \equiv GZ_W_M
\end{aligned} \tag{2.68}$$

4) Gradients at vorticity points for variables located at wind points: ($\overline{u_i' u_j'} \Longleftrightarrow \frac{\partial u_i}{\partial x_j}$, $\frac{\partial u_j}{\partial x_i}$)
For gradients localized at point UV:

$$\begin{aligned}
\frac{\partial \bullet}{\partial x} &= \frac{1}{\overline{d_{xx}}^{y}} \left[\delta_x \bullet - \overline{\overline{\left(\frac{\delta_z \bullet}{\overline{d_{zz}}^{y}} \right)}^{x} \overline{d_{zx}}^{y}}^{z} \right] && \equiv GX_V_UV \\
\frac{\partial \bullet}{\partial y} &= \frac{1}{\overline{d_{yy}}^{x}} \left[\delta_y \bullet - \overline{\overline{\left(\frac{\delta_z \bullet}{\overline{d_{zz}}^{x}} \right)}^{y} \overline{d_{zy}}^{x}}^{z} \right] && \equiv GY_U_UV
\end{aligned} \tag{2.69}$$

For gradients localized at point UW:

$$\begin{aligned}
\frac{\partial \bullet}{\partial x} &= \frac{1}{\overline{d_{xx}}^{z}} \left[\delta_x \bullet - \overline{\left(\frac{\overline{\delta_z \bullet}^{z}}{d_{zz}} \right)}^{x} d_{zx} \right] && \equiv GX_W_UW \\
\frac{\partial \bullet}{\partial z} &= \frac{\delta_z \bullet}{\overline{d_{zz}}^{x}} && \equiv GZ_U_UW
\end{aligned} \tag{2.70}$$

For gradients localized at point VW:

$$\begin{aligned}
\frac{\partial \bullet}{\partial y} &= \frac{1}{\overline{d_{yy}}^{z}} \left[\delta_y \bullet - \overline{\left(\frac{\overline{\delta_z \bullet}^{z}}{d_{zz}} \right)}^{y} d_{zy} \right] && \equiv GY_W_VW \\
\frac{\partial \bullet}{\partial z} &= \frac{\delta_z \bullet}{\overline{d_{zz}}^{y}} && \equiv GZ_V_VW
\end{aligned} \tag{2.71}$$

Making use of these operators, the discretized form of the turbulent fluxes in the Cartesian frame reads as follows:

$$\begin{aligned}
\overline{u_i' u_j'} &= \frac{2}{3}\delta_{ij}\,\overline{e}^{x_i,x_j} - \frac{4}{15}\frac{\overline{L}^{x_i,x_j}}{C_m}\overline{e^{\frac{1}{2}}}^{x_i,x_j}[GX_j_U_i_U_iU_j(u_i) + GX_i_U_j_U_iU_j(u_j) \\
&- \frac{2}{3}\delta_{ij}\sum_{m=1}^{3} GX_m_U_m_U_iU_j(u_m)] \qquad (2.72)\\
\overline{u_i'\theta'} &= -\frac{2}{3}\frac{\overline{L}^{x_i}}{C_s}\overline{e^{\frac{1}{2}}}^{x_i} GX_i_M_U_i(\theta)\phi_i \qquad (2.73)\\
\overline{u_i' r_v'} &= -\frac{2}{3}\frac{\overline{L}^{x_i}}{C_s}\overline{e^{\frac{1}{2}}}^{x_i} GX_i_M_U_i(r_v)\psi_i \qquad (2.74)\\
\overline{\theta' r_v'} &= C_2L^2\sum_{m=1}^{3} GX_m_M_M(\theta)GX_m_M_M(r_v)(\overline{\phi_m}^z + \overline{\psi_m}^z) \qquad (2.75)\\
\overline{\theta'^2} &= C_1L^2\sum_{m=1}^{3}(GX_m_M_M(\theta))^2)\overline{\phi_m}^z \qquad (2.76)\\
\overline{r_v'^2} &= C_1L^2\sum_{m=1}^{3}(GX_m_M_M(r_v))^2)\overline{\psi_m}^z \qquad (2.77)\\
\overline{u_i'\theta_v'} &= E_\theta\,\overline{u_i'\theta'}^{x_i} + E_{moist}\,\overline{u_i' r_v'}^{x_i} \qquad (2.78)
\end{aligned}$$

The ϕ_i and ψ_i stability functions are computed at W points. Their expression follows readily from (2.15, 2.16), using the discretized formulation of the Redelsperger numbers at W points:

$$\begin{aligned}
R_{\theta 1} &= \overline{\frac{g}{\theta_{v\,ref}}\frac{L^2}{e}}^z \overline{E_\theta}^z \cdot GZ_M_W(\theta) \qquad (2.79)\\
R^2_{\theta 3} &= R^2_{\theta 1} + (\overline{\frac{g}{\theta_{v\,ref}}\frac{L^2}{e}}^z \overline{E_\theta}^z)^2[\overline{\sum_{m=2}^{3} GX_m_M_M(\theta)\cdot GX_m_M_M(\theta)}^z] \qquad (2.80)\\
R_{r1} &= \overline{\frac{g}{\theta_{v\,ref}}\frac{L^2}{e}}^z \overline{E_{moist}}^z \cdot GZ_M_W(r_v) \qquad (2.81)\\
R^2_{r3} &= R^2_{r1} + (\overline{\frac{g}{\theta_{v\,ref}}\frac{L^2}{e}}^2 \overline{E_{moist}}^z)^2[\overline{\sum_{m=2}^{3} GX_m_M_M(r_v)\cdot GX_m_M_M(r_v)}^z] \qquad (2.82)\\
R^2_{\theta r3} &= R_{\theta 1}R_{r1} + (\overline{\frac{g}{\theta_{v\,ref}}\frac{L^2}{e}}^z)^2\overline{E_\theta}^z\overline{E_{moist}}^z[\overline{\sum_{m=2}^{3} GX_m_M_M(\theta)\cdot GX_m_M_M(r_v)}^z] \qquad (2.83)
\end{aligned}$$

Let us now describe the TKE equation discretization. The generic form of this equation is

$$\frac{\partial}{\partial t}(\tilde{\rho}e) = ADV(e) + \tilde{\rho}P^t - \frac{\partial}{\partial x}(\overline{\tilde{\rho}}^x\overline{u'e'}) - \frac{\partial}{\partial y}(\overline{\tilde{\rho}}^y\overline{v'e'}) - \frac{\partial}{\partial z}(\overline{\tilde{\rho}}^z\overline{w'e'}). \qquad (2.84)$$

The advections term $ADV(e)$ is not treated in the turbulence scheme, but in the routine taking care of the general advection of scalar quantities (see Part I, Chapter 4 on discretization). P^t contains

all the source terms, some of which are expressed at $t-1$, and others at t. This reads

$$\begin{aligned} P^t &= -\overline{u'^2}\frac{\partial u}{\partial x} - \overline{\overline{u'v'}}^{x,y}\frac{\partial}{\partial y}(\overline{u}^{y,x}) - \overline{\overline{u'w'}}^{x,z}\frac{\partial}{\partial z}(\overline{u}^{z,x}) - \overline{\overline{v'u'}}^{x,y}\frac{\partial}{\partial x}(\overline{v}^{x,y}) \\ &- \overline{v'^2}\frac{\partial v}{\partial y} - \overline{\overline{v'w'}}^{y,z}\frac{\partial}{\partial z}(\overline{v}^{z,y}) - \overline{\overline{w'u'}}^{x,z}\frac{\partial}{\partial x}(\overline{w}^{x,z}) - \overline{\overline{w'v'}}^{y,z}\frac{\partial}{\partial y}(\overline{w}^{y,z}) - \overline{w'^2}\frac{\partial w}{\partial z} \\ &+ \frac{g}{\theta_{v\,ref}}\overline{\overline{w'\theta'_v}}^{z} - C_\epsilon\frac{e^{3/2}}{L}. \end{aligned} \tag{2.85}$$

Using the Cartesian gradient operators and leaving the advection term aside, this become therefore

$$\begin{aligned} \delta_t\left[\overline{(\tilde{\rho}e)}^t\right] &= \tilde{\rho}[-\overline{u'^2}(GX\_U\_M(u)) - \overline{\overline{u'v'}}^{x,y}(GY\_V\_M(\overline{u}^{y,x})) - \overline{\overline{u'w'}}^{x,z}(GZ\_W\\_M(\overline{u}^{z,x})) \\ &- \overline{\overline{v'u'}}^{x,y}(GX\_U\_M(\overline{v}^{x,y})) - \overline{v'^2}(GY\_V\_M(v)) - \overline{\overline{v'w'}}^{y,z}(GZ\_W\\_M(\overline{v}^{z,y})) \\ &- \overline{\overline{w'u'}}^{x,z}(GX\_U\_M(\overline{w}^{x,z})) - \overline{\overline{w'v'}}^{y,z}(GY\_V\_M(\overline{w}^{y,z})) - \overline{w'^2}(GZ\_W\\_M(w)) \\ &+ \frac{g}{\theta_{v\,ref}}\overline{\overline{w'\theta'_v}}^{z} - C_\epsilon\frac{e^{3/2}}{L}] \\ &- (GX\_U\_M(\overline{\tilde{\rho}}^x\overline{u'e'})) - (GY\_V\_M(\overline{\tilde{\rho}}^y\overline{v'e'})) - (GZ\_W\\_M(\overline{\tilde{\rho}}^z\overline{w'e'})). \end{aligned} \tag{2.86}$$

This uses the turbulent fluxes of TKE, expressed at u_i points as

$$\overline{u'_ie'} = -C_{2m}\overline{Le^{\frac{1}{2}}}^{x_i}GX_i\_M\_U_i(e). \tag{2.87}$$

2.9 Boundary conditions

2.9.1 Lateral boundary conditions

An important point for lateral boundary conditions is to realize that the computation of the source term for any prognostic variable at (i, j) will involve only quantities of the same nature at (i-1, i+1, j-1, j+1), as shown in Fig. 2.3. As a consequence, a clean treatment of lateral boundary conditions is obtained with only one extra grid point on each side. Referring to the terminology of Chapter 5 (in Part I), HEXT=1 is sufficient for the turbulence scheme. The two basic options for lateral boundary conditions are therefore supported.

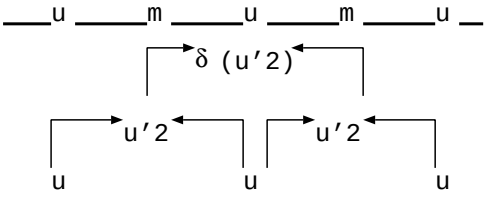

Figure 2.3: Discretization of second order terms.

Periodic LBC

In this case, the computation of all source terms in the turbulence routines is performed from I=1 to IMAX, and from J=1 to JMAX. It uses values of the mean variables at I=0 and IMAX+1, J=0 and

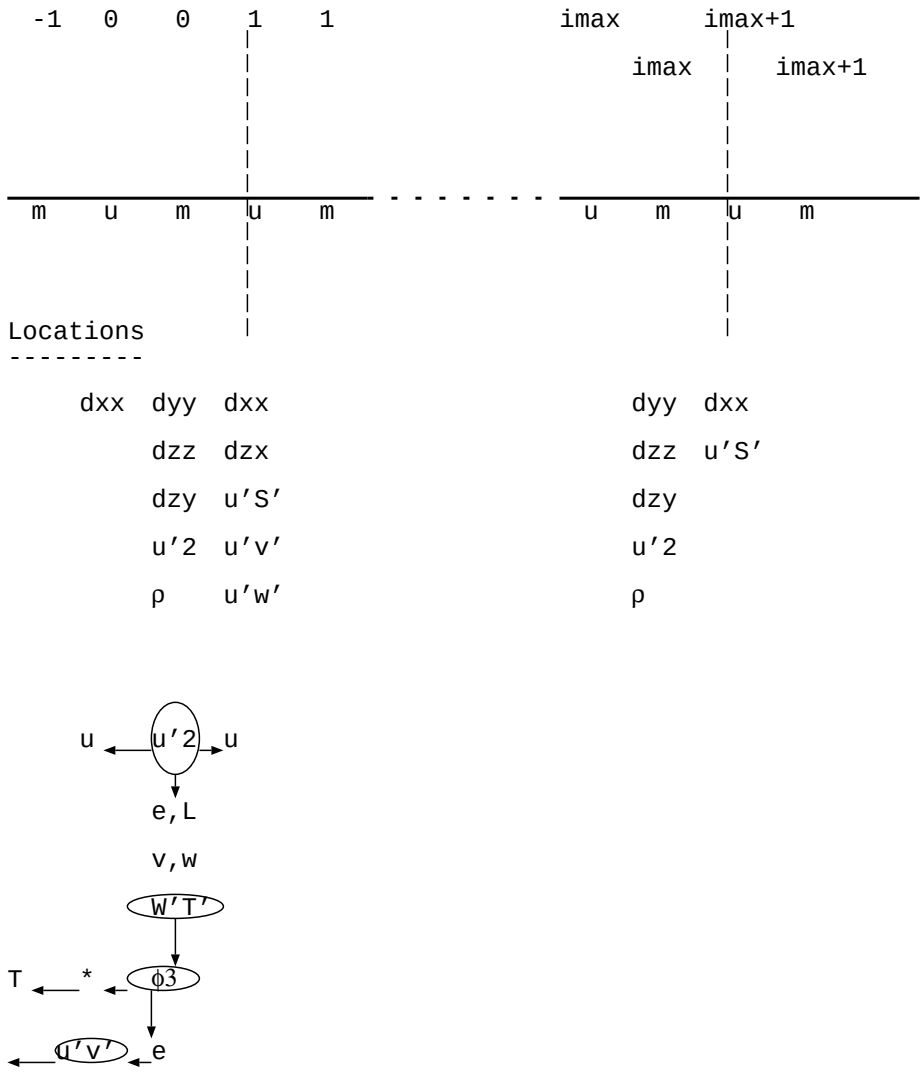

Figure 2.4: Cyclic lateral boundary conditions.

JMAX+1 (Fig. 2.4). These values are supplied by the routine BOUNDARY, as part of the general treatment of lateral boundaries. Note that the additional prognostic variables (the turbulence kinetic energy e and eventually the dissipation rate ϵ) are also made periodic by BOUNDARY.

Open LBC

In this case, the computation of the turbulent source terms is performed from I=1 to IMAX for scalars and non-normal velocity components, and from I=2 to IMAX for the normal velocity component. This is illustrated in Fig. 2.5. Indeed, there is no need to write an equation for the quantity u at I=1, since this value is to be prescribed by the open LBC scheme.

2.9.2 Upper boundary condition

In the Gal-Chen Sommerville coordinate system, the domain is terminated by a horizontal plane at $z = H$. This coincides with a plan of W points. The physical condition imposed at this level is that all turbulent vertical fluxes are zero.

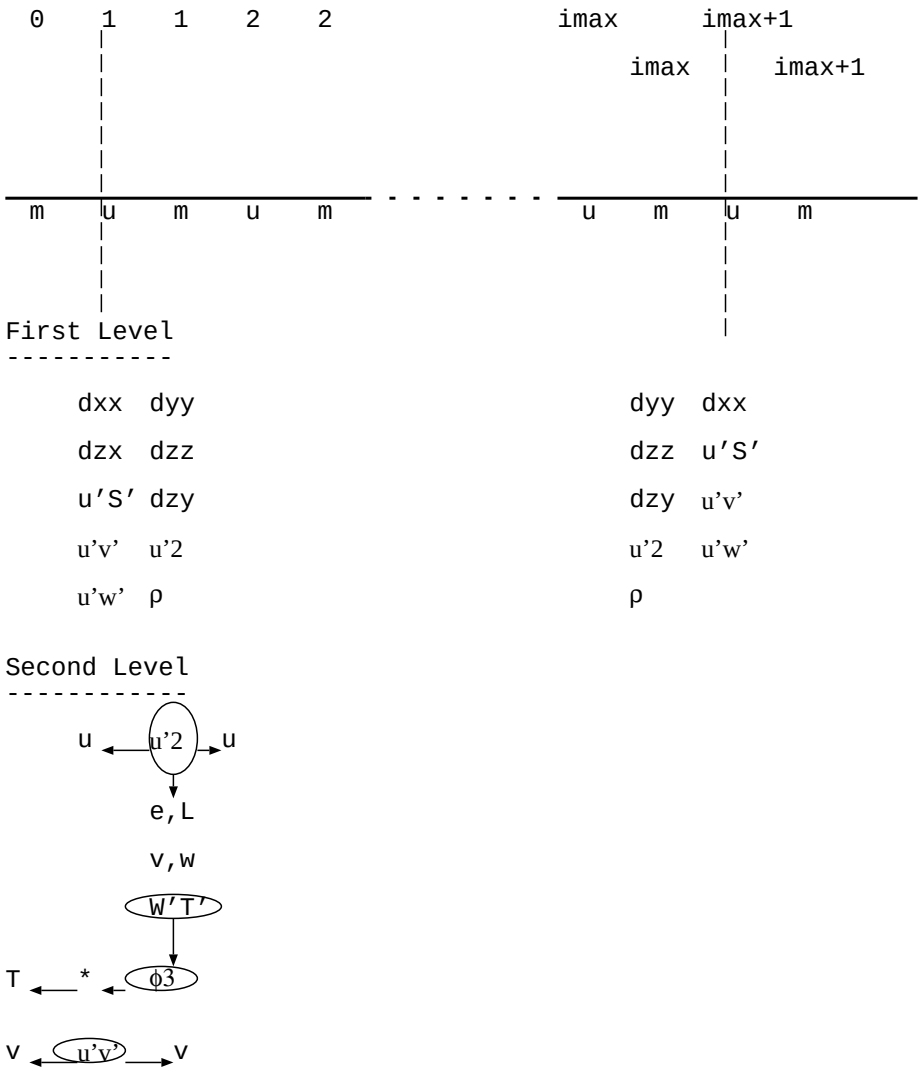

Figure 2.5: Open lateral boundary conditions.

Whenever vertical gradients of mean variables are needed at this height, they are computed by extrapolation of gradients immediately below. This procedure is assumed to have a negligible impact on the overall model results.

2.9.3 Surface boundary conditions

The physical forcing of turbulence at the surface is a major concern. We assume that the main information is contained in the value of the turbulent fluxes of heat, moisture and momentum, supplied by the soil-vegetation atmosphere transfer scheme (see Part II, Chapter 6). Depending on various options, these fluxes may be specified, or computed by bulk formulae.

One difficulty is to deal correctly with the terrain slope effect, in presence of steep orography. We assume that the soil vegetation atmosphere transfer scheme returns fluxes normal to the terrain. We then have to project these fluxes on to the Cartesian coordinates (Fig. 2.6).

If the flux ($\mathbf{\Phi}$) is normal to the surface, we can write it as $\mathbf{\Phi} = \Phi_n \boldsymbol{n}$. The projections over the

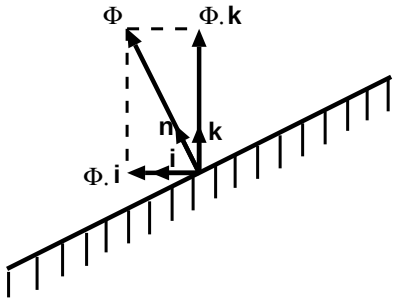

Figure 2.6: The Cartesian decomposition of the surface flux.

Cartesian coordinates are

$$\begin{aligned} \boldsymbol{\Phi i} &= \Phi_n \boldsymbol{n} \cdot \boldsymbol{i}, \\ \boldsymbol{\Phi j} &= \Phi_n \boldsymbol{n} \cdot \boldsymbol{j}, \\ \boldsymbol{\Phi k} &= \Phi_n \boldsymbol{n} \cdot \boldsymbol{k}. \end{aligned} \tag{2.88}$$

Referring to notations of Part I, Chapter 3, the contravariant vector basis normal to the surface is $\boldsymbol{e^3} = \|e^3\|\boldsymbol{n}$ (contravariant). Then,

$$e^3 = -\frac{d_{zx}}{d_{xx}d_{zz}}\boldsymbol{i} - \frac{d_{zy}}{d_{yy}d_{zz}}\boldsymbol{j} + \frac{1}{d_{zz}}\boldsymbol{k}, \tag{2.89}$$

and

$$\|e^3\| = \frac{1}{d_{zz}}(1 + (\frac{d_{zx}}{d_{xx}})^2 + (\frac{d_{zy}}{d_{yy}})^2)^{1/2}. \tag{2.90}$$

To get the Cartesian components, we just compute the scalar products

$$\boldsymbol{n} \cdot \boldsymbol{i} = \frac{\boldsymbol{e^3}}{\|e^3\|} \cdot \boldsymbol{i} = \frac{1}{\|e^3\|}(-\frac{d_{zx}}{d_{xx}d_{zz}}), \tag{2.91}$$

$$\boldsymbol{\Phi} \cdot \boldsymbol{i} = \Phi_n \boldsymbol{n} \cdot \boldsymbol{i} = \Phi_n \,(-\frac{d_{zx}}{d_{xx}(1 + (\frac{d_{zx}}{d_{xx}})^2 + (\frac{d_{zy}}{d_{yy}})^2)^{1/2}}), \tag{2.92}$$

and for the other components

$$\boldsymbol{\Phi} \cdot \boldsymbol{j} = \Phi_n \,(-\frac{d_{zy}}{d_{yy}(1 + (\frac{d_{zx}}{d_{xx}})^2 + (\frac{d_{zy}}{d_{yy}})^2)^{1/2}}), \tag{2.93}$$

$$\boldsymbol{\Phi} \cdot \boldsymbol{k} = \Phi_n \,(-\frac{1}{(1 + (\frac{d_{zx}}{d_{xx}})^2 + (\frac{d_{zy}}{d_{yy}})^2)^{1/2}}). \tag{2.94}$$

The projection $\boldsymbol{\Phi} \cdot \boldsymbol{k}$ is then used as the vertical surface flux .

2.9.4 Extrapolation of gradients

Another point to stress is that many flux computations at the boundaries require the use of points outside the domain. This is for instance the case at the ground for sloping terrain. The expression of the flux , $\overline{u'\theta'}$ by the GX_M_U operator involves a vertical differencing of θ, with information below the ground. Whenever this problem arises, the approach taken has been to extrapolate the gradients in the adjacent points.

2.10 Semi-implicit time discretization

For high resolution, full 3D experiments (LES or CRM type), the explicit time stepping is not expected to place major restrictions on the time step compared to the advection scheme. This is no longer true when the model is run in "meso-scale" mode, with highly anisotropic grids. In this case the vertical diffusion terms severely restrict the time step.
We have therefore implemented a Crank-Nicholson time implicit scheme for the vertical diffusion terms. The degree of implicitness may be varied at will by the user, adjusting the parameter XIMPL. XIMPL=1 will result in the fully implicit scheme, XIMPL=0.5 is the semi-implicit scheme, and XIMPL=0. reverts to the fully explicit scheme.
We will now formulate the matrix inversion problem associated with this Crank-Nicholson scheme. s stands for any prognostic variable, and we use the notations α =XIMPL and β =1-XIMPL. For short, we use the notation K for the vertical exchange coefficient (for instance, $K = \frac{2}{3}\frac{L}{C_s}e^{\frac{1}{2}}\phi_3$) for $s = \theta$). The evolution equation for s reads

$$\frac{\partial \tilde{\rho} s}{\partial t} = S^t + \alpha \frac{\partial}{\partial \overline{z}}\left(\frac{\overline{\tilde{\rho} K^t}^z}{d_{zz}^2}\frac{\partial s}{\partial \overline{z}}^{t+1}\right) + \beta \frac{\partial}{\partial \overline{z}}\left(\frac{\overline{\tilde{\rho} K^t}^z}{d_{zz}^2}\frac{\partial s}{\partial \overline{z}}^{t-1}\right), \tag{2.95}$$

where S^t represents the other source terms.
This expression, discretised for a given level k (with i, j omitted for comfort) becomes

$$\begin{aligned}
&\frac{\tilde{\rho} s^{t+1}(k) - \tilde{\rho} s^{t-1}(k)}{2\Delta t} = S^t(k) + \\
&\frac{\alpha}{\tilde{\rho}(k)}\left(\frac{\overline{\tilde{\rho} K^t(k+1)}^z}{d_{zz}^2(k+1)}(s^{t+1}(k+1) - s^{t+1}(k)) - \frac{\overline{\tilde{\rho} K^t(k)}^z}{d_{zz}^2(k)}(s^{t+1}(k) - s^{t+1}(k-1))\right) \\
&+\frac{\beta}{\tilde{\rho}(k)}\left(\frac{\overline{\tilde{\rho} K^t(k+1)}^z}{d_{zz}^2(k+1)}(s^{t-1}(k+1) - s^{t-1}(k)) - \frac{\overline{\tilde{\rho} K^t(k)}^z}{d_{zz}^2(k)}(s^{t-1}(k) - s^{t-1}(k-1))\right)
\end{aligned} \tag{2.96}$$

This gives the well known tri-diagonal matrix equation

$$s^{t+1}(k-1)(\alpha\frac{A(k)}{\tilde{\rho}(k)}) + s^{t+1}(k)(1 - \alpha\frac{A(k)}{\tilde{\rho}(k)} - \alpha\frac{C(k)}{\tilde{\rho}(k)}) + s^{t+1}(k+1)(\alpha\frac{C(k)}{\tilde{\rho}(k)}) = Y(k), \tag{2.97}$$

where

$$A(k) = -2\Delta t \frac{\overline{\tilde{\rho}(k) K^t(k)}^z}{d_{zz}^2(k)}, \tag{2.98}$$

$$C(k) = -2\Delta t \frac{\overline{\tilde{\rho}(k+1) K^t(k+1)}^z}{d_{zz}^2(k+1)}, \tag{2.99}$$

$$\begin{aligned}
Y(k) = {} & 2\Delta t S^t(k) + s^{t-1}(k-1)(-\beta\frac{A(k)}{\tilde{\rho}(k)}) \\
& + s^{t-1}(k)(1 + \beta\frac{A(k)}{\tilde{\rho}(k)} + \beta\frac{C(k)}{\tilde{\rho}(k)}) + s^{t-1}(k+1)(-\beta\frac{C(k)}{\tilde{\rho}(k)}).
\end{aligned} \tag{2.100}$$

This matrix problem is solved by a specialized routine called TRIDIAG.
In practice, the source term S^t contains only the surface fluxes. It is therefore a "split" treatment. After solving for s^{t+1}, the equivalent tendency $\frac{\partial s}{\partial t}$ is recomputed, and added to the other sources of the variable s.

2.11 References

Bister, M., and K. A. Emanuel, 1998: Dissipative heating and hurricane intensity. *Meteor. Atmos. Phys.*, **65**, 233-240.

Bougeault, P., and P. Lacarrère, 1989: Parameterization of orography-induced turbulence in a meso-beta scale model. *Mon. Wea. Rev.*, **117**, 1872-1890.

Cuxart, J., 1997: Planetary Boundary Layer Simulation: From LES to General Circulation Models, Ph.D. thesis, European thesis - Barcelone.

Cuxart, J., P. Bougeault, and J.-L. Redelsperger, 2000: A turbulence scheme allowing for mesoscale and large-eddy simulations. *Quart. J. Roy. Meteor. Soc.*, **126**, 1-30.

Duynkerke, P.G., 1988: Application of the E-ϵ turbulence closure model to the neutral and stable atmospheric boundary layer. *J. Atmos. Sci.*, **45**, 865-880.

Emanuel K. A. 1994, Atmospheric convection, Chp8: Theory of mixing in cumulus cloud, p215

Hanjalic, K., and B. E. Launder, 1972: A Reynolds stress model of turbulence and its application to thin shear flows. *J. Fluid Mech.*, **52**, 609-638.

Klaassen, G. P., and T. L. Clark, 1985: Dynamics of the cloud environment interface and entrainment in small cumuli: Two-dimensional simulations in the absence of ambient shear. *J. Atmos. Sci.*, **42**, 2621-2642.

Redelsperger, J.-L, and G. Sommeria, 1981: Méthode de représentation de la turbulence d'échelle inférieure à la maille pour un modèle tri-dimensionnel de convection nuageuse. *Boundary-Layer Meteor.*, **21(4)**, 509-530.

Squire, P., 1958: The spatial variation of liquid water and droplet concentration in cumuli. *Tellus*, **10**, 372-380

Squire, P., 1958: Penetrative downdraughts in cumuli. *Tellus*, **10**, 381-389

Tomas, S., and V. Masson, 2006: A parameterization of third-order moments for the dry convective boundary layer. *Bound.-Layer. Meteor.*, **120**, 437-454.

Chapter 3

EDKF Shallow Convection Scheme

Contents

3.1 Introduction

In a dry or cloudy convective boundary layer (CBL), the evolution of a variable ϕ is strongly influenced by vertical turbulent transport. Therefore, a good estimation of the second-order moment $\overline{w'\phi'}$ is needed to determine the tendency of $\overline{\phi}$ (the mean value of ϕ) in the CBL.
Siebesma and Teixeira (2000) and Hourdin et al. (2002) developed a new parameterization that combines eddy diffusivity and mass flux approaches in a consistent way. Organized strong updrafts are parameterized by the mass flux part while the remaining turbulence is parameterized using K-theory. This parameterization, named EDMF (Eddy-Diffusivity / Mass Flux), has been developed to model cloudy shallow convection and dry convection in a unified way. In the EDMF framework, the turbulent flux of a conservative variable ϕ is defined as:

$$\overline{w'\phi'} = -K\frac{\partial\overline{\phi}}{\partial z} + \frac{M_u}{\rho}(\phi_u - \overline{\phi}), \tag{3.1}$$

where ρ is the density, K is the turbulent diffusivity, M_u is the convective mass flux $M_u = \rho a_u w_u$ (a_u is the updraft grid fraction area and w_u is the vertical velocity in the updraft), $\overline{\phi}$ is the mean value and ϕ_u is the updraft value of the variable ϕ.

In this formulation, it is assumed that the size of the updraft area is very small compared to the grid size ($a_u \ll 1$), so the environmental field values are taken as the mean field values. The effect of downdrafts is neglected as this parameterization is used only for shallow convection. The eddy-diffusivity term represents the remaining fluctuations due to the non-organized small-scale local turbulence.
Our parameterization contains an eddy-diffusivity term which is computed by the turbulence scheme of Cuxart et al. (2000) and a mass flux term computed by an updraft scheme which is described in the following section. Due to the fact that we use the Kain-Fritsch scheme to diagnose entrainment and detrainment in the cloudy portion, we decided to call the new scheme EDKF for Eddy-Diffusivity / Kain-Fritsch.

3.2 Description of the scheme

3.2.1 Updraft model

The updraft model is defined as a single entraining/detraining rising parcel as in Soares et al. (2004). One resulting updraft described by the mass flux is used to represent the effect of several plumes, and its characteristics are determined as a function of mixing between the updraft and its environment through entrainment E (the inward mass flux from the environment to the updraft) and detrainment D (the outward mass flux from the updraft to the environment). Moreover, the mass flux approximation assumes that the cloud ensemble is considered in steady state. The mass flux is defined as $M_u = \rho a_u w_u$, and its evolution is determined by a diagnostic equation of the mass continuity between the updraft and its surrounding environment (Fig. 3.1),

$$\frac{\partial M_u}{\partial z} = (E - D) \tag{3.2}$$

$$\text{or, } \frac{1}{M_u}\frac{\partial M_u}{\partial z} = (\epsilon - \delta) \tag{3.3}$$

where ϵ and δ are respectively the entrainment rate ($E = \epsilon M_u$) and the detrainment rate ($D = \delta M_u$).
The evolution of a conserved parcel characteristic ϕ_u during the ascent is defined as in Siebesma (1998):

$$\frac{\partial M_u \phi_u}{\partial z} = E\overline{\phi} - D\phi_u \tag{3.4}$$

using (3.3) and simplified as:

$$\frac{\partial \phi_u}{\partial z} = -\epsilon(\phi_u - \overline{\phi}) \tag{3.5}$$

where ϕ_u and $\overline{\phi}$ are respectively an updraft conserved variable and its mean value on the grid. This equation is used to determine the evolution of updraft conservative variables such as the liquid potential temperature θ_{lu} and the total mixing ratio r_{tu} during ascent.
The vertical velocity (w_u) equation for the updraft is given by:

$$w_u \frac{\partial w_u}{\partial z} = B_u - \epsilon w_u^2 - P \tag{3.6}$$

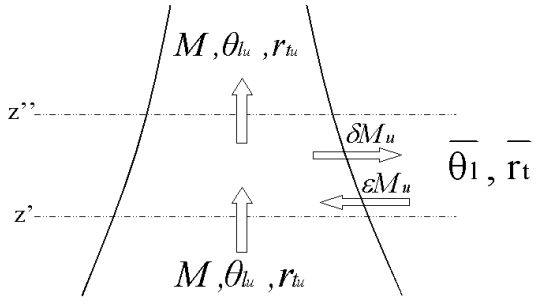

Figure 3.1: Variations of the updraft characteristics M_u, θ_{lu} and r_{tu} and dependent on the mixing with the environment dictated by the entrainment ϵM_u and the detrainment δM_u

.

where on the right-hand side (rhs), the first term is the buoyancy, the second term is the entrainment, and P represents the pressure term defined in, e.g. numerous studies (Simpson and Wiggert 1969; Siebesma et al. 2003; Soares et al. 2004) as a linear combination of the first two terms. Therefore, the equation is simplified as:

$$w_u \frac{\partial w_u}{\partial z} = aB_u - b\epsilon w_u^2 \tag{3.7}$$

where $a = 1$ and $b = 1$, defined respectively as a virtual mass coefficient and a drag coefficient (Simpson and Wiggert 1969). Numerical aspects are given in Appendix 3.3.2.
Using the definition of the mass flux, Soares et al. (2004) and Siebesma et al. (2007) were able to compute directly the mass flux in the dry portion of their updraft from the vertical velocity obtained from (3.7) and using a constant fraction area. At cloud base, they used a constant value of the cloud fractional area to compute the mass flux and to close the scheme.
Equation (3.7) is used to define the top of the updraft where w_u vanishes but also to diagnose the updraft fraction area, a_u, which is not a constant or a closure of the scheme as in Soares et al. (2004) and Siebesma et al. (2007).
Thanks to the independent computations of both mass flux M_u (3.3) and w_u (3.7), the updraft fraction area can vary vertically, and is defined as

$$a_u = \frac{M_u}{\rho w_u}. \tag{3.8}$$

The vertical variations of this last variable are important because a_u is used to diagnose the cloud fraction (see next section).
The mass flux approach is also used to realize a non-local mixing of momentum along the vertical in addition to the mixing yet realized by the turbulent scheme via the eddy-diffusivity approach. But, since the momentum is not conservative, the effect of pressure perturbations is added using a parameterization from Gregory et al. (1997). The evolution of the updraft horizontal wind component is defined as:

$$\frac{\partial u_u}{\partial z} = -\epsilon(u_u - \overline{u}) + C_u \frac{\partial \overline{u}}{\partial z}, \tag{3.9}$$

$$\frac{\partial v_u}{\partial z} = -\epsilon(v_u - \overline{v}) + C_v \frac{\partial \overline{v}}{\partial z}, \tag{3.10}$$

where $C_u = C_v = 0.5$, and u_u (v_u) represents the zonal (meridional) component of wind modified during the ascent in the updraft; $\overline{u}$ and $\overline{v}$ are zonal and meridional mean wind components respectively.

3.2.2 Lateral mass exchanges

The definition of entrainment and detrainment is the crucial issue in this type of parameterization. Various studies have used different definitions for various PBL regimes (e.g., Siebesma 1998; Neggers et al. 2002; De Rooy and Siebesma 2008).
We have chosen to define lateral mass exchanges from physical characteristics of the CBL. Arakawa (2004) explained that buoyancy is an important parameter in shallow convection. Moreover, the vertical velocity w_u is considered as a pertinent parameter in the description of mixing between dry updraft or the cloud and their environment in shallow convection. Neggers et al. (2002) defined the entrainment as inversely proportional to vertical velocity for shallow cumulus convection, and Cheinet (2003) also applies this formulation to dry plumes. This means that ϵ is not constant but decreases with higher vertical velocities. In other terms, an updraft with strong vertical velocity will be isolated from its environment.
In the dry portion of the CBL, ϵ and δ take into account physical characteristics of a buoyant ascending parcel. Equation (3.7) shows that buoyancy is linked to vertical velocity, ${w_u}^2$ being a vertical integral of the buoyancy. However, locally, both can be independent, for example in the non-buoyant part where negative buoyant air can still be ascending. Young (1988) explained that the correlation between buoyancy and w decreases in the upper part of the CBL, the buoyancy acting as a displacing force in the lower part of the CBL and as a restoring force in the upper part of the CBL. Thus, lateral mixing does not only depend on the vertical velocity as in Neggers et al. (2002) but must be locally defined as an equilibrium between w_u and buoyancy B_u. By dimensional analysis (Buckingham 1914), we obtain:

$$\epsilon_{dry}, \delta_{dry} \propto \frac{B_u}{w_u^2} \tag{3.11}$$

where $B_u = g(\theta_{v,u} - \overline{\theta_v})/\overline{\theta_v}$ is the buoyancy of the air parcels in the updraft.
Near the ground, a relative strong buoyancy and a weak vertical velocity allow strong entrainment to import many air parcels in the updraft, implying a positive proportionality coefficient for ϵ. Near the inversion, in the non-buoyant zone, much air is detrained implying a negative proportionality coefficient for δ. Since entrainment and detrainment rates cannot be negative, the entrainment rate is zero where the updraft is non-buoyant compared to its surrounding environment. Conditional sampling of detrainment in LES has shown that detrainment is not null in the mixed layer (see Fig. 9c of Pergaud et al. (2009)), so to keep a positive detrainment in the buoyant part of the updraft, a minimum detrainment is defined using a modified formulation from Lappen and Randall (2001): $\delta = (L_{up} - z)^{-1}$.
Eventually, in the dry portion of the CBL, entrainment and detrainment are defined as:

$$\epsilon_{dry} = Max\left[0, C_\epsilon \frac{B_u}{w_u^2}\right], \tag{3.12}$$

$$\delta_{dry} = Max\left[\frac{1}{L_{up} - z}, C_\delta \frac{B_u}{w_u^2}\right], \tag{3.13}$$

where L_{up} is the Bougeault and Lacarrère (1989) (BL89) upward mixing length, C_δ and C_ϵ have

been tuned to fit one-dimensional (1D) entrainment and detrainment to LES, $C_\delta = -10$ and $C_\epsilon = 0.55$. Numerical aspects are given in Appendix 3.3.3.
In the cloudy part, several descriptions of the exchanges exist.
We have chosen to define two different types of exchange differentiating the dry portion of the updraft from the moist one due to the fact that the environment of any updraft is strongly turbulent compared to the environment of a cloud. Taylor and Baker (1991) have emphasized the importance of buoyancy sorting in determining the cloud composition and in defining a continued lateral entrainment and detrainment. Zhao and Austin (2003) explained that a buoyancy sorting model can be used as a physically more realistic alternative to entraining plume models in shallow cumulus convection resolving notably the Warner paradox. In the parameterization presented here, if the lifting condensation level (LCL) is reached, lateral exchanges are computed using the parcel buoyancy sorting approach of Kain and Fritsch (1990) (KF90 in the following). Details are given in Kain and Fritsch (1990) and Bechtold et al. (2001) and you can see the chapter dealing with the Kain-Fritsch-Bechtold convection scheme. However, minor modifications have been put in the EDKF parameterization, the new parameterization uses a uniform distribution of the air parcels although, in the original formulation, the distribution was Gaussian.

3.2.3 Scheme initialization and closure

Since the scheme is integrated upward from the surface (level z_{grd}), $M_u(z_{grd})$ is computed as a function of w_* as in Grant (2001) but at the surface, contrary to the closure at the cloud base defined by Grant (2001),

$$M_u(z_{grd}) = C_{M_0}\rho(\frac{g}{\overline{\theta}_{vref}}\overline{w'\theta'_{vs}}L_{up})^{1/3} \tag{3.14}$$

where $\overline{w'\theta'_{vs}}$ is the surface buoyancy flux, L_{up} is the BL89 upward mixing length corresponding to the distance that a parcel leaving the ground travel due to buoyancy. The value of $C_{M_0} = 0.065$ is based on LES results according to Pergaud et al. (2009). Note that, in the surface layer, this value is larger than the value $C_{M_0} = 0.03$ originally proposed by Grant (2001) at the LCL.
The rising parcel characteristics are determined at the ground using the formulation of Soares et al. (2004) in which an excess is added to the environmental values. For example, the updraft liquid potential temperature near the ground is:

$$\theta_{lu}(z_{grd}) = \overline{\theta_l}(z_{grd}) + \alpha\frac{\overline{w'\theta'_{ls}}}{e^{1/2}(z_{grd})} \tag{3.15}$$

where the value of α is 0.3 as in Soares et al. (2004). Sensitivity tests in the range [0,1] indicate that results are independent of α. This excess is formulated as a function of the surface-layer variability according to Troen and Mahrt (1986) who demonstrated that the excess is well correlated with the ratio of the surface heat flux and the square root of turbulent kinetic energy. A similar equation is used for r_t.
At the surface, w_u is initialized from the turbulent kinetic energy e (provided by the turbulence scheme),

$${w_u}^2(z_{grd}) = \frac{2}{3}e(z_{grd}). \tag{3.16}$$

3.2.4 The subgrid condensation scheme

The updraft scheme represents the dynamical evolution of an air parcel during its ascent. Condensation can occur within the parcel. Therefore, a diagnostic sub-grid cloud based on the updraft

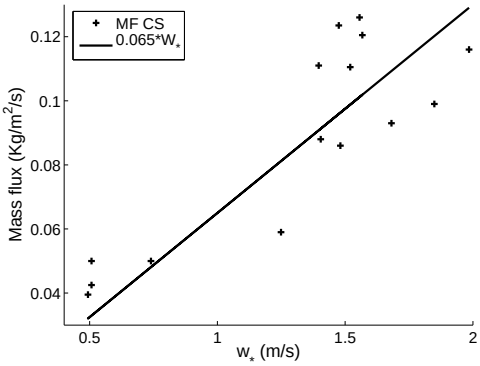

Figure 3.2: Mass flux in the surface layer computed using the Conditionnal Sampling defined in Pergaud et al. (2009) versus sub-cloud layer velocity scale w_*. Line shows $M = 0.065 w_*$.

characteristics is added. Although conservative variables are used, we can diagnose a sub-grid liquid mixing ratio $r_{c_{up}}$ and a cloud fraction CF. $r_{c_{up}}$ is computed from θ_l, r_t and pressure using a variation of all or nothing scheme since the updraft air parcels are considered completely cloudy. CF is defined proportional to the updraft fraction on the grid a_u:

$$CF = C_{cf} * a_u \tag{3.17}$$

where $C_{cf} = 2.5$. The horizontal size of the cloud is 2.5 times the size of the updraft. This parameter has been tuned to fit the 1D cloud fraction to LES results. This coefficient represents the difference between cloudy core fraction and cloud fraction.
The liquid mixing ratio can be approximated by the product between the cloud fraction previously computed and the updraft liquid mixing ratio computed from the updraft conservative variables (Bechtold and Cuijpers 1995):

$$\overline{r_c} = CF * r_{c_{up}} \tag{3.18}$$

In our parameterization, r_c is not a prognostic variable. If the mass flux becomes null, the cloud disappears totally. Only a prognostic cloud scheme can evaporate a cloud over several timesteps. So passive clouds that are not maintained by a thermal are not taken into account in the parameterization. However, here, $\overline{r_c}$ represents only the contribution of the shallow convection clouds. Others contributions for clouds can come from the subgrid turbulence scheme or from microphysics scheme (notably for resolved clouds).

3.3 Appendix

3.3.1 Mass flux in the surface layer compared to w_*

The mass flux near the surface has been set proportional to the convective vertical velocity scale w_* as in Grant (2001). The coefficient of proportionality C_{M_0} in our scheme cannot have the same value than the one used by Grant (2001) due to the fact that Grant (2001) defines this relation at the LCL. So we used the CS defined in Pergaud et al. (2009) to obtain mass flux values in the surface layer for different convective cases at different dates (IHOP, ARM).
Figure 3.2 is a plot of the surface layer mass flux against sub-cloud layer velocity scale. The LES data suggest that $C_{M_0} = 0.065$.

3.3.2 Analytical solution for the vertical velocity w_u

Equation (3.7) presents the computation for vertical velocity in the updraft w_u. Combining the equation for entrainment (3.13), the w_u equation becomes :

$$\frac{\partial {w_u}^2}{\partial z} = 2aB_u - 2bC_\epsilon max(0, B_u) \tag{3.19}$$

C_{BUO} is defined equal to $2a$ if $B_u < 0$ (entrainment is zero) and to $2(a - bC_\epsilon)$ if $B_u > 0$. This equation is integrated over each layer. Figure 3.3 presents this integral. If z' is layer bottom, z'' is layer top and $\Delta z_D = z'' - z'$, ${w_u}^2$ is defined by:

$$\int_{\Delta z_D} \frac{\partial {w_u}^2}{\partial z} dz = \int_{\Delta z_D} C_{BUO} B_u dz \tag{3.20}$$

$${w_u}^2(z'') - {w_u}^2(z') = C_{BUO} \frac{g}{\theta_{ref}} \int_{\Delta z_D} \left[\theta_{v_{up}}(z) - \overline{\theta_v}(z)\right] dz \tag{3.21}$$

θ_{vup} is assumed constant between z' and z'', and the variations of $\overline{\theta_v}$ is supposed linear between z' and z".

$$\overline{\theta_v}(z) = \alpha_1 z + \overline{\theta_v}(z') \tag{3.22}$$

$$\theta_{v_{up}}(z) = \theta_{v_{up}}(z') \tag{3.23}$$

So the integral for w_u becomes

$${w_u}^2(z'') - {w_u}^2(z') = C_{BUO} \frac{g}{\theta_{ref}} \int_{\Delta z_D} \left[-\alpha_1 z - \overline{\theta_v}(z') + \theta_{v_{up}}(z')\right] dz \tag{3.24}$$

After computation, w_u at the level z'' computed from the level z' is :

$${w_u}^2(z'') = C_{BUO} \frac{g}{\theta_{ref}} \Delta z_D \left(\frac{-\alpha_1}{2} \Delta z_D - \overline{\theta_v}(z') + \theta_{v_{up}}(z')\right) + {w_u}^2(z') \tag{3.25}$$

3.3.3 Analytical integrated solution for entrainment and detrainment

The entrainment ϵ is defined by equation (3.13). This equation is integrated, as for w_u, on each vertical grid size for example between z' and z'' (see on Fig. 3.3):

$$\epsilon = \frac{C_\epsilon}{\Delta z_D} \int_{\Delta z_D} \frac{B}{{w_u}^2} dz \tag{3.26}$$

Using (3.25), ϵ becomes

$$\epsilon = \frac{C_\epsilon g}{\Delta z_D \theta_{ref}} \int_{\Delta z_D} \frac{\theta_{v_{up}}(z') - \alpha_1 z + \overline{\theta_v}(z')}{C_{BUO} \frac{g}{\theta_{ref}} z(-\alpha_1 z - \overline{\theta_v}(z') + \theta_{v_{up}}(z')) + {w_u}^2(z')} dz \tag{3.27}$$

$$\epsilon = \frac{C_\epsilon}{\Delta z_D C_{BUO}} \int_{\Delta z_D} \frac{-\alpha_1 z + \theta_{v_{up}}(z') + \overline{\theta_v}(z')}{\frac{-\alpha_1}{2} z^2 - \overline{\theta_v}(z') z + \theta_{v_{up}}(z') z) + \frac{\theta_{ref} {w_u}^2(z')}{g C_{BUO}}} dz. \tag{3.28}$$

noting $X = \frac{-\alpha_1}{2} z^2 - \overline{\theta_v}(z') z + \theta_{v_{up}}(z') z) + \frac{\theta_{ref} {w_u}^2(z')}{g C_{BUO}}$:

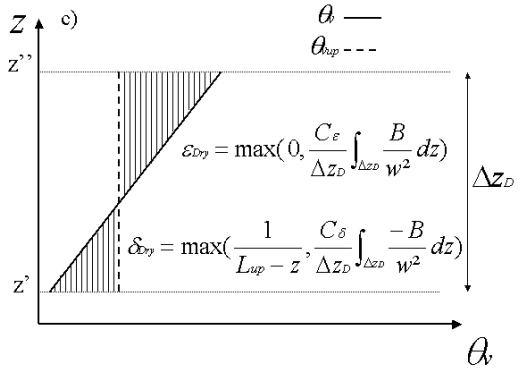

Figure 3.3: Parameterized entrainment and detrainment for dry layer

$$dX = ((-\alpha_1)z + \theta_{v_{up}}(z') + \overline{\theta_v}(z'))dz \tag{3.29}$$

$$\epsilon = \frac{C_\epsilon}{C_{BUO}\Delta z_D}\int_{\Delta z_D}\frac{dX}{X} \tag{3.30}$$

$$\epsilon = \frac{C_\epsilon}{C_{BUO}\Delta z_D}[Ln(X)]_{\Delta z_D} \tag{3.31}$$

After computation, ϵ is defined as :

$$\epsilon = \frac{C_\epsilon}{C_{BUO}\Delta z_D} ln\left[1 + \frac{C_{BUO}\Delta z_D}{{w_u}^2(z')\theta_{ref}}(\frac{-\alpha_1}{2}\Delta z - \theta_{v_{up}}(z') + \overline{\theta_v}(z'))\right] \tag{3.32}$$

where α_1 is defined as previously. An identical solution can be found for δ taking the absolute value of the buoyancy.
A formulation of the transition between cloudy and dry regime is added to limit the sensitivity of the scheme to the change in the computation of entrainment and detrainment. If a liquid mixing ratio is detected at z" using an "all or nothing" adjustment from updraft variables, the LCL height is determined assuming a linear increase of r_c with height. A weight for the KF90 lateral exchanges is defined proportional to the cloudy part occupying grid and integral dry entrainment and detrainment are computed only on the height of the dry part.

3.4 References

Arakawa, A., 2004: The Cumulus Parameterization Problem: Past, Present, and Future. *J. Clim.*, **17**, 2493–2525.

Bechtold, P., and J. W. M. Cuijpers, 1995: Cloud perturbations of temperature and humidity: A LES study. *Bound. Layer. Meteor.*, **76**, 377–386.

Bechtold, P., E. Bazile, P. Mascart and E. Richard, 2001: A Mass flux convection scheme for regional and global models. *Quart. J. Roy. Meteor. Soc.*, **127**, 869-886.

Bougeault, P, and P. Lacarrère, 1989: Parameterization of Orography-Induced Turbulence in a Mesobeta-Scale Model. *Mon. Wea. Rev.*, **117**, 1872–1890.

Buckingham, E., 1914: On physically similar systems: Illustrations of the use of dimensional equations. *Phys. Rev.*, **IV**, 345–376.

Cheinet, S., 2003: A multiple Mass-Flux Parameterization for the Surface-Generated Convection. Part1: Dry Plumes. *J. Atmos. Sci.*, **60**, 2313–2327.

Cuxart, J., P. Bougeault, and J.-L. Redelsperger, 2000: A turbulence scheme allowing for mesoscale and large-eddy simulations. *Quart. J. Roy. Meteor. Soc.*, **126,** 1–30.

De Rooy, W. C., and P. Siebesma, 2008: A simple parameterization for detrainment in shallow cumulus. *Mon. Wea. Rev.*, **136**, 560–576.

Grant, A. L. M., 2001: Cloud-base fluxes in the cumulus-capped boundary layer. *Quart. J. Roy. Meteor. Soc.*, **127**, 407–421.

Gregory, D., R. Kershaw, and P. M. Inness, 1997: Parametrization of momentum transport by convection. II: Tests in single-column and general circulation models. *Quart. J. Roy. Meteor. Soc.*, **123**, 1153–1183.

Hourdin, F., F. Couvreux, and L. Menut, 2002: Parameterization of the Dry Convective Boundary Layer Based on a Mass Flux Representation of Thermals. *J. Atmos. Sci.*, **59**, 1105–1122.

Kain, J. S., and J. M. Fritsch, 1990: A one-dimensional entraining/detraining plume model and its application in convective parameterizations. *J. Atmos. Sci.*, **47**, 2784-2802.

Lappen, C. L., and D. A. Randall, 2001: Toward a Unified Parameterization of the Boundary Layer and Moist Convection. Part2 : Lateral Mass Exchanges and Subplume-Scale Fluxes. *J. Atmos. Sci.*, **58**, 2037–2051.

Neggers, R. A. J., P. Siebesma, and H. J. J. Jonker, 2002: A Multiparcel Model for Shallow Cumulus Convection. *J. Atmos. Sci.*, **59**, 1655–1668.

Pergaud, J., V. Masson, S. Malardel, and F. Couvreux, 2009: A Parameterization of Dry Thermals and Shallow Cumuli for Mesoscale Numerical Weather Prediction. *submitted to Bound. Layer. Meteor*.

Siebesma, P., 1998: Shallow Cumulus Convection. In *"Buoyant convection in geophysical flows"* (Eds. E.J. Plate et al), 441–486.

Siebesma, P., C. S. Bretherton, A. Brown, A. Chlond, J. Cuxart, P. G. Duynkerke, H. Jiang, M. Khairoutdinov, D. Lewellen, C. H. Moeng, E. Sanchez, B. Stevens, and D. E. Stevens, 2003: A Large Eddy Simulation Intercomparaison Study of Shallow Cumulus Convection. *J. Atmos. Sci.*, **60**, 1201–1219.

Siebesma, P., P. M. M. Soares, and J. Teixeira, 2007: A combined Eddy-Diffusivity Mass-Flux approach for the convective boundary layer. *J. Atmos. Sci.*, **64**, 1230–1248.

Simpson J, and V. Wiggert, 1969: Models of precipitating cumulus towers. *Mon. Wea. Rev.*, **97**, 471–489.

Soares, P. M. M., P. M. A. Miranda, A. P. Siebesma, and J. Teixeira, 2004: An Eddy-Diffusivity/Mass-Flux parameterization for dry and shallow cumulus convection. *Quart. J. Roy. Meteor. Soc.*, **130**, 3055–3079.

Taylor, G. R., and M. B. Baker, 1991: Entrainment and Detrainment in cumulus clouds. *J. Atmos. Sci.*, **48**, 112–121.

Troen, I. B., and L. Mahrt, 1986: A simple model of the atmospheric boundary layer: Sensitivity to surface evaporation. *Bound. Layer. Meteor*, **37**, 129–148.

Young, G. S., 1988: Turbulence Structure of the convective Boundary Layer. Part II: Phoenix 78 Aircraft Observations of Thermals and their environment. *J. Atmos. Sci.*, **45**, 727–735.

Zhao, M., and P. H. Austin, 2003: Episodic Mixing and Buoyancy-Sorting Representations of Shallow Convection: A Diagnostic Study. *J. Atmos. Sci.*, **60**, 892–912.

Chapter 4

Convection Scheme

Contents

4.1 Introduction

It has been well recognized since the 1960s (e.g. Charney and Eliassen 1964; Manabe and Strickler 1964; Kuo 1965; Ooyama 1971; Yanai et al. 1973) that cumulus convection is one of the major processes that affects the dynamics and energetics of atmospheric circulation systems. Since then many cumulus parameterization schemes have been developed for numerical weather prediction (NWP) models and General Circulation Models (GCMs), to account for the subgrid-scale release of latent heat and mass transport associated with convective clouds. A non-exhaustive list of these

schemes includes e.g. Arakawa and Schubert (1974), Anthes (1977), Kuo and Raymond (1980), Fritsch and Chappell (1980), Bougeault (1985), Betts and Miller (1986), Tiedtke (1989), Gregory and Rowntree (1990), Kain and Fritsch (1990), Emanuel (1991), Donner (1993), Grell (1993), Wang and Randall (1996), Sun and Haines (1996), and Hu (1997). The common point of all cumulus parameterizations is that they aim to diagnose the presence of larger-scale conditions that would support the development of convective activity and, under appropriate conditions, to introduce tendencies for temperature and moisture (and possibly momentum) that would be consistent with the effects of convective activity. In particular, most parameterizations are designed to drive the model atmosphere towards a convectively adjusted state when they activate. This adjusted state is either predefined ("adjustment" schemes) or is computed using a bulk or spectral cloud model and adjusting the atmosphere through mass exchange between the cloud and the environment (mass flux schemes).

Two necessary characteristics of any convective parameterization are i) a reasonable set of criteria to determine when convective adjustment should be initiated, and ii) reasonable procedures for determining the characteristics of a final convectively-adjusted state. In fully prognostic dynamic models, the efficacy of a convection parameterization is often measured by factors such as i) does it activate at the right time and place? ii) does it produce the right amount and areal coverage of precipitation? and iii) does it enhance the predictive skill of its host model? Of course, there are many ways of evaluating these measures, and the third criteria above, in particular, depends on the needs of the user. For example, from the practical point of view of a weather forecaster, a convection scheme used in a mesoscale model for a 1-2 day forecast provides valuable information if it has skill in predicting the initiation and evolution of convective events, especially if they involve severe convection. In addition, convective parameterization plays a critically important role in the accurate quantitative prediction of rainfall, especially heavy rain episodes, which present a major challenge for forecasters (Kuo et al. 1997; Fritsch et al. 1998). In contrast, for long-range GCM integrations a convective parameterization may be judged to be successful if it enhances the ability of the model to accurately represent the mean climate and variability of the tropical atmosphere. Because of these seemingly disparate expectations, cumulus parameterizations have been developed typically with a particular application in mind and may contain inherent biases toward that application.

It seems reasonable, however, to expect that, to the extent that the essential physics of convection can be represented in the crude framework of a parameterization in a manner that is compatible with the numerics of modeling systems, it might be possible to develop a parameterization that is useful over a broad range of scales and type of applications. Fundamentally, we believe that, beyond the detection of convective activity, a primary purpose of convective parameterization is to mitigate the effects of inappropriate scale-selection in a modeling system's representation of deep convection. In particular, we propose that if a parameterization nudges towards a reasonable adjusted state, that its imposed time-scale of adjustment is reasonable, and that it activates in a timely manner, it can perform well in a variety of convective environments and model configurations. In this context a convection parameterization has been developped on the basis of existing frameworks, essentially the rather general framework proposed by Kain and Fritsch (1993). The parameterization is intended to provide an efficient representation of atmospheric shallow and deep convection for both mesoscale and global applications.

A detailed description of the scheme is provided below, however numerical applications in different 1D, mesoscale and global contexts are discussed in Bechtold et al. (2001) and Mallet et al. (1999). Further 1D evaluations of the scheme and intercomparisons with other models/schemes are presented in Xie et al. (2002) and Bechtold et al. (2000) in the context of the international pro-

gram GCSS (GEWEX Cloud System Study). The corresponding computer code is also available as an optimized portable routine (both in Meso-NH and ECMWF/ARPEGE IFS code structure) in Fortran 90 on upon request from P. Bechtold (now at ECMWF).

4.2 Mass flux equations

Briefly, with the aid of the mass flux approximation the effect of a convective cloud population on its environment can be written (see e.g. Arakawa and Schubert (1974), Gregory and Miller (1989), Betts (1997) for various derivations)

$$\left.\frac{\partial\overline{\Psi}}{\partial t}\right|_{\rm conv} = \frac{\partial(\overline{w'\Psi'})}{\partial z} \tag{4.1}$$

$$\approx \frac{1}{\overline{\rho}A}\frac{\partial}{\partial z}\left[M^u(\Psi^u-\overline{\Psi})+M^d(\Psi^d-\overline{\Psi})+\tilde{M}(\tilde{\Psi}-\overline{\Psi})\right]$$

$$\approx \frac{1}{\overline{\rho}A}\frac{\partial}{\partial z}\left[M^u\Psi^u+M^d\Psi^d-(M^u+M^d)\overline{\Psi}\right], \tag{4.2}$$

where Ψ is a conserved variable, $M=\overline{\rho}wA$ is the mass flux (kg s^{-1}), w the vertical velocity, and $A=A^u+A^d+\tilde{A}$ denotes the horizontal domain (grid size). Overbars denote ensemble mean (horizontal grid mean) values, tildes denote environmental values, up-and downdraft values are denoted by superscripts u and d, respectively. Furthermore, describing the mass exchange of the cloud ensemble with its environment by entrainment ϵ and detrainment δ, i.e.

$$\frac{\partial}{\partial z}(M^u\Psi^u)=\epsilon^u\overline{\Psi}-\delta^u\Psi^u; \qquad \frac{\partial}{\partial z}(M^d\Psi^d)=\epsilon^d\overline{\Psi}-\delta^d\Psi^d \tag{4.3}$$

we obtain the final result

$$\left.\frac{\partial\overline{\Psi}}{\partial t}\right|_{\rm conv}=\frac{1}{\overline{\rho}A}\left[\frac{\partial}{\partial z}([M^u+M^d]\overline{\Psi})-[\epsilon^u+\epsilon^d]\overline{\Psi}+\delta^u\Psi^u+\delta^d\Psi^d\right]. \tag{4.4}$$

It can be shown that this equation is also valid for non-conserved variables, i.e. temperature or water mixing ratios.

4.3 Cloud model

The ensemble average updraft and downdraft properties in (4.4) are determined with the aid of a one-dimensional cloud model that consists of a classical steady-state plume convective updraft, and a corresponding steady-state plume convective downdraft. The cloud model is designed to represent shallow and deep convective clouds that are characterized by their respective cloud radius.

4.3.1 Key cloud levels

First, it is useful to define the model cloud and a certain number of important levels in the cloud that will be needed in the following discussion. As illustrated in Fig. 4.1 the model cloud extends upward from the lifting condensation level (LCL) of an air parcel with departure level DPL

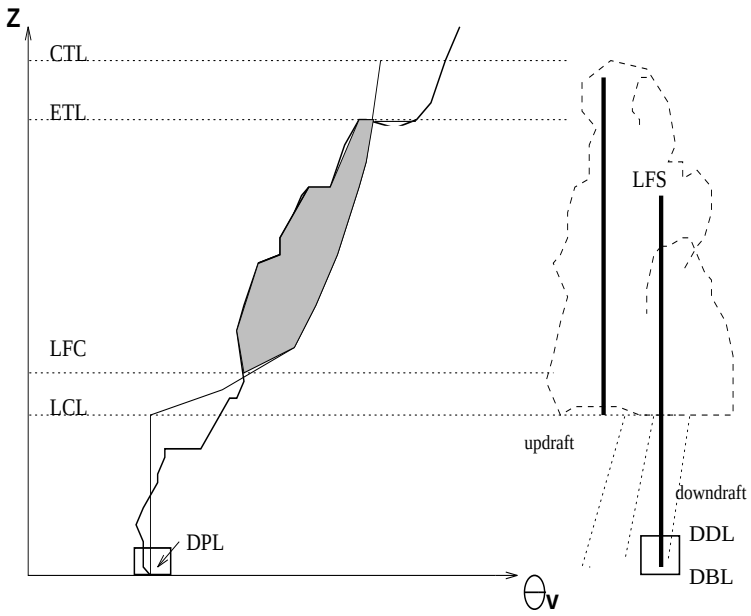

Figure 4.1: Environmental (thick solid line) and parcel sounding (thin solid line) of θ_v in a deep convective cloud. The convective available energy (CAPE) corresponds to the shaded area. The different key cloud levels are related to condensation and buoyancy. The updraft and downdraft regions are illustrated by the fat solid lines (the cloud is supposed to precipitate).

(DPL actually denotes a 60 hPa thick mixed layer) to the cloud top level (CTL). The level of free convection (LFC) is the level where the updraft becomes positively buoyant with respect to the environment, and the equilibrium temperature level (ETL) is the level where the buoyancy of the updraft redrops to zero. The convective available potential energy is defined as the positive area (from the LFC to the ETL) between the incloud virtual potential temperature sounding and the environmental sounding. The downdraft originates within the cloud at the level of free sink (LFS), and extends down to the downdraft base level (DBL). All downdraft mass is detrained over a fixed layer extending from DDL to DBL. Finally, note that the DPL and the DBL are of course not necessarily equal to the surface level, the present figure serving only as an example.
The following discussion of the different parts of the convection scheme is straightforward in the way that it closely follows the sequential structure of the scheme.

4.3.2 Trigger function

At present time, the physical processes initiating convection are not well understood. There is no general criterion that tells us when we should allow for convective overturning of the atmosphere; i.e. when we should allow a moist convective parcel to overcome the stable layer at cloud base and to have access to the CAPE that is stored aloft due to large scale forcing associated with e.g. midlatitude frontal systems, upper level jets or tropical waves. However, another important issue is the determination of the moist source layer for convection that will be lifted up and will finally determine the properties of the convective cloud (cloud top level, precipitation, etc.). It turns out that over the tropical ocean this initial moist layer corresponds to the 500-m deep boundary layer (Raymond 1995) and the most difficult problem is to locate the convection. However, in midlatitude convection, especially at night time, convection might root at upper atmospheric levels.

The numerical formalism is as follows. Starting from the ground level, we first construct an at least 60-hPa deep mixed layer with mean potential temperature $\overline{\theta}^{mix}$ and vapor mixing ratio $\overline{r}_v^{mix}$. Then this mixed air parcel is lifted without entrainment to its LCL. We directly determine the temperature at the LCL using an algorithm proposed by Davies-Jones (1983), and compute the pressure at the LCL as $P(\mathrm{LCL}) = P_{00}[T(\mathrm{LCL})/\theta^{mix}]^{C_{pd}/R_d}$, where P_{00} is the reference pressure. The air parcel is unstable with respect to moist convection if at the LCL

$$\overline{\theta}_v^{mix} - \overline{\theta}_v + \Delta T/\Pi \ > 0, \tag{4.5}$$

with θ_v the virtual potential temperature, and with the Exner function defined as $\Pi = (P/P_{00})^{R_d/C_{pd}}$. For shallow convection the temperature increment ΔT is simply set to 0.2 K. For deep convection ΔT is intended to crudely trigger/suppress convection as a function of grid-scale motion, where it is defined by $\Delta T = \pm c_w \ |\overline{w}|^{1/3}$, with c_w=6 (K m$^{-1/3}$ s$^{1/3}$). The sign of ΔT is equal to the sign of $\overline{w}$. As the large-scale vertical velocity varies quasi-linearly as a function of the grid size, it is normalized by $\overline{w}\sqrt{A}/\Delta x_{ref}$, with Δx_{ref} the 25-km reference grid space. Furthermore, we test if the air parcel is able to produce a sufficient cloud depth (at least 3 km for deep convection, and 500 m for shallow convection) by lifting the mixed layer parcel conserving the equivalent potential temperature $\theta_e(\overline{\theta}^{mix}, \overline{r}_v^{mix})$, and searching for the intersection with the environmental saturated curve $\theta_{es}(\overline{T})$ (see e.g. Raymond 1995). If the air parcel is stable with respect to moist convection or if its probable cloud thickness is smaller than the specified value, the above procedure is repeated starting at the next higher 60-hPa mixed layer, and so on.

4.3.3 Updraft

Updrafts are assumed to originate at the DPL, entrain environmental air in the mixed layer, and then undergo undilute ascent up to the LCL. Starting from the LCL the thermodynamic characteristics of the updraft are computed assuming conservation (except from precipitation processes) of enthalpy or "liquid water static energy" h_{il} and total water mixing ratio r_w

$$h_{il} = C_{pm}T - L_v r_c - L_s r_i + (1 + r_w)gz \tag{4.6}$$
$$r_w = r_v + r_c + r_i. \tag{4.7}$$

where the specific heat of moist air is defined as $C_{pm} = C_{pd} + r_w C_{pv}$, g denotes the gravity constant, and r_v, r_c and r_i denote the maxing ratios of water vapor and non-precipitating cloud water/ice, respectively. A derivation of h_{il} is provided in the Appendix together with a definition of the various thermodynamic constants and functions used. The choice of h_{il} is motivated by the fact that it is linear, conserved in the presence of glaciation processes, and easily allows to switch on/off glaciation processes in the model.
The updraft computations are initiated at the LCL using $h_{il}^u = C_{pm}T(\mathrm{LCL}) + (1 + r_v^{mix})gz(\mathrm{LCL})$ and $r_w^u = r_v^{mix}$. The initial updraft mass flux is set to a unit value of $M^u(\mathrm{LCL}) = \overline{\rho}\, w_{\mathrm{LCL}}\, \pi R_0^2$, with a vertical velocity w_{LCL} of 1 m s^{-1} and an updraft radius R_0 of 1500 m for deep and 50 m for shallow convection - all the different parameter switches for deep and shallow convection are summarized in Table 4.1.
Hereafter we switch to the discretized equations on a vertical model grid k, with k increasing with height. The upstream operator is denoted by $\Delta\Psi = \Psi^{k+1} - \Psi^k$, layer mean values are denoted by the additional superscript m. If no superscript is indicated we simply mean the current model level k. Furthermore, it is convenient to denote the entrainment/detrainment rates ϵ and δ in mass

Table 4.1: Parameters and settings for deep and shallow convection

Parameter	deep	shallow
cloud radius (m)	1500	50
minimum cloud thickness (m)	3000	500
adjustment time (h)	$0.5 < \tau < 1$	3
ΔT (K) in "trigger"	computed from $\overline{w}$	0.2
downdraft	yes	no
precipitation	yes	no

flux units kg s^{-1} instead of units mass flux per length as used in (4.2)-(4.4). In this notation the updraft mass flux as well as the updraft values of h_{il} and r_w change through mixing, detrainment and precipitation according to

$$\Delta M^u = \epsilon^{um} - \delta^{um} \tag{4.8}$$

$$\Delta(M^u h^u_{il}) = \epsilon^{um}\overline{h}_{il} - \delta^{um} h^u_{il} + M^{u(k+1)}(L_v \Delta r_r + L_s \Delta r_s) \tag{4.9}$$

$$\Delta(M^u r^u_w) = \epsilon^{um}\overline{r}_w - \delta^{um} r^u_w - M^{u(k+1)}(\Delta r_r + \Delta r_s). \tag{4.10}$$

The system (4.8)-(4.10) is solved together with a parameterization of microphysics and mixing that are described separately.

Microphysics and updraft velocity

The condensate mixing ratios r^u_c, r^u_i are deduced from h^u_{il} and r^u_w using a saturation adjustment, and allowing a gradual glaciation of the cloud in the temperature range between 268 and 248 K (see also Tao et al. 1989). The liquid and solid precipitation $\Delta r_r + \Delta r_s$ produced in each model layer is computed following Ogura and Cho (1973)

$$\Delta r_r + \Delta r_s = (r^{um}_c + r^{um}_i)(1 - exp[-c_{pr}\Delta z / w^{um}]), \tag{4.11}$$

where $c_{pr} = 0.02$ s^{-1} is a condensate to precipitation conversion factor. This formulation is essentially based on the fact that in high speed updrafts precipitation particles do not have time to form or are carried upward by the draft. The updraft vertical velocity w^u is evaluated with the aid of

$$\Delta((w^u)^2) = \frac{2g}{1+\gamma}\left[\frac{\theta^{um}_v - \overline{\theta}^m_v}{\overline{\theta}^m_v}\right]\Delta z - 2\frac{\epsilon^u}{M^u}(w^u)^2, \tag{4.12}$$

where $\theta_v = \theta(1 + R_v/R_d\ r_v)/(1 + r_w)$, and $\gamma = 0.5$ is the virtual mass coefficient that approximately takes into account non-hydrostatic pressure perturbations (Kuo and Raymond 1980). The last term of the rhs of (4.12) accounts for zero environmental momentum. The vertical velocity is also used to compute the cloud top level CTL, which is defined as the level where $(w^u)^2$ becomes negative. Finally, the total precipitation flux produced by the updraft is simply given by

$$\mathrm{Pr} = \sum_{k=\mathrm{LCL}}^{k=\mathrm{CTL}} [\Delta r_r + \Delta r_s] M^u. \tag{4.13}$$

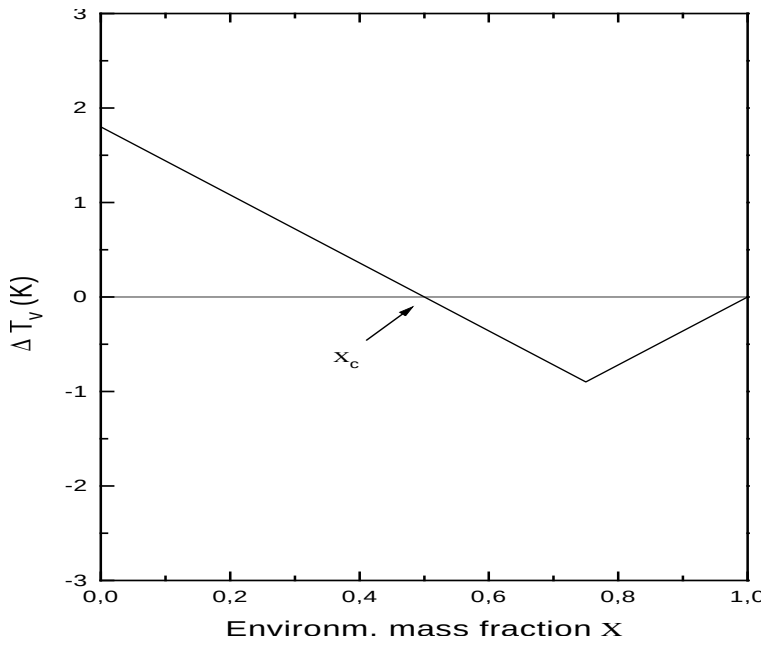

Figure 4.2: Plot of typical virtual temperature differences between updraft-environment mixtures and that of the environment as a function of the fraction of environmental mass in the mixtures.

Entrainment and detrainment

Unfortunately, the performance of a plume cloud model critically depends on the specification of updraft entrainment/detrainment rates which are functions of the cloud radius, and are generally assumed to be constant with height. We initially adopted the mixing formalism proposed by Kain and Fritsch (1990) where an ensemble of mixed parcels is generated, with positively buoyant parcels supposed to follow the cloudy updraft (entrain) and negatively buoyant parcels supposed to detrain. Denoting the fractional amount of environmental mass that just yields a neutrally buoyant mixture as χ_c, the net environmental entrainment rate and the updraft entrainment rate are given by

$$\epsilon^u = \Delta M_t \int_0^{\chi_c} \chi \ f(\chi) d\chi \tag{4.14}$$

$$\delta^u = \Delta M_t \int_{\chi_c}^{1} (1-\chi) f(\chi) d\chi \tag{4.15}$$

$$\Delta M_t = M^u c_{\rm etr} \Delta z / R_0, \tag{4.16}$$

where ΔM_t with $c_{etr} = 0.2$ is the total rate at which mass enters the transition region between clear and cloudy air (Simpson 1983); $f(\chi)$ is a Gaussian type distribution satisfying $f(0) = f(1) = 0$ (Kain and Fritsch 1990).
The critical mixed fraction χ_c is solved for directly, knowing that the virtual temperature difference between updraft-environment mixtures and that of the unmixed environment varies linearly as a function of the environmental mass fraction χ (see Fig. 4.2). The zero crossing of this curve is evaluated from

$$\theta_v^{mix} - \overline{\theta}_v = 0 = \theta_v^u - \overline{\theta}_v - \frac{\theta_v^u - \theta_v^{mix}}{\chi} \chi_c \tag{4.17}$$

so that χ_c is given by

$$\chi_c = \frac{\theta_v^u - \overline{\theta}_v}{\theta_v^u - \theta_v^{mix}}\chi; \quad \chi = 0.1; \quad 0 \leq \chi_c \leq 1; \tag{4.18}$$

we use a small value of 0.1 for χ which is supposed to be smaller than the critical value. θ_v^{mix} is determined as a function of h_{il}^{mix} and r_w^{mix}, where $h_{il}^{mix} = \chi\overline{h}_{il} + (1-\chi)h_{il}^u$; idem for r_w^{mix}.
However, it turned out that in deep convective situations this mixing formulation often produced $\epsilon^u > \delta^u$ so that the convective mass flux always increased with height, and the upper-level mass flux was overestimated. Therefore, this mixing procedure was only retained for shallow convection. For deep convection we simply use vertically constant entrainment/detrainment rates with $\epsilon^u = \delta^u = 0.5\Delta M_t$.

Updraft flow summary

The updraft computations are an important part of the convection scheme as here we build up a characteristic precipitating cloud whose nominal mass flux is later modified by the closure assumption. The updraft computations can be summarized as follows:
1) Update CAPE for undilute ascent, i.e. assuming conservation of undilute θ_e at the LCL.
2) Estimate r_c^u and r_i^u at level $k+1$ setting $h_{il}^u(k+1) = h_{il}^u(k), r_w^u(k+1) = r_w^u(k)$, and applying a saturation adjustment procedure defined.
3) Compute $\theta_v^u(k+1)$ and square of vertical velocity using the just computed values of r_c^u and r_i^u in (4.12).
4) Compute precipitation produced in model layer using (4.11). Update total precipitation.
5) Update $r_c^u, r_i^u, h_{il}^u, r_w^u$ at level $k+1$ for precipitation.
6) Compute entrainment and detrainment rates at level $k+1$ using
7) Compute final values of updraft mass flux, h_{il}^u, r_w^u at level $k+1$ using (4.9)-(4.10).
8) Exit the updraft computations when the CTL is attained, i.e. when the updraft velocity becomes negative.
9) Adjust the updraft mass flux to reflect a linear decrease of the mass flux between the ETL and the CTL.

4.3.4 Downdraft

In contrast to the updraft computations where condensate production and glaciation processes are important and therefore h_{il} is a very convenient variable, the downdraft computations become simplified when using the equivalent potential temperature θ_e as it implicitly takes into account the evaporational cooling effect. The definition of θ_e is taken from Bolton (1980) and proved to be highly accurate

$$\theta_e = T(P_{00}/P)^{R_d/C_{pd}(1-0.28r_v)}\exp[(3374.6525/T - 2.5403)r_v(1+0.81r_v)]. \tag{4.19}$$

The downdraft is assumed to be driven by cooling through melting and evaporation of precipitation. It originates at the level of free sink (LFS), defined by the level of minimum environmental saturated θ_e between the LCL and the ETL. The initial values of the downdraft mass flux, θ_e and moisture at the LFS can be estimated as follows

$$M^d(LFS) = -(1 - \mathrm{Pr}_{\mathrm{eff}})M^u(LCL) \tag{4.20}$$

where the precipitation efficiency $\mathrm{Pr_{eff}}$ is given as a function of wind shear and cloud base height (Zhang and Fritsch 1986). The initial humidity is obtained by mixing updraft and environmental air

$$r_w^d(\mathrm{LFS}) = \chi \overline{r}_w + (1-\chi) r_w^u; \quad \chi = (\theta_e^u - \overline{\theta}_{es})/(\theta_e^u - \overline{\theta}_e). \tag{4.21}$$

This definition of the mixed fraction gives a very smooth variation of χ, with a value that is close to χ_c defined in (4.18). According to (4.21) the value of θ_e^d at the LFS is set to its saturated environmental value corrected by melting effects, with the cooling due to melting estimated by $\Delta T_{\mathrm{melt}} = L_m/C_{ph}[r_w^u(\mathrm{LCL}) - r_w^u(\mathrm{CTL})]$. This method is motivated by the fact that the amount of downdraft mass flux is dependent on the total downdraft evaporation rate which is not known initially and is itself dependent on the magnitude of the melting effect. We know the amount of solid precipitation but we do not know the amount of ice that is evaporated in the downdraft.

The following equations are used to compute the downdraft properties starting from the LFS down to the downdraft base level (DBL) which is defined as the level where $\theta_e^d(\mathrm{LFS}) > \overline{\theta}_{\mathrm{es}}(\overline{\mathrm{T}})$.

$$\begin{aligned}
\epsilon^d &= -M^d(\mathrm{LFS}) c_{\mathrm{etr}} \Delta z / R_0; \quad k > \mathrm{DDL} && (4.22)\\
\delta^d &= 0; \qquad\qquad\qquad\qquad\quad k > \mathrm{DDL} && (4.23)\\
\Delta M^d &= \epsilon^d && (4.24)\\
\Delta(M^d \theta_e^d) &= \epsilon^d \overline{\theta}_e && (4.25)\\
\Delta(M^d r_w^d) &= \epsilon^d \overline{r}_w. && (4.26)
\end{aligned}$$

Note that M^d is negative but ϵ^d and δ^d are positive. All downdraft detrainment is assumed to occur over the 60 hPa deep layer DDL-DBL (Fig. 4.1). For the closure adjustment procedure we will need the values of h_{il}^d. As δ^d is zero everywhere apart from the detrainment layer, we only need to compute the values of h_{il}^d for this layer. It is computed from θ_e^d and r_w^d. The total downdraft evaporation rate is estimated using a specified value of 90% for the relative humidity. If the actual value of humidity in the downdraft in the detrainment layer is less than the specified value, water is evaporated to give the required value. If no water is evaporated, no downdraft is allowed and the downdraft mass flux is set to zero.

4.3.5 Closure

Finally, a closure assumption is needed to control the intensity of convection. Here we adopt a Fritsch Chappell type closure which is based on the assumption that all convective available potential energy (CAPE) in a grid element is removed within an adjustment period τ. For deep convection τ is set to the advective time period $\tau = \sqrt{A}/|\boldsymbol{v}|$, with $\boldsymbol{v}$ the mean horizontal wind vector between the LCL and the 500-hPa level, and is limited by 0.5 h $< \tau <$ 1 h. The upper limit roughly corresponds to one life cycle of a convective cloud. For shallow convection an adjustment time τ of 3 h is used. With the aid of the above presented cloud model we have already computed the initial guess updraft and downdraft mass fluxes and the corresponding entrainment/detrainment rates. Therefore, we are now able to compute the final convectively-adjusted environmental values (see also the main mass flux equations (4.4)) using a time integration over τ together with an iterative procedure

$$\overline{\Psi}^{(n+1)} = \overline{\Psi}^{(n)} + (\tau/m_t) \left[- \Delta(\tilde{M}^{(n)}\overline{\Psi}^{(n)}) - [\epsilon^{u(n)} + \epsilon^{d(n)}]\ \overline{\Psi}^{(n)} + \delta^{u(n)}\Psi^u + \delta^{d(n)}\Psi^d \right] \tag{4.27}$$

$$\tilde{M} = \overline{\rho}\tilde{w}A; \quad \tilde{w} = \int (\partial\tilde{w}/\partial z)dz; \quad \left(\frac{\partial\tilde{w}}{\partial z}\right) = \frac{\epsilon^u + \epsilon^d - \delta^u - \delta^d}{m_t}, \tag{4.28}$$

where n denotes the iteration number, Ψ stands for either h_{il} or the various water species r_w, r_c, r_i. The total mass of the model layer is denoted by m_t, and $\tilde{M}$ is the compensating environmental mass flux. The esssential point of the present adjustment procedure is that only the environmental values $\Psi = h_{il}, r_w, r_c, r_i$ are updated and the mass fluxes are adjusted in the closure adjustment procedure, but no updraft or downdraft computations are repeated so that the updraft and downdraft values of the thermodynamic variables keep unchanged.
Now, computing the new environmental values of θ and r_v from $\overline{h}_{il}$ and $\overline{r}_w$ using (4.6)-(4.7), we can compute $\overline{\theta}_e$ and a new value of CAPE by using undilute parcel ascent

$$\mathrm{CAPE^{(n+1)}} = \int_{\mathrm{LCL^{(n+1)}}}^{\mathrm{ETL}} g \left[\frac{\overline{\theta}_e^{(n+1)}(\mathrm{DPL})}{\overline{\theta}_{es}^{(n+1)}} - 1 \right] dz, \tag{4.29}$$

where the new value $\mathrm{LCL}^{(n+1)}$ is obtained from $\overline{\theta}_v^{(n+1)}$(DPL) by the same procedure as used in the trigger function. The use of the conserved variable $\overline{\theta}_e(DPL)$ instead of θ_v^u in (4.29) is motivated by the fact that this formulation allows to determine CAPE directly without executing additional updraft computations.
Then, at all model levels the updraft and downdraft mass fluxes as well as the entrainment/detrainment fluxes and the precipitation flux are multiplied by the adjustment factor

$$F_{adj}^{(n+1)} = F_{adj}^{(n)} \frac{\mathrm{CAPE}^{(0)}}{\mathrm{CAPE}^{(0)} - \mathrm{CAPE}^{(n+1)}}, \tag{4.30}$$

where $\mathrm{CAPE}^{(0)}$ is the initial value of CAPE. The above described procedure (4.27)-(4.30) is repeated until $\mathrm{CAPE}^{(n+1)} < 0.1\ \mathrm{CAPE}^{(0)}$. At the end of the adjustment procedure the final convective tendencies are simply evaluated as

$$\left.\frac{\partial\overline{\Psi}}{\partial t}\right|_{\mathrm{conv}} = (\overline{\Psi}^{(n)} - \overline{\Psi}^{(0)})/\tau, \tag{4.31}$$

where Ψ now stands for either θ, r_v, r_c, r_i.
A final remark concerns the conservation properties of the scheme, a point that is particularly important for long time or global applications. The scheme is designed to conserve mass and energy as can be verified numerically from the integral relationships

$$\int_0^{\mathrm{CTL}} \frac{(\epsilon^u + \epsilon^d - \delta^u - \delta^d)}{m_t} dz = 0 \tag{4.32}$$

$$\int_0^{\mathrm{CTL}} \left(\frac{\overline{\rho}}{\rho_l}\right) \left.\frac{\partial \overline{r}_w}{\partial t}\right|_{\mathrm{conv}} dz = \frac{\mathrm{Pr}}{\rho_l A} \tag{4.33}$$

$$\int_0^{\mathrm{CTL}} \left(\frac{\overline{\rho}}{\rho_l}\right) \left.\frac{\partial \overline{h}_{il}}{\partial t}\right|_{\mathrm{conv}} dz = L_v \frac{\mathrm{Pr}}{\rho_l A} \tag{4.34}$$

where ρ_l is the density of liquid water, and $\mathrm{Pr}\ \rho_l^{-1} A^{-1}$, is the adjusted surface precipitation flux in m s^{-1}.

4.4 Discussion

Our aim was to design a parameterization that incorporates the effects of the essential physics of moist convection while remaining as straightforward and numerically efficient as possible. In adhering to these guidelines, however, it is inevitable that numerous simplifications of real physical processes become necessary.

The limitations of a convective plume model to represent properties of a cloud ensemble are discussed in Warner (1970), Raymond and Blyth (1986), and Lin and Arakawa (1997). To limit these drawbacks, we also developed an ensemble version of the code, where the deep part can be called several times using different entrainment/detrainment rates (=different cloud radius), and different temperature/moisture perturbations for triggering. The resulting convective tendency is then the sum of the shallow part and the deep convective part (which is an average of the convective tendencies and mass fluxes of its individual ensemble members).

In the case of the present parameterization, an explicit dependence on grid-length is included in two places. First, grid-resolved vertical velocity, as it is used in the trigger function (see discussion related to (5)) is scaled as a linear function of grid length. Second, the convective time period is computed as the advective time period, based on the mean wind speed in the cloud layer and the model grid-length. This time period is constrained to be between 0.5 and 1 hour, however. In addition to these implicit sensitivities to horizontal resolution, certain physical processes have been neglected in the current parameterization. For example, convective transport of momentum is not yet included, but could be easily done using the scheme equations for passive tracers together with a pressure perturbation term (Kershaw and Gregory 1997) Also, we do not explicitly account for mesoscale transports that might give a substantial contribution to the mass flux at upper levels (Donner 1993; Betts 1997; Alexander and Cotton 1998), but the significance of this is largely unknown. This parameterization contains several parameters that are difficult to assess. However, extensive testing revealed minimal sensitivity to the values used for most of them, within a range of reasonable values. The most significant sensitivities appear in relation to specification of cloud radius (determining entrainment/detrainment), the precipitation efficiency (used to drive downdrafts), and to a lesser extent the adjustment time scale.

Finally, lets also mention a limitation that is related to the effects of convective downdrafts. In the atmosphere, convectively generated "cold pools" often spread out over significant areas in the vicinity of thunderstorms, and the leading edge of this cold outflow can be a region of active generation of new convective cells. Since prognostic variables are represented as horizontally-averaged values in each layer within a grid-column, parameterization schemes introduce the effects of downdrafts as a mean cooling and drying of individual layers. When these stabilizing tendencies are introduced as a mean effect, parameterized convection may "turn off" due to cooling and drying from parameterized downdrafts, whereas in reality only a portion of the total area represented by a grid element might experience intense downdraft cooling. Thus parameterization schemes may

have a tendency to underpredict convective overturning at coarser resolutions. A possible solution for this problem would be to allow for partial coverage by downdraft outflow and appropriate subgrid-scale forcing associated with outflow propagation (Liang et al. 1998).

4.5 Appendix

4.5.1 Definition of latent and specific heats

The specific latent heats of vaporisation, sublimation and melting as a function of temperature are defined by

$$\begin{aligned} L_v(T) &= L_v(T_t) + (C_{pv} - C_l)(T - T_t) && (4.35)\\ L_s(T) &= L_s(T_t) + (C_{pv} - C_s)(T - T_t) && (4.36)\\ L_m(T) &= L_s(T) - L_v(T), && (4.37) \end{aligned}$$

with

$$T_t = 273.16; \quad L_v(T_t) = 2.5008 \times 10^6 \quad L_s(T_t) = 2.8345 \times 10^6, \tag{4.38}$$

where T_t is given in K and where the specific heats for phase change are given in J kg^{-1}. The specific heat constants are defined as

$$C_{pv} = 4\ R_v; \quad C_l = 4.218 \times 10^3; \quad C_s = 2.106 \times 10^3, \tag{4.39}$$

with R_v=461.525 J kg^{-1} K^{-1}. The gas constant and specific heat for dry air are defined as R_d=287.06 J kg^{-1} K^{-1} and $C_{pd} = 7/2R_d$.

4.5.2 Derivation of h_{il}

Following Dufour and van Mieghem (1975) an accurate and natural formulation of h_{il} can be derived from the enthalpy equation

$$C_{ph}dT - T(R_d + r_v R_v)d\ln P = d(L_v r_c + L_s r_i) - \left[r_c \frac{dL_v}{dT} + r_i \frac{dL_s}{dT} \right] dT, \tag{4.40}$$

with $C_{ph} = C_{pd} + r_v C_{pv} + r_c C_l + r_i C_s$. Making use of the hydrostatic approximation and the relations (4.35)-(4.37), (4.40) can be integrated to obtain

$$h_{il} = C_{pm}T - L_v r_c - L_s r_i + (1 + r_w)gz, \tag{4.41}$$

with $C_{pm} = C_{pd} + r_w C_{pv}$.

4.5.3 Definition of saturation mixing ratios

The saturation pressure for water vapor over liquid water and ice is derived from an integration of the Clausius-Clapeyron equation

$$e_{sl}(T) = exp\left[\alpha_l - \frac{\beta_l}{T} - \gamma_l \ln(T)\right] \tag{4.42}$$

$$e_{si}(T) = exp\left[\alpha_s - \frac{\beta_s}{T} - \gamma_s \ln(T)\right], \tag{4.43}$$

where

$$\alpha_l = \ln[e_s(T_t)] + \frac{\beta_l}{T_t} + \gamma_l \ln(T_t); \quad \beta_l = \frac{L_v(T_t)}{R_v} + \gamma_l T_t$$

$$\gamma_l = \frac{(C_l - C_{pv})}{R_v}, \tag{4.44}$$

and $e_s(T_t)$ =611.14 Pa. The corresponding coefficients for the saturation pressure over ice are obtained by simply replacing in (4.44) and (4.44) the index l (liquid) by the index s (solid) and by replacing L_v by L_s. Finally, the saturated water vapor mixing ratio is defined as $r_{vs}(T) = (m_v/m_d)(e_s(T)/P - e_s(T))$, with $m_v/m_d = R_d/R_v = 0.622$ the ratio of dry air to water vapor Mol mass.

4.5.4 Precipitation efficiency

Defining the windshear by

$$S = \frac{|\boldsymbol{v}(\mathrm{CTL}) - \boldsymbol{v}(\mathrm{LCL})|}{z(\mathrm{CTL}) - z(\mathrm{LCL})} \frac{|\boldsymbol{v}(\mathrm{CTL})| - |\boldsymbol{v}(\mathrm{LCL})|}{\big||\boldsymbol{v}(\mathrm{CTL})| - |\boldsymbol{v}(\mathrm{LCL})|\big|}, \tag{4.45}$$

with $\boldsymbol{v}$ the horizontal wind vector, the precipitation efficiency as a function of wind shear is expressed as

$$\mathrm{Pr}_{\mathrm{Sef}} = 1.591 - 0.639\,S + 0.0953\,S^2 - 0.00496\,S^3. \tag{4.46}$$

The precipitation efficiency as a function of cloud base height is given as

$$\begin{aligned} \mathrm{Pr}_{\mathrm{Zef}} = 0.967 &- 0.7 z_b + 1.62 \times 10^{-1} z_b^2 - 1.26 \times 10^{-2} z_b^3 \\ &+ 4.27 \times 10^{-4} z_b^4 - 5.44 \times 10^{-6} z_b^5, \end{aligned} \tag{4.47}$$

with z_b the height difference between the LCL and the model surface level normalized by a cloud base height of 3280 m. Both $\mathrm{Pr}_{\mathrm{Sef}}$ and $\mathrm{Pr}_{\mathrm{Zef}}$ are limited to values between 0.4 and 0.92. Finally, the actual precipitation efficiency is given by $\mathrm{Pr}_{\mathrm{eff}} = 0.5(\mathrm{Pr}_{\mathrm{Sef}} + \mathrm{Pr}_{\mathrm{Zef}})$.

4.6 References

Alexander, G. D., and W. R. Cotton, 1998: The use of cloud resolving simulations of mesoscale convective systems to build a mesoscale parameterization scheme. *J. Atmos. Sci.*, **55**, 2137-2161.

Arakawa, A., and W. H. Schubert, 1974: Interaction of a cumulus cloud ensemble with the large-scale environment: Part I. *J. Atmos. Sci.*, **31**, 674-701.

Anthes, R. A., 1977: A cumulus parameterization scheme utilizing a one-dimensional cloud model. *Mon. Wea. Rev.*, **105**, 270-286.

Bechtold, P., E. Bazile, P. Mascart and E. Richard, 2001: A Mass flux convection scheme for regional and global models. *Quart. J. Roy. Meteor. Soc.*, **127**, 869-886.

Bechtold, P., J. L. Redelsperger, I. Beau, M. Blackburn, S. Brinkop, J. Y. Grandpeix, A. Grant, D. Gregory, F. Guichard, C. Hoff and E. Ioannidou, 2000: A GCSS model intercomparison for a tropical squall line observed during TOGA-COARE. II: Intercomparison of single-column models and a cloud-resolving model. *Quart. J. Roy. Meteor. Soc.*, **126**, 865-888.

Betts, A. K., and M. J. Miller, 1986: A new convective adjustment scheme. Part II: Single column tests using GATE wave, BOMEX, ATEX, and arctic air-mass data sets. *Quart. J. Roy. Meteor. Soc.*, **112**, 693-709.

———-, 1997: 'The parameterization of deep convection'. In *"The physics and parameterization of moist atmospheric convection"* (Ed. R. K. Smith), *NATO ASI Series*, **505**, 255-279.

Bolton, D., 1980: The computation of equivalent potential temperature. *Mon. Wea. Rev.*, **108**, 1046-1053.

Bougeault, P., 1985: A simple parameterization of the large-scale effects of cumulus convection. *Mon. Wea. Rev.*, **113**, 2108-2121.

Bretherton, C. S., and P. K. Smolarkiewicz, 1989: Gravity waves, compensating subsidence and detrainment around cumulus clouds. *J. Atmos. Sci.*, **46**, 740-759.

Charney, J., and A. Eliassen, 1964: On the growth of the hurricane depression. *J. Atmos. Sci.,* **21,** 68-75.

Davies-Jones, R. P., 1983: An accurate theoretical approximation for adiabatic condensation temperature. *Mon. Wea. Rev.*, **111**, 1119-1121.

Donner, L. J., 1993: A cumulus parameterization including mass fluxes, vertical momentum dynamics, and mesoscale effects. *J. Atmos. Sci.*, **50**, 889-906.

———–, C. J. Seman, and R. S. Hemler, 1999: Three dimensional cloud-system modeling of GATE convection. *J. Atmos. Sci.*, **56**, 1885-1912.

Dufour L., and J. van Mieghem, 1975: Thermodynamique de l'atmosphère. Institut Royal Météorologique de Belgique, 278 pp.

Emanuel, K. A., 1991: A scheme for representing cumulus convection in large-scale models. *J. Atmos. Sci.*, **48**, 2313-2335.

———-, 1997: The problem of convective moistening. In *"The physics and parameterization of moist atmospheric convection"* (Ed. R. K. Smith), *NATO ASI Series*, **505**, 447-462.

Fritsch, J. M., and C. F. Chappell, 1980: Numerical prediction of convectively driven mesoscale pressure systems. Part I: Convective parameterization. *J. Atmos. Sci.*, **37**, 1722-1733.

Fritsch, J. M., R. A. Houze, R. Adler, H. Bluestein, L. Bosart, J. Brown, F. Carr, C. Davies, R. H. Johnson, N. Junker, Y.-H. Kuo, S. Rutledge, J. Smith, Z. Toth, J. W. Wilson, E. Zipser, and D. Zrnic, 1998: Quantitative precipitation forecasting: Report of the eighth prospectus development team, U. S. weather research program. *Bull. Am. Meteorol. Soc.*, **79**, 285-299.

Gregory, D., and M. J. Miller, 1989: A numerical study of the parameterization of deep tropical convection. *Quart. J. Roy. Meteor. Soc.*, **115**, 1209-1241.

Gregory, D., and P. R. Rowntree, 1990: A mass-flux convection scheme with representation of cloud ensemble characteristics and stability dependent closure. *Mon. Wea. Rev.*, **118**, 1483-1506.

Grell, G. A., 1993: Prognostic evaluation of assumptions used by cumulus parameterizations. *Mon. Wea. Rev.*, **121**, 764-787.

Hu, Q., 1997: A cumulus parameterization based on a cloud model of intermittently rising thermals. *J. Atmos. Sci.*, **54**, 2292-2307.

Kain, J. S., and J. M. Fritsch, 1990: A one-dimensional entraining/detraining plume model and its application in convective parameterizations. *J. Atmos. Sci.*, **47**, 2784-2802.

————, and ————, 1993: Convective parameterization for mesoscale models: The Kain-Fritsch scheme. *Meteor. Monographs*, **46**, 165-170.

Kershaw, R., and D. Gregory, 1997: Parameterization of momentum transport by convection. Part I: Theory and cloud modelling results. *Quart. J. Roy. Meteor. Soc.*, **123**, 1133-1151.

Kuo, H. L., 1965: On formation and intensification of tropical cyclones through latent heat release by cumulus convection. *J. Atmos. Sci.*, **22**, 40-63.

————-, and W. H. Raymond, 1980: A quasi-one-dimensional cumulus cloud model and parameterization of cumulus heating and mixing effects. *Mon. Wea. Rev.*, **108**, 991-1009.

Kuo, Y.-H., J. F. Bresch, M.-D. Cheng, J. Kain, D. B. Parsons, W.-K. Tao and D.-L. Zhang, 1997: Summary of a mini workshop on cumulus parameterization for mesoscale models. *Bull. Am. Meteorol. Soc.*, **78**, 475-490.

Lin, C., and A. Arakawa, 1997: The macroscopic entrainment process of simulated cumulus ensemble. Part II: Testing the entraining-plume model *J. Atmos. Sci.*, **54**, 1027-1043.

Liang, Q., G. S. Young, and W. M. Frank, 1998: A convective wake parameterization scheme for use in general circulation models. *Mon. Wea. Rev.*, **126**, 456-469.

Mallet, I., J.-P. Cammas, P. Mascart and P. Bechtold, 1999: Effects of cloud diabatic heating on a FASTEX cyclone (IOP17) early development. *Quart. J. Roy. Meteor. Soc.*, **125**, 3415-3438.

Manabe, S., and R. Strickler, 1964: Thermal equilibrium of the atmopshere with a convective adjustment. *J. Atmos. Sci.*, **21**, 361-385.

Mapes, B. E., 1997: Equilibrium versus activation control of large-scale variations of tropical deep convection. In *"The physics and parameterization of moist atmospheric convection"* (Ed. R. K. Smith), *NATO ASI Series*, **505**, 321-358.

Moncrieff, M. W., D. Gregory, S. K. Krueger, J. L. Redelsperger, and W. K. Tao, 1997: GEWEX Cloud System Study (GCSS) working group 4: Precipitating convective cloud systems. *Bull. Am. Meteorol. Soc.*, **78**, 831-845.

Ogura, Y., and H.-R. Cho, 1973: Diagnostic determination of cumulus populations from large-scale variables. *J. Atmos. Sci.*, **30**, 1276-1286.

Ooyama, K., 1971: A theory on parameterization of cumulus convection. *J. Meteor. Soc. Japan*, **49**, 744-756.

Raymond, D. J., 1995: Regulation of moist convection over the West Pacific warm pool. *J. Atmos. Sci.*, **52**, 3945-3959.

————-, and A. M. Blyth, 1986: A stochastic mixing model for nonprecipitating clouds. *J. Atmos. Sci.*, **43**, 2708-2718.

Sun, W.-H., and P. A. Haines, 1996: Semi-prognostic tests of a new cumulus parameterization scheme for mesoscale modeling. *Tellus*, **48A**, 272-289.

Simpson, J., 1983: Cumulus clouds: interactions between laboratory experiments and observations as foundations for models. *Mesoscale Meteorology*, D. K. Lilly and T. Gal-Chen, Eds., Reidel, 399-412.

Slingo, J. M., M. Blackburn, A. K. Betts, R. Brugge, K. D. Hodges, B. J. Hoskins, M. J. Miller, L. Steenman-Clark, and J. Thuburn, 1994: Mean climate and transience in the tropics of the UGAMP GCM: Sensitivity to convective parameterization. *Q. J. R. Meteorol. Soc.*, **120**, 881-922.

Tao, W.-K., J. Simpson, and M. McCumber, 1989: An ice-water saturation adjustment. *Mon. Wea. Rev.*, **117**, 231-235.

Tiedtke, M., 1989: A comprehensive mass flux scheme for cumulus parameterization in large-scale models. *Mon. Wea. Rev.*, **117**, 1779-1800.

Wang, J., and D. A. Randall, 1996: A cumulus parameterization based on the generalized convective available potential energy. *J. Atmos. Sci.*, **53**, 716-727.

Warner, J., 1970: On steady-state one-dimensional models of cumulus convection. *J. Atmos. Sci.*, **27**, 1035-1040.

Xie, S.-C., K.-M. Xu, R. T. Cederwall, P. Bechtold, A. D. Del Genio, S. A. Klein, D. G. Cripe, S. J. Ghan, D. Gregory, S. F. Iacobellis, S. K. Krueger, U. Lohmann, J. C . Petch, D. A. Randall, L. D. Rotstayn, R. C. J. Somerville, Y. C. Sud, K. von Salzen, G. K. Walker, A. Wolf, J. J. Yio, G. J. Zhang and M. Zhang, 2002: Intercomparison and evaluation of cumulus parameterizations under summertime midlatitude continental conditions. *Q. J. R. Meteorol. Soc.*, **128**, 1095-1135.

Yanai, M., S. K. Esbensen, and J.-H. Chu, 1973: Determination of bulk properties of tropical cloud clusters from large-scale heat and moisture budgets. *J. Atmos. Sci.*, **30**, 611-627.

Zhang, D.-L., and J. M. Fritsch, 1986: Numerical simulation of the meso-β scale structure and evolution of the 1977 Johnstown flood. Part I: Model description and verification. *J. Atmos. Sci.*, **43**, 1913-1943.

Chapter 5

Microphysical Schemes for Warm Clouds

Contents

Three microphysical schemes for warm clouds are implemented into Meso-NH. The most simple scheme is the Kessler one, a one-moment scheme that prognoses mixing ratio of cloud and rain water. The two others are some two-moment schemes that predicts the mixing ratio and the concentrations of cloud and rain drops. The C2R2 scheme is the most general one while the KHKO scheme is designed for stratocumulus.

5.1 Kessler scheme

5.1.1 Equations

We note r_v, r_c, and r_r the water vapor, cloud water and rainwater mixing ratios, as defined in MESO-NH. For any constituent, r is the mass of the constituent divided by the reference mass of dry air.[1] The consevation equations for these quantities are written:

$$\frac{d}{dt}(\rho_{dref} r_v) = \rho_{dref}(P_{RE} - P_{CON}) \tag{5.1}$$

$$\frac{d}{dt}(\rho_{dref} r_c) = \rho_{dref}(-P_{RA} - P_{RC} + P_{CON}) \tag{5.2}$$

$$\frac{d}{dt}(\rho_{dref} r_r) = \rho_{dref}(P_{RA} + P_{RC} - P_{RE} + P_{RS}) \tag{5.3}$$

where P designates the sources and where the subscripts CON, RE, RA, RC and RS respectively refer to the following processes: evaporation/condensation, rain evaporation, accretion of cloud droplets by raindrops, conversion of cloud droplets into raindrops (autoconversion), and rain sedimentation. Condensation/evaporation is a very fast process, it cannot be computed explicitly and is obtained through an implicit saturation adjustment procedure, taking subgrid-scale processes into account (see Chapter on the sub-grid condensation schemes). All others terms are computed explicitly.

[1] Notice that $\rho_{dref} r = \rho_d \tilde{r}$ where $\tilde{r}$ is the usual mixing ratio i.e. the mass of the constituent divided by the mass of dry air.

5.1.2 Raindrops characteristics

Distribution

Raindrops are assumed to follow a Marshall-Palmer distribution. The number of raindrops whose diameter lies in the interval D and $D + dD$ is given by:

$$N(D)dD = N_0 \exp(-\lambda D)dD \tag{5.4}$$

Observations for different types of rain show a range of values for N_0 from $0.4\ 10^7$ to $3.5\ 10^7$ m^{-4}. $N_0 = 10^7$ m^{-4} is a value frequently used.
The λ parameter is obtained from

$$\rho_{dref} r_r = \int_0^\infty \frac{\pi}{6} \rho_{lw} D^3 N_0 \exp(-\lambda D)dD = \frac{\pi \rho_{lw} N_0}{\lambda^4}, \tag{5.5}$$

which leads to

$$\lambda = \Big(\frac{\pi \rho_{lw} N_0}{\rho_{dref} r_r}\Big)^{\frac{1}{4}}. \tag{5.6}$$

Fall velocity

The terminal fall velocity for a raindrop of diameter D is expressed as

$$V(D) = \big(\frac{\rho_{00}}{\rho_{dref}}\big)^{\alpha} a D^b, \tag{5.7}$$

with $\alpha = 0.4$, $a = 842$ m$^{0.2}$/s and $b = 0.8$, ρ_{00} being the air density at the reference pressure level P_{00}. This parameterization follows Liu and Orville (1969) and includes the effect of mean density variation as suggested by Foote and Du Toit (1969).
The rain terminal fall velocity is then given by

$$V_T \rho_{dref} r_r = \int_0^\infty \frac{\pi}{6} \rho_{lw} D^3 V(D) N(D) dD, \tag{5.8}$$

which leads to

$$V_T = \frac{a}{6} \big(\frac{\rho_{00}}{\rho_{dref}}\big)^{\alpha} \frac{\Gamma(b+4)}{\lambda^b}, \tag{5.9}$$

or

$$V_T = \frac{a}{6} \Gamma(b+4) \big(\frac{\rho_{00}}{\rho_{dref}}\big)^{\alpha} \big(\frac{\rho_{dref} r_r}{\pi \rho_{lw} N_0}\big)^{\frac{b}{4}}. \tag{5.10}$$

5.1.3 Explicit sources

Autoconversion

The sole rainwater initiation mechanism is the autoconversion process which is parameterized according to Kessler (1969). The Kessler rate relies on intuitive considerations: the autoconversion rate increases linearly with the cloud water content $(\rho_{dref} r_c)$ but cloud conversion does not occur below a threshold value q_{crit}.

$$P_{RC} = k\ \max(r_c - \frac{q_{crit}}{\rho_{dref}}, 0) \tag{5.11}$$

The parameters k and q_{crit} are usually set to 10^{-3} s^{-1} et 0.5 g/m^3.
In the code P_{RC} is written as:

$$P_{RC} = C1_{RC} Max(r_c - \frac{C2_{RC}}{\rho_{dref}}, 0) \tag{5.12}$$

with $C1_{RC} = k$ and $C2_{RC} = q_{crit}$.

Accretion

Once embryonic precipitation particles are formed, rainwater mixing ratio growth occurs primarily by accretion of cloud water in the form

$$P_{RA} = \int_0^\infty \frac{\pi}{4} D^2 V(D) E r_c N(D) dD, \tag{5.13}$$

where E is the collision efficiency (here taken equal to 1). After integration,

$$P_{RA} = \frac{\pi}{4} a N_0 (\frac{\rho_{00}}{\rho_{dref}})^\alpha r_c \frac{\Gamma(b+3)}{\lambda^{b+3}}. \tag{5.14}$$

After replacing λ,

$$P_{RA} = \frac{\pi}{4} a N_0 (\frac{\rho_{00}}{\rho_{dref}})^\alpha r_c \Gamma(b+3) \big(\frac{\rho_{dref} r_r}{\pi \rho_{lw} N_0}\big)^{\frac{b+3}{4}}. \tag{5.15}$$

In the code P_{RA} is written as:

$$P_{RA} = C_{RA} (\rho_{dref})^{C'_{RA} - \alpha} r_c (r_r)^{C'_{RA}} \tag{5.16}$$

with

$$C_{RA} = \frac{\pi}{4} a N_0 (\rho_{00})^\alpha \Gamma(b+3) \big(\frac{1}{\pi \rho_{lw} N_0}\big)^{\frac{b+3}{4}}$$

and

$$C'_{RA} = \frac{b+3}{4}$$

The accretion and autoconversion sources are limited by the amount of available cloud water. In the case where both processes are simultaneously operating, accretion is computed first.

Rain evaporation

According to Pruppacher and Klett (1978, p 420), the evaporation rate of a drop of diameter D is given by

$$D \frac{dD}{dt} = \frac{4 S \bar{f}}{\rho_{lw} A}, \tag{5.17}$$

where $\bar{f}$ is a ventilation factor and

$$S = \frac{r_{vs} - r_v}{r_{vs}}, \tag{5.18}$$

$$A = \frac{R_v T}{e_s(T) D_v} + \frac{L_v(T)}{k_a T} (\frac{L_v(T)}{R_v T} - 1) \tag{5.19}$$

$$\simeq \frac{R_v T}{e_s(T) D_v} + \frac{L_v(T)^2}{k_a R_v T^2}. \tag{5.20}$$

r_{vs} is the saturated vapor mixing ratio, D_v is the diffusivity of water vapor in air and k_a is the heat conductivity of air. For simplicity, D_v and k_a are taken constants: $D_v = 2.26\ 10^{-5}$ m^2/s and $k_a = 24.3\ 10^{-3}$ J/(msK).
e_s is the saturation vapor pressure and is computed according to

$$e_s(T) = \exp\big(\alpha_w - \frac{\beta_w}{T} - \gamma_w \ln(T)\big), \tag{5.21}$$

with

$$\alpha_w = \ln(e_s(T_t)) + \frac{\beta_w}{T_t} - \gamma_w \ln(T_t), \tag{5.22}$$

$$\beta_w = \frac{L_v(T_t)}{R_v}\gamma_w T_t, \tag{5.23}$$

$$\gamma_w = \frac{C_l - C_{pv}}{R_v}. \tag{5.24}$$

L_v is the latent heat of vaporization and is computed according to

$$L_v(T) = L_v(T_t) + (C_{pv} - C_l)(T - T_t). \tag{5.25}$$

The ventilation factor $\bar{f}$ is given by

$$\bar{f} = 1 + F(Re)^{0.5}, \tag{5.26}$$

where Re is the Reynolds number which can be expressed as

$$Re = \frac{V(D)D}{\nu}, \tag{5.27}$$

ν being the air kinematic viscosity which is here assumed to be constant: $\nu = 0.15\ 10^{-4}$ kg/(ms).
F is a ventilation coefficient taken equal to 0.22.
After replacing (5.7) and (5.27) in (5.26), one gets

$$\bar{f} = 1 + F\big[\big(\frac{\rho_{00}}{\rho_{dref}}\big)^{\alpha}\frac{aD^{b+1}}{\nu}\big]^{0.5}. \tag{5.28}$$

The integration of (5.17) over the rain drop spectrum leads to the expression of the evaporation source

$$P_{RE} = \frac{1}{\rho_{dref}}\int_0^{+\infty}\frac{2\pi S\bar{f}}{A}DN(D)dD. \tag{5.29}$$

After replacing $\bar{f}$,

$$P_{RE} = \frac{2\pi SN_o}{A}\frac{1}{\rho_{dref}}\big[\frac{1}{\lambda^2} + F\big(\frac{\rho_{00}}{\rho_{dref}}\big)^{\alpha/2}\big(\frac{a}{\nu}\big)^{1/2}\frac{\Gamma(\frac{b+5}{2})}{\lambda^{\frac{b+5}{2}}}\big], \tag{5.30}$$

or

$$P_{RE} = \frac{2\pi SN_o}{A}\frac{1}{\rho_{dref}}\big[\big(\frac{\rho_{dref}r_r}{\pi\rho_{lw}N_o}\big)^{\frac{1}{2}} + F\big(\frac{\rho_{00}}{\rho_{dref}}\big)^{\alpha/2}\big(\frac{a}{\nu}\big)^{1/2}\Gamma\big(\frac{b+5}{2}\big)\big(\frac{\rho_{dref}r_r}{\pi\rho_{lw}N_o}\big)^{\frac{b+5}{8}}\big]. \tag{5.31}$$

In the code P_{RE} is written as

$$P_{RE} = \frac{S}{A}\big[C1_{RE}(\rho_{dref})^{-\frac{1}{2}}(r_r)^{\frac{1}{2}} + C2_{RE}(\rho_{dref})^{C'_{RE}-1-\alpha/2}(r_r)^{C'_{RE}}\big], \tag{5.32}$$

with

$$C1_{RE} = 2\pi N_o(\frac{1}{\pi\rho_{lw}N_o})^{\frac{1}{2}}$$

$$C2_{RE} = 2\pi N_o F\big(\rho_{00})^{\alpha/2}(\frac{a}{\nu})^{1/2}\Gamma(\frac{b+5}{2})\big(\frac{1}{\pi\rho_{lw}N_o}\big)^{\frac{b+5}{8}}\big)$$

$$C'_{RE} = \frac{b+5}{8}$$

The rain evaporation source is limited by the amount of available rainwater.

Rain sedimentation

The sedimentation rate is given by

$$P_{RS} = \frac{1}{\rho_{dref}}\frac{\partial}{\partial z}\int_0^\infty N(D)V(D)\frac{\pi}{6}\rho_{lw}D^3V(D)N(D)dD \tag{5.33}$$

$$= \frac{1}{\rho_{dref}}\frac{\partial}{\partial z}(V_T\rho_{dref}r_r). \tag{5.34}$$

In the code, P_{RS} is written as

$$P_{RS} = \frac{1}{\rho_{dref}}\frac{\partial}{\partial z}\big[C_{RS}(\rho_{dref})^{C'_{RS}-\alpha}(r_r)^{C'_{RS}}\big], \tag{5.35}$$

with

$$C_{RS} = \frac{a}{6}\Gamma(b+4)(\rho_{00})^{\alpha}\big(\frac{1}{\pi\rho_{lw}N_0}\big)^{\frac{b}{4}},$$

$$C'_{RS} = \frac{4+b}{4}.$$

In order to maintain stability, the rain sedimentation source is computed with a time splitting technique and with an upstream differencing scheme. The small time step used for this computation is determined from the CFL stability criterion based on a maximum raindrop fall velocity V_{TRmax} of 7 m s^{-1}.

The sedimentation rate can be alternatively calculated using a Probability Density Function (PDF) -based approach. A general description of the method is done in Geleyn et al. (2008). The sedimentation rate is given by

$$P_{RS} = \frac{1}{\rho_{dref}}\frac{\partial}{\partial z}F_r \tag{5.36}$$

where F_r is the sedimentation flux. The sedimentation flux is computed from the top to the bottom of the atmosphere following

$$F_r(j) = P_1\frac{\Delta z}{\Delta t}\rho_{dref}r_r + P_2F_r(j-1) \tag{5.37}$$

Δt is the time step and Δz the thickness of the layer. P_1 and P_2 are computed as in Geleyn et al. (2008) in the case where the PDF of the fall speeds of the drops is a simple step function

$$P_1 = \min\left(1, \frac{V_{T1}\Delta t}{\Delta z}\right) \tag{5.38}$$

$$P_2 = \max\left(0, 1 - \frac{\Delta z}{V_{T2}\Delta t}\right) \tag{5.39}$$

V_{T1} and V_{T2} are the terminal velocities of the two groups of drops. The first one is computed using equation (5.10) and r_r of the level j. V_{T2} is computed with the same equation but using a mixing ratio representative of the incoming flux

$$r'_r = \frac{\Delta t}{\rho_{dref}\Delta z} F_r(j-1) \tag{5.40}$$

This method is unconditionally stable and avoids the use of a time splitting technique.

5.1.4 Implicit sources

Once the explicit sources are computed, the condensation/evaporation rate is obtained through a saturation adjustment procedure following Langlois (1973). If T^* and r_v^* are the temperature and vapor mixing ratio obtained after adding the explicit sources, we seek the zero-crossing of $F(T)$, defined as

$$F(T) = (T - T^*) + \frac{L_v(T)}{C_{ph}}(r_{vs}(T) - r_v^*). \tag{5.41}$$

To obtain a rapidly convergent algorithm, Langlois suggests to use a generalized Newton-Raphson procedure which employs the first and second derivatives of F:

$$T \simeq T^* - \frac{F(T^*)}{F'(T^*)}\left[1 + \frac{F(T^*)F''(T^*)}{2F'^2(T^*)}\right]. \tag{5.42}$$

The saturated vapor mixing ratio is given by

$$r_{vs}(T) = \frac{\epsilon e_s(T)}{p - e_s(T)}, \tag{5.43}$$

where $\epsilon = M_v/M_d$.
According to (5.21),

$$e'_s(T) = (\frac{\beta_w}{T^2} - \frac{\gamma_w}{T})e_s(T) = A(T)e_s(T). \tag{5.44}$$

r'_{vs} is then given by

$$r'_{vs} = A(T)r_{vs}(T)(1 + \frac{r_{vs}(T)}{\epsilon}). \tag{5.45}$$

It follows:

$$T = T^* - \Delta_1(1 + \frac{1}{2}\Delta_1\Delta_2), \tag{5.46}$$

with

$$\Delta_1 = \frac{F(T^*)}{F'(T^*)} = \frac{L_v(T)}{C_{ph} + L_v(T) r'_{vs}(T^*)} \big[r_{vs}(T^*) - r_v^* \big], \tag{5.47}$$

$$\Delta_2 = \frac{F''(T^*)}{F'(T^*)} = \frac{L_v(T) r'_{vs}(T^*)}{C_{ph} + L_v(T) r'_{vs}(T^*)} \big[\frac{A'(T^*)}{A(T^*)} + A(T^*) + \frac{2 r_{vs}(T^*)}{\epsilon} \big], \tag{5.48}$$

and

$$A(T) = \frac{\beta_w}{T^2} - \frac{\gamma_w}{T}, \tag{5.49}$$

$$A'(T) = -\frac{2\beta_w}{T^3} + \frac{\gamma_w}{T^2}. \tag{5.50}$$

$$\tag{5.51}$$

In the above derivation, the variations of L_v with respect to T are ignored, being considered much smaller than the variations of r_{vs}. Langlois shows that with this procedure, iteration is unnecessary. The condensation/evaporation rate is then computed as:

$$P_{CON} = -\Delta_1 (1 + \frac{1}{2} \Delta_1 \Delta_2) \frac{C_{ph}}{L_v(T)} \frac{1}{2\Delta t} \tag{5.52}$$

In the case of evaporation (condensation), P_{CON} is limited by the amount of available cloud water (water vapor).

5.1.5 Global correction for negative values

The microphysical sink/sources are computed in such a way they never return negative values for r_v, r_c, or r_r. However, following the user's choice, the advection scheme can be not positive definite. It could be therefore necessary to remove all the negative mixing ratio values before applying the microphysical calculations. This is currently done inside the microphysical scheme, by a global filling algorithm based on a multiplicative method (Rood 1987). The negative values of the mixing ratio source distribution found are corrected (i.e set equal to zero). The total mass of the corrected distribution is calculated. Then the corrected distribution is mutiplied grid point by grid point by the ratio of the mass of the original distribution to the mass of the corrected distribution.

5.1.6 Practical implementation

The microphysical constants (N_o, a, b, α, $C1_{RC}$, $C2_{RC}$, C_{RA}, C'_{RA}, D_v, k_a, $C1_{RE}$, $C2_{RE}$, C'_{RE}, C_{RS}, C'_{RS} and V_{TRmax}) are set up in routine INI_CLOUD called during the initialization process. During the model run, the computations related to the resolved cloud and rain parameterization are monitored by the routine RESOLVED_CLOUD. When entering RESOLVED_CLOUD, the source array ψS of a variable ψ contains

$$\frac{\hat{\rho}\psi^{t-1}}{2\Delta t} + \sum_i S_i(\hat{\rho}\psi^t)$$

where S_i designate the previously computed tendencies (i.e. advection, numerical diffusion, turbulence, ...). ψS can be interpreted as a guess of $\hat{\rho}\psi^{t+1}/2\Delta t$. RESOLVED_CLOUD computes the microphysical tendencies and returns updated values of the source arrays affected by the explicit cloud and rain parameterization i.e. θS, $r_v S$, $r_c S$, and $r_r S$. The main steps of the scheme are the following

- The negative mixing ratios sources (r_vS, r_cS, and r_rS) are corrected according to the global filling algorithm described in the previous subsection.
- The θ, r_v, r_c, and r_r sources are divided by $\hat{\rho}$ to minimize computations in this section.
- Routine SLOW_TERMS is called and proceeds to the computation of the explicit sources:
  - Computes the rain sedimentation source P_{RS} and updates the rain source [$r_rS = r_rS + P_{RS}$].
  - Computes the accretion source P_{RA}, limits the accretion source by the amount of cloud water available at this stage [$P_{RA} = Min(P_{RA}, r_cS)$] and updates the cloud water and rainwater sources [$r_cS = r_cS - P_{RA}$ and $r_rS = r_rS + P_{RA}$].
  - Computes the autoconversion source P_{RC}, limits the autoconversion source by the amount of cloud water available at this stage [$P_{RC} = Min(P_{RC}, r_cS)$] and updates the cloud water and rainwater sources [$r_cS = r_cS - P_{RC}$ and $r_rS = r_rS + P_{RC}$].
  - Computes the rain evaporation source P_{RE}, limits the rain evaporation source by the amount of rainwater available at this stage [$P_{RE} = Min(P_{RE}, r_rS)$] and updates the water vapor, rainwater, and potential temperature sources [$r_vS = r_vS + P_{RE}$, $r_rS = r_rS - P_{RE}$ and $\theta S = \theta S - P_{RE}L_v/(\pi_{ref}C_{ph})$].
- Routine FAST_TERMS is called and performs the implicit saturation adjustment:
  - Computes the condensation/evaporation source P_{CON}, limits this source by the amount of cloud water (water vapor) available at this stage in the case of evaporation (condensation) [$P_{CON} = Min(P_{CON}, r_vS)$ or $P_{CON} = Min(P_{CON}, r_cS)$], and updates the water vapor, cloud water, and potential temperature sources [$r_vS = r_vS - P_{CON}$, $r_cS = r_cS + P_{CON}$ and $\theta S = \theta S + P_{CON}L_v/(\pi_{ref}C_{ph})$].
- The θ, r_v, r_c, and r_r sources are multiplied by $\hat{\rho}$ to go back to the original tendencies.

5.1.7 Available options and summary of the ajustable constants

According to the value of the CLOUD parameter given in namelist (see the Meso_NH user's guide), the one-moment microphysical scheme for warm clouds can be used in three different ways:

- CLOUD = 'NONE' : no microphysics, the water vapor (if present) is computed as a passive tracer,
- CLOUD = 'REVE' : only reversible processes are considered, no rain is generated (i.e the call to SLOW_TERM is by-passed),
- CLOUD = 'KESS' : the full scheme is operating.

Some others parameters might be reasonably modified by the user in routine INI_CLOUD. These are:
N_o the Marshall-Palmer distribution parameter,
a, b, and α the parameters used in the raindrop fall velocity expression,
$C1_{RC}$ and $C2_{RC}$, the autoconversion time constant and threshold,
V_{TRmax}, the maximum raindrop fall velocity used to ensure stability of the sedimentation computation.

5.2 The two-moment microphysical scheme for warm clouds

5.2.1 Purpose

This section describes the warm bulk microphysical scheme hereafter called C2R2 that predicts the concentration and the mixing ratio of both cloud droplets and rain drops. The salient feature of the scheme is the explicit incorporation of aerosol characteristics in the activation parameterization (a major sink in the big sized aerosol budget). The C2R2 scheme contains also a revised analysis of the coalescence terms that lead to a more reliable formation of the rain drops. The explicit evolution of the droplet concentration in C2R2 makes the scheme attractive for several topics such as the cloud chemistry and the radiative transfer. On the other side, the prognostic rain drop concentration provides a better description of the big precipitating drops which are a critical issue for an accurate modeling of either light drizzle or heavy showers.
The C2R2 scheme aims to extend the domain of applicability of crude bulk schemes like the Kessler scheme, for small cloud scale problems where generally expensive bin microphysical schemes are recommended. The scheme opens also an interesting field area by linking the cloud microphysical properties to the aerosol load in a rather simple way. The development of a similar two-moment approach to describe the microphysical evolution of cold clouds, is underway.

5.2.2 Introduction to the "rain_C2R2" code

It is customary in bulk microphysical schemes to consider two modes around which liquid water is distributed thus providing a natural partition between cloud and rain water. These two modes are characterized by an equivalent mixing ratio (mass of condensate scaled by the mass of dry air) but by very different number concentrations from a few tens or hundreds per cubic centimeter for the cloud droplets down to a few units or tens per liter for the raindrops.
The present scheme assumes that each mode follows a generalized gamma distribution, so the droplet/drop size distributions are described by the normalized form:

$$n_i(D) = N_i \frac{\alpha_i}{\Gamma(\nu_i)} \lambda_i^{\alpha_i \nu_i} D^{\alpha_i \nu_i - 1} \exp\big(-(\lambda_i D)^{\alpha_i}\big) \tag{5.53}$$

where $\Gamma(x)$ is the gamma function (see Press *et al.* (1992) for the coding) and where the index $i \in [c, r]$ stands for cloud or rain, respectively. Our strategy is to predict only two of the most significant moments of (5.53) that possess a clear physical meaning, namely the zeroth N_i and third order moments $r_i = (1/\rho_a) \int_0^\infty (\pi/6) \rho_w D^3 n_i(D) dD$. As these two moments are determined from (5.53), the variable slope parameter λ_i can be deduced from

$$\lambda_i = \Big(\frac{\pi}{6} \rho_w \frac{\Gamma(\nu_i + 3/\alpha_i)}{\Gamma(\nu_i)} \frac{N_i}{\rho_a r_i}\Big)^{1/3} \tag{5.54}$$

whereas the remaining parameters α_i and ν_i that are mostly related to the spectral breadth of (5.53), are held fixed for the moment. Equation (5.54) is an application of a general formula to compute the p-moment of (5.53), that is

$$\int_0^\infty D^p n_i(D) dD = \frac{N_i}{\lambda_i^p} \frac{\Gamma(\nu_i + p/\alpha_i)}{\Gamma(\nu_i)} = N_i M_i(p). \tag{5.55}$$

5.2.3 The bulk microphysical scheme

System of equation

The continuity equations of the condensed phases, described in terms of concentration and mixing ratio, are written in symbolic form as follows:

$$\frac{\partial N_c}{\partial t} = \sum \frac{\partial N_c}{\partial t}\Big|_{NMT} + CVHENC - CCACCR - CCSCOC \tag{6.89a}$$

$$\frac{\partial r_c}{\partial t} = \sum \frac{\partial r_c}{\partial t}\Big|_{NMT} + RVHENC + RVCONC - RCAUTR - RCACCR \tag{6.89b}$$

$$\frac{\partial N_r}{\partial t} = \sum \frac{\partial N_r}{\partial t}\Big|_{NMT} + CCAUTR - CRSCOR - CSEDR \tag{6.89c}$$

$$\frac{\partial r_r}{\partial t} = \sum \frac{\partial r_r}{\partial t}\Big|_{NMT} + RCAUTR + RCACCR - RREVAV - RSEDR \tag{6.89d}$$

In addition to (6.89a-d), an equation of conservation for N_a, the number concentration of the activated Cloud Condensation Nuclei (CCN),

$$\frac{\partial N_a}{\partial t} = \sum \frac{\partial N_a}{\partial t}\Big|_{NMT} + CVHENC. \tag{5.58}$$

is introduced to keep track of the CCN upon which cloud droplets have been already activated (see also the diagram of Fig. 5.1 which summarizes the scheme). The system is closed by expressing the conservation of the water vapor mixing ratio r_v and of the dry potential temperature θ:

$$\frac{\partial r_v}{\partial t} = \sum \frac{\partial r_v}{\partial t}\Big|_{NMT} + RREVAV - RVCONC - RVHENC \tag{6.91a}$$

$$\frac{\partial \theta}{\partial t} = \sum \frac{\partial \theta}{\partial t}\Big|_{NMT} + \frac{L_v}{\Pi C_{ph}}\Big(RVCONC - RREVAV\Big) \tag{6.91b}$$

In (6.89a)-(6.91b), the subscript $_{NMT}$ refers to Non-Microphysical Tendencies (advection, turbulence, numerics and other physical processes) while the meaning of the other symbols, given in Table 5.1, is detailed in the following section. A list of symbols is provided in the appendix and the coefficients appearing in the next formula are expressed in SI units unless specified.

CCN activation (CVHENC) and reversible condensation/evaporation of droplets (RVCONC)

The CCN activation and the condensation growth of cloud droplets are the dominant processes affecting distinctly the number concentration (N_c) and the mixing ratio (r_c) of cloud liquid water at the early stage of the cloud lifetime. These processes are difficult to model explicitly because they depend upon the maximum (CCN activation) and mean (condensation) local supersaturation values $s_{v,w}$ in contact with the CCN and the droplets. This quantity is not generally well captured in cloud models because its scale is highly variable and because the activation process results from an unstable thermodynamical equilibrium at short timescales in competition with the condensation growth that just tends to absorb any excess of supersaturation.
The parameterization of the CCN activation follows the diagnostic and integral approach of Twomey (1959) as improved by Cohard et al. (1998) where CCN activation spectra are expressed in the following functional form:

$$N_{CCN} = C s_{v,w}^k F(\mu, \frac{k}{2}, \frac{k}{2}+1; -\beta s_{v,w}^2). \tag{5.61}$$

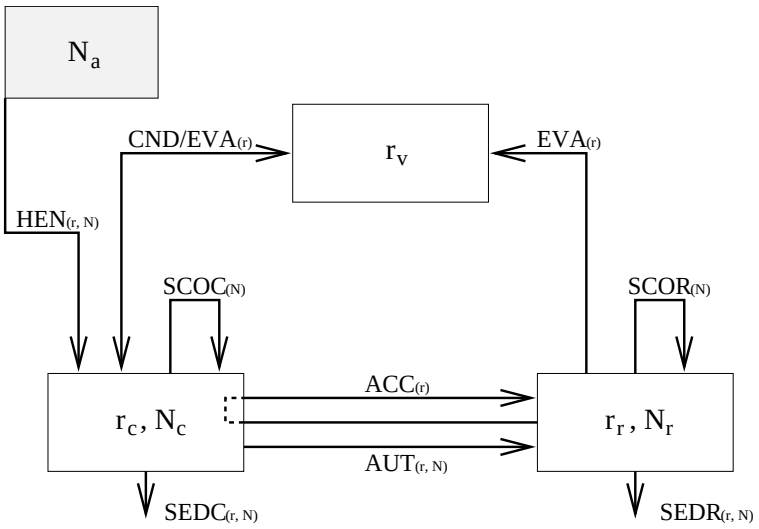

Figure 5.1: Warm microphysical processes included in the C2R2 scheme (see text for the acronyms and explanations).

$F(a,b,c;x)$ is the hypergeometric function. This form adheres more closely to observations of N_{CCN} at large $s_{v,w}$ (N_{CCN} is finite as $s_{v,w}$ goes to infinity) as compared to the traditional $Cs_{v,w}^k$ law. Furthermore Cohard et al. (2000c) show that it is possible to establish parametric relations between the four unknowns in (5.61) and characteristics of lognormal distributions of underlying aerosols with variable chemical composition and solubility. Thus the k, β and μ parameters of (5.61) can be expressed with the following formulas:

$$\frac{k}{k_0} = \left(\frac{\ln(\sigma)}{\ln(\sigma)_0}\right)^{\alpha_k^\sigma}, \tag{5.62a}$$

$$\frac{\beta}{\beta_0} = \left(\frac{\overline{r}}{\overline{r}_0}\right)^{\alpha_\beta^{\overline{r}}} \exp\left(\alpha_\beta^\sigma\left(\frac{\ln(\sigma)}{\ln(\sigma)_0} - 1\right)\right)\left(\frac{\epsilon_m}{\epsilon_{m0}}\right)^{\alpha_\beta^{\epsilon m}}\left(\frac{T}{T_0}\right)^{\alpha_\beta^T}, \tag{5.62b}$$

$$\frac{\mu}{\mu_0} = \left(\frac{\ln(\sigma)}{\ln(\sigma)_0}\right)^{\alpha_\mu^\sigma}. \tag{5.62c}$$

The values of the new coefficients in (5.62a-c) can be taken from Tables 2 and 3 of Cohard et al. (2000c). The remaining parameter C in (5.61) is deduced from the total CCN number concentration (N_{CCN}^{max}) using

$$\lim_{s_{v,w}\to+\infty} N_{CCN}(s_{v,w}) = N_{CCN}^{max} = \frac{C}{\beta^{k/2}}\frac{\Gamma(k/2+1)\Gamma(\mu-k/2)}{\Gamma(\mu)} \tag{5.64}$$

under the condition that k verifies $k < 2\mu$ which is always satisfied here.
Using (5.61) and following Twomey's method, Cohard et al. (1998) showed that an estimate of the maximum supersaturation $s_{v,w_{MAX}}$ is the root of

$$s_{v,w_{MAX}}^{k+2} F(\mu, \frac{k}{2}, \frac{k}{2}+\frac{3}{2}, -\beta s_{v,w_{MAX}}^2) = \frac{\rho_a(\psi_1 w)^{3/2}}{2kC\pi\rho_w\psi_2(G)^{3/2}B(\frac{k}{2},\frac{3}{2})}. \tag{5.66}$$

Substituting values of $s_{v,w} = s_{v,w_{MAX}}$ into (5.61) provides an estimate of the potentially activable CCN number concentration, so the production rate of newly nucleated droplets is given by comparison with CCN that have been already activated. It is also worth to note that (5.61) and (5.66) can be easily generalized to a mixture of aerosols.

Table 5.1: Nomenclature of the microphysical processes involved in (6.89a-d).

Symbols	Mechanisms	Sinks	Sources	Processes
$RVHENC$	$r_v \Longrightarrow r_c$	r_v	r_c	nucleation
$CVHENC$	$N_n \Longrightarrow N_a$	N_n	N_a	(implicitly)
	$N_a \Longrightarrow N_c$	N_a	N_c	
$RVCONC$	$r_v \Longrightarrow r_c$	r_v	r_c	condensation
	$r_v \Longleftarrow r_c$	r_c	r_v	& evaporation
$RCAUTR$	$r_c + r_c \Longrightarrow r_r$	r_c	r_r	autoconversion
$CCAUTR$	$N_c + N_c \Longrightarrow N_r$	N_c	N_r	
$RCACCR$	$r_c + r_r \Longrightarrow r_r$	r_c	r_r	accretion
$CCACCR$	$N_c + N_c \Longrightarrow N_r$	N_c	N_r	
$RREVAV$	$r_r \Longrightarrow r_v$	r_r	r_v	evaporation
$CRSCOR$	$N_r + N_r \Longrightarrow N_r$	N_r	N_r	self-collection
$CCSCOC$	$N_c + N_c \Longrightarrow N_c$	N_c	N_c	& break-up
$RSEDR$	$r_r \Longrightarrow r_r$	r_r	r_r	sedimentation
$CSEDR$	$N_r \Longrightarrow N_r$	N_r	N_r	

The reversible condensation/evaporation process is treated implicitly as a result of a non-iterative vapor saturation adjustment (see Cohard and Pinty, 2000a). This treatment is well justified by observations that show that the interior of clouds is nearly in thermodynamical equilibrium ($s_{v,w} < 1\%$). The condensation rate is obtained after solving for T the equation of the first law of thermodynamics,

$$(T - T^*) + \frac{L_v(T)}{C_{ph}}(r_{vs}(T) - r_v^*) = 0 \tag{5.67}$$

where T^* and r_v^* are the temperature and vapor mixing ratio of an intermediate state after integrating all the other explicit processes. $r_{vs}(T)$ is the saturated water vapor mixing ratio, $L_v(T)$ the latent heat of vaporization and C_{ph} the heat capacity of cloudy air. The condensation rate is given by

$$RVCONC = max(-r_c, r_v^* - r_{vs}(T))/\delta t \tag{5.68}$$

Coalescence

A short analysis of the stochastic collection equation indicates that bulk microphysical schemes always need a parameterization for the autoconversion terms (formation of raindrops by droplet coalescence) while the other processes (including raindrop growth by accretion and self-collection) can be treated analytically using the collection kernels of Long (1974).

Autoconversion (RCAUTR and CCAUTR) The parameterization relies on the work of Berry and Reinhardt (1974) for the computation of the RCAUTR term. The parameterization is built on the observation that a characteristic water content L of small drops develops steadily over a characteristic timescale τ. These two positive quantities are expressed in the ranges 20 μm $\leq D_c \leq$

36 μm and $0 \leq \nu_c \leq 3$ by:

$$L = 2.7 \times 10^{-2} \rho_a r_c \left(\frac{1}{16} \times 10^{20} \sigma_c^3 D_c - 0.4\right) \tag{5.69a}$$

$$\tau = 3.7 \frac{1}{\rho_a r_c} \left(0.5 \times 10^6 \sigma_c - 7.5\right)^{-1} \tag{5.69b}$$

where the mean-volume drop diameter D_c and the standard deviation σ_c are computed using (5.55). Eqs(5.69a) and (5.69b) are combined to get:

$$RCAUTR = - \, max\left(\frac{L}{\tau}, 0.\right) \tag{5.71}$$

A suitable parameterization of the CCAUTR rate is more difficult to obtain because the original Berry and Reinhardt's parameterization tends to accumulate the freshly formed drops by autoconversion in the lowest part of the raindrop spectrum thus preventing the development of sizeable raindrops. This led Cohard and Pinty (2000a) to the conclusion that it is important to restrict the original Berry and Reinhardt formulation:

$$CCAUTR = - \, 3.5 \times 10^9 \, \frac{\rho_a L}{\tau} \tag{5.72}$$

to situations where $D_r < D_h$ where D_h is the "hump diameter" defined by Berry and Reinhardt (1974). For cases where $D_r > D_h$, it is assumed that the autoconversion of the cloud droplets does not modify the mean-volume diameter so (5.72) is replaced by:

$$CCAUTR = \frac{N_r}{r_r} RCAUTR \tag{5.73}$$

Accretion (RCACCR and CCACCR) and self-collections (CCSCOC and CRSCOR) The processes of accretion and self-collections associated to polynomial collection kernels, can be integrated analytically in bulk schemes as shown by Cohard and Pinty (2000a). The collection kernels of Long (1974), already used by Ziegler (1985), are considered in this study:

$$K(D_1, D_2) = \begin{cases} K_2 (D_1^6 + D_2^6) & \text{if } D_1 \leq 100 \mu\text{m}, \\ K_1 (D_1^3 + D_2^3) & \text{if } D_1 > 100 \mu\text{m}. \end{cases} \tag{5.74}$$

with $K_2 = 2.59 \times 10^{15}$ m^{-3}s^{-1} and $K_1 = 3.03 \times 10^3$ s^{-1}. As recommended by Berry and Reinhardt (1974), the accretion and the self-collection of raindrops are accounted for once $r_r > 1.2 \times L/\rho_a$. The cumbersome expressions of the different ACC and SCO terms have been obtained by Cohard and Pinty (2000a) for the raindrops:

If $D_r \geq 100 \mu$m

$$\begin{aligned} CCACCR &= -K_1 N_c N_r \left(\frac{\Gamma(\nu_c + 3/\alpha_c)}{\Gamma(\nu_c) \lambda_c^3} + \frac{\Gamma(\nu_r + 3/\alpha_r)}{\Gamma(\nu_r) \lambda_r^3} \right) \\ RCACCR &= -\frac{\pi}{6} \frac{\rho_w}{\rho_a} K_1 \frac{N_c N_r}{\lambda_c^3} \left(\frac{\Gamma(\nu_c + 6/\alpha_c)}{\Gamma(\nu_c) \lambda_c^3} + \frac{\Gamma(\nu_c + 3/\alpha_c)}{\Gamma(\nu_c)} \frac{\Gamma(\nu_r + 3/\alpha_r)}{\Gamma(\nu_r) \lambda_r^3} \right) \\ CRSCOR &= -K_1 N_r^2 \frac{\Gamma(\nu_r + 3/\alpha_r)}{\Gamma(\nu_r) \lambda_r^3} \end{aligned} \tag{5.75}$$

If $D_r < 100\mu$m

$$\begin{aligned} CCACCR &= -K_2 N_c N_r \Big(\frac{\Gamma(\nu_c + 6/\alpha_c)}{\Gamma(\nu_c)\lambda_c^6} + \frac{\Gamma(\nu_r + 6/\alpha_r)}{\Gamma(\nu_r)\lambda_r^6} \Big) \\ RCACCR &= -\frac{\pi}{6}\frac{\rho_w}{\rho_a} K_2 \frac{N_c N_r}{\lambda_c^3} \Big(\frac{\Gamma(\nu_c + 9/\alpha_c)}{\Gamma(\nu_c)\lambda_c^6} + \frac{\Gamma(\nu_c + 3/\alpha_c)}{\Gamma(\nu_c)} \frac{\Gamma(\nu_r + 6/\alpha_r)}{\Gamma(\nu_r)\lambda_r^6} \Big) \\ CRSCOR &= -K_2 N_r^2 \frac{\Gamma(\nu_r + 6/\alpha_r)}{\Gamma(\nu_r)\lambda_r^6} \end{aligned} \tag{5.76}$$

and for the cloud droplets

$$CCSCOC = -K_1 N_c^2 \frac{\Gamma(\nu_c + 3/\alpha_c)}{\Gamma(\nu_c)\lambda_c^3} \tag{5.77}$$

Break-up

Break-up is an efficient process acting on the concentration of the large drops (a key role to explain the high reflectivity core of the tropical rainband in the present case study).
Firstly, collisional break-up is introduced as in Verlinde and Cotton (1993), where a bulk collection efficiency $E_c < 1$ is used to damp the growth of the raindrops by self-collection. In the scheme, the preceeding $CRSCOR$ term is multiplied by the E_c factor with the following definition:

$$E_c = \begin{cases} 1 & \text{if } D_r < 600\mu\text{m}, \\ \exp(-2.5 \times 10^3 (D_r - 6 \times 10^{-4})) & \text{if } 600\mu\text{m} \leq D_r < 2000\mu\text{m}, \\ 0 & \text{if } D_r \geq 2000\mu\text{m}. \end{cases} \tag{5.78}$$

Values of the cutoff diameters in (5.78) have been subjected to a specific evaluation in Cohard and Pinty (2000b).
Secondly and as discussed by Cohard and Pinty (2000b), the inclusion of an additional drop size limiter (a substitute for a spontaneous break-up parameterization) is necessary to remove the giant drops that can be produced spuriously by an unaccurate differential transport of r_r and N_r (advection and sedimentation terms). The correction is applied whenever D_r is larger than 3000 μm so beyond the range of active collisional break-up (see Cohard and Pinty (2000b) for further details).

Evaporation (RREVAV)

The evaporation rate of a raindrop population, falling in an undersaturated environment ($s_{v,w} \ll 0$) is obtained after performing an analytical integration over the whole drop mass spectrum. The size evolution of a single evaporating drop of diameter D is given by

$$\frac{dD}{dt}\Big|_{EVA} = \frac{4 s_{v,w} \bar{f} G}{D} \tag{5.79}$$

where the ventilation factor $\bar{f}$, an empirical function of the Reynolds number $Re = VD/\nu_{cin}$ of the flow, is given by:

$$\bar{f} = 0.78 + FRe^{0.5} = 0.78 + 0.265 \Big[\Big(\frac{\rho_{00}}{\rho_a} \Big)^{0.4} \frac{cD^{d+1}}{\nu_{cin}} \Big]^{0.5} \tag{5.80}$$

after inserting (5.85). Integrating (5.79) with (5.80) and (5.53) leads to an analytical expression of the evaporation rate that is:

$$RREVAV = \frac{1}{\rho_a}\int_0^{+\infty} \frac{\pi}{2}\rho_w D^2 \frac{dD}{dt}\Big|_{EVA} n_r(D)dD \tag{5.81}$$
$$= \frac{2\pi s_{v,w} N_r G}{\lambda\Gamma(\lambda)}\frac{\rho_w}{\rho_a}\Big[0.78 + 0.265\Big(\frac{\rho_{00}}{\rho_a}\Big)^{0.2}\Big(\frac{c}{\nu_{cin}}\Big)^{0.5}\frac{\Gamma(\nu_r + (d+3)/2\alpha_r)}{\lambda_r^{(d+1)/2}}\Big].$$

Concentrations N_r are not affected by evaporation in the present scheme. However if the mean volume drop diameter becomes smaller than 82 μm (the hypothetical size separation between the droplet and drop modes) then all raindrops are converted into cloud droplets, i.e. $N_c = N_c + N_r; r_c = r_c + r_r$ and $N_r = r_r = 0$.

Sedimentation (RSEDR and CSEDR)

Due to the fact that the terminal velocity of drops depends on their size, the gravitational sedimentation of hydrometeors is selective if one considers the whole range of raindrop spectra. This leads to an efficient size sorting phenomenom which is important in the case of warm cumuli where some drops can be large enough to fall while smaller ones are delayed and maintained in updraft cores for further growth. This differential settling between drops is accounted for in two-moment schemes because both sedimentation fluxes of N_r and r_r are computed:

$$RSEDR = \frac{1}{\rho_a}\frac{\partial}{\partial z}\int_0^{\infty} \frac{\pi}{6}\rho_w D^3 V(D) n_r(D)dD$$
$$= \frac{1}{\rho_a}\frac{\partial}{\partial z}\Big[c\Big(\frac{\rho_{00}}{\rho_a}\Big)^{0.4}\rho_a r_r \frac{\Gamma(\nu_r + (d+3)/\alpha_r)}{\lambda_r^d \Gamma(\nu_r + 3/\alpha_r)}\Big], \tag{5.83}$$
$$CSEDR = \frac{\partial}{\partial z}\int_0^{\infty} V(D) n_r(D)dD = \frac{\partial}{\partial z}\Big[c\Big(\frac{\rho_{00}}{\rho_a}\Big)^{0.4} N_r \frac{\Gamma(\nu_r + d/\alpha_r)}{\lambda_r^d \Gamma(\nu_r)}\Big]. \tag{5.84}$$

In (5.83)-(5.84), a simple power law dependence in diameter including air density effect (Foote and Du Toit 1969) has been assumed:

$$V(D) = \Big(\frac{\rho_{00}}{\rho_a}\Big)^{0.4} cD^d, \tag{5.85}$$

Appendix: List of symbols

A	$= 4\sigma_{w/a}/R_v T\rho_w$
$B(a,b)$	beta function
c and d	parameters of the fall speed-diameter relationship for the water drops
C	activation spectrum coefficient
C_{vv}	heat capacity at constant volume of water vapor
C_{pd}, C_{pv} and C_w	heat capacity at constant pressure of dry air, water vapor and liquid water
C_{ph}	$= C_{pd} + r_v C_{pv} + (r_c + r_r)C_w$
D, D_1 and D_2	drop diameters
D_c, D_r	mean volume drop diameter for cloud droplet and raindrop

	distributions
D_v	diffusivity of water vapor in the air
e_v	water vapor pressure
e_{vs}	saturation vapor pressure over water
E_c	collection efficiency
$\bar{f}$	ventilation factor
F	ventilation coefficient
$F(a,b,c;x)$	hypergeometric function
$G(D,T,P)$	$= \frac{1}{\rho_w}\Big(\frac{R_v T}{e_{vs}(T) D_v} + \frac{L_v(T)}{k_a T}(\frac{L_v(T)}{R_v T} - 1)\Big)^{-1}$
k and k_0	activation spectrum coefficients
k_a	heat conductivity of air
$K(x,y)$ and $K(D_1,D_2)$	collection kernels
K_1 and K_2	Long's collection kernel coefficients
L	autoconversion water mass
L_v	latent heat of vaporization
n, n_c and n_r	total, cloud droplet and raindrop size distributions
N_0	intercept parameter of an exponential distribution law
N_c, N_r	cloud droplet and raindrop number concentration
N_n, N_a	condensation nuclei and activated CCN number concentration
N_{CCN}	total activable CCN number concentration
M_w	molar weight of water
$M_i(p)$	p_moment of the i_drop size distribution
P and P_{00}	pressure and reference pressure (1000 hPa)
$\overline{r}$	geometric mean radius of the CCN lognormal distribution
r_v, r_c and r_r	water vapor, cloud water and rain water mixing ratios
r_{vs}	saturated vapor mixing ratio
R_d and R_v	gas constant for dry air and water vapor
Re	Reynolds number
$s_{v,w}$	supersaturation ($= e_v/e_{vs} - 1$)
$s_{v,w_{MAX}}$	maximum supersaturation
t	time
T and T_{00}	temperature and reference temperature (273.16 K)
$V(D)$	drop fall speed of diameter D
w	updraft velocity
x and y	drop mass
z	height or vertical coordinate
$\alpha^{\{\overline{r},\ln(\sigma),\epsilon_m,T\}}_{\{k,\beta,\mu\}}$	adjusted parameters defining the CCN spectrum coefficients
α_c, α_r	dispersion parameter of the generalized gamma distribution law for the cloud droplets and the raindrops
β and β_0	activation spectrum coefficient
δt	time step
$\Gamma(a)$	complete gamma function
ϵ	$= R_v/R_d$
ϵ_m	aerosol soluble fraction
θ	potential temperature
λ_c, λ_r	slope parameter of the generalized gamma distribution law

	for the cloud droplets and the raindrops
μ and μ_0	activation spectrum coefficients
ν_c, ν_r	dispersion parameter of the generalized gamma distribution law for the cloud droplets and the raindrops
ν_{cin}	kinematic viscosity of air
Π	$=(P/P_{00})^{R_d/C_{pd}}$
ρ_a and ρ_w	air and liquid water densities
ρ_{00}	air density at $P = P_{00}$ and $T = T_{00}$
σ	geometric standard deviation of the CCN lognormal distribution
σ_c	standard deviation of cloud droplet distribution
$\sigma_{w/a}$	surface tension of water over the air
τ	timescale for autoconversion
$\psi_1(T,P)$	$= \frac{g}{TR_d}\left(\frac{L_v}{c_pT} - 1\right)$
$\psi_2(T,P)$	$= \left(\frac{P}{\epsilon e_{vs}(T)} + \frac{\epsilon L_v^2}{R_d T^2 c_p}\right)$

5.3 The two-moment microphysical scheme for LES of stratocumulus

5.3.1 Introduction

The KHKO scheme is a 2-moment microphysical scheme specially designed for boundary layer clouds. These clouds are low precipitating warm clouds, and not sufficiently thick to produce heavy rain. The precipitating hydrometeors are drizzle only: their diameter are of the order of several dozens of micrometers. The conversion rates that impact drizzle formation and evolution are parameterized according to Khairoutdinov and Kogan (2000) (KK00) microphysical scheme. These processes are autoconversion, accretion, drizzle sedimentation and drizzle evaporation. Microphysical processes that impact cloud formation are parameterized as in the C2R2 scheme: cloud droplet condensation and evaporation follow Langlois (1973) and activation follows Cohard et al. (1998) (see the C2R2 scientific documentation). Moreover cloud droplet sedimentation is resolved by assuming a Stokes flow to calculate the cloud droplets terminal velocity and an analytical distribution to describe the cloud droplet spectra as in the C2R2 scheme. Microphysical prognostic variables are the same as in the C2R2 scheme: cloud droplet number concentration N_c and mixing ratio r_c, precipitating hydrometeors number concentration N_r and mixing ratio r_r, activated cloud condensation nuclei number concentration N_a.
The next section describes KK00 (the original scheme of Khairoutdinov and Kogan (2000)) and KHKO (the corresponding scheme implemented in Meso-NH) specificities and limits.

5.3.2 KK00 scheme specifities

The KK00 scheme is a 2-moment bulk microphysical scheme. All processes are parameterized only as a function of mixing ratios and number concentrations of each category (cloud droplet and drizzle). The methodology developed in KK00 consisted to assume firstly a power law relationship between conversion rate and the prognostic variables. Each power law introduces coefficients that have to be determined. These coefficients have been empirically adjusted by using about 100 000

hydrometeors spectra obtained from four 3-D LES simulations of stratocumulus clouds using an explicit (bin) microphysical model. For each of these spectra, autoconversion and accretion conversion rates are calculated by integrating the stochastic collection equation. Then the coefficients in the parameterized expressions are evaluated by regression analysis.

Figure 5.2a shows the range of cloud droplet mixing ratios and number concentrations of spectra used to evaluate conversion rates. These values are typical of values encountered in stratocumulus as shown in Fig 5.2b and Fig 5.2c that represent cloud droplet mixing ratios and number concentrations of spectra measured respectively during the ACE-1 and ACE-2 field experiments. The advantage of adjusting coefficients using spectra simulated with an explicit model is that these spectra are representative of boundary layer clouds realistic distributions.

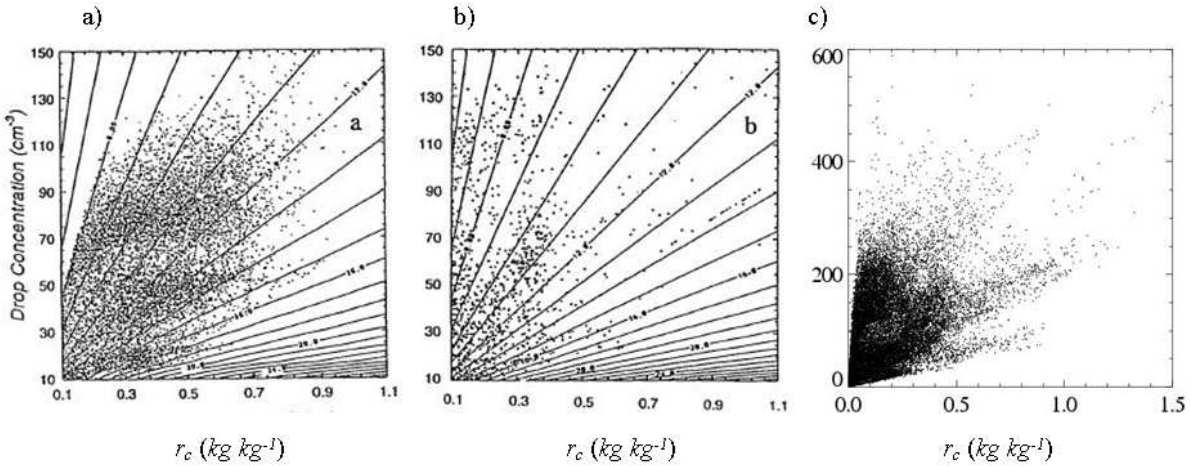

Figure 5.2: a) A scatterplot of the parameter space used to evaluate the coefficients of the KK00 microphysical processes parameterizations. Each data point represents the cloud droplet mixing ratio and the number concentration calculated from an individual hydrometeor size spectrum simulated by the explicit microphysical model. b) Similar to a) but for the spectra averaged over each aircraft flight leg in stratocumulus cloud during the first phase of ACE-1, (following Khairoutdinov et Kogan (2000)), c) Similar to a) but for the ensemble of spectra measured during ACE-2 field experiments (8 flights). Each spectra is averaged with a resolution of about 100 m horizontally. Note that different scales are used for this plot.

Note that a value for r_c of 1.1 g kg^{-1} (the maximum value in Fig. 5.2a) corresponds to an adiabatic cloud with a depth equal to about 550 m. This value can be calculated by assuming an adiabatic linear relationship between the mixing ratio at cloud top $r_c(H)$ and the cloud depth H with an adiabatic coefficient C_w equal to 2 10^{-6} kg m^{-4} : $r_c(H) = C_w H$. This scheme cannot be extended to deep convective clouds.

In the KK00 scheme, separation between cloud droplets and drizzle is defined at a diameter D_0 equal to 50 μm. This low value permits consideration of drizzle in the precipitating category.

Parameterizations are expressed as a function of local microphysical values. Thus the scheme is valid only for simulations where microphysical fields are explicitly resolved i.e. in the LES configuration. Resolution must not be more than 200 m horizontally and a few ten of meters vertically (a vertical resolution of 10 m in the cloud is recommended).

5.3.3 System of equations

For each prognostic variable, conservative equations in KHKO scheme are the following ones:

$$\frac{\partial N_a}{\partial t} = \sum \frac{\partial N_a}{\partial t}\Big|_{NMT} + \frac{\partial N_a}{\partial t}\Big|_{ACT} + \frac{\partial N_a}{\partial t}\Big|_{EVAPC} \tag{5.86a}$$

$$\frac{\partial N_c}{\partial t} = \sum \frac{\partial N_c}{\partial t}\Big|_{NMT} + \frac{\partial N_c}{\partial t}\Big|_{ACT} + \frac{\partial N_c}{\partial t}\Big|_{SEDC} + \frac{\partial N_c}{\partial t}\Big|_{AUTO} + \frac{\partial N_c}{\partial t}\Big|_{ACCR} + \frac{\partial N_c}{\partial t}\Big|_{EVAPC} \tag{5.86b}$$

$$\frac{\partial r_c}{\partial t} = \sum \frac{\partial r_c}{\partial t}\Big|_{NMT} + \frac{\partial r_c}{\partial t}\Big|_{ACT} + \frac{\partial r_c}{\partial t}\Big|_{SEDC} + \frac{\partial r_c}{\partial t}\Big|_{AUTO} + \frac{\partial r_c}{\partial t}\Big|_{ACCR} + \frac{\partial r_c}{\partial t}\Big|_{CONDC} + \frac{\partial r_c}{\partial t}\Big|_{EVAPC} \tag{5.86c}$$

$$\frac{\partial N_r}{\partial t} = \sum \frac{\partial N_r}{\partial t}\Big|_{NMT} + \frac{\partial N_r}{\partial t}\Big|_{SEDR} + \frac{\partial N_r}{\partial t}\Big|_{AUTO} + \frac{\partial N_r}{\partial t}\Big|_{ACCR} + \frac{\partial N_r}{\partial t}\Big|_{EVAPR} \tag{5.86d}$$

$$\frac{\partial r_r}{\partial t} = \sum \frac{\partial r_r}{\partial t}\Big|_{NMT} + \frac{\partial r_r}{\partial t}\Big|_{SEDR} + \frac{\partial r_r}{\partial t}\Big|_{AUTO} + \frac{\partial r_r}{\partial t}\Big|_{EVAPR} \tag{5.86e}$$

where the subscript NMT refers to Non-Microphysical Tendencies (advection, turbulence, numerics and other physical processes), ACT, $SEDC$, $SEDR$, $AUTO$, $ACCR$, $CONDC$, $EVAPC$, $EVAPR$ are the microphysical contributions, i.e. respectively, activation, cloud droplet sedimentation, drizzle sedimentation, autoconversion, accretion, cloud droplet condensation, cloud droplet evaporation and drizzle evaporation.
The KK00 scheme does not take into account the drizzle self-collection (on the contrary to C2R2 for raindrops): drizzle diameters are too low for this process to impact the drizzle number concentration N_r. Moreover in the KHKO scheme, water vapor condensation on precipitating hydrometeors is not taken into account (as in C2R2).
In order to close this system of equations the rhs terms are parameterized as a function of the prognostics variables. The next sections describe parameterizations of these processes except for cloud droplet condensation/evaporation and activation, that are identical to the C2R2 scheme. For a description of the latter the reader should refer to the C2R2 documentation.

5.3.4 Collection processes

Autoconversion Autoconversion is the process that initializes precipitating hydrometeor spectra. It depends on cloud droplet spectra characteristics. In the KK00 scheme it is assumed to depend on cloud droplets number concentration N_c and mixing ratio r_c. After regression analysis on bin model simulations, KK00 obtain the following parameterized expressions for the mixing ratios conversion rates by autoconversion:

$$\frac{\partial r_r}{\partial t}\Big|_{AUTO} = 1350.r_c^{2.47}N_c^{-1.79} \tag{5.88}$$

$$\frac{\partial r_c}{\partial t}\Big|_{AUTO} = -\frac{\partial r_r}{\partial t}\Big|_{AUTO} \tag{5.89}$$

The cloud droplet number concentration source term is evaluated by assuming that all collected cloud droplet diameters are equal to the mean volume diameter D_c:

$$\left.\frac{\partial N_c}{\partial t}\right|_{AUTO} = -\frac{\left.(\frac{\partial r_r}{\partial t})\right|_{AUTO}}{\frac{\pi\rho_w}{6\rho_a}D_c^3} \tag{5.90}$$

New drizzle drops are assumed to have the diameter D_0 equal to 50 μm. Thus the drizzle number concentration source term due to autoconversion is:

$$\left.\frac{\partial N_r}{\partial t}\right|_{AUTO} = \frac{\left.\frac{\partial r_r}{\partial t}\right|_{AUTO}}{\frac{\pi\rho_w}{6\rho_a}D_0^3} \tag{5.91}$$

Accretion

Accretion rate has to be expressed as a function of cloud droplets spectra and precipitating hydrometeors spectra because accretion represents an interaction between the two categories. KK00 assume that accretion rate depends only on cloud droplet and drizzle mixing ratios. After regression analysis the following expressions for mixing ratios conversion rates are obtained:

$$\left.\frac{\partial r_r}{\partial t}\right|_{ACCR} = 67(r_c r_r)^{1.15} \tag{5.92}$$

$$\left.\frac{\partial r_c}{\partial t}\right|_{ACCR} = -\left.\frac{\partial r_r}{\partial t}\right|_{ACCR} \tag{5.93}$$

Similar to autoconversion, cloud droplets number concentration accretion sink term is expressed as the following:

$$\left.\frac{\partial N_c}{\partial t}\right|_{ACCR} = -\frac{\left.\frac{\partial r_r}{\partial t}\right|_{ACCR}}{\frac{\pi\rho_w}{6\rho_a}D_c^3} \tag{5.94}$$

Cloud droplets collection by precipitating hydrometeors involves an increase of precipitating hydrometeors mass but not of their number. For that reason there is no accretion source term for the drizzle number concentration.

5.3.5 Break-up

Break-up is applied to achieve a numerical goal only. Drizzle drops are not large enough to take into account this process. However, at some grid point, the drizzle drops number concentration and mixing ratio have non-physical low values that can result in an inconsistency between these two values and thus overly large drizzle mean volume diameters. In order to avoid this divergence, break-up is applied to limit too low values of drizzle number concentration and keep consistency between the drizzle number concentration and mixing ratio. The same protection is done for the cloud droplets number concentration. The latter is corrected when necessary in order that the cloud droplets mean volume diameter do not exceed the limit diameter between cloud droplets and drizzle i.e. 50 μm.

5.3.6 Drizzle evaporation

Precipitating drops evaporation rate can be expressed as:

$$\frac{\partial r_r}{\partial t}\Big|_{EVAPR} = \frac{2\pi\rho_w}{\rho_a} G(T,P) s_{v,w} \int_0^\infty D n_r(D) dD \tag{5.95}$$

where $G(T,P)$ is a function of temperature and pressure, $n_r(D)$ is the drizzle density function and $s_{v,w}$ is the subsaturation ($s_{v,w} = e_v/e_{vs} - 1$). Note that drizzle drops have a sufficiently low diameter to ignore the ventilation factor. By introducing a coefficient C_{evap} equal to the ratio of the drizzle drop mean diameter to the drizzle drop mean volume diameter, it becomes:

$$\frac{\partial r_r}{\partial t}\Big|_{EVAPR} = 12 C_{evap} G(T,P) (\frac{\pi\rho_w}{6\rho_a})^{\frac{2}{3}} r_r^{\frac{1}{3}} N_r^{\frac{2}{3}} s_{v,w} \tag{5.96}$$

KK00 assume that C_{evap} is a constant parameter. Its value has been adjusted using the spectra derived from the bin model simulations. They propose: $C_{evap} = 0.86$. The uncertainty of this parameter is estimated on the order of $15 - 20\%$.
KK00 calculate the rate of change of drizzle number concentration as:

$$\frac{\partial N_r}{\partial t}\Big|_{EVAPR} = \frac{N_r}{r_r} \frac{\frac{\partial r_r}{\partial t}\Big|_{EVAPR}}{\frac{\pi\rho_w}{6\rho_a} D_r^3} \tag{5.97}$$

Water vapor condensation on drizzle is not taken into account in the model. In the presence of cloud droplets, the amount of water vapor condensed on drizzle is negligible. Because positive supersaturation is encountered in clouds only, it is consistent to neglect condensation on drizzle.

5.3.7 Sedimentation

Generalities

For the two categories of liquid water, number concentration and mixing ratio sedimentation rates can be expressed respectively as function of the number concentration sedimentation flux F_{N_i} (in $\mathrm{m^{-2}\ s^{-1}}$) and the mixing ratio sedimentation flux F_{r_i} (in kg $\mathrm{m^{-2}\ s^{-1}}$) with $i = [c, r]$.

$$\frac{\partial N_i}{\partial t}\Big|_{SED_i} = \frac{\partial F_{N_i}}{\partial z} \tag{5.98}$$

$$\frac{\partial r_i}{\partial t}\Big|_{SED_i} = \frac{1}{\rho_a} \frac{\partial F_{r_i}}{\partial z} \tag{5.99}$$

with : $F_{N_i} = V_{N_i} N_i$ and $F_{r_i} = V_{r_i} \rho_a r_i$,
and :

$$V_{N_i} = \frac{F_{N_i}}{N_i} = \frac{\int_0^\infty v(D) n_i(D) dD}{\int_0^\infty n_i(D) dD} \tag{5.100}$$

$$V_{r_i} = \frac{F_{r_i}}{\rho_a r_i} = \frac{\int_0^\infty \frac{\pi}{6}\rho_w D^3 v(D) n_i(D) dD}{\int_0^\infty \frac{\pi}{6}\rho_w D^3 n_i(D) dD} \tag{5.101}$$

V_{r_i} is an average weighted by the third momentum of the distribution. For a non-monodispersed distribution, the mean terminal velocity of the mixing ratio V_{r_i} is different and greater than the mean terminal velocity of the hydrometeors V_{N_i}, because the flux of the hydrometeor mixing ratio is driven by hydrometeors of larger diameter.

Drizzle sedimentation

KK00 propose parameterized expressions of the velocity of the drizzle number concentration and the velocity of the mixing ratio as a function of the drizzle distribution mean volume diameter D_r:

$$V_{N_r} = 0.0035 D_r - 0.1 \tag{5.102}$$

$$V_{r_r} = 0.006 D_r - 0.2 \tag{5.103}$$

The coefficients have been tuned against the spectra simulated with the explicit model.

Cloud droplets sedimentation

KHKO introduces cloud droplet sedimentation on the contrary to KK00 parameterization, because this process has an impact on cloud evolution by reducing entrainment at cloud top (Ackerman et al. 2004; Bretherton et al. 2007). As in the C2R2 scheme, it is parameterized by assuming a Stokes law to calculate the cloud droplets terminal velocity and by assuming an analytical distribution to represent cloud droplet spectra. The analytical distribution used is a generalized gamma law (cf. C2R2 documentation). This law can be expressed as a function of r_c and N_c and two free parameters α_c and ν_c.
After integration, the sedimentation fluxes for the cloud droplet number concentration and the mixing ratio respectively are the following:

$$F_{N_c} = k_1 N_c D_c^2 \frac{\Gamma(\nu_c + \frac{2}{\alpha_c})}{\Gamma(\nu_c + \frac{3}{\alpha_c})^{\frac{2}{3}}} \Gamma(\nu_c)^{-\frac{1}{3}} \tag{5.104}$$

$$F_{r_c} = k_2 N_c D_c^5 \frac{\Gamma(\nu_c + \frac{5}{\alpha_c})}{\Gamma(\nu_c + \frac{3}{\alpha_c})^{\frac{5}{3}}} \Gamma(\nu_c)^{\frac{2}{3}} \tag{5.105}$$

where $\Gamma(x)$ is the gamma function and $\alpha_c = 3$, $\nu_c = 2$. These values have been adjusted by comparison with measured cloud droplet spectra during ACE-2 field campaign (Geoffroy 2007).

Appendix: List of symbols

C_{evap}	ratio of the drizzle drop mean radius to the drizzle drop mean volume radius
D_0	separation between cloud droplets and drizzle (=50 μm)
D_c, D_r	mean volume drop diameter for cloud droplet and drizzle distributions
D_v	diffusivity of water vapor in the air
e_v	water vapor pressure
e_{vs}	saturation vapor pressure over water
F_{N_c}, F_{r_c}	cloud number concentration and mixing ratio sedimentation flux
F_{N_r}, F_{r_r}	drizzle number concentration and mixing ratio sedimentation flux
$G(T,P)$	$= = \frac{1}{\rho_w}(\frac{R_v T}{e_{vs}(T) D_v} + \frac{L_v(T)}{k_a T}(\frac{L_v(T)}{R_v T} - 1))^{-1}$
k_a	heat conductivity of air
L_v	latent heat of vaporisation

n, n_c and n_r	total, cloud droplet and drizzle size distributions
N_c, N_r	cloud droplet and drizzle number concentration
N_a	activated CCN number concentration
P	pressure
r_v, r_c and r_r	water vapor, cloud droplets and drizzle mixing ratios
r_{vs}	saturated water vapor mixing ratio
R_v	gaz constant for water vapor
$s_{v,w}$	supersaturation ($= e_v/e_{vs} - 1$)
T	temperature
$v(D)$	Hydrometeor of diameter D terminal velocity
V_{N_r}, V_{r_r}	drizzle number concentration and mixing ratio mean terminal velocity
α_c, ν_c	dispersion parameters of the generalized gamma distribution
	law for the cloud droplets distribution
ρ_a and ρ_w	air and liquid water densities
$\Gamma(a)$	complete gamma function

5.4 References

Berry, E. X., and R. L. Reinhardt, 1974: An analysis of cloud drop growth by collection: Part II. single initial distributions. *J. Atmos. Sci.*, **31**, 1825-1831.

Bretherton, C. S., P. N. Blossey, and J. Uchida, 2007: Cloud droplet sedimentation, entrainment efficiency, and subtropical stratocumulus albedo. *Geophys. Res. Lett.*, **34,** L03813

Cohard, J.-M., J.-P. Pinty, and C. Bedos, 1998: Extending Twomey's analytical estimate of nucleated cloud droplet concentrations from CCN spectra. *J. Atmos. Sci.*, **55,** 3348-3357.

Cohard, J.-M., and J.-P. Pinty, 2000a: A comprehensive two-moment warm microphysical bulk scheme. Part I: Description and selective tests. *Q. J. R. Meteorol. Soc.*, **126**, 1815-1842.

Cohard, J.-M., and J.-P. Pinty, 2000b: A comprehensive two-moment warm microphysical bulk scheme. Part I: 2D experiments with a non-hydrostatic model. *Q. J. R. Meteorol. Soc.*, **126**, 1843-1859.

Cohard, J.-M., J.-P. Pinty, and K. Suhre, 2000c: On the parameterization of activation spectra from CCN microphysical properties. *J. Geophys. Res.*, **105**, D9, 11753-11766.

Foote, G. B., and P. S. Du Toit, 1969: Terminal velocity of raindrops aloft. *J. Appl. Meteor.*, **8**, 249-253.

Geleyn, J.-F., B. Catry, Y. Bouteloup, and R. Brozkova, 2008. A statistical approach for sedimentation inside a micro-physical precipitation scheme. *Tellus*, **60A**, 649-662.

Geoffroy, O., 2007: Modelisation LES des precipitations dans les nuages de couche limite et parametrisation pour les GCM, Ph.D. thesis, Universite Paul Sabatier (Toulouse III).

Kessler, E., 1969: On the distribution and continuity of water sustance in atmospheric circulations. *Meteor. Monog.*, **10**, N° 32, 84pp.

Khairoudinov, M., and Y. Kogan, 2000: A new cloud physics parameterization in a large-eddy simulation model of marine stratocumulus. *Mon. Wea. Rev.*, **128,** 229-243.

Langlois, W.E., 1973: A rapidly convergent procedure for computing large-scale condensation in a dynamical weather model. *Tellus*, **25**, 86-87.

Long, A. B., 1974: Solutions to the droplet collection equation for polynomial kernels. *J. Atmos. Sci.*, **31**, 1040-1057.

Liu, J. Y, and H. D. Orville, 1969: Numerical modeling of precipitation and cloud shadow effects on mountain-induced cumuli. *J. Atmos. Sci.*, **26**, 1283-1298.

Press, W. H., S. A. Teukolsky, W. T. Vetterling, and B. P. Flannery, 1992: *Numerical Recipes in FORTRAN: The Art of Scientific Computing.* 2nd Ed. Cambridge University Press, 963 pp.

Pruppacher, H. R and J. D. Klett, 1978: Microphysics of clouds and precipitation. Reidel, 714pp

Rood, R. B., 1987: Numerical advection algorithms and their role in atmospheric transport and chemistry models. *Review of Geoph.*, **25**, 71-100.

Twomey, S., 1959: The nuclei of natural cloud formation. Part II: The supersaturation in natural clouds and the variation of cloud droplet concentration. *Geophys. Pure Appl.*, **43**, 243-249.

Verlinde, J, P. J. Flatau, and W. R. Cotton, 1990: Analytical solution to the collection growth equation: comparison with approximate methods and application to cloud microphysics parameterization schemes. *J. Atmos. Sci.*, **47**, 2871-2880.

Chapter 6

Microphysical Scheme for Atmospheric Ice

Contents

6.1 Introduction

6.1.1 Purpose of the parameterization

The importance of ice microphysics to radiation transfer, energy budget and precipitation formation in convective storms has been widely stressed until recently (Chen and Cotton 1988; Mc Cumber et al. 1991; Chin 1994; Caniaux et al. 1995; Krueger et al. 1995; Yang and Houze 1995). There are several features that differ between the liquid and the ice phase in clouds. First, the reversible transformation between the liquid and the ice is accompagnied by a significant latent heat release ($\sim 10\%$ of the latent heat of condensation/evaporation), which can contribute to a further growth of convective clouds aloft or cooling beneath by precipitating particles falling in an unsaturated environment. Second, the terminal fall speed of the solid hydrometeors is significantly reduced compared to that of the liquid drops of the same weight. A direct consequence of these different aerodynamical properties, is that a larger time scale for the life cycle of partially glaciated convective clouds can be expected due to a larger residence time of the solid hydrometeores and a modified spatial redistribution of precipitations as well. Finally due to their different habit, the light scattering properties of the ice crystals are different from those of the cloud droplets of equivalent size and thus must be specifically accounted for in a cloud radiative transfer scheme when the ice phase is present.

6.1.2 Representation of the ice categories

The most striking feature of the ice phase in clouds is the extreme diversity and complexity of the crystal habits (see Pruppacher and Klett 1978) which lead to some uncertainity in their morphological and aerodynamical properties. This is why a great amount of curve fitting relationships have been proposed in the past to relate a characteristic dimension of an ice crystal to its volume, mass and terminal fall speed. So in order to elucidate the impact of the ice phase in a mesoscale model such as **Meso-NH**, many practical arguments are in favor of unavoidable but necessary assumptions in the bulk representation of some selected ice categories.

Actual ice parameterizations retain 2 (Rutledge and Hobbs 1983; Cotton et al. 1982[1]), 3 (Lin et al. 1983; Rutledge and Hobbs 1984; Ziegler 1985) or 4 (Ferrier 1994) and even 5 (Walko et al. 1995) ice categories. In a recent evaluation of the impact of the number of ice categories, Mc Cumber et al. (1991) concluded that at least 3 different ice types are necessary to cover most of their precipitating case study but they draw attention on the fact that application and tuning of the scheme might be case specific. The common agreement about an ice phase microphysical scheme is that it must include the pristine or primary ice phase issuing from heterogeneous nucleation processes, the aggregates or snowflakes type corresponding to lightly rimed large ice crystals or dry assemblages and a third category of more or less heavily rimed crystals which are graupels, frozen drops or hail, depending of considerations on the density of the particles. A matter of discussion can be found regarding the last category of ice particles as a physical discrimination exists in the growth mode of low density (~ 0.4) rimed particles (assumed to be dry for the graupels) from that of the high density (~ 0.9) hailstones which grow in the wet mode. In the definition of the present scheme, the user can handle either 3 categories of ice for simplification or 4 categories that distinguish hail from graupel.

Another point of concern is related to the supplementary prognostic equations for the number concentration of ice crystal in each category. For instance Cotton et al. (1986) and others use a specific equation to predict the primary ice number concentration which is motivated by the representation of both the heterogeneous ice-nucleation processes (see for instance, the revised version of Meyers et al. (1992)) and the secondary production of ice crystals known as the Hallett-Mossop (HM) or rime-splitering mechanism (Hallett annd Mossop 1974). Furthermore, several authors (Ziegler 1985; Murakami 1990; Ferrier 1994; Meyeers et al. 1996) have included a number concentration equation for their precipitating ice particles in their scheme which is in contrast with other simplified approaches where the intercept parameter of the crystal distribution or the total number concentration is given. In the present scheme, a somewhat different solution have been adopted. For this first version of the scheme, neither the HM process nor the immersion freezing of cloud droplets will be considered at once thus giving the opportunity to simply diagnose[2] the primary ice total number in the manner described in Ferrier (1994)[3]. Secondly, rather than working with more or less fixed number concentrations of precipitating ice or developping prognostic equations where the shaping of the spectra by self-aggregation/break-up processes is difficult to control, we followed Caniaux (1993) who after compiling various published experimental observations, established that the total number concentration N can be simply related to the slope parameter λ of the

[1] This reference is purely historical as the CSU-RAMS ice microphysical scheme has been greatly improved by Cotton et al. (1986)

[2] Although there is no serious physical difficulty to consider a prognostic equation for the primary ice total number concentration, we shall consider this improvement in a future version of the code with a high priority.

[3] see his equation 4.33, which condenses the results of Meyers et al. (1992)

ice precipitating category as[4]:

$$N = C\lambda^x. \tag{6.1}$$

Taking $x = 0$ means that the total number concentration is held fixed while for $x = -1$, it is the intercept parameter ($N_0 \equiv C$) of a Marshall-Palmer distribution law ($n(D) = N_0\, e^{-\lambda D}$) which is assumed to be a constant. In fact, as we want to grossly reproduce the broadening of the spectra (a decrease of λ) by the self-aggregation processes (a reduction of N), it is imperative to have $x > 0$. In (6.1), both C and x depend on the ice category and must be specified from physical arguments. However, experimental evidence and a sensitivity study leads Caniaux (1993) to link C and x by the following relationship:

$$\log_{10} C = -3.55\, x + 3.89, \tag{6.2}$$

thus reducing the degree of freedom for the choice of C and x.

To summarize and as a first step toward a more advanced scheme, the following strategy is adopted:

- the scheme contains a prognostic equation for the primary ice mixing ratio r_i, the snowflakes mixing ratio r_s, and the rimed crystals mixing ratio r_g,
- the total number concentration of the primary ice N_i is diagnosed while the total number concentration of the snowflakes N_s and of the rimed crystals N_g follow (6.1),
- power law relationships are used to relate the mass to the diameter[5],

  $$m(D) = aD^b \tag{6.3}$$

  and the terminal speed velocity to the diameter

  $$v(D) = cD^d\, (\rho_{00}/\rho_{dref})^{0.4}, \tag{6.4}$$

  where the last factor is the Foote and Du Toit (1969) correction of the air density, ρ_{00} being the air density at the reference pressure level P_{00}.
- each category of ice particle is assumed to be distributed according to

  $$n(D) = N\, g(D), \tag{6.5}$$

  where $g(D)$ is a normalized distribution law to be chosen in Table 6.1.

  It can be noticed that according to Tripoli and al. (1988), the use of the generalized Gamma law allows the maximal flexibility without requiring much computation effort as for instance, $M(p)$, the p^{th} moment of the law is simply expressed as:

  $$M(p) = \int_0^\infty D^p g(D)\, dD = \frac{G(p)}{\lambda^p}, \tag{6.6}$$

  where

  $$G(p) = \frac{\Gamma(\nu + p/\alpha)}{\Gamma(\nu)}, \tag{6.7}$$

[4]The intercept parameter N_0 of a Marshall-Palmer law is used in the original formulation of Caniaux (1993), but we found more convenient to generalize the relationship in (6.1) to the total number concentration.

[5]The diameter D refers to the maximum ice particle dimension. From (6.3), it is easy to show that D_{sph}, the equivalent spherical diameter is $D_{sph} = (6/\pi\ a/\rho_{ice})^{1/3} D^{b/3}$ with ρ_{ice} being the density of the ice (taking $\rho_{ice} = \rho_w$ means that D_{sph} is the melted diameter).

Table 6.1: Analytical formulation of various normalized distribution laws (from Tripoli and al. 1988).

Name of the distribution law	Mathematical expression
generalized Gamma	$g(D) = \frac{\alpha}{\Gamma(\nu)} \lambda^{\alpha\nu} D^{\alpha\nu-1} \exp\big(-(\lambda D)^{\alpha}\big)$
Gamma ($\alpha = 1$)	$g(D) = \frac{\lambda^{\nu}}{\Gamma(\nu)} D^{\nu-1} \exp(-\lambda D)$
Marshall-Palmer ($\alpha = 1$ and $\nu = 1$)	$g(D) = \lambda \exp(-\lambda D)$
Weibull ($\nu = 1$)	$g(D) = \alpha \lambda^{\alpha} D^{\alpha-1} \exp\big(-(\lambda D)^{\alpha}\big)$
Rayleigh ($\alpha = 2$ and $\nu = 3/2$)	$g(D) = \frac{\lambda^3}{\sqrt{\pi}} D^2 \exp\big(-(\lambda D)^2\big)$
Lognormal	$g(D) = \frac{1}{\sqrt{2\pi}\sigma D} \exp\big[-\big(\frac{\log(\lambda D)}{\sqrt{2}\sigma}\big)^2\big]$

for a generalized Gamma law or

$$G(p) = \exp\big(\frac{p^2\sigma^2}{2}\big), \tag{6.8}$$

in case of lognormal distribution.

- the ice content, ρr, of any specy i, s or g is defined by:

$$\rho r = \int_0^{\infty} m(D) n(D)\, dD = aNM(b), \tag{6.9}$$

where (6.3), (6.5), and (6.6) have been used. The slope parameter λ is then easily computed by inserting (6.1) and (6.6) into (6.9) to give:

$$\lambda = \Big(\frac{\rho r}{aCG(b)}\Big)^{\frac{1}{x-b}}. \tag{6.10}$$

Corollarily, it can be seen from the above equation that $x < b$ to ensure an opposite sense of variation for ρr and λ (see Fig. 6.1) that is the presence of large ice particles (low λ) are associated with high mixing ratios r and probably low concentration $x > 0$ as shown above.

6.1.3 General characteristics of the ice crystals

Each ice category is characterized by a specific set of value for the parameters involved in (6.1) according to their relative size abundance and in (6.3; mass-diameter), (6.4; fall speed-diameter), (6.38; vapor growth capacity-diameter), and (6.39; ventilation factor-diameter) depending upon their habit and growth mode. Note that each ice crystal is potentially precipitating even if the terminal fall speed of the primary ice crystal is negligible compared to that of the aggregates and the rimed particles. Doing so ensures the long term dissipation of unactive cirrus clouds or thunderstorm anvils by the sublimation of crystals falling in the subsaturated layers underneath.
Cloud ice is assumed to be distributed by a low dispersion (high ν) generalized Gamma law corresponding to an exponential distribution of the volume of quasi-spherical crystals ($\alpha = 3$) (see,

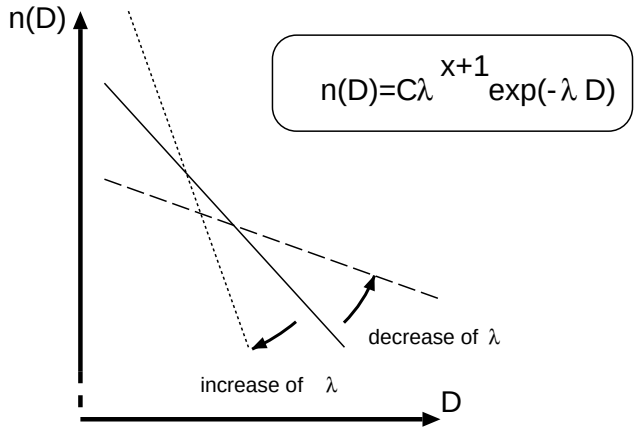

Figure 6.1: Modified Marshall-Palmer distribution $n(D)$ as a function of the slope parameter λ in log scale (from Caniaux 1993).

Ziegler 1985) while the precipitating particles follow the more classical exponential (or Marshall-Palmer) law.

In Table 6.2, the parameters of the r_s class describe the behavior of unrimed radiating assemblages of plates, side planes, bullets and columns or that of densely rimed radiating assemblages of dendrites. The parameters chosen for the r_g class correspond to those of lump graupels[6]. All the values of the a, b, c and d parameters are taken from Locatelli and Hobbs (1974) for the icy hydrometeors and from Starr and Cox (1985) and Heymsfield (1972) for the primary crystals (hexagonal plates)[7]. The ventilation coefficients ($\overline{f}_{0,1,2}$), based on Hall and Pruppacher (1977), are valid for spheres and for oblate spheroids as well. The $C - x$ values have been selected after the work of Passarelli (1978) and Mitchell (1988)[8] on the snowflake distribution theory and of Houze et al. (1979), but with a large uncertainty on the fact that the measured crystals could be graupels. It is important to stress that $x = 1$ is an acceptable value for snow because these particles are bidimensional particles ($b = 1.9$) with a variable density.

[6]For hailstones, $a = 470$ and $b = 3$ corresponding to spherical particles of density $\rho_{ice} = 900$ kg/m^3 together with $c = 207$ and $d = 0.64$ (Böhm 1989) and $C \sim 5\ 10^{-4}$ with $x \sim 2$ are recommended values from the analysis made by Cheng and English (1983).

[7]Starr and Cox (1985) provided several sets for a, b, c and d suitable for different crystal habits in cirrus clouds. They are recalled in the table below for completness.

Crystal habit	Columns	Bullet rosettes	Plates
a	$2.14\ 10^{-3}$	44	0.82
b	1.7	3.0	2.5
c	$2.1\ 10^{5}$	$4.3\ 10^{5}$	$8.0\ 10^{2}$
d	1.585	1.663	1.000

Note that the fall speed parameters are valid for the crystal size range of 0-200 μm and that c contains the air density correction ($\rho = 0.58$ kg/m^3 assumed at 40 kPa). The bullet rosettes with a quasi spherical shape ($b = 3$) impose to take $\mathcal{C}_{1_i}$ closer to 0.5 in such a case.

[8]Values for x close to 2 have been retrieved by recent radar and aircraft data analysis (see, Thomason et al. 1995 in 27^{th} *Conf. on Radar Met.* but for spectrum tails due to large particles). However taking x too much close to 2 leads to some inconsistancies in computing λ from (6.10)

Table 6.2: Set of parameters used to characterize each ice category and the raindrops (Kessler scheme).

Parameters	r_i	r_s	r_g		r_r	r_c
α	3	1	1		1	3 on sea; 1 on land
ν	3	1	1		1	1 on sea; 3 on land
a	0.82	0.02	19.6		524	524
b	2.5	1.9	2.8		3	3
c	800	5.1	124		842	3.2 10^7
d	1.00	0.27	0.66		0.8	2
C		5	5 10^5		8 10^6	
x		1	-0.5		-1	
$\overline{f}_0$	1.00	0.86	0.86		1.00	
$\overline{f}_1$		0.28	0.28		0.26	
$\overline{f}_2$	0.14					
$\mathcal{C}_1$	$1/\pi$	1/π	0.5		0.5	

6.1.4 Nomenclature

The different rates at which microphysical processes involving one ice specy at least, have a symbolic name which is built according to the following rules:

- a first letter (R or C) to mean that the rate is relevant for a mixing Ratio or for a Concentration,
- a second letter (V, C, I, R, S or G) to identify the Sink specy,
- a group of three letters to shorten the name of the MICrophysical process,
- an optional letter to recall the name of the "Reactant" specy in case of three-component process,
- a last letter (I, R, S or G) to identify the Source specy.

6.1.5 Outlines of the microphysical scheme for mixed phase clouds

Warm processes

Cloud droplets nucleate and grow by condensation of water vapor or are forced to evaporate instantaneously according to the supply of water vapor by transport. Then autoconversion and accretion processes take place to form and accelerate the growth of the precipitable raindrops which evaporate when falling below the cloud base.

Table 6.3: List of the warm microphysical processes (not involving ice particles).

Symbol	Mechanism	Sink	Source	Process
$RVCNDC$	$r_v \implies r_c$	r_v	r_c	condensation on cloud droplets
$RCAUTR$	$r_c + r_c \implies r_r$	r_c	r_r	autoconversion of cloud droplets
$RCACCR$	$r_c + r_r \implies r_r$	r_c	r_r	accretion of cloud droplets by raindrops
$RREVAV$	$r_r \implies r_v$	r_r	r_v	evaporation(condensation)

Cold processes

Small ice crystals are initiated by two heterogeneous nucleation processes:

- deposition: formation of ice embryos in a supersaturated environment over ice,
- contact: freezing of supercooled droplet subsequent to the attraction of aerosol particles by Brownian motion or by phoretic diffusion (a function of temperature).

Also, when the temperature drops below $-35°$C, the homogeneous nucleation or droplet freezing takes place to deplete very rapidly the cloud droplets.
Ice crystals can grow by water vapor deposition or decay by sublimation depending on the level of saturation of the environment with respect to ice. Aggregates are formed by autoconversion process of pristine ice crystals while the primary source of graupel is either raindrop contact freezing or heavy riming of the snowflakes. When the air temperature is warmer than T_t, the small primary ice crystals are immediately converted into cloud water, the snowflakes are transfered into the graupel category at a rate proportional to their partial melting (Walko et al. 1995) and finally the graupels melt by shedding all the liquid water into raindrops.
The representation of ice crystal growth by collection processes (for instance by aggregation, riming or rain contact freezing) remains the most difficult and controversial task. As in many bulk parameterizations, the assumptions of continuous growth and the simple geometric sweep-out concept for the collection kernel K are retained. So the mutual gravitational interaction between species X and Y leads to a general definition of K,

$$K(D_x, D_y) = \frac{\pi}{4}(D_x + D_y)^2 |v_x(D_x) - v_y(D_y)| E_{xy}, \tag{6.11}$$

where E_{xy} is the collection efficiency (often, a poorly known quantity).
In the most general case, the collection process COL involving X and Y can lead to the formation of a third specy Z (simultaneous collection and conversion processes with sometimes further external conditions on the mixing ratios r_x and r_y), so the mixing ratio tendency of specy Y (a loss for Y) due to the mass collection of X is:

$$RYCOLXZ = \rho^{-1} \int_0^\infty \Big\{ \int_0^\infty K(D_x, D_y)\, m_y(D_y) n_y(D_y) dD_y \Big\} n_x(D_x) dD_x, \tag{6.12}$$

Table 6.4: List of the cold microphysical processes (involving ice particles).

Symbol	Mechanism	Sink	Source	Process
$RVHENI$	$r_v \Longrightarrow r_i$	r_v	r_i	heterogeneous nucleation
$RCHONI$	$r_c \Longrightarrow r_i$	r_c	r_i	homogeneous nucleation
$RRHONG$	$r_r \Longrightarrow r_g$	r_r	r_g	homogeneous nucleation
$RCBERI$	$r_c \Longrightarrow r_i$	r_c	r_i	Bergeron-Findeisen effect
$RVDEPI$	$r_v + r_i \Longrightarrow r_i$	r_v	r_i	deposition(sublimation)
$RVDEPS$	$r_v + r_s \Longrightarrow r_s$	r_v	r_s	deposition(sublimation)
$RVDEPG$	$r_v + r_g \Longrightarrow r_g$	r_v	r_g	deposition(sublimation)
$RIAUTS$	$r_i + r_i \Longrightarrow r_s$	r_i	r_s	autoconversion of pristine ice
$RIAGGS$	$r_i + r_s \Longrightarrow r_s$	r_i	r_s	aggregation of pristine ice
$RRCFRIG$	$r_i + r_r \Longrightarrow r_g$	r_r	r_g	raindrops contact freezing
$RICFRRG$	$r_i + r_r \Longrightarrow r_g$	r_i	r_g	raindrops contact freezing
$RCRIMSS$	$r_c + r_s \Longrightarrow r_s$	r_c	r_s	light riming of aggregates
$RCRIMSG$	$r_c + r_s \Longrightarrow r_g$	r_c	r_g	heavy riming of aggregates
$RSRIMCG$	$r_c + r_s \Longrightarrow r_g$	r_s	r_g	heavy riming of aggregates
$RRACCSS$	$r_r + r_s \Longrightarrow r_s$	r_r	r_s	accretion of rain and aggregates
$RRACCSG$	$r_r + r_s \Longrightarrow r_g$	r_r	r_g	accretion of rain and aggregates
$RSACCRG$	$r_r + r_s \Longrightarrow r_g$	r_s	r_g	accretion of rain and aggregates
$RCDRYG$	$r_c + r_g \Longrightarrow r_g$	r_c	r_g	dry growth of the graupels
$RIDRYG$	$r_i + r_g \Longrightarrow r_g$	r_i	r_g	dry growth of the graupels
$RRDRYG$	$r_r + r_g \Longrightarrow r_g$	r_r	r_g	dry growth of the graupels
$RSDRYG$	$r_s + r_g \Longrightarrow r_g$	r_s	r_g	dry growth of the graupels
$RCWETG$	$r_c + (r_g) \Longrightarrow r_r$	r_c	r_r & r_g	partial freezing & water shedding
$RRWETG$	$r_r + (r_g) \Longrightarrow r_g$	r_r	r_g	partial freezing & water shedding
$RIWETG$	$r_i + r_g \Longrightarrow r_g$	r_i	r_g	wet growth of the graupels
$RSWETG$	$r_s + r_g \Longrightarrow r_g$	r_s	r_g	wet growth of the graupels
$RIMLTC$	$r_i \Longrightarrow r_c$	r_i	r_c	melting
$RGMLTR$	$r_g \Longrightarrow r_r$	r_g	r_r	melting
$RSCVMG$	$r_s \Longrightarrow r_g$	r_s	r_g	conversion melting

conversely the mixing ratio tendency for X (a loss too but for X) is:

$$RXCOLYZ = \rho^{-1} \int_0^\infty \Big\{ \int_0^\infty K(D_x, D_y)\; m_x(D_x) n_x(D_x) dD_x \Big\} n_y(D_y) dD_y, \tag{6.13}$$

and the mixing ratio tendency of specy Z (a gain for Z) is simply $RXCOLYZ + RYCOLXZ$. When Z identifies to one of the initial specy X or Y, i. e. a two component process, a single mixing ratio collection rate needs to be computed as for instance Eq. (6.13) if $Z \equiv Y$ or Eq. (6.12) if $Z \equiv X$ as for instance

$$RYCOLX = \rho^{-1} \int_0^\infty \Big\{ \int_0^\infty K(D_x, D_y)\, m_y(D_y) n_y(D_y) dD_y \Big\} n_x(D_x) dD_x = -RXCOLY \tag{6.14}$$

is the mixing ratio rate of change of specy X due to the single collection of specy Y.
More complicated and as discussed by Farley et al. (1989) and Ferrier (1994), collection processes might be envisionned as both two and three component processes when threshold diameters are introduced for instance to convert specy Y into specy Z if and only if the diameter D_y of Y is larger than a required value D_y^{lim}. This means than only a fraction (generally the upper diameter one) of specy Y, collecting specy X, will be converted into specy Z and thus be removed from the Y category, while the remaining fraction of the former specy Y increases its mass as a binary collection process between X and Y. So, the growth of X from Y is now:

$$RYCOLXX = \rho^{-1} \int_0^\infty \Big\{ \int_0^{D_y^{lim}} K(D_x, D_y)\, m_y(D_y) n_y(D_y) dD_y \Big\} n_x(D_x) dD_x, \tag{6.15}$$

the growth of Z from both X and Y is:

$$\begin{aligned} RYCOLXZ &= RYCOLX - RYCOLXX \\ &= \rho^{-1} \int_0^\infty \Big\{ \int_{D_y^{lim}}^\infty K(D_x, D_y)\, m_y(D_y) n_y(D_y) dD_y \Big\} n_x(D_x) dD_x, \end{aligned} \tag{6.16}$$

while $RYCOLX$, the total loss of Y (leading to the growth of X in Eq. (6.15) and to the growth of Z in Eq. (6.16)), is given by Eq. (6.14).
Although, this approach has much more physical basis, it needs a (technically more complicated) partial integration over the dimensional spectrum of at least a specy to compute the mixing ratio tendencies.
In the present parameterization, any accreted material on the graupels cannot change the type of this crystal but the concurrent dry/wet growth regimes will compete in the manner described by Lin et al. (1983). So much of these collection processes will be described by integrals of type (6.14). Considering now the collection processes on aggregates, it is postulated that beyond a critical size of the initial aggregate, the riming of cloud droplets may modify so much the crystal characteristics that it is converted into a graupel. Furthermore, the collection of raindrops on aggregates is also very efficient to convert the upper part of the aggregate spectrum into graupels in the manner suggested by Ferrier (1994). So partial integrals of the form (6.15) need to be computed to represent the two latter collection processes.

6.2 Microphysical processes

6.2.1 Summary of the scheme

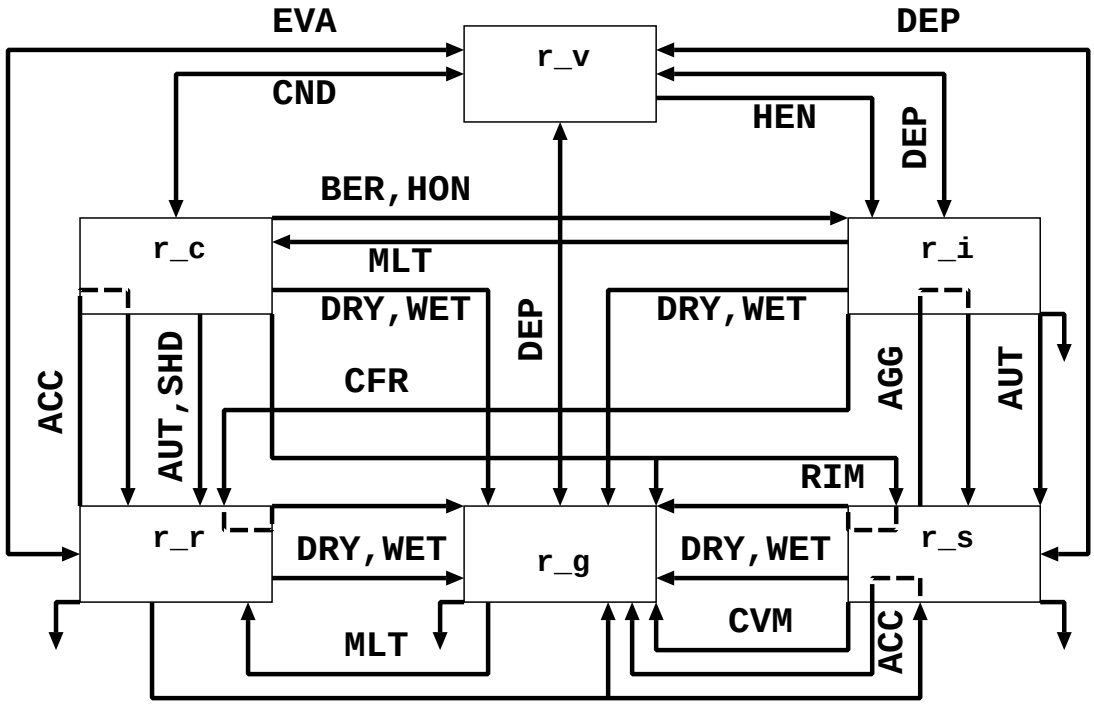

Figure 6.2: Diagram of the microphysical processes for mixed phase cloud in the present scheme.

6.2.2 Warm processes

The parameterization of these processes is borrowed from the widespread Kessler scheme described elsewhere, so the mathematical expression of these processes is only recalled here for completness.

$$RCAUTR = k_{cr}\ Max(0, r_c - r_c^*), \tag{6.17}$$

with $k_{cr} = 10^{-3}$ s^{-1} and $q_c^* = r_c^*/\rho_{dref} = 0.5\ 10^{-3}$ kg/m^3.

$$RCACCR = \frac{\pi}{4} N_r r_c c_r M(d_r + 2)\Big(\frac{\rho_{00}}{\rho_{dref}}\Big)^{0.4} \tag{6.18}$$

and

$$RREVAV = \frac{4\pi}{\rho}\frac{(-SS_w)}{A_w(T,P)} N_r \mathcal{C}_{1r}\big[\overline{f}_{0r} M_r(1) + \overline{f}_{1r} c_r' M_r(\frac{d_r+3}{2})\big], \tag{6.19}$$

where $SS_w = r_v/r_{vs_w} - 1$ and

$$A_w(T,P) = \frac{L_v(T)^2}{k_a(T) R_v T^2} + \frac{R_v T}{D_v(T,P) e_{sw}(T)}.$$

Table 6.5: Set of parameters used to parameterize the nucleation processes (from Ferrier 1994).

N_{NU1_0}	N_{NU2_0}	α_1	β_1	α_2	β_2	m_{NU_0}
50 m^{-3}	1000 m^{-3}	4.5	0.6 K^{-1}	12.96	0.639	6.88 10^{-13} kg

$\mathcal{C}_{1r}$, f_{0r} and f_{1r} are taken from Table 6.2 and $c'_r = Sc_v^{1/3}(c_r\rho/\eta)^{1/2}(\rho_{00}/\rho_{dref})^{0.2}$ with $Sc_v \sim 0.635$ (see after (6.39)). Note that according to the nomenclature and sign convention: $RREVAV > 0$ in case of rain evaporation.
In order to reproduce the small drizzle of the fog necessary for its dissipation, the sedimentation of cloud droplets $RSEDC$ can be taken into account. The slope parameter for the cloud λ_c used for the mass sedimentation rate is defined by :

$$\lambda_c = \left[\frac{\pi}{6}\rho_w \frac{\Gamma(\nu_c + \frac{3}{\alpha_c})}{\Gamma(\nu_c)} \frac{N_c}{\rho_d r_c}\right]^{\frac{1}{3}}$$

α_c, ν_c and N_c are defined according to the fractions of sea and land surface cover of the grid mesh, with $N_{c_{sea}}$ =100 cm^{-3} and $N_{c_{land}}$ =300 cm^{-3}.

6.2.3 Heterogeneous nucleation

As in Ferrier (1994) and according to Meyers et al. (1992), the number concentration of primary ice crystals N_{NU} formed by heterogeneous nucleation is given by:

$$N_{NU} = \begin{cases} N_{NU1}, & T - T_t \geq -5\text{K}, \\ N_{NU2}, & T - T_t < -5\text{K} \end{cases} \tag{6.20}$$

where

$$N_{NU1} = N_{NU1_0}\left[(r_v - r_{vs_i})/(r_{vs_w} - r_{vs_i})\right]^{\alpha_1} exp(-\beta_1(T - T_t)), \tag{6.21}$$
$$N_{NU2} = N_{NU2_0} exp(\alpha_2 SS_i - \beta_2), \tag{6.22}$$

where $SS_i = r_v/r_{vs_i} - 1$ is the supersaturation ratio with respect to ice and r_{vs_w} is the saturated mixing ratio over supercooled water.
Assuming that $N_i = N_{NU}$ (because the secondary ice production is not yet considered) and for m_{NU_0}, the mass of a nucleated ice crystal, the mass nucleation rate $RVHENI$ equals to:

$$RVHENI = (\rho\Delta t)^{-1} m_{NU_0} Max(N_{NU} - N_i^{t-\Delta t}, 0). \tag{6.23}$$

The typical values of the unknown parameters are given in Table 6.5.
In (6.23), the previous ice crystal concentration $N_i^{t-\Delta t}$ is available because the diagnostic variable $N_i = N_{NU}$ is stored after an update by the mean of (6.20).

Table 6.6: Values of $J_{HOM}(T)$ after Pruppacher (1995).

$T - T_t$ (K)	-35	-36	-37	-38	-39
J_{HOM} ($m^{-3}s^{-1}$)	$2\ 10^{11}$	$1\ 10^{13}$	$3\ 10^{14}$	$5\ 10^{15}$	$9\ 10^{16}$

$T - T_t$ (K)	-40	-41	-42	-43	-44
J_{HOM} ($m^{-3}s^{-1}$)	$1\ 10^{18}$	$2\ 10^{19}$	$1\ 10^{21}$	$5\ 10^{22}$	$2\ 10^{23}$

6.2.4 Homogeneous nucleation

When the temperature drops below $-35°$C, the spontaneous freezing of cloud droplets in absence of ice nuclei (the homogeneous nucleation) is an active process to convert any remaining small droplets into pristine crystals. This is an essential process in cirriform clouds so it needs to be modeled accurately in such cases.
The probability $\mathcal{P}$ of a water droplet of volume V to freeze in the interval of time $[t,\ t + \Delta t]$ is governed by the nucleation formula

$$\mathcal{P} = 1 - \exp\Big(- \int_t^{t+\Delta t} J_{HOM}(T) V \, dt \Big), \tag{6.24}$$

where V is the droplet volume and $J_{HOM}(T)$ the freezing rate, tabulated by Pruppacher (1995) and reported in Table 6.6[9],
The above set of data has been approximated by a fitting curve which is:

$$J_{HOM} = \exp(\alpha_3 (T - T_t) - \beta_3), \tag{6.25}$$

with $\alpha_3 = -3.075$ K^{-1} and $\beta_3 = 81.00356$.
Considering $J_{HOM}(T)$ and V as constant during the timestep Δt, (6.24) can be reduced to

$$\mathcal{P} \approx J_{HOM}(T) V \Delta t. \tag{6.26}$$

Integrating (6.26) over the cloud droplet spectrum and differentiating with respect to time and using (6.9) with an appropriate form for the cloud droplets, gives the final homogeneous nucleation rate

$$RCHONI = Min\Big\{ \frac{r_c}{\Delta t}, \frac{\pi}{6} J_{HOM}(T) (\rho r_c) \frac{M_c(6)}{M_c(3)} \Big\}. \tag{6.27}$$

To compute the M_c ratio in (6.27), it is assumed that $\lambda_c = 1.1\ 10^5$ m^{-1} corresponding to a cloud droplet number concentration $N_c \sim 400\ 10^6$ m^{-3} and a mixing ratio $r_c \sim 10^{-3}$ kg/kg for $\rho \sim 1$ kg/m^3.
Because the scheme assumes that the ice crystal concentration is determined by the only heterogeneous nucleation parameterization, the diagnostic concentration of these pristine crystals is not modified by the present homogenous nucleation scheme. This is a source of error indeed because this concentration must be accounted for in computing the very slow speed of sedimentation of cirrus clouds in long lived simulations. The solution which has been adopted in the present scheme

[9]Note that J_{HOM} goes to infinity as $T - T_t < -44$ K

employs a specific ice crystal number concentration relationship to compute a sedimentation flux of these small crystals (see the subsection relative to the computation of $RSEDI$).
We assume also that the raindrops cannot survive to temperature colder than $-35°$C because they are spontaneously converted to graupels by homogenous freezing (nucleation)

$$RRHONG = \frac{r_r}{\Delta t} H(T_t - 35), \tag{6.28}$$

where $H(x)$ is the Heaviside distribution ($H(x) = 0$ if $x < 0$ and $H(x) = 1$ if $x \geq 0$)

6.2.5 Deposition (sublimation) of water vapor

The rate of mass growth or decay of a single aggregate or graupel particle by vapor deposition or sublimation can be written as:

$$\partial m/\partial t \mid_{DEP/SUB} = 4\pi S S_i \mathcal{C} \overline{f} / A_i(T, P), \tag{6.29}$$

where $\mathcal{C}$ is the capacity of the ice crystal, $\overline{f}$ is a ventilation factor and $A_i(T, P)$ is a thermodynamic function:

$$A_i(T, P) = \frac{L_s(T)^2}{k_a(T) R_v T^2} + \frac{R_v T}{D_v(T, P) e_{si}(T)}, \tag{6.30}$$

where e_{si} is the saturation vapor pressure over ice:

$$e_{si}(T) = exp\big(\alpha_i - \frac{\beta_i}{T} - \gamma_i \ln(T)\big), \tag{6.31}$$

with

$$\alpha_i = \ln(e_{si}(T_t)) + \frac{\beta_i}{T_t} - \gamma_i \ln(T_t) \tag{6.32}$$

$$\beta_i = \frac{L_s(T_t)}{R_v} \gamma_i T_t \tag{6.33}$$

$$\gamma_i = \frac{C_i - C_{pv}}{R_v} \tag{6.34}$$

and L_s is the latent heat of sublimation:

$$L_s(T) = L_s(T_t) + (C_{pv} - C_i)(T - T_t). \tag{6.35}$$

The thermal conductivity of the air $k_a(T)$ and the diffusivity of water vapor in the air $D_v(T, P)$ are given by (see Pruppacher and Klett 1978, pp. 418 and 413):

$$D_v(T, P) = 0.2138\ 10^{-4} (T/T_t)^{1.94} (P_{00}/P), \tag{6.36}$$

$$k_a(T) = 2.38\ 10^{-2} + 0.0071\ 10^{-2} (T - T_t). \tag{6.37}$$

In (6.29), $\mathcal{C}$ and $\overline{f}$ have the following expressions depending upon the crystal shape and size

$$\mathcal{C} = \mathcal{C}_1 D \tag{6.38}$$

$$\overline{f} = \overline{f}_0 + \overline{f}_1\chi + \overline{f}_2\chi^2 \tag{6.39}$$

where $\chi = Sc_v^{1/3}Re^{1/2}$ is a function of $Sc_v = \nu(T,P)/D_v(T,P)$, the Schmidt number for water vapor and of $Re = v(D)D\rho/\eta(T)$, the Reynolds number of the flow around a crystal of size D. The dynamic viscosity $\eta(T) = \rho(T,P)\nu(T,P)$ of the air of density $\rho(T,P)$ is given by (see Pruppacher and Klett 1978, p. 323):

$$\eta(T) = 1.718\,10^{-5} + 0.0049\,10^{-5}(T - T_t). \tag{6.40}$$

In the following, $Sc_v \approx 0.635$ with a very good approximation.
In 6.38, a cylindrical shape is assumed for the aggregates while the rimed particles are spherical (see Table 6.2). Furthermore, as the pristine ice category is assumed to contain small crystals only, in contrast to the aggregates and rimed particles which are rather large-size hydrometeors, the formulas of Hall and Pruppacher (1977) have been split for a simplified application to the $D < 70\mu$m range, relevant of the r_i specy (see below for the parameterization of the Bergeron-Findeisen effect), and for the $D > 70\mu$m range corresponding to the r_s and r_g categories (see Table 6.2).
Integration of (6.29) over the whole particle spectral range gives for $X(=j)$ being $S(=s)$ or $G(=g)$:

$$RVDEPX = \frac{4\pi}{\rho}\frac{SS_i}{A_i(T,P)}N_j\mathcal{C}_{1j}\left[\overline{f}_{0j}M_j(1) + \overline{f}_{1j}c'_jM_j(\frac{d_j+3}{2}) + \overline{f}_{2j}c'^2_jM_j(d_j+2)\right], \tag{6.41}$$

where $c'_j = Sc_v^{1/3}(c_j\rho/\eta)^{1/2}(\rho_{00}/\rho_{dref})^{0.2}$ and where the moments M_j of the ice category $_j$ can be expanded according to (6.6.)
Although the water vapor exchanges over the pristine ice crystals (and the cloud droplets) in the present scheme are treated implicitly by an adjustment process (see paragraph 6.3.4), an expression equivalent to the explicit rate $RVDEPX$ needs to be computed for the purpose of parameterizing the Bergeron-Findeisen effect described hereafter.

6.2.6 Bergeron-Findeisen effect

A mixed phase cloud is characterized by the simultaneous existence of cloud droplets and small ice crystals in equilibrium with the vapor saturation level over liquid water and ice water, respectively (Fig. 6.3). As the later is always lower that the former ($e_{si}(T) < e_{sw}(T)$), there is a systematic evaporation of the cloud droplets for deposition onto the ice crystals. This process is independent of the droplet and crystal growth or decay due to the supply or deficit of water vapor as for instance by vertical transport.
In the present scheme, it is assumed that $RCBERI$, the resulting rate of mass transfer from the cloud droplets to the ice crystals, is determined by the rate of water vapor deposition onto the pristine ice crystals. This rate is assumed to be equal to the rate of evaporation of the cloud droplets so the process is neutral with respect to the water vapor reservoir but not for the heat budget as the corresponding heat of freezing is accounted to warm the environmental air. The expression of $RCBERI$ is a case application of (6.41) for the pristine ice that is:

$$RCBERI = \frac{4\pi}{\rho}\frac{SS_i}{A_i(T,P)}N_i\mathcal{C}_{1i}\left[\overline{f}_{0i}M_i(1) + \overline{f}_{2i}c'^2_iM_i(d_i+2)\right], \tag{6.42}$$

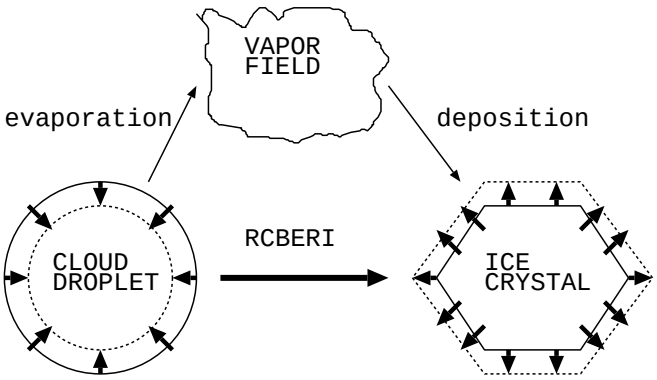

Figure 6.3: Illustration of the Bergeron-Findeisen effect and its parameterization.

where d_i, $\mathcal{C}_{1i}$, f_{0i} and f_{2i} are taken from Table 6.2 and $c'_i = Sc_v^{1/3}(c_i\rho/\eta)^{1/2}(\rho_{00}/\rho_{dref})^{0.2}$ with $Sc_v \sim 0.635$.

6.2.7 Autoconversion of primary ice crystal to form aggregates

This process is the only way to initiate aggregates in a cold cloud and generally two approaches are employed to describe it. In the first one (Cotton et al. 1986), the aggregation rate has some physical root as it is based upon the stochastic collection kernel (K_{PS}) of Passarelli and Srivastava (1978). In the second one (adopted in the present scheme because of its simplicity), a formula analogous to the cloud droplet autoconversion parameterization of Kessler is used with:

$$RIAUTS = k_{is}\ Max(0, r_i - r_i^*). \tag{6.43}$$

The inverse time constant k includes a temperature efficiency factor as in Lin et al. (1983) ($k_{is} = 10^{-3}\ e^{0.015(T-T_t)}$) while the critical ice mixing ratio r_i^* varies with temperature. This threshold, expressed as critical ice specific humidity q_i^*, was initially set equal to a fixed value of $0.5\ 10^{-3}$ kg/m^3, in the "realistic" range of $0.1\ 10^{-3}$ kg/m^3 to $1\ 10^{-3}$ kg/m^3 according to some suggestions of q_i^* ($\sim 1\ 10^{-3}$ kg/m^3 by Lin et al. (1983) or $\sim 0.7\ 10^{-3}$ kg/m^3 by Rutledge and Hobbs (1983)). The threshold was then reduced to the assigned value of $r_i^\star = 2 \times 10^{-5}$ kg kg^{-1} as deduced from an extended thick cloud regime over Atlantic (Chaboureau et al. 2002). Finally, in order to apply the formulation to several ice cloud types, Ryan (2000) parameterizes $r_i^\star$ as a function of the air temperature, T. This suggestion is now incorporated into the model setting as an adjustment for low temperature limits, which leads to:

$$r_i^\star = \min(2 \times 10^{-5}, 10^{0.06\times(T-273.16)-3.5}). \tag{6.44}$$

An improvement of the cirrus cover was shown by comparison with satellite observations (Chaboureau and Pinty 2006).

6.2.8 Contact freezing of raindrops to form graupels

The production of frozen drops due to collision between pristine ice crystals and raindrops is a typical three component collection process. As in other schemes, the effects of small ice crystal fall speeds on the collection kernel (6.11) can be legitimately ignored so (6.12) and (6.13) are

easily integrated to give:

$$RRCFRIG = \frac{1}{\rho}\frac{\pi^2}{24} E_{ir} N_i \rho_w c_r M(5+d_r) \Big(\frac{\rho_{00}}{\rho_{dref}}\Big)^{0.4}, \tag{6.45}$$

$$RICFRRG = \frac{\pi}{4} E_{ir} N_r r_i c_r M(2+d_r) \Big(\frac{\rho_{00}}{\rho_{dref}}\Big)^{0.4} \tag{6.46}$$

where (6.3)-(6.6) have been used. The terminal fall speed of the raindrops is assumed to follow (6.4) but for $c_r = 842$(m/s)$^{0.2}$ and for $d_r = 0.8$ (see Table 6.2) while $E_{ir} = 1$.

6.2.9 Collection growth of the aggregates

Aggregates grow by collecting small pristine crystals ($RIAGGS$) and by the partial riming of cloud droplets ($RCRIMSS$) and small raindrops ($RRACCSS$). In case of heavy riming by droplets or when the collected raindrops are large, the growth of the aggregates is followed by a conversion into the graupel category.

Collection of pristine crystals

Neglecting the relative size and fall speed of the pristine crystals compared to that of the aggregates and integrating over the dimensional spectrum of the aggregates give:

$$RIAGGS = \frac{\pi}{4} E_{is} N_s r_i c_s M(2+d_s) \Big(\frac{\rho_{00}}{\rho_{dref}}\Big)^{0.4}, \tag{6.47}$$

where (6.12) have been used with $D_x \sim 0$ in (6.11). The collection efficiency, estimated from Kajikawa and Heymsfield (1989) that is:

$$E_{is} = 0.25\, e^{0.05(T-T_t)}, \tag{6.48}$$

is consistent with the decrease of the sticking efficieny of the interacting solid crystals when the temperature is cooler than T_t.

Riming by cloud droplets

The approach of Farley et al. (1989) is used with the assumption that conversion of aggregates into graupels may occur for riming aggregates of size larger than $D_{cs}^{lim} = 7$mm[10] , thus the growth of aggregates by riming is reduced to:

$$RCRIMSS = \frac{\pi}{4} E_{cs} N_s r_c c_s M(2+d_s; D_{cs}^{lim}) \Big(\frac{\rho_{00}}{\rho_{dref}}\Big)^{0.4}, \tag{6.49}$$

where $E_{cs} = 1$ and where $M(p; D^{lim})$ is the incomplete integration version of (6.6) which is evaluated numerically for computational efficiency, namely:

$$M(p; D^{lim}) = \int_0^{D^{lim}} D^p g(D)\, dD \sim \sum_0^{D^{lim}} D^p g(D) \Delta D. \tag{6.50}$$

[10]The diameter D_{cs}^{lim} can be also estimated by considering the Macklin formula (see, Heymsfield and Pflaum 1985) which relates the rime density to the size of the collector particle

Conversely, the graupel conversion rate consecutive to the heavy riming of the cloud droplets on the flakes is:

$$RCRIMSG = RCRIMS - RCRIMSS = \frac{\pi}{4} E_{cs} N_s r_c c_s M(2+d_s) \Big(\frac{\rho_{00}}{\rho_{dref}}\Big)^{0.4} - RCRIMSS, \tag{6.51}$$

while the simultaneous rate of transfer of aggregate mixing ratio to the graupel category is simply estimated as the mass of aggregate larger than D_{cs}^{lim} that is readily available at each time step thus,

$$RSRIMCG = \frac{1}{\Delta t} N_s \int_{D_{cs}^{lim}}^{\infty} a_s D_s^{b_s} g(D_s)\, dDs = \frac{N_s}{\Delta t} a_s (M(b_s) - M(b_s; D_{cs}^{lim})). \tag{6.52}$$

Collection of raindrops

As for the riming of cloud droplets, it is postulated that the collection of small raindrops do not change the structure of an aggregate but larger colliding raindrops reshape it as a graupel. Furthermore as both raindrops and aggregates have significant fall speeds, it is not easy to solve the integrals of the form of (6.12) and (6.15) together with (6.11) and so the numerical technique suggested by Ferrier (1994) have been adopted. For instance, (6.14) with the full expansion of (6.11) is rewritten as:

$$RZCOLX = \frac{1}{\rho} \frac{\pi}{4} \Big(\frac{\rho_{00}}{\rho_{dref}}\Big)^{0.4} a_z N_x N_z \Lambda(\lambda_x, \lambda_z) \Delta v_{xz}(\lambda_x, \lambda_z), \tag{6.53}$$

where

$$\Delta v_{xz} = \Lambda(\lambda_x, \lambda_z)^{-1} \int_0^{\infty} \Big\{ \int_0^{\infty} E_{xz} (D_x + D_z)^2 |c_x D_x^{d_x} - c_z D_z^{d_z}| D_z^{b_z} g_z(D_z)\, dD_z \Big\} g_x(D_x)\, dD_x \tag{6.54}$$

and with the normalizing factor $\Lambda(\lambda_x, \lambda_z)$ obtained by removing E_{xz} and the absolute fall speed difference in (6.54) that leads to the formal expression:

$$\begin{aligned} \Lambda(\lambda_x, \lambda_z) &= \int_0^{\infty} \Big\{ \int_0^{\infty} (D_x + D_z)^2 D_z^{b_z} g_z(D_z)\, dD_z \Big\} g_x(D_x)\, dD_x \\ &= M_x(2) M_z(b_z) + 2 M_x(1) M_z(1+b_z) + M_z(2+b_z). \end{aligned} \tag{6.55}$$

As Δv_{xz} is only a function of the time and space local values of λ_x and λ_z, a two-dimensionnal look-up table is created to contain numerical solutions of (6.54) for a series of logarithmically spaced couplet of λ_x and λ_z in the physically expected ranges $[\lambda_x^{min}, \lambda_x^{max}]$ and $[\lambda_z^{min}, \lambda_z^{max}]$, respectively. Then accurate estimates of Δv_{xz} can be obtained by bilinear interpolation with respect to the tabulated values of λ_x and λ_z.
For the specific case of raindrop-aggregate process, the growth of the aggregates $RRACCSS$ (at the expense of rain) by raindrop merging and freezing can be written:

$$RRACCSS = \frac{1}{\rho} \frac{\pi^2}{24} \rho_w \Big(\frac{\rho_{00}}{\rho_{dref}}\Big)^{0.4} N_s N_r \Lambda(\lambda_s, \lambda_r) \Delta v_{sr}(\lambda_s, \lambda_r), \tag{6.56}$$

with

$$\Delta v_{sr} = \Lambda(\lambda_s, \lambda_r)^{-1} \int_0^{\infty} \Big\{ \int_0^{D_r^{lim}} E_{sr} (D_s + D_r)^2 |c_s D_s^{d_s} - c_r D_r^{d_r}| D_r^3 g_r(D_r)\, dD_r \Big\} g_s(D_s)\, dD_s \tag{6.57}$$

and the conversion rate into the graupels becomes:

$$RRACCSG = RRACCS - RRACCSS \tag{6.58}$$

with $RRACCS$ computed as in (6.53). The threshold diameter D_r^{lim} beyond which aggregates collecting raindrops are considered as graupels, is defined as in Ferrier (1994) by computing the density ρ_{sr} of the newly formed aggregate-raindrop mixture from

$$\frac{\pi}{6}\rho_w D_r^3 + \frac{\pi}{6}\Big[\underbrace{a_s\frac{6}{\pi}D_s^{b_s-3}}_{\rho_s}\Big]D_s^3 = \frac{\pi}{6}\rho_{sr}D_s^3. \tag{6.59}$$

The resulting particle is classified as graupel (of density ρ_g) if $\rho_{sr} > 0.5(\rho_g + \rho_s)$. Considering the graupels as quasi spheroids ($b_g \sim 3$ in Table 6.2), D_r^{lim} can be expressed as:

$$D_r^{lim} = \Big[\frac{3}{\pi}\frac{(a_g - a_s D_s^{b_s-3})}{\rho_w}\Big]^{1/3} D_s. \tag{6.60}$$

In addition to (6.58), conversion of aggregates into graupels drain a fraction of aggregate mixing ratio onto the graupel category at a rate:

$$RSACCRG = \frac{1}{\rho}\frac{\pi}{4}\Big(\frac{\rho_{00}}{\rho_{dref}}\Big)^{0.4} N_s N_r a_s \Lambda(\lambda_r,\lambda_s)\Delta v_{rs}(\lambda_r,\lambda_s), \tag{6.61}$$

with

$$\Delta v_{rs} = \Lambda(\lambda_r,\lambda_s)^{-1}\int_0^\infty \Big\{\int_{D_r^{lim}}^\infty E_{sr}(D_s+D_r)^2|c_s D_s^{d_s} - c_r D_r^{d_r}|g_r(D_r)\,dD_r\Big\}D_s^{b_s}g_s(D_s)\,dD_s \tag{6.62}$$

6.2.10 Wet/dry growth of the graupels

Graupeln are very efficient collectors for condensed water so during their accretional growth, their surface temperature (T_s) is generally larger than the temperature of the environment because of the latent heat release by the liquid accreted material. At equilibrium this temperature excess is balanced by the convective heating of the ambiant air. Until the mean surface temperature of the graupels remains below T_t all the collected droplets and raindrops can freeze: this stage corresponds to the DRY growth mode. As soon as T_s reaches the value of T_t, a thin liquid film persists at the surface of the graupels and any excess of accreted liquid condensate is shed away: this second stage is the WET growth mode corresponding to the formation of hail.

Dry growth

The dry growth of the graupels by collection processes contains the sum of individual accretion processes that is:

$$RDRYG = RCDRYG + RRDRYG + RIDRYG + RSDRYG. \tag{6.63}$$

The expressions for $RCDRYG$ and for $RIDRYG$ are similar to that of $RIAGGS$ in Eq. (6.47), they read:

$$RCDRYG = \frac{\pi}{4}E_{cg}N_g r_c c_g M(2+d_g)\Big(\frac{\rho_{00}}{\rho_{dref}}\Big)^{0.4}, \tag{6.64}$$

$$RIDRYG = \frac{\pi}{4} E_{ig} N_g r_i c_g M(2+d_g) \Big(\frac{\rho_{00}}{\rho_{dref}} \Big)^{0.4}, \tag{6.65}$$

but with different efficiencies that is:

$$E_{cg} = 1 \qquad \text{and} \qquad E_{ig} = 0.01\ e^{0.1(T-T_t)} \tag{6.66}$$

as revised by Ferrier et al. (1995).[11]
The accretional growth of the graupels with large hydrometeors (aggregates and raindrops) is computed using the numerical technique of Ferrier (1994) which has been already applied for the aggregates collecting raindrops. However the present collection processes are simpler because the graupels are the final products regardless the type of collected particle; so one gets:

$$RSDRYG = \frac{1}{\rho} \frac{\pi}{4} \Big(\frac{\rho_{00}}{\rho_{dref}} \Big)^{0.4} N_g N_s a_s \Lambda(\lambda_g, \lambda_s) \Delta v_{gs}(\lambda_g, \lambda_s), \tag{6.67}$$

with

$$\Delta v_{gs} = \Lambda(\lambda_g, \lambda_s)^{-1} \int_0^\infty \Big\{ \int_0^\infty E_{gs} (D_g + D_s)^2 |c_g D_g^{d_g} - c_s D_s^{d_s}| D_s^{b_s} g_s(D_s)\ dD_s \Big\} g_g(D_g)\ dD_g \tag{6.68}$$

for graupels collecting flakes and

$$RRDRYG = \frac{1}{\rho} \frac{\pi^2}{24} \rho_w \Big(\frac{\rho_{00}}{\rho_{dref}} \Big)^{0.4} N_g N_r \Lambda(\lambda_g, \lambda_r) \Delta v_{gr}(\lambda_g, \lambda_r), \tag{6.69}$$

with

$$\Delta v_{gr} = \Lambda(\lambda_g, \lambda_r)^{-1} \int_0^\infty \Big\{ \int_0^\infty E_{gr} (D_g + D_r)^2 |c_g D_g^{d_g} - c_r D_r^{d_r}| D_r^3 g_r(D_r)\ dD_r \Big\} g_g(D_g)\ dD_g \tag{6.70}$$

for graupels collecting raindrops. The collision efficiencies are computed as in (6.66) with $E_{gr} = E_{cg}$ and $E_{gs} = E_{ig}$.

Wet growth

The study of this mode growth has been made by Musil (1970) and reviewed by Nelson (1983). The heat balance equation of a graupel collecting liquid droplets/raindrops ($|_l$), solid pristine ice ($|_i$) and flakes ($|_s$) with $T_s = T_t$ can be written as:

$$\begin{aligned} &\frac{dm}{dt}\ |_l\ (L_m(T_t) - C_w(T_t - T)) - \Big[\frac{dm}{dt}\ |_i + \frac{dm}{dt}\ |_s \Big] C_i(T_t - T) \\ &\quad = 4\pi \mathcal{C}_g \overline{f}_g \Big[k_a(T)(T_t - T) + \frac{L_v D_v(T,P)}{R_v T} (e_{vs}(T_t) - e_v) \Big]. \end{aligned} \tag{6.71}$$

As the mass increase of the individual graupel is

$$\frac{dm}{dt}\ |_g = \frac{dm}{dt}\ |_l + \frac{dm}{dt}\ |_i + \frac{dm}{dt}\ |_s, \tag{6.72}$$

[11] The expression used to simulate the E_{ig} effect has a great importance to adjust the relative abundance of the snow/aggregate because giving a large value to E_{ig} tends to deplete rapidly this category of ice particles. Note that the solid-solid sticking coefficients are the poorest known quantities in cloud physics

the integration of (6.71) over the whole graupel spectrum using (6.1), (6.4), (6.5), (6.6), and (6.72), leads to an expression for the graupel wet growth ($RWETG$) which is:

$$\begin{aligned} RWETG = \frac{4\pi \mathcal{C}_{1_g} N_g}{\rho(L_m(T_t) - C_w(T_t - T))} \Big[k_a(T)(T_t - T) + \frac{L_v D_v(T,P)}{R_v T}(e_{vs}(T_t) - e_v) \Big] \\ \times \big[\overline{f}_{0g} M_g(1) + \overline{f}_{1g} c'_g M_g(\frac{d_g+3}{2}) \big] \\ + (RIWETG + RSWETG) \Big[1 + \frac{C_i(T_t - T)}{\rho(L_m(T_t) - C_w(T_t - T))} \Big]. \end{aligned} \tag{6.73}$$

In the above expression, c'_g is defined in (6.41) and $RIWETG(RSWETG)$ is the graupel collection rate of pristine ice(aggregates) in the wet mode that is with $E_{ig}(E_{sg})$ in Eq. (6.66)(6.67) taken equal to unity in order to represent an enhanced sticking efficiency due to the wetting of the graupels.

Which growth mode?

To determine whether the dry (6.63) or the wet (6.73) growth mode is active, the two rates $RDRYG$ and $RWETG$ are compared and the lowest value is retained. For instance, if $RWETG > RDRYG$ means that enough water can freeze on the graupels and so the growth can operate in the dry regime. Conversely if $RDRYG > RWETG$, the growth is in the wet mode because potentially accreting water cannot freeze entirely as $RWETG$ represents the maximal freezing rate of the graupels.

Water shedding

In case of wet growth regime, any excess of liquid water at the surface of the graupels is removed (shed) and converted into raindrops. Although this process is active for large ice particles only (Rasmussen et al. 1984), it is assumed to occur even for small sized particles as the present parameterization does not contain any mixed phase category of ice. Lin et al. (1983) emphasized the role of the water shedding mechanism as a rapid transformation of cloud water into raindrops in the 0°C to -10°C region of clouds and they gave details how to handle this effect.
The key is to expand the wet growth rate $RWETG$ of (6.73) into the explicit form of (6.63), which is used to define the dry growth rate $RDRYG$, so:

$$RWETG = RRWETG + RCWETG + RIWETG + RSWETG. \tag{6.74}$$

Note that $RCWETG \equiv RCDRYG$ and that $RWETG - RIWETG - RSWETG$ is exactly the wet growth due to the liquid water collected so,

- if $RWETG - RIWETG - RSWETG > RCWETG$: there is no explicit water shedding as some raindrops can still be frozen on the surface of the graupels at the rate $RRWETG$ defined by Eq. (6.74) that is:

$$RRWETG = RWETG - RCWETG - RIWETG - RSWETG. \tag{6.75}$$

- if $RWETG - RIWETG - RSWETG < RCWETG$: even all the collected cloud droplets cannot freeze on the graupels and so are shed as raindrops at a rate $RRWETG$ defined in (6.75). In that case $RRWETG$, a negative quantity but a gain for the raindrops as it identifies to the rate of transfer of unfrozen cloud droplets into rain, is renamed as $RCSHDR$ with:

$$RCSHDR = -Min\Big\{0, RWETG - RCWETG - RIWETG - RSWETG\Big\}. \tag{6.76}$$

Finally (6.75) is recast as:

$$RRWETG = Max\Big\{0, RWETG - RCWETG - RIWETG - RSWETG\Big\}. \tag{6.77}$$

6.2.11 Melting of ice crystals

Pristine ice melting

When $T > T_t$, the small ice crystal cannot survive as they are supposed to melt instantaneously into cloud droplets at a rate:

$$RIMLTC = \frac{r_i}{\Delta t} H(T_t). \tag{6.78}$$

Melting of the graupels

In analogy with the wet growth mode of the graupels, the melting water formed at the surface of the graupels and the continuously collected water is shed away into raindrops. According to Mason (1956), the heat balance equation of a partially melting graupel is:

$$L_m(T_t)\frac{dm}{dt}\,|_g - \frac{dm}{dt}\,|_l\, C_w(T_t - T) = 4\pi \mathcal{C}_g \overline{f}_g \Big[k_a(T)(T_t - T) + \frac{L_v D_v(T,P)}{R_v T}(e_{vs}(T_t) - e_v)\Big]. \tag{6.79}$$

where $\frac{dm}{dt}\,|_g$ is the rate of change of the ice mass of a graupel and $\frac{dm}{dt}\,|_l$ the collected cloud droplets and raindrops (supposed to be at the same temperature T of the environment).
Integration of (6.79) over the whole dimensional spectrum of the graupels lead to an expression of the graupel melting rate,

$$\begin{aligned} RGMLTR = &-\frac{4\pi \mathcal{C}_{1_g} N_g}{\rho L_m(T_t)}\Big[k_a(T)(T_t - T) + \frac{L_v D_v(T,P)}{R_v T}(e_{vs}(T_t) - e_v)\Big] \\ &\times \big[\overline{f}_{0g} M_g(1) + \overline{f}_{1g} c'_g M_g(\frac{d_g + 3}{2})\big] \\ &-(RCWETG + RRWETG)\frac{C_w(T_t - T)}{L_m(T_t)}. \end{aligned} \tag{6.80}$$

Melting of the aggregates

The behavior of the snowflakes and aggregates is somewhat different from that of the graupels at the onset of melting. Tunnel experiments showed that during this stage, the structure of the aggregates collapse while the melting water is trapped in the gaps of the porous structure. Thus melting aggregates tend to densify and as a result get some ressemblance to the graupels in mixed phase. From a similar heat balance equation of (6.79), one can derive the melting rate of the aggregates which is:

$$\begin{aligned} RSMLT = &-\frac{4\pi \mathcal{C}_{1_s} N_s}{\rho L_m(T_t)}\Big[k_a(T)(T_t - T) + \frac{L_v D_v(T,P)}{R_v T}(e_{vs}(T_t) - e_v)\Big] \\ &\times \big[\overline{f}_{0s} M_s(1) + \overline{f}_{1s} c'_s M_s(\frac{d_s + 3}{2})\big] \\ &-(RCRIMSS + RRACCSS)\frac{C_w(T_t - T)}{L_m(T_t)}. \end{aligned} \tag{6.81}$$

Next, it is assumed that a given portion of aggregates is transfered into (melting) graupels at a rate $RSCVMG$ proportional to $RSMLT$. The former conversion rate represents the mixture of

melted water and icy assemblages which is dense enough to be categorized as graupel

$$RSCVMG = \alpha_{S\rightarrow G} RSMLT. \tag{6.82}$$

In the present parameterization, $\alpha_{S\rightarrow G}$ has a value of 2 which means that an equal portion of solid ice and liquid water is required for the aggregates to build a graupel-like structure during their melting stage. It is worth to emphasize that in the spirit of the scheme, the "melting-conversion" of the aggregates do not exchange heat with the environment, so the graupels must integrate the rate $RSCVMG$ prior the computation of their own melting rates $RGMLTR$.

6.2.12 Sedimentation rates

The present parameterization postulates that the pristine ice crystals have no significant fall speed however, in order to reproduce the slow erosion of cirrus sheets, an estimate of $RSEDI$ has been provided for that specific purpose. The sedimentation fluxes are computed by assuming that the crystals are shaped as columns with a concentration N_{Ci} given by Mc Farquhar and Heymsfield (1997) that is:

$$N_{Ci} = \frac{1}{4\pi\rho_i}\rho r_i (MAX\{0.05\ 10^6, -0.1532\ 10^6 - 0.021454\ 10^6 Log(\rho r_i)\})^3, \tag{6.83}$$

where $\rho_i = 900 kg/m^3$ is the density of the ice. The sedimentation rate is thus given by

$$RSEDI = \frac{\partial}{\partial z}\Big[N_{Ci} a_i c_i M(b_i + d_i)\Big(\frac{\rho_{00}}{\rho_{dref}}\Big)^{0.4}\Big], \tag{6.84}$$

where $M(b_i + d_i) = G(b_i + d_i)(\rho r_i / a_i N_{Ci} G(b_i))^{\frac{b_i + d_i}{b_i}}$.
The ice mass sedimentation rates for precipitating particles $X = S$ or G are given by

$$\begin{aligned} RSEDX &= \frac{1}{\rho_{dref}}\frac{\partial}{\partial z}\Big[\int_0^\infty v(D_x) m(D_x) n(D_x)\, dD_x\Big] \\ &= \frac{1}{\rho_{dref}}\frac{\partial}{\partial z}\Big[N_x a_x c_x M(b_x + d_x)\Big(\frac{\rho_{00}}{\rho_{dref}}\Big)^{0.4}\Big] \\ &= \frac{1}{\rho_{dref}}\frac{\partial}{\partial z}\Big[C_x a_x c_x G(b_x + d_x)\Big(\frac{\rho_{dref} r_x}{a_x C_x G(b_x)}\Big)^{\frac{b+d-x}{b-x}}\Big(\frac{\rho_{00}}{\rho_{dref}}\Big)^{0.4}\Big], \end{aligned} \tag{6.85}$$

where (6.1), (6.6), and (6.10) have been used. As for the fallout of rain, the ice sedimentation terms are computed with a time splitting technique and with an upstream differencing scheme.

6.2.13 Extension to hail

The scheme described above is a three-ice category scheme where hailstones are implicitly mixed with less-dense graupel particles to form the broad class of heavily rimed particles. However hailstones may be of special interest in convective storms. Furthermore they have a specific growth rate which can be modeled in the manner of the "wet growth" regime of the graupel particles. The physical basis is that hail particles are very efficient to collect particles so their growth rate is mostly limited by the capability of the collected drops to freeze out at the surface of the hailstones (heat budget equation). Therefore unfrozen drops are shed away and feed back the raindrop category of the condensate. The whole process corresponds to the RWETG growth rate expressed by Eq.

(6.73). The drawback of the present method, which does not distinguish between graupel and hail particles is twofold: first, the relevant relationships (mass-size, fall speed-size, etc.) of the hail particles are not explicitly taken into account and second, the DRY/WET switch of the graupel growth mode is not size-segregated and affects the whole graupel spectrum while only the largest graupel particles are prone to grow in the wet mode. So in order to better represent the initiation of hail from the graupel reservoir and the microphysical evolution of these hydrometeors, a fourth category of ice is introduced. The extended microphysical scheme (Lascaux et al. 2006) is now referred to the ICE4 scheme.

Introduction to hail particles

All the variables relative to the "hail" category are suffixed with an "h". For instance, the hail mixing ratio is r_h. The parameters used to characterize hail (here treated as ice spheres) are given in Table 6.7. The shape parameter ν is set to a high value of 8 in order to favor a narrow size distribution of the hailstones around the biggest sizes of the particles.

Table 6.7: Set of parameters used to characterize the hailstones.

Parameters	α	ν	a	b	c	d	C	x	$\overline{f}_0$	$\overline{f}_1$	$\overline{f}_2$	$\mathcal{C}_1$
r_h	1	8	470.	3.0	207.	0.64	4.E4	-1.0	0.86	0.28	0	0.5

Microphysical processes involving hail particles

The hail category originates from the graupel reservoir, which largest particles likely experience a wet growth mode. Once formed, hailstones exclusively grow in the wet growth mode too and do not go back to the graupel stage. Hailstones partially melt under the freezing level in the same way graupel particles do. There is no deposition/sublimation of the hailstones.

Formation from graupel particles

The formation rate of hail particles is derived from the **WET** and **DRY** growth modes of the graupel particles. The partial conversion of graupels into hailstones is then approximated by

$$\left.\frac{\partial r_h}{\partial t}\right|_{g\to h} = \left(\frac{\partial r_g}{\partial t}\right)^* \times \frac{\mathbf{DRY}}{\mathbf{DRY}+\mathbf{WET}} \tag{6.86}$$

where $\left(\partial r_g/\partial t\right)^*$ is the sum of the r_g tendencies before the conversion into hail. The corresponding sink on the r_g budget is $\left.\partial r_g/\partial t\right|_{g\to h} = -\left.\partial r_h/\partial t\right|_{g\to h}$. The above formulation allows for a progressive transition from graupel to hail. It is based on the simple idea that the more the graupel particles can grow in the **WET** mode (**DRY**$\gg$**WET** case), the more they are depleted and converted into hailstones. This macroscopic approach is in contrast with Ziegler (1985) who suggested a size distinction between graupel and hail which is based on a dry/wet growth threshold diameter to integrate by part over the graupel size distribution. We found that this technique is not easily applicable in a four-class microphysical scheme insofar the scheme is rendered increasingly complex (Ferrier 1994). The ratio introduced in Eq. (6.86) lies between 1 (full conversion into hail

when **WET**$\ll$**DRY**) and 1/2 (no conversion into hail when **WET**$\leq$ **DRY**) so hail is produced only when $0 <$**WET**$\leq$**DRY**.
The ratio expressed in Eq. (6.86) can be easily modified and adjusted to improve the transfer rate in accord with experimental data.

Growth of hail particles

Rigorously speaking, hailstones exclusively grow in the wet regime but these conditions are not strictly checked for the moment to simplify the coding. The consequence is that hail does not revert to the graupel category in the scheme. This situation will be improved in the future. The wet growth rate ($RWETH$) is analogous to (6.73), it writes:

$$\begin{aligned} RWETH = & \frac{4\pi \mathcal{C}_{1_h} N_h}{\rho(L_m(T_t) - C_w(T_t - T))} \Big[k_a(T)(T_t - T) + \frac{L_v D_v(T,P)}{R_v T}(e_{vs}(T_t) - e_v) \Big] \\ & \times \big[\overline{f}_{0h} M_h(1) + \overline{f}_{1h} c'_h M_h(\frac{d_h+3}{2}) \big] \\ & + (RIWETH + RSWETH + RGWETH) \Big[1 + \frac{C_i(T_t - T)}{\rho(L_m(T_t) - C_w(T_t - T))} \Big]. \end{aligned} \tag{6.87}$$

In the above expression, $RGWETH$ is the hail collection rate of graupel particles in the wet mode with $E_{gh} = 1$. $RIWETH$ and $RSWETH$ have a similar meaning to $RIWETG$ and $RSWETG$ in (6.73) but for hail. The $RSWETH$ and $RGWETH$ rates are tabulated and interpolated from lookup tables.

Melting of hail particles

We proceed the same way as for the graupel particles (in Eq. (6.80)).

$$\begin{aligned} RHMLTR = & -\frac{4\pi \mathcal{C}_{1_h} N_h}{\rho L_m(T_t)} \Big[k_a(T)(T_t - T) + \frac{L_v D_v(T,P)}{R_v T}(e_{vs}(T_t) - e_v) \Big] \\ & \times \big[\overline{f}_{0h} M_h(1) + \overline{f}_{1h} c'_h M_h(\frac{d_h+3}{2}) \big] \\ & - (RCWETH + RRWETH) \frac{C_w(T_t - T)}{L_m(T_t)}. \end{aligned} \tag{6.88}$$

During the melting, hailstones can collect liquid water at $RCWETH$ and $RRWETH$ rates for the cloud droplets and raindrops, respectively. The collection rate $RRWETH$ is precomputed and interpolated from a lookup table.

Sedimentation of hail particles

The fallout of the hailstones is treated in the same way as rain, snow and graupel particles. The time splitting number is determined from the CFL stability criterium based on a maximum fall velocity of 40 m.s^{-1} instead of 10 m.s^{-1} without hail.

6.3 Integration of the equations of conservation

6.3.1 System of equation

The ice scheme predicts the evolution of the three specific ice categories r_i, r_s and r_g and also modifies the evolution of r_v and of the two other microphysical variables r_c and r_r. The system

of equation for the ice variables differ considerably with respect to the temperature T and so two distinct systems of equation can be written.

- $T < T_t$

$$\begin{aligned}\frac{\partial r_i}{\partial t} &= \sum \frac{\partial r_i}{\partial t}\Big|_{DYN} + RSEDI + RVHENI + RCHONI + RCBERI + RVDEPI \\ &-RIAUTS - RICFRRG - RIAGGS - \delta_{DRY} RIDRYG - (1-\delta_{DRY}) RIWETG,\end{aligned} \tag{6.89}$$

$$\begin{aligned}\frac{\partial r_s}{\partial t} &= \sum \frac{\partial r_s}{\partial t}\Big|_{DYN} + RSEDS + RVDEPS + RIAUTS + RIAGGS + RCRIMSS \\ &-RSRIMCG + RRACCSS - RSACCRG - \delta_{DRY} RSDRYG \\ &-(1-\delta_{DRY}) RSWETG,\end{aligned} \tag{6.90}$$

$$\begin{aligned}\frac{\partial r_g}{\partial t} &= \sum \frac{\partial r_g}{\partial t}\Big|_{DYN} + RSEDG + RVDEPG + \underbrace{RICFRRG + RRCFRIG}_{} \\ &+\underbrace{RCRIMSG + RSRIMCG}_{} + \underbrace{RRACCSG + RSACCRG}_{} \\ &+\delta_{DRY}(RCDRYG + RRDRYG + RIDRYG + RSDRYG) \\ &+(1-\delta_{DRY})(\underbrace{RRWETG + RCWETG + RIWETG + RSWETG}_{RWETG} - RCSHDR)\end{aligned} \tag{6.91}$$

where $\sum \frac{\partial r_x}{\partial t}\Big|_{DYN}$ includes the advection and the numerical and turbulent diffusions affecting the variable r_x. One recalls that $RCDRYG \equiv RCWETG$ and that $RRWETG + RCWETG + RIWETG + RSWETG = RWETG$ above. The other underbraced terms mark the conversion terms producing graupels namely, the contact freezing of the raindrops, the heavy riming of the aggregates by cloud droplets and by accretion of raindrops respectively. The switch δ_{DRY} tags the graupel growth mode so it is set to 1(0) in case of $DRY(WET)$ growth.

$$\begin{aligned}\frac{\partial r_v}{\partial t} &= \sum \frac{\partial r_v}{\partial t}\Big|_{DYN} + RREVAV - RVCNDC \\ &-RVHENI - RVDEPI - RVDEPS - RVDEPG\end{aligned} \tag{6.92}$$

$$\begin{aligned}\frac{\partial r_c}{\partial t} &= \sum \frac{\partial r_c}{\partial t}\Big|_{DYN} - RCAUTR - RCACCR \\ &-RCBERI - RCHONI - RCRIMSS - RCRIMSG \\ &-\delta_{DRY} RCDRYG - (1-\delta_{DRY}) RCWETG\end{aligned} \tag{6.93}$$

$$\begin{aligned}\sum \frac{\partial r_r}{\partial t} &= \frac{\partial r_r}{\partial t}\Big|_{DYN} + RSEDR + RCAUTR + RCACCR - RREVAV \\ &-RRCFRIG - RRACCSS - RRACCSG - \delta_{DRY} RRDRYG \\ &-(1-\delta_{DRY})(RRWETG - RCSHDR)\end{aligned} \tag{6.94}$$

$$\begin{aligned}\frac{\partial \theta}{\partial t} = \sum \frac{\partial \theta}{\partial t}\Big|_{DYN} &+\frac{L_v}{\Pi_{ref} C_{ph}}\Big[RVCNDC - RREVAV\Big] \\ &+\frac{L_f}{\Pi_{ref} C_{ph}}\Big[RCHONI + RCBERI + RRCFRIG + RCRIMSS \\ &+RCRIMSG + RRACCSS + RRACCSG + \delta_{DRY}(RCDRYG \\ &+RRDRYG) + (1-\delta_{DRY})(RCWETG + RRWETG - RCSHDR)\Big] \\ &+\frac{L_s}{\Pi_{ref} C_{ph}}\Big[RVHENI + RVDEPI + RVDEPS + RVDEPG\Big]\end{aligned} \tag{6.95}$$

where the warm microphysical processes have been included.

- $T > T_t$

$$\frac{\partial r_i}{\partial t} = \sum \frac{\partial r_i}{\partial t}\Big|_{DYN} + RSEDI - RIMLTC, \tag{6.96}$$

$$\begin{aligned}\frac{\partial r_s}{\partial t} &= \sum \frac{\partial r_s}{\partial t}\Big|_{DYN} + RSEDS - RSCVMG \\ &+RCRIMSS + RRACCSS - RSRIMCG - RSACCRG - RSWETG,\end{aligned} \tag{6.97}$$

$$\begin{aligned}\frac{\partial r_g}{\partial t} &= \sum \frac{\partial r_g}{\partial t}\Big|_{DYN} + RSEDG - RGMLTR + RSCVMG \\ &+\underbrace{RCRIMSG + RSRIMCG}+\underbrace{RRACCSG + RSACCRG}+RSWETG,\end{aligned} \tag{6.98}$$

$$\frac{\partial r_v}{\partial t} = \sum \frac{\partial r_v}{\partial t}\Big|_{DYN} - RVCNDC + RREVAV, \tag{6.99}$$

$$\begin{aligned}\frac{\partial r_c}{\partial t} &= \sum \frac{\partial r_c}{\partial t}\Big|_{DYN} + RVCNDC + RIMLTC \\ &-RCRIMSS - RCRIMSG - RCWETG,\end{aligned} \tag{6.100}$$

$$\begin{aligned}\frac{\partial r_r}{\partial t} &= \sum \frac{\partial r_r}{\partial t}\Big|_{DYN} RSEDR - RREVAV + RGMLTR \\ &-RRACCSS - RRACCSG + RCWETG,\end{aligned} \tag{6.101}$$

$$\begin{aligned}\frac{\partial \theta}{\partial t} = \sum \frac{\partial \theta}{\partial t}\Big|_{DYN} &+\frac{L_v}{\Pi_{ref} C_{ph}}\Big[RVCNDC - RREVAV\Big] \\ &+\frac{L_f}{\Pi_{ref} C_{ph}}\Big[RCRIMSS + RCRIMSG + RRACCSS + RRACCSG \\ &-RIMLTC - RGMLTR\Big].\end{aligned} \tag{6.102}$$

Note that $\delta_{DRY} = 0$ in warm clouds for the melting graupels and that the liquid water collected by the melting graupels is shed immediately so $RCWETG$ is a conversion rate of cloud droplets into raindrops in that case.
In the two above systems of equations, the condensation/evaporation term for r_c ($RVCNDC$) and the deposition/sublimation term for r_i ($RVDEPI$) are integrated implicitly during the final water vapor adjustment step (see below).

6.3.2 Positivity adjustments

As done for the variables used in the warm microphysics parameterization, it is necessary to check at first the positivity of the mixing ratios after the integration of the sole $\sum \frac{\partial r_x}{\partial t}\Big|_{DYN}$ terms in the preceeding systems of equation. Mixing ratios ending with negative values are corrected (reset to zero) and the global filling algorithm of Rood (1987) is applied to ensure the total mass conservation of each microphysical specy.

6.3.3 Ordering the integration of the microphysical sources

The time integration of the explicit rates in Eqs (6.89) up to (6.102) must be done carefully because some important processes are fueled by cloud ice or cloud droplets which contents are not necessary updated after the successive action of the numerous microphysical processes. As a result this may lead to situations where excessive depletion of a key specy by a single process has a dramatic effect on the long-term (chaotic) behavior of a cloud parcel. More practical arguments, such as the

positiveness requirement of the final mixing ratios are also in favor of a strict control and update when adding up all the source terms (transport followed by a local growth/depletion) of the system of equations.
As shown by Lin et al. (1983) and Ziegler (1988) but for a different scheme and case study too, the highest rates in a mixed phase cloud are found for the accretion of cloud droplets and raindrops onto the snowflakes and the graupels (in the dry mode) and the freezing of the drops. Thus the source terms associated to these processes should be integrated at the end of the sequence and just before the late cloud ice and droplet transfers which anticipate the final water vapor-temperature adjustment.
In the present scheme, it is suggested to proceed as follow:

- first integrate the slow "cold" processes: nucleations, vapor deposition/sublimation, aggregation and autoconversion
- then the "warm" processes: accretion, autoconversion and rain evaporation
- then include the accretional growth of the aggregates, the contact freezing of the raindrops and the conversion-melting of the aggregates,
- then the accretional growth of the graupels and their melting
- then add the pristine ice melting and Bergeron-Findeisen transfer
- and finally integrate the sedimentation terms

Each process is computed with the prognostic variables (especially the mixing ratios) defined at the current time step but it is limited by the current state of the guess of the depleted prognostic variable before integration. This means that at the end of each step, the partially integrated mixing ratios of the decaying microphysical species are strictly checked for positivity so, in some circumstances, some specy may be available or not for the next process depending on the chosen order in the sequence of integration. It is clear that this systematic control makes the job easier at the end because no other algorithm for local compensation of negative value needs to be developped. But the drawback is that it introduces a dependency to the order of the processes.
A summary of the general algorithm for integrating the microphysical cold and warm processes is presented in Fig. 6.4.

6.3.4 Water vapor adjustments

All the concurrent microphysical processes involving an exchange of heat and water vapor on the condensed particles are computed independently each other. In the warm microphysical scheme an implicit adjustment of the temperature, water vapor and cloud water fields is performed in order to introduce some consistency between θ and r_v with a strict saturation criterium in clouds leading to a subsequent passive adjustment of r_c. A by-product of this adjustment is the derivation of a condensation/evaporation rate ($RVCNDC$) of the cloud droplets. In mixed phase clouds the problem is far more complex because of the presence of cloud droplets and ice (so two species to re-adjust) and the difficulty of defining unambiguously a single level of saturation. The solution which has been chosen here is to perform an implicit adjustment as in Lord et al. (1984) or in Tao et al. (1989) because it seems superior to the explicit closure exposed in Ferrier (1994) where

Figure 6.4: Algorithm of the step-by-step integration of the microphysical processes.

a simple saturation over ice is assumed leading to some controversial account of the Bergeron-Findeisen effect[12] and a single correction of r_i. In the present scheme the Bergeron-Findeisen conversion rate ($RCBERI$) is explicitly pre-integrated and so the traditional linear partition of water vapor correction as a function of temperature can be subjected to some revision. Another advantage of using an implicit adjustment scheme in the spirit of that of Lord et al. (1984) is that it can revert to a classical adjustment scheme in case of warm cloud ($r_i = 0$) or fully glaciated cloud ($r_c = 0$).
The major assumptions used in the proposed saturation adjustment scheme are the following:

- the saturation vapor mixing ratio ($r_{vs_{iw}}$) inside a mixed phase cloud results from the barycentric formula introduced by Lord et al. (1984) that is:

$$r_{vs_{iw}} = \frac{r_c^* r_{vs_w}(T) + r_i^* r_{vs_i}(T)}{r_c^* + r_i^*} \tag{6.103}$$

[12]Note that Krueger et al. (1995) emphasized the fact that the original adjustment introduced by Lord et al. (1984) cannot reproduce an implicit Bergeron-Findeisen transfer of mass

- the super/sub-saturation adjustment over cloud ice/droplets is made isobarically and proportionnal to the explicitly estimated cloud water and cloud ice content, this gives:

$$\Delta r_c = r_c - r_c^* = \Delta r_v CND \qquad \text{and} \qquad \Delta r_i = r_i - r_i^* = \Delta r_v DEP \tag{6.104}$$

with

$$\Delta r_v = r_v^* - r_v = r_v^* - r_{vs_{iw}} \tag{6.105}$$

and with

$$CND = \frac{r_c^*}{r_c^* + r_i^*} \qquad \text{and} \qquad DEP = \frac{r_i^*}{r_c^* + r_i^*}. \tag{6.106}$$

So any deficit or excess of water vapor is compensated or absorbed by each cloudy condensed phase in proportion to their respective content and as a consequence, Δr_c and Δr_i have always the same sign. This way of doing seems raisonnable since once the Bergeron-Findeisen effect is accounted for, water vapor can be supplied or gathered by r_c and r_i in proportion to their actual amount[13] .

However, the above adjustment formulation was found to produce to much ice at weakly negative temperature. As a consequence, since the Masdev 4.1 version, the CND and DEP terms are calculated following Tao et al. (1989) as:

$$CND = \frac{T - T_{00}}{T_0 - T_{00}} \qquad \text{and} \qquad DEP = 1 - CND \tag{6.107}$$

with $T_0 = 0°\text{C}$ and $T_{00} = 40°\text{C}$.

The saturation adjustment then proceeds as for Tao et al. (1989) where a zero-crossing solution of

$$\begin{aligned} F(T) &= T - T^* - \frac{L_v(T)\Delta r_c + L_s(T)\Delta r_i}{C_{ph}} \\ &= T - T^* + \Big(\frac{L_v(T)CND + L_s(T)DEP}{C_{ph}}\Big)(r_{vs_{iw}}(T) - r_v^*) \end{aligned} \tag{6.108}$$

is sought using (6.103) to (6.106) and the non-iterative algorithm of Langlois (1973) already experienced for the warm microphysical adjustment is preferred to the first order solution of Tao et al. (1989). Of course, this adjustment is performed after integrating explicitly all the source terms in the θ and the r_v prognostic equations, the cloud condensation and ice deposition terms excepted. The procedure used for solving (6.108) is based upon the quasi-second order expansion of $F(T) = 0$, namely[14]

$$T \simeq T^* - \frac{F(T^*)}{F'(T^*)}\Big[1 + \frac{1}{2}\frac{F(T^*)}{F'(T^*)}\frac{F''(T^*)}{F'(T^*)}\Big] \tag{6.109}$$

where

$$\begin{aligned} \Delta_1 &= \frac{F(T^*)}{F'(T^*)} = \frac{\big[L_v(T^*)CND + L_s(T^*)DEP\big](r_c^* r_{vs_w}(T^*) + r_i^* r_{vs_i}(T^*) - (r_c^* + r_i^*)r_v^*)}{C_{ph}(r_c^* + r_i^*) + \big[L_v(T^*)CND + L_s(T^*)DEP\big]\big[r_c^* r'_{vs_w}(T^*) + r_i^* r'_{vs_i}(T^*)\big]}, \\ \Delta_2 &= \frac{F''(T^*)}{F'(T^*)} = \frac{\big[L_v(T^*)CND + L_s(T^*)DEP\big](r_c^* r''_{vs_w}(T^*) + r_i^* r''_{vs_i}(T^*))}{C_{ph}(r_c^* + r_i^*) + \big[L_v(T^*)CND + L_s(T^*)DEP\big]\big[r_c^* r'_{vs_w}(T^*) + r_i^* r'_{vs_i}(T^*)\big]}, \end{aligned} \tag{6.110}$$

[13] In the remaining text, the starred variables are the most recently updated (or "guess") variables

[14] The slow variations of $L_v(T)$ and of $L_s(T)$ with the temperature are neglected but not those of $r_{vs_w}(T)$ and of $r_{vs_i}(T)$.

and where

$$\begin{aligned}
r'_{vs_w}(T^*) &= A_w(T^*) r_{vs_w}(T^*)\Big[1+\frac{r_{vs_w}(T^*)}{\epsilon}\Big],\\
r'_{vs_i}(T^*) &= A_i(T^*) r_{vs_i}(T^*)\Big[1+\frac{r_{vs_i}(T^*)}{\epsilon}\Big],\\
r''_{vs_w}(T^*) &= r'_{vs_w}(T^*)\Big[\frac{A'_w(T^*)}{A_w(T^*)}+A_w(T^*)\big(1+2\frac{r_{vs_w}(T^*)}{\epsilon}\big)\Big],\\
r''_{vs_i}(T^*) &= r'_{vs_i}(T^*)\Big[\frac{A'_i(T^*)}{A_i(T^*)}+A_i(T^*)\big(1+2\frac{r_{vs_i}(T^*)}{\epsilon}\big)\Big]
\end{aligned} \tag{6.111}$$

with $\epsilon = M_v/M_d$ and

$$\begin{aligned}
A_w(T) &= \frac{\beta_w}{T^2}-\frac{\gamma_w}{T} \qquad \text{and} \qquad A'_w(T) = -\frac{2\beta_w}{T^3}+\frac{\gamma_w}{T^2}\\
A_i(T) &= \frac{\beta_i}{T^2}-\frac{\gamma_i}{T} \qquad \text{and} \qquad A'_i(T) = -\frac{2\beta_i}{T^3}+\frac{\gamma_i}{T^2}.
\end{aligned} \tag{6.112}$$

Finally the rates $RVDEPI$ and $RVCNDC$ in the r_c and r_i equations, are estimated by:

$$\begin{aligned}
RVDEPI &= \frac{(r_v^*-r_{vs_{iw}})DEP}{2\Delta t} = \frac{C_{ph}}{L_v(T^*)CND+L_s(T^*)DEP}\Big[-\Delta_1(1+\frac{1}{2}\Delta_1\Delta_2)\Big]\frac{DEP}{2\Delta t}\\
RVCNDC &= \frac{(r_v^*-r_{vs_{iw}})CND}{2\Delta t} = \frac{C_{ph}}{L_v(T^*)CND+L_s(T^*)DEP}\Big[-\Delta_1(1+\frac{1}{2}\Delta_1\Delta_2)\Big]\frac{CND}{2\Delta t}.
\end{aligned} \tag{6.113}$$

6.4 References

Böhm, H. P., 1989: A general equation for the terminal fall speed of solid hydrometeors. *J. Atmos. Sci.*, **46**, 2419-2427.

Caniaux, G., 1993: Paramétrisation de la glace dans un modèle non-hydrostatique de nuage: Application à une ligne de grain tropicale. Thèse de Doctorat de l'Université Paul-Sabatier, 257 pp.

Chaboureau, J.-P., J.-P. Cammas, P. J. Mascart, J.-P. Pinty, and J.-P. Lafore, 2002: Mesoscale model cloud scheme assessment using satellite observations. *J. Geophys. Res.*, **107(D16)**, 4301, doi:10.1029/2001JD000714.

Chaboureau, J.-P. and J.-P. Pinty, 2006: Evaluation of a cirrus parameterization with Meteosat Second Generation. *Geophys. Res. Let.*, **33**, L03815, doi:10.1029/2005GL024725.

Cheng, L., and M. English, 1983: A relationship between hailstone concentration and size. *J. Atmos. Sci.*, **40**, 204-213.

Chin, H.-N. S., 1994: The impact of the ice phase and radiation on a midlatitude squall line system. *J. Atmos. Sci.*, **51**, 3320-3343.

Cotton, W. R., G. J. Tripoli, R. M. Rauber and E. A. Mulvihill, 1986: Numerical simulations of the effects of varying ice crystal nucleation rates and aggregation processes on orographic snowfall. *J. Climate Appl. Meteor.*, **25**, 1658-1680.

Farley, R. D., P. A. Price, H. D. Orville and J. H. Hirsch, 1989: On the numerical simulation of graupel/hail initiation via the riming of snow in bulk water microphysical cloud models. *J. Appl. Meteor.*, **28**, 1128-1131.

Ferrier, B. S., 1994: A double-moment multiple phase four-class bulk ice scheme. Part I: description. *J. Atmos. Sci.*, **51**, 249-280.

Ferrier, B. S., W.-K. Tao and J. Simpson, 1995: A double-moment multiple phase four-class bulk ice scheme. Part II: simulations of convective storms in different large-scale environments and comparison with other bulk parameterizations. *J. Atmos. Sci.*, **52**, 1001-1033.

Foote, G. B., and P. S. Du Toit, 1969: Terminal velocity of raindrops aloft. *J. Appl. Meteor.*, **8**, 249-253.

Hall, W. D., and H. R. Pruppacher, 1977: The survival of ice particles falling from cirrus clouds in subsaturated air. *J. Atmos. Sci.*, **33**, 1995-2006.

Hallett, J., and S. C. Mossop, 1974: Production of secondary ice particles during the riming process. *Nature*, **249**, 26-28.

Heymsfield, A. J., 1972: Ice crystals terminal velocities. *J. Atmos. Sci.*, **29**, 1348-1356.

Heymsfield, A. J. and J. C. Pflaum, 1985: A quantitative assessment of the accuracy of techniques for calculating graupel growth. *J. Atmos. Sci.*, **42**, 2264-2274.

Houze, R. A. Jr., P. V. Hobbs, P. H. Herzegh and D. B. Parsons, 1979: Size distributions of precipitation particles in frontal clouds. *J. Atmos. Sci.*, **36**, 156-162.

Kajikawa, M., and A. J. Heymsfield, 1989: Aggregation of ice crystals in cirrus. description *J. Atmos. Sci.*, **46**, 3108-3121.

Langlois, W. E., 1973: A rapidly convergent procedure for computing large-scale condensation in a dynamical weather model. *Tellus*, **25**, 86-87.

Krueger, S. K., Q. Fu, K. N. Liou, and H.-N. S. Chin, 1995: Improvements of an ice-phase microphysics parameterization for use in numerical simulations of tropical convection. *J. Appl. Meteor.*, **34**, 281-287.

Lascaux, F., E. Richard, and J.-P. Pinty, 2006: Numerical simulations of three MAP IOPs and the associated microphysical processes. *Quart. J. Roy. Meteor. Soc.*, **132**, 1907-1926.

Lin, Y.-L., R. D. Farley, and H. D. Orville, 1983: Bulk parameterization of snow field in a cloud model. *J. Climate Appl. Meteor.*, **22**, 1065-1092.

Locatelli, J. D., and P. V. Hobbs, 1974: Fall speeds and masses of solid precipitation particles. *J. Geophys. Res.*, **79D**, 2185-2197.

Lord, S. J., H. E. Willoughby, and J. M. Piotrowicz, 1984: Role of a parameterized ice-phase microphysics in an axisymmetric non-hydrostatic tropical cyclone model. *J. Atmos. Sci.*, **41**, 2836-2848.

Nelson, S. P., 1983: The influence of storm flow structureon hail growth. *J. Atmos. Sci.*, **40**, 1965-1983.

Mc Cumber, M., W.-K. Tao, J. Simpson, R. Penc, and S. T. Soong, 1991: Comparaison of ice-phase microphysical parameterization schemes using numerical simulations of tropical convection. *J. Appl. Meteor.*, **30**, 985-1004.

Mc Farquhar, G. M., A. J. Heymsfield, 1997: Parameterization of tropical cirrus ice crystal size distributions and implications for radiative transfer: Results from CEPEX *J. Atmos. Sci.*, **54**, 2187-2200.

Masson, B. J., 1956: On the melting of hailstones. *Quart. J. R. Met. Soc.*, **82**, 209-216.

Meyers, M. P., P. J. DeMott, and W. R. Cotton, 1992: New primary ice-nucleation parameterizations in an explicit cloud model. *J. Appl. Meteor.*, **31**, 708-721.

Meyers, M. P., R. L. Walko, J. Y. Harrington and W. R. Cotton, 1996: New RAMS cloud microphysics parameterization. Part II: The two-moment scheme. *submitted to Atm. Res.*

Murakami, M., 1990: Numerical modeling of dynamical and microphysical evolution of an isolated convective cloud -the 19 July 1981 CCOPE cloud. *J. Meteor. Soc. Japan*, **68**, 107-128.

Musil, D. J., 1970: Computer modeling of hailstone growth in feeder clouds. *J. Atmos. Sci.*, **27**, 474-482.

Passarelli, R. E., Jr., 1978: An approximate analytical model of the vapor deposition and aggregation growth of snow. *J. Atmos. Sci.*, **35**, 118-124.

Pruppacher, H. R., and J. D. Klett, 1978: *Microphysics of Clouds and Precipitation*. Reidel,714 pp.

Rutledge, S. A. and P. V. Hobbs, 1983: The mesoscale and microscale structure and organization of clouds and precipitation in midlatitude cyclones. Part VIII: A model for the "Seeder-Feeder" process in warm-frontal rainbands. *J. Atmos. Sci.*, **40**, 1185-1206.

Rutledge, S. A. and P. V. Hobbs, 1984: The mesoscale and microscale structure and organization of clouds and precipitation in midlatitude cyclones. Part XII: A diagnostic modeling study of precipitation development in narrow cold-frontal rainbands. *J. Atmos. Sci.*, **41**, 2949-2972.

Ryan, B. F., 2000: A bulk parameterization of the ice particle size distribution and the optical properties in ice clouds, *J. Atmos. Sci.*, **57**, 1436-1451.

Starr, D. O'C. and S. K. Cox, 1985: Cirrus clouds. Part I: A cirrus cloud model. *J. Atmos. Sci.*, **42**, 2663-2681.

Sue Chen, and W. R. Cotton, 1988: The sensitivity of a simulated extratropical mesoscale convective system to longwave radiation and ice-phase microphysics. *J. Atmos. Sci.*, **45**, 3897-3910.

Tao, W.-K., J. Simpson, and M. Mc Cumber, 1989: An ice-water saturation adjustment. *Mon. Wea. Rev.*, **117**, 231-235.

Tripoli, G. J., P. J. Flatau, and W. R. Cotton, 1988: Generalized microphysics scheme for use in mesoscale cloud model. *Preprints 10^{th} International Cloud Physics Conference*. Bad-Homburg. FRG August, 1988, 109-111.

Walko, R. L., W. R. Cotton, M. P. Meyers, and J. Y. Harrington, 1995: New RAMS cloud microphysics parameterization. Part I: The single-moment scheme. *Atm. Res.*, **38**, 29-62.

Yang M.-J. and R. A. Houze, 1995: Sensitivity of squall-line rear inflow to ice microphysics and environmental humidity. *Mon. Wea. Rev.*, **123**, 3175-3193.

Ziegler, C. L., 1985: Retrieval of thermal and microphysical variables in observed convective storms. Part I: Model development and preliminary testing. *J. Atmos. Sci.*, **42**, 1487-1509.

Ziegler, C. L., 1988: Retrieval of thermal and microphysical variables in observed convective storms. Part II: Sensitivity of cloud processes to variation of the microphysical parameterization. *J. Atmos. Sci.*, **45**, 1072-1090.

Chapter 7

Sub-Grid Condensation Schemes

Contents

7.1 Sub-Grid Condensation Scheme for warm-phase clouds

7.1.1 Introduction

Sommeria and Deardorff (1977) have first suggested that taking into account sub-grid condensation in the turbulence parameterization would improve the physical behaviour of a model: The numerical shocks between cloudy and non cloudy grid cells are attenuated, and the vertical turbulent flux of virtual potential temperature can then be positive in partially cloudy layers.
The turbulence scheme of Meso-NH has been described in the previous chapter in the hypothesis of a cloudless atmosphere. Here we explain how the sub-grid clouds are represented. This presentation assumes that the reader knows the gross characteristics of the turbulence scheme. The principle of the sub-grid cloud scheme is to use *conservative forms* of the prognostic variables describing the entropy and the total non-precipitating water content. This was first proposed by Betts (1973). As a consequence, there are only minor modifications to the general turbulence computations.

7.1.2 Definition of conservative variables

The difficulty of treating the source terms for the mixing ratios r_* due to such processes as evaporation/condensation, accretion of cloud droplets by raindrops, etc. , can be considerably reduced by using quasi-conservative variables. Let us consider the equations for r_v, r_c, and r_r:

$$\frac{d(\rho_{dref} r_v)}{dt} = \rho_{dref}(S_{RE} - S_{CON}), \tag{7.1}$$

$$\frac{d(\rho_{dref} r_c)}{dt} = \rho_{dref}(-S_{RA} - S_{RC} + S_{CON}), \tag{7.2}$$

$$\frac{d(\rho_{dref} r_r)}{dt} = \rho_{dref}(S_{RA} + S_{RC} - S_{RE} + S_{RS}), \tag{7.3}$$

where the S_* represent the source terms, with subscripts CON, RE, RA, RC, RS corresponding respectively to evaporation/condensation, rain evaporation, accretion of cloud droplets by raindrops, conversion of cloud droplets into raindrops, and rain sedimentation. If one defines a new variable

$$r_{np} = r_v + r_c, \tag{7.4}$$

the equation of evolution of r_{np} will read

$$\frac{d(\rho_{dref} r_{np})}{dt} = \rho_{dref}(S_{RE} - S_{RA} - S_{RC}). \tag{7.5}$$

Note that the standard Meso-NH notations compell to use the subscript np (for *non precipitating*) instead of w, since r_w is already defined as the sum of all species r_*. r_{np} is the sum of the mixing ratios of water species which *accompany air movements*, as opposed to r_r, whose evolution equation involves rain sedimentation, thus an independent fall velocity, assumed to be much larger than the air velocity. *For the time beeing, we consider that the turbulent fluctuations of rain are negligible, and the turbulence scheme will only take into account the vapour vapor and the cloud liquid water.* The right-hand side of Eq.(7.5) involving only source terms that have slow characteristic time scales, r_{np} can be considered as quasi-conservative. In the future, the inclusion of ice (r_i), snow (r_s), or graupels (r_g) in Meso-NH may require careful attention to the definition of a suitable, quasi-conservative mixing ratio.

Similarly, we may define

$$\theta_l = \theta - \frac{L_v}{C_{ph}} {\Pi_{ref}}^{-1} r_c, \tag{7.6}$$

where L_v is the latent heat of vaporization of water, C_{ph} is the specific heat at constant pressure for moist air ($C_{ph} = C_{pd} + r_v C_{pv} + (r_c + r_r) C_l + (r_i + r_s + r_g + r_h) C_i$), and $\Pi_{ref}^{-1} = \left(\frac{\theta}{T}\right)_{ref}$. θ_l is a quasi-conservative potential temperature, except for the same source terms that remain in the equation of evolution of r_{np}, as can be seen if we come back to the equation of evolution of θ in the absence of moist correction, solid species of water, and diabatic effects due to radiation and diffusion: starting from the usual expressions

$$\frac{d(\rho_{dref}\theta)}{dt} = \frac{L_v}{C_{ph}} \Pi_{ref}^{-1} \underbrace{\rho_{dref}(-S_{RE} + S_{CON})}_{=-\frac{d(\rho_{dref} r_v)}{dt}}, \tag{7.7}$$

$$\frac{d(\rho_{dref} r_c)}{dt} = \rho_{dref}(-S_{RA} - S_{RC} + S_{CON}), \tag{7.8}$$

we deduce

$$\frac{d(\rho_{dref}\theta_l)}{dt} = \frac{L_v}{C_{ph}} \Pi_{ref}^{-1} \rho_{dref}(S_{RA} + S_{RC} - S_{RE}). \tag{7.9}$$

This shows that except for the slow microphysical terms, the new variables are approximately as well conserved as θ and r_v in the absence of condensation. We take advantage of this to apply the turbulence scheme described in the previous chapter to θ_l and r_{np}, with a single modification linked to the expression of the buoyancy.

The course of computations is therefore the following:

- enter the turbulence scheme with the usual prognostic variables
- compute conservative variables
- compute turbulent fluxes of conservative variable formally as in the cloudless case (except for the expression of the buoyancy flux $\overline{u_i' \theta_v'}$)
- diagnose turbulent fluxes in non-conservative variables from their conservative counterparts
- come back to non-conservative variables
- come back to the main model

7.1.3 Retrieval of cloud water mixing ratio

As shown by Sommeria and Deardorff (1977), the mean value of r_c can be diagnosed from the grid scale values of θ_l and r_{np}, and their variances, which are supplied by the general turbulence scheme. This diagnosis relies on a simple statistical theory based on the shape of the sub-grid scale fluctuations histogram.

We first note that whenever cloud is present, the mixing ratio is equal to the saturation mixing ratio $r_{vs}(\theta, p)$. This can be expressed using θ_l and a first-order Taylor expansion as

$$r_v = r_{vs}(\theta, p) \approx r_{vs}(\theta_l) + (\frac{\partial r_{vs}}{\partial \theta})_{\theta_l}(\theta - \theta_l). \tag{7.10}$$

Here, the variations of r_{vs} with pressure have been neglected, because $|\frac{\partial r_{vs}}{\partial \theta}\Delta\theta| \gg |\frac{\partial r_{vs}}{\partial p}\Delta p|$. In the following, we will use the notation $J = \left(\frac{\partial r_{vs}}{\partial \theta}\right)_{\theta_l}$. Using the Clausius-Clapeyron relation, we have $J = \frac{r_{vs}(T_l)L_v}{R_v T_l \theta_l}$. Thus, we get

$$r_c = r_{np} - r_v = r_{np} - r_{vs}(\theta_l) - J(\theta - \theta_l). \tag{7.11}$$

Since by definition, $\theta - \theta_l = \frac{L_v}{C_{ph}}\Pi_{ref}^{-1} r_c$, this gives

$$r_c = r_{np} - r_{vs}(\theta_l) - J\frac{L_v}{C_{ph}}\Pi_{ref}^{-1} r_c, \tag{7.12}$$

$$r_c = \frac{r_{np} - r_{vs}(\theta_l)}{1 + M}, \tag{7.13}$$

where $M = J\frac{L_v}{C_{ph}}\Pi_{ref}^{-1}$.

On the other hand, in the unsaturated case, $r_c = 0$, thus a general expression is

$$r_c = \text{Max}\left(0, \frac{r_{np} - r_{vs}(\theta_l)}{1 + M}\right). \tag{7.14}$$

The mean cloud water mixing ratio in the grid cell is then obtained by averaging (7.14). For historical reasons, we use the notation

$$s = \frac{r_{np} - r_{vs}(\theta_l)}{2(1 + M)}. \tag{7.15}$$

s may be seen as a turbulent quantity that controls local saturation within the grid. Whenever $s \geq 0$, there is saturation. Then, $s = \overline{s} + s'$, and saturation may be defined as $s' \geq -\overline{s}$.
Note that the standard deviation σ_s of s may be easily computed, since to first order approximation,

$$s' = \frac{r'_{np} - J\theta'_l}{2(1 + M)}, \tag{7.16}$$

leading to

$$\sigma_s = \frac{\left(\overline{r'^2_{np}} + J^2\overline{\theta'^2_l} - 2J\overline{r'_{np}\theta'_l}\right)^{\frac{1}{2}}}{2(1 + M)}. \tag{7.17}$$

To compute the statistical average of r_c within the grid, it is useful to introduce the centered, normalized variable $t = s'/\sigma_s$, and its probability distribution $G(t)dt$. In terms of t, saturation is present whenever $t \geq -\overline{s}/\sigma_s$. We will therefore define the quantity

$$Q_1 = \frac{\overline{r_{np}} - r_{vs}(\overline{\theta_l})}{2(1 + M)\sigma_s}. \tag{7.18}$$

The fraction of the grid cell occupied by clouds is then

$$N = \int_{-Q_1}^{+\infty} G(t)dt, \tag{7.19}$$

and the mean cloud water content is

$$\frac{\overline{r_c}}{2\sigma_s} = \int_{-Q_1}^{+\infty} (Q_1 + t)G(t)dt. \tag{7.20}$$

The problem is therefore solved.
Note that in the case of elongated grids with $\Delta x, \Delta y \gg \Delta z$, it will be useful to assimilate the cloud fraction N to the cloud *cover*, in the usual meteorological sense. For isotropic grid, the cloud fraction is more of a three dimensional nature.

7.1.4 Flux of liquid water

We also need to compute the fluxes $\overline{u_i' r_c'}$, where u_i can be any of the three components of the velocity u_1, u_2, or u_3. Indeed, these fluxes will be used to compute the buoyancy fluxes $\overline{u_i' \theta_v'}$ (appearing in the TKE prognostic equation), and to retrieve the fluxes of non-conservative variables, once the fluxes of conservative variables are known.
With the same notations as in the previous section, according to Bougeault (1981, 1982), we have

$$\frac{\overline{s' r_c'}}{2{\sigma_s}^2} = \int_{-Q_1}^{+\infty} t(Q_1 + t)G(t)dt \; . \tag{7.21}$$

We assume that this second-order correlation can be used as a generic model for the $\overline{u_i' r_c'}$ correlations. However, Bechtold et al. (1993) have shown this to underestimate the real correlation in cases of low cloud fraction. We therefore introduce an empirical coefficient λ_i to obtain more realistic results:

$$\frac{\overline{u_i' r_c'}}{\overline{u_i' s'}} = \lambda_i \frac{\overline{s' r_c'}}{\sigma_s^2}. \tag{7.22}$$

Once the turbulent fluxes of cloud liquid water are known, going back to turbulent fluxes in non-conservative variables is straightforward, because they are linear combinations of turbulent fluxes in conservative variables. From (7.4, 7.6), we obtain readily

$$\overline{u_i' \theta'} = \overline{u_i' \theta_l'} + \frac{L_v}{C_{p_h}} \Pi_{ref}{}^{-1} \overline{u_i' r_c'}, \tag{7.23}$$

$$\overline{u_i' r_v'} = \overline{u_i' r_{np}'} - \overline{u_i' r_c'}. \tag{7.24}$$

7.1.5 Closure of the scheme

The closure relies on adequate choices for G and λ_i. In their original paper, Sommeria and Deardorff proposed to use by simplicity a gaussian distribution for G. However, Bougeault (1981, 1982) showed that this would underestimate the cloud fraction in most cases, because actual distributions are skewed. He proposed several solutions, the most general being the Gamma probability density. The importance of using skewed distributions has been confirmed by later work (Cuijpers and Bechtold 1995).

Using this theory, N, $\frac{\overline{r_c}}{2\sigma_s}$, and $\frac{\overline{s'r'_c}}{2{\sigma_s}^2}$ are then computed from equations 7.19, 7.20, and 7.21 and expressed as:

$$N = F_0(Q_1, A_s), \tag{7.25}$$

$$\frac{\overline{r_c}}{2\sigma_s} = F_1(Q_1, A_s), \tag{7.26}$$

$$\frac{\overline{s'r'_c}}{2\sigma_s^2} = F_2(Q_1, A_s). \tag{7.27}$$

Q_1 has been defined above, and A_s is the skewness of the distribution of t, that requires parametrization. The detailed expressions of F_0, F_1, and F_2 may be found in Bougeault (1982).
As far as the coefficients λ_i are concerned, they are unfortunately not well known when $i = 1$ or $i = 2$. By simplicity, we will assume $\lambda_1 = \lambda_2 = 1$. For $i = 3$, the study of Cuijpers and Bechtold (1995) shows that its value can range from 1 when G is a gaussian function, to 3 when Q_1 is of the order of -2, and up to 50 when Q_1 is as low as -4. However, in the later case, these values of Q_1 are sparse and the dispersion of the numerical value of λ_3 obtained after LES 3D simulations for different conditions of saturation is high, which makes difficult the fitting of any curve for λ_3.

The current choice of parameters in Meso-NH is the following:

1. For 1D or quasi-1D mode,

   - $Q_1 \geq 0$: $A_s = 0$ and $\lambda_3 = 1$,
   - $Q_1 < -2$: $A_s = 2$ and $\lambda_3 = 3$,
   - $-2 \leq Q_1 < 0$: $A_s = -Q_1$ and $\lambda_3 = 1 - Q_1$.

   The values of A_s for the first two cases correspond respectively to a gaussian function and a skewed exponential function. The latter case is only a linear interpolation of the two previous ones. In any of the three previous cases, $\lambda_1 = \lambda_2 \equiv 1$.

2. For the LES mode,

   - $A_s \equiv 0$ and $\lambda_1 = \lambda_2 = \lambda_3 \equiv 1$ in all cases.

The expression of the fluxes of cloud water is finally obtained from Eqs. (7.16), (7.22), and (7.27), as

$$\overline{u'_i r'_c} = A_{moist}\overline{u'_i r'_{np}} + A_\theta \overline{u'_i \theta'_l}, \tag{7.28}$$

with

$$A_{moist} = \frac{\lambda_i F_2(Q_1, A_s)}{1 + M}, \tag{7.29}$$

$$A_\theta = -J\frac{\lambda_i F_2(Q_1, A_s)}{1 + M}. \tag{7.30}$$

7.1.6 Buoyancy flux

As mentionned above, the only modification in the turbulence scheme in presence of saturation is the expression of the virtual potential temperature. Cloud water increase the density of the parcel, but the latent heat produced by condensation has an opposite effect. In general cloudy parcels are therefore more buoyant than clear air parcels. Using the conservative variables, this is expressed as

$$\begin{aligned}\theta_v &= \theta(1+\delta\frac{r_v}{1+r_w}-\frac{r_c}{1+r_w}-\frac{r_w-r_v-r_c}{1+r_w}) \\ &= \left(\theta_l+\frac{L_v}{C_{p_h}}{\Pi_{ref}}^{-1}r_c\right)\left(1+\delta\frac{r_{np}}{1+r_w}-(1+\delta)\frac{r_c}{1+r_w}-\frac{r_w-r_{np}}{1+r_w}\right). \end{aligned} \quad (7.31)$$

The fluctuations of θ are then given by

$$\begin{aligned}\theta_v' &\approx \delta\frac{\overline{\theta}}{1+\overline{r_w}}r'_{np} \\ &+ \left(\frac{L_v}{C_{p_h}}{\Pi_{ref}}^{-1}\left(1+\delta\frac{\overline{r_{np}}}{1+\overline{r_w}}-(1+\delta)\frac{\overline{r_c}}{1+\overline{r_w}}-\frac{\overline{r_w}-\overline{r_{np}}}{1+\overline{r_w}}\right)-(1+\delta)\frac{\overline{\theta}}{1+\overline{r_w}}\right){r_c}' \\ &+ \left(1+\delta\frac{\overline{r_{np}}}{1+\overline{r_w}}-(1+\delta)\frac{\overline{r_c}}{1+\overline{r_w}}-\frac{\overline{r_w}-\overline{r_{np}}}{1+\overline{r_w}}\right)\theta'_l, \end{aligned} \quad (7.32)$$

where $\delta=\dfrac{R_v}{R_d}-1$. This shows that the expression of $\overline{u_i'\theta_v'}$ will include a $\overline{u_i'r_c'}$ term.

It is convenient to define the following coefficients:

$$A = 1+\delta\frac{\overline{r_{np}}}{1+\overline{r_w}}-(1+\delta)\frac{\overline{r_c}}{1+\overline{r_w}}-\frac{\overline{r_w}-\overline{r_{np}}}{1+\overline{r_w}}, \quad (7.33)$$

$$B = \delta\frac{\overline{\theta}}{1+\overline{r_w}}, \quad (7.34)$$

$$\begin{aligned}C &= \frac{L_v}{C_{p_h}}{\Pi_{ref}}^{-1}\left(1+\delta\frac{\overline{r_{np}}}{1+\overline{r_w}}-(1+\delta)\frac{\overline{r_c}}{1+\overline{r_w}}-\frac{\overline{r_w}-\overline{r_{np}}}{1+\overline{r_w}}\right)-(1+\delta)\frac{\overline{\theta}}{1+\overline{r_w}} \\ &= \frac{L_v}{C_{p_h}}{\Pi_{ref}}^{-1}A-\frac{1+\delta}{\delta}B. \end{aligned} \quad (7.35)$$

With these notations, the buoyancy flux $\overline{u_i'\theta_v'}$ can be written

$$\overline{u_i'\theta_v'}=A\overline{u_i'\theta_l'}+B\overline{u_i'r_{np}'}+C\overline{u_i'r_c'}\,. \quad (7.36)$$

A more compact expression may be obtained by use of (7.28):

$$\overline{u_i'\theta_v'}=E_\theta\overline{u_i'\theta_l'}+E_{moist}\overline{u_i'r_{np}'}\,, \quad (7.37)$$

where $E_\theta=A+CA_\theta$ and $E_{moist}=B+CA_{moist}$.

7.1.7 Modification to the mixing length

There are three different ways of computing the mixing length in Meso-NH.

- For the LES mode, the mixing length is usually set equal to $(d_{xx}d_{yy}d_{zz})^{1/3}$. In this case, no change is necessary to account for SGC.
- In the case of a K-ϵ turbulence scheme, condensation processes will be taken into account implicitely in the length scale when working in conservative variables.
- Finally, when the Bougeault-Lacarrère scheme is adopted, one has to use the potential temperature $\theta_v = \theta\left(\frac{1+\delta r_v}{1+r_w}\right)$ to obtain the level, either upward or downward, where all the TKE has been transformed into potential energy due to buoyancy, yielding:

$$-\overline{e}(z) = \int_z^{z+l_{up}} \beta(\overline{\theta_{vp}}(z') - \overline{\theta_{ve}}(z'))dz' = \int_{z-l_{down}}^{z} \beta(\overline{\theta_{ve}}(z') - \overline{\theta_{vp}}(z'))dz' \ ,$$

  where the subscripts e and p refer respectively to the environment and to the particle which has left its initial height.

If the transformation is adiabatic, when a particle leaves its initial height, then:

$$\overline{\theta_{vp}}(z') = \overline{\theta}_p(z')\left(\frac{1+\delta\overline{r_{vp}}(z')}{1+\overline{r_{wp}}(z')}\right) \ , \tag{7.38}$$

$$\overline{\theta_{ve}}(z') = \overline{\theta}_e(z')\left(\frac{1+\delta\overline{r_{np_e}}(z')}{1+\overline{r_{we}}(z')}\right) \ , \tag{7.39}$$

where $\overline{\theta}_p(z')$, $\overline{r_{vp}}(z')$, and $\overline{r_{wp}}(z')$ account for the change of phase of water when the particle is lifted from height z.

7.1.8 Spatial Discretization

The discretization in space follows from the general turbulence scheme. The cloud fraction, the cloud mixing ratio, the conservative variables and the variances are all located at mass points. The application of the theory is therefore straightforward.
On the other hand, the fluxes are located at u_i points. Thus, application of (7.28) requires an average of A_r and A_θ in the direction i. This reads:

$$\overline{u_i'r_c'} = \overline{A_r}^{x_i}\overline{u_i'r_{np}'} + \overline{A_\theta}^{x_i}\overline{u_i'\theta_l'}. \tag{7.40}$$

The buoyancy flux ....

7.1.9 Practical implementation

As this method is providing a diagnostic estimate of the cloud water mixing ratio, it substitutes to the condensation adjustment procedure. This could be done in the turbulence scheme very conveniently. However, the general code organization would become very complicated, and different wether the SGC is used or not. Therefore, we decided not to mix the turbulence scheme and the condensation adjustment in one routine and to adhere to the usual order of call of the routines inside one model time step, where the condensation adjustment is the last routine called before the end of the time step.
The code organization follows from these considerations. It is understood that the objective of the time step is to compute values at $t+1$.

1. The input variables to the turbulence scheme are the usual prognostic variables at t and $t-1$, their sources, and the value of $\lambda_3 \overline{s'r'_c}/2\sigma_s^2 \equiv \lambda_3 F_2(Q_1, A_s)$, saved from the previous time step.

2. In routine TURB, the conservative variables and their sources are computed from the input variables, through (7.4, 7.6).

3. The computation of turbulent fluxes follows as described in the previous chapter. However, when the buoyancy flux is needed, the formulation of the E_θ and E_{moist} coefficients uses the formulation (7.37) instead of the formulation given in the previous chapter. Note that the two formulations coincides in the total absence of cloud. This computation is based on the value of $\lambda_3 \overline{s'r'_c}/2\sigma_s^2$.

4. The fluxes of cloud water $\overline{u'_i r'_c}$ are diagnosed through (7.28). This uses also (7.29). Note that only $\lambda_3 F_2$ is transmitted to the routine to save ressources. This trick is possible because in the present version of the scheme, λ_1 and λ_2 are not used in the 1DIM case, and equal to λ_3 in the 3DIM case.

5. The divergence of $\overline{u'_i r'_c}$ is used to evaluate the source of r_c due to the turbulent exchanges, at the exclusion of the condensation/evaporation process.

6. The value of σ_s^t is computed, and is an output of the turbulence scheme.

7. At the end of the TURB routine, we get back to the usual form of the temperature, the water mixing ratio, and their sources. Note that the cloud water mixing ratio r_c is not modified during the turbulence computation, but its source now includes the effect of turbulent transport, as do the sources of the potential temperature and water vapor.

8. At the end of the model time step, routine FAST_TERMS receives as input the non-adjusted value of the prognostic variables at time $t+1$. We shall call these θ^*, r_v^*, and r_c^*. It also receives σ_s^t.

9. FAST_TERMS computes the final value of the conservative variables by applying (7.4, 7.6) to θ^*, r_v^*, and r_c^*. This does not involve any approximation, since the conservative variables are conserved by definition in the saturation adjustment.

10. It computes Q_1 by applying (7.48) with the final values of the conservative variables, and σ_s^t. This step thus assimilates σ_s^t to σ_s^{t+1}. This is done in order to save computer ressources. The alternative would be to carry a large number of additionnal variables, or to redo part of the turbulence computation. This is a price to pay for clarity and efficiency of the code.

11. The adjusted value r_c^{**} is obtained from (7.26), again assimilating σ_s^t to σ_s^{t+1}. At the same time, $\lambda_3 \overline{s'r'_c}/2\sigma_s^2$ is computed and saved for the next time step.

12. Finally, the adjusted value of the non-conservative, prognostic variables at time $t+1$ are obtained through

$$\overline{r_c}^{t+\Delta t} = \overline{r_c}^{**} \tag{7.41}$$

$$\overline{\theta}^{t+\Delta t} - \overline{\theta}^{*} = \frac{L_v}{C_{p_h}} {\Pi_{ref}}^{-1} \left(\overline{r_c}^{**} - \overline{r_c}^{*}\right) \tag{7.42}$$

$$\overline{r_v}^{t+\Delta t} - \overline{r_v}^{*} = -\left(\overline{r_c}^{**} - \overline{r_c}^{*}\right) \tag{7.43}$$

7.2 Sub-Grid condensation scheme for ice-phase and convective clouds

7.2.1 Introduction

The application of a statistical sub-grid condensation scheme to deep convective tropospheric clouds and to upper tropospheric stratiform clouds requires a couple of extensions to the warm-phase scheme presented in the previous chapter. These extensions include i) the representation of ice phase and mixed-phase clouds ii) a definition of statistical cloud relations that approximately hold for all types of tropospheric clouds, and iii) a proper definition of sub-grid variance including a convective contribution. These specific developments are described below and closely follow the Méso-nh Cloud Resolving Model (CRM) study by Chaboureau and Bechtold (2002). However, all issues concerning the coupling of the sub-grid condensation scheme with the Méso-nh prognostic thermodynamic framework (section "practical implementation") as described in the previous chapter keep unchanged.

7.2.2 Thermodynamic framework

The properties of a moist adiabatically ascending air parcel are conveniently expressed assuming conservation (in the absence of precipitation) of enthalpy or "liquid water static energy" h_l and total water mixing ratio r_w

$$\begin{aligned} h_l &= C_{pm}T - L_v r_c - L_s r_i + (1 + r_w)gz \quad (7.44)\\ r_w &= r_v + r_c + r_i, \quad (7.45) \end{aligned}$$

where the specific heat of moist air is defined as $C_{pm} = C_{pd} + r_w C_{pv}$, L_v and L_s are the specific latent heats of vaporization and sublimation, g denotes the gravitational acceleration, z is height, and r_v, r_c and r_i denote the mixing ratios of water vapor and non-precipitating cloud water/ice, respectively. We further define a "liquid" temperature as

$$\begin{aligned} T_l &= T - L_v/C_{pm}\, r_c - L_s/C_{pm}\, r_i \\ &= (h_l - (1 + r_w)gz)/C_{pm}, \quad (7.46) \end{aligned}$$

and combine the moisture and temperature effects to one single variable $s = ar_w - bT_l$ (see e.g. Mellor 1977) with

$$\begin{aligned} a = (1 + Lr_{sl}/C_{pm})^{-1}, \qquad b = a\ r_{sl},\\ r_{sl} = \partial r_{sat}/\partial T(T = T_l) = Lr_{sat}(T_l)/(R_v T_l^2). \quad (7.47) \end{aligned}$$

Here L and r_{sat} are the latent heat and water vapor saturation mixing ratio that inside a given glaciation interval $T_0 > T > T_1$ are linearly interpolated as a function of temperature between their respective values for liquid water and ice, i.e. $L = (1 - \chi)L_v + \chi L_s$, $r_{sat} = (1 - \chi)r_{satw} + \chi r_{sati}$, with $\chi = (T_0 - T)/(T_0 - T_1)$, T_0 =273.16 K, and T_1=253 K. r_{satw} and r_{sati} are the saturation mixing ratios over water and ice, respectively.
Finally, with the above definitions Q_1 is expressed as the saturation deficit of the ensemble or grid average (denoted by overbars) normalized by σ_s, the variance of s, with primes denoting deviations from the ensemble (grid) mean

$$\begin{aligned} Q_1 = \overline{a}\,(\overline{r}_w - r_{sat}(\overline{T}_l))/\sigma_s,\\ \sigma_s = (\overline{a}^2\,\overline{r_w'^2} - 2\overline{a}\overline{b}\ \overline{r_w' T_l'} + \overline{b}^2\,\overline{T_l'^2})^{1/2}. \quad (7.48) \end{aligned}$$

7.2.3 Fractional cloudiness and cloud condensate

As shown in Chaboureau and Bechtold (2002) using CRM data, the cloud fraction N and the grid-mean condensate mixing ratio $r_l = r_c + r_i$ of tropospheric clouds can be represented by the following relations that have been earlier established for boundary-layer clouds

$$N = \max\{0, \min[1, 0.5 + 0.36 \arctan(1.55 Q_1)]\} \tag{7.49}$$

$$\begin{aligned} \frac{\overline{r}_l}{\sigma_s} &= e^{(1.2Q_1 - 1)}, && Q_1 < 0. \\ \frac{\overline{r}_l}{\sigma_s} &= e^{-1} + 0.66 Q_1 + 0.086 Q_1^2 && 0 \leq Q_1 \leq 2 \\ \frac{\overline{r}_l}{\sigma_s} &= Q_1 && Q_1 > 2. \end{aligned} \tag{7.50}$$

The respective mixing ratios for cloud water and cloud ice are then retrieved using $r_c = (1 - \chi)\, r_l$, and $r_i = \chi\, r_l$.

7.2.4 Parameterization of σ_s

The practical application of the cloud relations (7.49) and (7.50) in meteorological models requires the knowledge of the second-order moment σ_s. This quantity is provided by the Méso-nh turbulence scheme and used as that in the warm-phase sub-grid condensation scheme.
However, it turned out that this formulation is not yet well adapted to deep and upper tropsopheric clouds as it generally has zero value above the boundary-layer. Here, a simple parameterization is suggested representing the total variance of s as a sum of a turbulent and a convective contribution

$$\sigma_s^2 = \sigma_{sturb}^2 + \sigma_{sconv}^2 \tag{7.51}$$

Turbulent contribution

The turbulent contribution is either the value computed by the turbulence scheme (possible option in the computer code) or (present default option) expressed as

$$\sigma_s = c_\sigma\, l \left[\overline{a}^2 \left(\frac{\partial \overline{r}_w}{\partial z} \right)^2 - 2\overline{a}\overline{b}\, C_{pm}^{-1} \frac{\partial \overline{h}_l}{\partial z} \frac{\partial \overline{r}_w}{\partial z} + \overline{b}^2\, C_{pm}^{-2} \left(\frac{\partial \overline{h}_l}{\partial z} \right)^2 \right]^{1/2}, \tag{7.52}$$

where $C_{pm}^{-1}\, \partial h_l / \partial z = \partial T_l / \partial z \; + g / C_{pm}(1 + r_w)$, l is a constant length-scale of value $l_0 = 600$ m (for $z > l_0$; $l = z$ for $z <= l_0$), and c_σ is a constant of value 0.2 (Cuxart et al. 2000).

Convective contribution

Using the top-hat approximation, the variance and the flux of a quantity s can be expressed as (see e.g. Lappen and Randall 2001)

$$\overline{s'^2} = N\,(1 - N)(s^c - s^e)^2, \tag{7.53}$$

where N is the cloud fraction, and where c and e denote cloud and environmental values, respectively. However, as noted by the authors and Siebesma (personal communication) the top-hat approximation reasonably represents the convective fluxes but not the variances, and is also sensible to the decomposition chosen, i.e. cloud/environment or updraft/downdraft. Therefore, instead

of (7.53) we seek a simple expression as a function of the convective mass flux (a quantity that is readily available from the mass flux convection parameterization):

$$\sigma_s^{conv} = \overline{s'^2}^{1/2} \approx \frac{\overline{w's'}}{w^*} \approx M \, \frac{(s^c - s^e)}{w^* \rho^*} \tag{7.54}$$

where $M = \overline{\rho} \, N \, w$ is the convective mass flux (kg s^{-1} m^{-2}), w^* a convective scale velocity and ρ^* a tropospheric density scale. Finally, (7.54) is further simplified to

$$\sigma_s^{conv} \approx M \, \frac{(s^c - s^e)}{w^* \rho^*} \approx \alpha \, M \, f(z/z^*) \tag{7.55}$$

where a vertical scaling function f has been introduced. It turns out that σ_s is mainly determined (especially in the tropics and the upper troposphere) by the moisture variance. For simplicity the scaling function is set to $f = a^{-1}$ so that it is proportional to the saturation mixing ratio.
Finally, the value of the proportionality coefficient α can be obtained by minimizing the function $(\sigma_s^2 - \sigma_{sturb}^2 - \sigma_{sconv}^2)^2$, where σ_s^2 are the values derived from convective data sets and where σ_{sturb} and σ_{sconv} are replaced by the expressions (7.52) and (7.55), respectively. A value $\alpha = 3 \times 10^{-3}$ is obtained using the cloud mass flux from the CRM.

7.3 Treatment of mixed-phase clouds

7.3.1 Definition of new conservative variables

The standard Meso-NH sub-grid condensation scheme computes the turbulent fluxes in a moist atmosphere assuming a reversible condensation/evaporation process for non-precipitating cloud droplets. The inclusion of the ice phase leads to a generalization of the scheme to mixed-phase clouds. This is done using new quasi-conservative variables. First, the total *non precipitating* mixing ratio is redefined by

$$r_{np} = r_v + r_c + r_i, \tag{7.56}$$

where the additional term r_i is the non-precipitating pristine ice mixing ratio. Second, the ice-liquid potential temperature, θ_{il}, is substituted for θ_l which is only applicable to warm clouds

$$\theta_{il} = \theta - \frac{L_v}{C_{ph}} {\Pi_{ref}}^{-1} r_c - \frac{L_s}{C_{ph}} {\Pi_{ref}}^{-1} r_i, \tag{7.57}$$

where L_s is the latent heat of sublimation of ice and with the usual definition of C_{ph}. Note that r_{np} and θ_{il} still revert to r_v and θ in a cloudless atmosphere so the moist turbulence scheme can be employed with only slight modifications to account for the presence of the ice phase.

7.3.2 Some weighted thermodynamical functions

In most of the cases, a simple weighting function $f_{ice} = \dfrac{r_i}{r_c + r_i}$ is sufficient to update some ancillary thermodynamical functions from their "warm cloud" definition. For instance the mixed-phase saturation mixing ratio is defined by the barycentric formula $r_{vs}(T) = (1 - f_{ice}) r_{vs}^l(T) + f_{ice} r_{vs}^i(T)$

with $r_{vs}^l(T)$ and $r_{vs}^i(T)$ being the saturation mixing ratios over water and ice, respectively. Consequently, the function $J = \left(\frac{\partial r_{vs}^l}{\partial \theta}\right)_{\theta_{il}}$ which is introduced in the warm cloud case ($J \equiv J_l$) becomes

$$J \equiv J_{il} = (1 - f_{ice})J_l + f_{ice}J_i, \tag{7.58}$$

where $J_i = \frac{r_{vs}^i(T_{il})L_s}{R_v T_{il}\theta_{il}}$. The same approximation is made for the function M, for the stability functions ϕ_i and ψ_i, and hence for the resulting A_{moist} and A_θ functions. We recall that the assumption of saturation mixing ratio is always made when a cloud is present (although this may not be accurate in the case of cold ice clouds where a significant degree of supersaturation over ice can be found), so:

$$r_c + r_i = \frac{r_{np} - r_{vs}(\theta_l)}{1 + M}, \tag{7.59}$$

with a new definition of M which can be derived analytically as $M \equiv M_{il} = J_{il}\frac{L_v(1 - f_{ice}) + L_s f_{ice})}{C_{ph}}\Pi_{ref}^{-1}$.

7.3.3 Ice and liquid fluxes

Then we need to compute the divergence of the turbulent fluxes $\overline{u_i' r_c'}$ and $\overline{u_i' r_i'}$, where u_i can be any of the three components of the velocity. This is done using the same theory developed in the pure warm cloud case but with $r'_{(c+i)} = r_c' + r_i'$

$$\frac{\overline{s' r'_{(c+i)}}}{2{\sigma_s}^2} = \int_{-Q_1}^{+\infty} t(Q_1 + t)G(t)dt\ , \tag{7.60}$$

and with an actualized definition of $s' = \frac{r'_{np} - J\theta'_{il}}{2(1 + M)}$ which now incorporates both r_c' and r_i' fluctuations. Q_1 still has its usual meaning. Similar characteristics of the probability distribution $G(t)dt$ are implicitly assumed for liquid and mixed-phase clouds. The simplest way to partition the liquid and ice turbulent fluxes of condensed material is to consider the following closure

$$\overline{u_i' r'_{(c+i)}} = \lambda_i \frac{\overline{u_i' s'}\ .\ \overline{s' r'_{(c+i)}}}{\sigma_s^2} = \overline{u_i' r_c'} + \overline{u_i' r_i'} \tag{7.61}$$

with $\overline{u_i' r_c'} = (1 - f_{ice})\overline{u_i' r'_{(c+i)}}$ and with $\overline{u_i' r_i'} = f_{ice}\overline{u_i' r'_{(c+i)}}$.

7.3.4 Buoyancy flux

The last point of concern is the computation of the buoyancy term in presence of ice in the TKE equation. The expression of θ_v in 7.31 is slightly modified when switching from θ_l to θ_{il} and when using the new expression for r_{np}

$$\begin{aligned}
\theta_v &= \theta(1 + \delta\frac{r_v}{1 + r_w} - \frac{r_c + r_i}{1 + r_w} - \frac{r_w - r_v - r_c - r_i}{1 + r_w}) \\
&= \left(\theta_{il} + \frac{L_v}{C_{p_h}}{\Pi_{ref}}^{-1} r_c + \frac{L_s}{C_{p_h}}{\Pi_{ref}}^{-1} r_i\right) \\
&\times \left(1 + \delta\frac{r_{np}}{1 + r_w} - (1 + \delta)\frac{r_c + r_i}{1 + r_w} - \frac{r_w - r_{np}}{1 + r_w}\right),
\end{aligned} \tag{7.62}$$

where again $\delta = \dfrac{R_v}{R_d} - 1$. The fluctuations of θ_v now depend on both r_c and r_i

$$\begin{aligned}
\theta'_v &\approx \delta \frac{\overline{\theta}}{1+\overline{r_w}} r'_{np} \\
&+ \left(\frac{L_v}{C_{ph}} \Pi_{ref}{}^{-1} \left(1 + \delta \frac{\overline{r_{np}}}{1+\overline{r_w}} - (1+\delta) \frac{\overline{r_c}+\overline{r_i}}{1+\overline{r_w}} - \frac{\overline{r_w}-\overline{r_{np}}}{1+\overline{r_w}} \right) - (1+\delta) \frac{\overline{\theta}}{1+\overline{r_w}} \right) r'_c \\
&+ \left(\frac{L_s}{C_{ph}} \Pi_{ref}{}^{-1} \left(1 + \delta \frac{\overline{r_{np}}}{1+\overline{r_w}} - (1+\delta) \frac{\overline{r_c}+\overline{r_i}}{1+\overline{r_w}} - \frac{\overline{r_w}-\overline{r_{np}}}{1+\overline{r_w}} \right) - (1+\delta) \frac{\overline{\theta}}{1+\overline{r_w}} \right) r'_i \\
&+ \left(1 + \delta \frac{\overline{r_{np}}}{1+\overline{r_w}} - (1+\delta) \frac{\overline{r_c}+\overline{r_i}}{1+\overline{r_w}} - \frac{\overline{r_w}-\overline{r_{np}}}{1+\overline{r_w}} \right) \theta'_{il}, \qquad (7.63)
\end{aligned}$$

After recasting the above expression as $\theta'_v = A^{il}\theta'_{il} + Br'_{np} + C^l r'_c + C^i r'_i$ (see 7.37), a good approximation of $\overline{u'_i \theta'_v}$ is deduced

$$\overline{u'_i \theta'_v} \approx E_\theta \overline{u'_i \theta'_{il}} + E_{moist} \overline{u'_i r'_{np}}, \qquad (7.64)$$

where the updated factors $E_\theta = A + CA_\theta$ and $E_{moist} = B + CA_{moist}$ are a function of $A \equiv A^{il}$ (including $\overline{r_i}$) and of $C = (1 - f_{ice})C^l + f_{ice}C^i$.

7.4 Mixing length

No modification is brought for the moment.

7.5 Fractional nebulosity of mixed-phase clouds

Although all ingredients of the "warm cloud" scheme are available and are directly applicable to mixed-phase clouds, the partial cloudiness N has not yet been tested in this case. Note that N is already coupled to the radiative transfer scheme.

7.6 References

Bechtold, P., J.-P. Pinty and P. Mascart, 1993: The use of partial cloudiness in a warm-rain parameterization: a subgrid-scale precipitation scheme, *Mon. Wea. Rev.*, **121**, 3301-3311.

Betts, A. K., 1973: on precipitating cumulus convection and its parameterization, *Quart. J. Roy. Meteorol. Soc.*, **99**, 178-196.

Bougeault, P. 1981: Modeling the trade-wind cumulus boundary layer. Part I: testing the ensemble cloud relations against numerical data, *J. Atmos. Sci.*, **38**, 2414-2428, 1981.

Bougeault, P., 1982: Cloud-ensemble relations based on the gamma probability distribution for the higher-order models of the planetary boundary layer, *J. Atmos. Sci.*, **39**, 2691-2700.

Bougeault, P., and P. Lacarrère, 1989: Parameterization of orography-induced turbulence in a meso-beta scale model, *Mon. Wea. Rev.*, **117**, 1872-1890.

Chaboureau J.-P., and P. Bechtold, 2002: A simple cloud parameterization derived from cloud resolving model data: Diagnostic and prognostic applications. *J. Atmos. Sci.*, **59**, 2362-2372.

Chaboureau J.-P., and P. Bechtold, 2005: Statistical representation of clouds in a regional model and the impact on the diurnal cycle of convection during Tropical Convection, Cirrus and Nitrogen Oxides (TROCCINOX). *J. Geophys. Res.*, **110**, D17103, doi:10.1029/2004JD005645.

Cuxart, J., P. Bougeault, and J.-L. Redelsperger, 2000: A turbulence scheme allowing for mesoscale and large-eddy simulations. *Quart. J. Roy. Meteor. Soc.*, **126,** 1–30.

Cuijpers, J. W. M. and P. Bechtold, 1995: A Simple Parameterization of Cloud Water Related Variables for Use in Boundary Layer Models, *J. Atmos. Sci.*, **52**, 2486-2490.

Lappen, C.-L., and D. A. Randall, 2001: Toward a unified parameterization of the boundary layer and moist convection. Part I: A new type of mass-flux model. *J. Atmos. Sci.,* **58,** 2021-2036.

Mellor, G. L., 1977: The Gaussian cloud model relations. *J. Atmos. Sci.,* **34,** 356-358.

Sommeria, G. and J. W. Deardorff, 1977: Subgrid scale condensation in models for non precipitating clouds, *J. Atmos. Sci.*, **34**, 344-355.